КРИСТАЛЛОГРАФИЯ

SOVIET PHYSICS

Crystallography

VOLUME 2 NUMBER 1

A Translation
of the journal
Crystallography
of the
Academy of Sciences of the USSR

(RUSSIAN ORIGINAL VOL. 2, NO. 1)

Published by the
AMERICAN INSTITUTE OF PHYSICS
INCORPORATED

SOVIET PHYSICS

Crystallography

A translation of the journal "Crystallography" of the Academy of Sciences of the USSR

A publication of the
**AMERICAN INSTITUTE
OF PHYSICS**

Governing Board

FREDERICK SEITZ, *Chairman*

Members

WALTER S. BAIRD
JESSE W. BEAMS
RAYMOND T. BIRGE
R. H. BOLT
J. W. BUCHTA
J. H. DILLON
VERNET E. EATON
HERBERT A. ERF
IRVINE C. GARDNER
S. A. GOUDSMIT
C. KITTEL
WINSTON E. KOCK
R. BRUCE LINDSAY
WALTER C. MICHELS
G. E. PAKE
R. RONALD PALMER
JOSEPH B. PLATT
RALPH A. SAWYER
H. D. SMYTH
JOHN STRONG
GEORGE E. UHLENBECK

Officers and Staff

ELMER HUTCHISSON
Director
HENRY A. BARTON
Associate Director
WALLACE WATERFALL
Secretary and Treasurer
EDWARD P. TOBER
Mgr., Production and Distribution
THEODORE VORBURGER
Advertising Manager
RUTH F. BRYANS
Publication Manager
KATHRYN SETZE
Assistant Treasurer
ALICE MASTROPIETRO
Circulation Manager
EUGENE H. KONE
Director of Public Relations

American Institute of Physics Advisory Board on Russian Translations

ROBERT T. BEYER, *Chairman*

FREEMAN DYSON, DWIGHT GRAY, MORTON HAMERMESH,
DAVID HARKER, VLADIMIR ROJANSKY, HAROLD F. WEAVER

Advisory Editor, Soviet Physics – Crystallography: DAVID HARKER, Protein Structure Project, Polytechnic Institute of Brooklyn, Brooklyn 2, New York.

"Soviet Physics – Crystallography" is published by the American Institute of Physics, with the cooperation of the American Crystallographic Association, for the purpose of making available in English reports of current Soviet research in crystallography as contained in the journal "Crystallography" of the Academy of Sciences of the USSR. The translation begins with the 1957 issues.

Transliteration of the names of Russian authors follows the system employed by the Library of Congress.

This translating and publishing project was undertaken by the Institute in the conviction that dissemination of the results of research everywhere in the world is invaluable to the advancement of science. The National Science Foundation of the United States encouraged the project initially and is supporting it in large part by a grant. Translation and printing are being handled by Consultants Bureau, Inc.

The American Institute of Physics and its translators propose to translate faithfully all of the scientific material in the "Crystallographic Journal of the Academy of Sciences of the USSR" appearing after January 1, 1957. The views expressed in the translated material, therefore, are intended to be those expressed by the original authors, and not those of the translators nor of the American Institute of Physics.

One volume is published annually. The volume numbering coincides with that of the original Russian journal.

Subscription Prices:

Per year (6 issues), starting with Vol. 2, No. 1

General: *United States and Canada*	$25.00
Elsewhere	27.00
Libraries of non-profit academic institutions:	
United States and Canada	10.00
Elsewhere	12.00
Back numbers, all issues	5.00

Subscriptions should be addressed to the American Institute of Physics, 335 East 45th Street, New York 17, New York.

Copyright by American Institute of Physics 1958

SOVIET PHYSICS

Crystallography

VOLUME 2, NUMBER 1 JANUARY-FEBRUARY, 1957

ANNOUNCEMENT

The present issue marks the beginning of the translation of the Soviet journal "Crystallography". This translation is being published by the American Institute of Physics with the cooperation of the American Crystallographic Association, and is supported in large measure by the National Science Foundation.

It further represents the second expansion in the translation program of the American Institute of Physics, which is now carrying out translations of six Soviet journals with a total of approximately 10,000 pages per year. This program, which began in 1955, has been fortunate in the widespread support of the work, not only, by the organizations mentioned above, but also by translators, subscribers and the original editors in the Soviet Union. It is hoped that such cooperation will continue for this new enterprise.

SOVIET PHYSICS

Crystallography

VOLUME 2, NUMBER 1 JANUARY-FEBRUARY, 1957

ALEKSEI VASIL'EVICH SHUBNIKOV

Aleksei Vasil'evich Shubnikov was born in Moscow on March 17, (29), 1887. He lost his father, who was a business clerk, at an early age; but through the efforts of his mother he won a scholarship to one of the best secondary schools in Moscow, the Imperial Commercial School, which was also attended at other times by I. A. Goncharov and S. M. Solov'ev. The brothers, N. I. and S. I. Vavilov, were schoolmates of Shubnikov.

In 1908, after being graduated from the secondary school with honors and with the title of Bachelor of Commerce, Shubnikov was enrolled in the Physico-Mathematical Faculty of Moscow University to specialize in physical chemistry. He published his first articles in the journal "The Physics Amateur," during his university years. During his first year he was attracted by the lectures on crystallography given by Iu. V. Wulff, Ia. V. Samoilov and V. I. Vernadskii and decided to specialize in this field without officially changing his specialty of "physical chemistry."

In 1910 Shubnikov began to work in Wulff's laboratory and soon became the latter's assistant. During the next year he published the results of his first independent experimental investigation, on the symmetry of potassium bichromate crystals. In order to obtain a diploma of the highest grade it was necessary to submit a second paper. This was an investigation of the influence of the degree of supersaturation of a potash alum solution on the shape of the precipitated crystals. The results were subsequently published and Shubnikov frequently returned to this work.

After his graduation from the university with a first-grade diploma, in order to perform his military service Shubnikov joined one of the regiments of grenadiers stationed in Moscow. This enabled him to continue scientific investigations which he had begun together with Wulff. This work was interrupted by the outbreak of the First World War in 1914. Shubnikov was called into the army with the rank of ensign and was sent to the front, where he was soon seriously wounded. After his recuperation he was appointed a military chemist and worked in munitions plants from the beginning of 1915 until 1918.

In 1919 Shubnikov finally returned to his scientific work, at first in the Shaniavskii University and then, in 1920, at the newly established Ural University in Ekaterinburg (Sverdlovsk), where he was appointed professor. During his stay in Sverdlovsk from 1920 to 1925 Shubnikov organized a department of crystallography and a research laboratory which immediately became closely associated with the Ural diamond-cutting factory. Shubnikov enthusiastically undertook the development of rational methods of grinding and polishing precious and industrial stones. In particular, he organized the production of quartz wedges for microscopes and of other crystal optical products at the factory. In his publications during these and later years we find papers on a disk saw for the cutting of small stones, on the grinding and polishing of stones, on the preparation of crystalline products, etc. These practical labors grew with time into a great branch of science and Shubnikov can with complete justification be regarded as the founder of applied crystallography in the USSR.

In his teaching Shubnikov was the first in the USSR to make extensive pedagogical use of the basic instrument of modern geometric crystallography, the Wulff net, and was the author of the first textbooks based on its use.

By 1925 Shubnikov's reputation was so great that when the chair of crystallography at Leningrad University, which had previously been held by Academician A. E. Fersman, became vacant it was immediately offered to Shubnikov. In addition, he was invited by Fersman to work in the Mineralogical Museum of the Academy of Sciences at Leningrad. Soon afterwards, when the death of Wulff left the chair of crystallography vacant at Moscow University, Shubnikov was asked to take the place of his beloved teacher. But he declined to participate in either competition and concentrated on his work for the Academy of Sciences as a senior research associate of the Mineralogical Museum, in which he headed the department of crystallography.

In 1927 and 1929 Shubnikov was sent abroad to familiarize himself with the status of crystallographic and x-ray investigations. He visited the crystallographic institutions of Germany and Norway and worked for some time at the Institute of Mineralogy and Crystallography of Leipzig University under Rinne.

In Leningrad Shubnikov considerably enlarged the range of his scientific and technical interests by working in the Radium Institute, the Physico-Technical Institute, the Central Radio Engineering Laboratory, the Leningrad divisions of the Institute of Applied Mineralogy and in the Ceramics Institute. At that time he assisted in the organization of a great laboratory for the processing of precious and industrial stones connected with the combine "Russian Gems," which still exists under a different name. During this period he conducted a large number of experimental investigations concerning the practical utilization of the piezoelectrical properties of quartz, and with the determination of the role of the environment as an integral factor in crystal formation, and he published a number of theoretical papers on symmetry, expecially on the symmetry of the continuum, which to some extent is contrasted with the symmetry of the noncontinuum in a crystal regarded as a medium. This fruitful activity of Shubnikov received public recognition in 1933 when he was appointed a corresponding member of the Academy of Sciences of the USSR.

During his Leningrad period Shubnikov was surrounded by a group of students and colleagues among whom were G. G. Lemmlein, G. B. Bokii B. V. Vitovskii, E. V. Tsinzerling and others.

In 1934 the Academy of Sciences was transferred to Moscow by governmental decree. This transfer was followed by the transformation of the crystallography division of the Lomonosov Institute of the Academy of Sciences, then heated by Shubnikov, into an independent Institute of Crystallography. Fedorov and Wulff had hoped for the establishment of such an institute, which Shubnikov was able to accomplish.

The first step in this direction was the conversion of the crystallography division of the Lomonosov Institute into an independent Crystallographic Laboratory of the Academy of Sciences. At first this laboratory remained in the Department of Geological and Geographical Sciences, but was later transferred to the Department of Physical and Mathematical Sciences.

Shubnikov then had to change his rule of being the "soul" of all work issuing from his division because the laboratory had expanded its scope to include such departments as x-rays, electron diffraction, the growth of industrial crystals, the mechanical properties of crystals, etc. During these years Shubnikov wrote a number of large monographs on crystallography. The first of these was "How Crystals Grow" in 1935, which was a reference book for everyone concerned with the growth of crystals. Almost at the same time there appeared "Quartz and its Uses" (1940), "Symmetry" (1940), and the "Elements of Crystallography" written in collaboration with E. E. Flint and G. B. Bokii in 1940. A large number of shorter but always brilliant papers and lectures by Shubnikov were devoted to the introduction of the fundamental crystallographic concept of symmetry and the associated way of thinking into related sciences, principally physics and chemistry. During this period Shubnikov made a very great discovery: he brought into realization and studied piezoelectric textures whose possibility he had predicted from a study of the theory of piezoelectricity.

At the end of 1937 Shubnikov organized and headed the laboratory of combine No. 13 of the Ministry of Electrotechnical Industry, out of which during the war there grew a special factory which has now been transformed into a research institute. He was similarly connected with other research and industrial organizations.

In 1941, at the beginning of the Second World War, the Crystallographic Laboratory was evacuated to the Sverdlovsk region, where it very soon was switched to important war work on supplying the communications service of the army and heavy industry with piezoelectric devices. While engaged in this work Shubnikov completed a book on piezoelectric textures for which he was awarded a Stalin Prize in 1947.

In 1947 the Laboratory returned to Moscow. In the following year, at the suggestion of the Presidium of the Academy of Sciences, the Council of Ministers of the USSR transformed it into the Crystallographic Institute of the Academy of Sciences of the USSR. Shubnikov's closest collaborators at this time, in addition to those previously mentioned, were N. V. Belov, L. M. Beliaev, Z. G. Pinsker, N. E. Vedeneeva, M. V. Klassen-Nekliudova, N. N. Sheftal', A. S. Shein and others.

Twelve years after the organization of the Institute it has become on of the great research institutions of the country. At the same time its material and technological equipment has been expanding. At the present time new buildings are being erected. Some of these are already being used, such as the machine shops, high pressure and high temperature laboratories and an independent department of low-temperature crystallography. Shubnikov's attention to the practical work of the Institute did not prevent him from continuing important theoretical studies. In 1947 there appeared his book "The Formation of Crystals," which is a thorough revision of his classic work "How Crystals Grow." A large number of Shubnikov's original ideas on crystal optics appeared in 1950 in his "Optical Crystallography," with very unusual illustrations executed by the author himself. In 1951 he published his book "The Symmetry and Antisymmetry of Finite Figures" in which he attempted to make practical use of four-dimensional crystallography. His new ideas unexpectedly found an application in the structural analysis of crystals, as was shown simultaneously by B. K. Vainshtein, a member of the Crystallographic Institute and the Englishman W. Cochran. From the study of antisymmetry the 230 Fedorov space symmetry groups can be replaced by 1651 infinite Shubnikov symmetry and antisymmetry groups which include the 230 groups as a special case.

At almost the same time that the Crystallographic Institute was established Shubnikov was instrumental in establishing the specialty of solid-state physics at Gor'kii University, where he went to give brief courses for two years, after which this work was turned over to his assistants.

In 1955 there appeared a new book, "A Study of Piezoelectric Textures," which Shubnikov wrote in collaboration with I. S. Zheludev, V. P. Konstantinova and I. M. Sil'vestrova.

Shubnikov's great creative activity, which is reflected in 250 published works, received official recognition in 1953 when he was elected an Academician in the Division of Physical and Mathematical Sciences of the Academy of Sciences USSR.

In the same year, 1953, Shubnikov headed the department of crystal physics in the physics faculty of Moscow University. He was attracted by the possibility of expounding the subject matter of crystallography and crystal physics to mathematics and physics students, using the language of the exact mathematical sciences and the tensor notation. In his skillful and creative mastery and development of the tensor method Shubnikov has been a successor of the most eminent crystallographers and crystal physicists of recent times – Curie, Fedorov, Voigt and Wulff. At the present time a creative group has assembled around Shubnikov, consisting of G. G. Lemmlein, V. R. Regel' and Shubnikov's young students V. A. Koptsik and I. S. Zheludev.

The great results of the activity of the Institute during the last ten years were summed up by Shubnikov himself in his address at the annual meeting of the Academy of Sciences on February 2, 1956, which was published in a profusely illustrated brochure during the same year. Shubnikov's merits were also recognized by a second Stalin Prize in 1950 as well as by the awarding of the Order of the Red Banner of Labor in 1945 and the Order of Lenin in 1953.

Aleksei Vasil'evich Shubnikov is now doing much work towards the development and strengthening of scientific relations between Soviet crystallographers and foreign scientists. In 1945 he was elected an honorary member of the English Mineralogical Society and in 1947 became an honorary member of the French Mineralogical Society. In 1946 he participated in the work of the committee for the organization of the International Crystallographic Union and of its official organ "Acta Crystallographica." The name of this journal was suggested by him.

At the present time Shubnikov is full of productive energy directed toward the solutions of great theoretical and practical problems which have been entrusted to the Crystallographic Institute of our nation. We wish Aleksei Vasil'evich Shubnikov many years of life, health and further success for the benefit of Soviet science.

SYMMETRY AND VARIOUS KINDS OF ANTISYMMETRY OF FINITE BODIES

A. M. Zamorzaev, E. I. Sokolov

Shubnikov antisymmetry can be generalized to a different kind of antisymmetry by assigning not one, but two, three, or more signs with different meanings to the points of a body. The general theory is developed, and a classification is given for symmetry groups and different kinds of antisymmetry groups, after which we calculate the number of finite crystallographic groups of these types. This calculation is nontrivial for the case of two and three signs, but becomes trivial for finite bodies if four or more signs are used.

1. The concept of antisymmetry introduced by A. V. Shubnikov consists of the following: a) to each point of a body undergoing transformation we assign a positive or negative sign; b) symmetry transformations are called those isometric* transformations which do not change a sign, and antisymmetry transformations are those which change a sign [1, 2]. The groups of symmetry and antisymmetry transformations are naturally divided into three types: a) those not containing antisymmetry transformations ("generating" groups), b) those containing anti-identity transformations ("major" groups), and c) those containing antisymmetry transformations without any anti-identity ("minor" [4]).

Symmetry and antisymmetry groups of finite bodies were investigated by Shubnikov himself; in generalizing 32 crystallographic symmetry ("generating") groups, he found 32 "major" and 58 "minor" groups [1-3]. The derivation of the "minor" groups with the separation of the dissimilar ones among them was the nontrivial part of the problem he solved, which was later extended to infinite space groups [4, 5].

Let us assign two signs to each point of the body undergoing transformation; these will be either ++, or +−, or −+, or −− [2]. Let us call symmetry transformations those isometric transformations which change none of the signs, and antisymmetry transformations of kind I, II or III (mixed) those isometric transformations which change only the first, only the second, or both signs, respectively. Antisymmetry of the third (mixed) kind can also be called antisymmetry of kind (1, 2).

The present work is devoted to a study of this generalization of Shubnikov groups for finite bodies.

2. It is easily seen that the method for deriving symmetry or any type of antisymmetry groups represents nothing new, and is based on theorems 1 and 2 given by Zamorzaev [4]. For the derivation of groups of essentially new structure, we indicate some new theorems.

Theorem 1. Every group of symmetry and antisymmetry transformations of more than one kind contain antisymmetry transformations of all three kinds, and contains three subgroups of index 2, each of which consist of the set of all symmetry transformations and the antisymmetry transformations of one kind.

Corollary. Every group of symmetry and antisymmetry transformations of more than one kind contains a subgroup of index 4 consisting of the set of all its symmetry transformations, and this subgroup is the intersection of three different subgroups of index 2 in the given group.

---

* Isometric transformations are those which do not change distances between points.

Theorem 2. Any group of symmetry and antisymmetry transformations can be obtained from a group of symmetry transformations in one of the following ways:

a) by extending it with an anti-identity of any kind as a generating element;

b) by extending it by two anti-identity elements of different kinds as generating elements;

c) by replacing all the elements of a coset of a subgroup of index 2 by the corresponding antisymmetry transformations of one kind;

d) by extending the group obtained by c) by a generating element which is the anti-identity of a kind not already contained in the group;

e) by replacing all the elements in each of the three cosets of one of its subgroups of index 4 (which is the intersection of three different subgroups of index 2) by the corresponding antisymmetry transformations of any kind (using different kinds for different cosets).

It is important to prove here that any group of symmetry and antisymmetry transformations of more than one kind is obtained from some symmetry group by one of the methods b, d, or e, corresponding to extending the given group by more than one anti-identity, a single anti-identity, or no anti-identity.

Let us classify the groups of symmetry and various kinds of anti-symmetry transformations.

We shall call a family any set of symmetry and antisymmetry transformation groups which can be obtained from a single symmetry transformation group by one of the methods given in the theorem. We shall call the symmetry group the generating group.

The remaining groups of the family, depending on the method by which they are derived, are of the following type:

a) those containing antisymmetry transformations of one kind, with an anti-identity, or major groups of kind of I, II, or III;

b) that containing the anti-identity of two (and therefore three) kinds, or the major group of all three kinds;

c) those containing antisymmetry transformations of only one kind without the anti-identity, or minor groups of kind I, II, or III;

d) those containing antisymmetry transformations of all three kinds with only one kind of anti-identity, or a major group of this kind (I, II, or III) and a minor group of some other kind;

e) those containing antisymmetry transformations of all three kinds without anti-identities, or minor groups of all three kinds.

Our problem is to calculate the number of all finite crystallographic groups of the above types. As is known, there are 32 generating groups; it is clear that there are 32 groups of each kind corresponding to type a), as well as 32 of type b). It is easily seen (see Section 1) that there are 58 groups of each kind of type c), and it is clear that there are also 58 groups for each case of type d).

The nontrivial problem is the derivation of all minor groups of more than one kind, that is of groups of type d). This derivation is most easily performed by replacing various elements of each of the 32 generating groups by the corresponding antisymmetry transformations of different kinds. In addition, one must count the number of repetitions in each family of groups obtained, and count the number of different groups.

3. Let us introduce the following notation for the symmetry and antisymmetry elements of various kinds (for finite bodies):

n is an axis of revolution of n-th order.
$\underline{n}$ is an anti-axis of rotation of kind I of n-th order.
n' is an anti-axis of rotation of kind II of n-th order.
$\underline{n}'$ is an anti-axis of rotation of kind III of n-th order.
$\bar{n}$ is a reflection-rotation axis of n-th order;

$\overline{\underline{n}}$, $\overline{n}'$, $\overline{\underline{n}}'$ are reflection-rotation anti-axes of kind I, II, and III of n-th order.
m is a symmetry plane.
$\underline{m}$, m', $\underline{m}'$ are antisymmetry planes of kind I, II, and III.

The symbols for the symmetry and antisymmetry elements are used to denote the groups corresponding to them [1].

We shall use a centered dot · to indicate that the elements of symmetry and antisymmetry are parallel, and a colon : to indicate that they are perpendicular [1].

We here present the most important theorems on the relation between the symmetry elements and various types of antisymmetry elements.

Theorem A. Two double axes (anti-axes of the same kind) intersecting at an angle of π/n are equivalent to an n-th order axis perpendicular to them and either one of the original axes;

a double axis and an anti-axis of any kind intersecting at any angle of π/n are equivalent to an n-th order anti-axis (of the same kind) perpendicular to them and either one of the original axes;

two double anti-axes of different kinds intersecting at an angle of π/n are equivalent to an n-th order anti-axis (of the other kind) perpendicular to them and either one of the original axes.

Theorem B. Two planes (anti-planes of the same kind) intersecting at an angle of π/n are equivalent to an n-th order axis along their intersection line and either one of the original planes; a plane and an anti-plane of any kind intersecting at an angle of π/n are equivalent to an anti-axis (of the same kind) of n-th order along their intersection line and either one of the original planes;

two anti-planes of different kinds intersecting at an angle of π/n are equivalent to an anti-axis (of the third kind) of n-th order along their intersection line and either one of the original planes.

These theorems can be used to identify the equivalent minor groups of more than one kind in each family.

We here give all such different groups.

1) $\underline{2}:2'(=\underline{2}:\underline{2}'=\underline{2}':\underline{2}=\underline{2}':2'=2':\underline{2}'=2':\underline{2})$; 2) $\underline{4}:2'(=4:\underline{2}')$
3) $\overline{4'}:\underline{2}(=\overline{4'}:\overline{2'})$, 4) $\overline{4'}:\underline{2}(=\overline{4}':2')$; 5) $\overline{6}:2'(=\overline{6}:\underline{2}')$, 6) $\overline{6'}:\underline{2}(=\overline{6'}:\overline{\underline{2}}')$,
7) $\underline{6}':\overline{\underline{2}}(=\underline{6}':\overline{2}')$; 8) $\overline{2}\cdot\overline{m'}(=\overline{\underline{2}}\cdot\underline{m}')$, 9) $\overline{2'}\cdot\underline{m}(=\overline{2'}\cdot\overline{m'})$, 10) $\underline{2}'\cdot\overline{\underline{m}}(=\underline{2}'\cdot\overline{m}')$;
11) $\overline{4}\cdot\overline{m}'(=\overline{4}\cdot\underline{m}')$, 12) $\overline{4}'\cdot\underline{m}(=\overline{4'}\cdot\underline{m}')$, 13) $\overline{\underline{4'}}\cdot\underline{m}(=\overline{\underline{4'}}\cdot m')$; 14) $\overline{\underline{6}}\cdot\overline{m}'(=\overline{6}\cdot\underline{m}')$,
15) $\overline{6}'\cdot\underline{m}(=\overline{6}'\cdot\overline{m'})$, 16) $\overline{6'}\cdot\underline{m}(=\overline{\underline{6'}}\cdot m')$; 17) $\overline{2}:\overline{m'}$, 18) $2':\overline{\underline{m}}$, 19) $\overline{2}:\overline{\underline{m}}'$,
20) $2':\overline{\underline{m}}'$, 21) $\overline{\underline{2'}}:\underline{m}$, 22) $\overline{2}':\overline{m}'$, 23) $\underline{4}:m'$, 24) $\overline{4'}:\underline{m}$, 25) $4:\overline{\underline{m}}'$, 26) $\overline{4'}:\overline{\underline{m}}'$,
7) $4':\overline{\underline{m}}$, 28) $\overline{\underline{4}}':\overline{m}'$; 29) $\overline{\underline{6}}:m'$, 30) $\overline{6}':\underline{m}$, 31) $\underline{6}:\overline{\underline{m}}'$, 32) $\overline{6}':\overline{\underline{m}}'$, 33) $\underline{6}':\overline{\underline{m}}$,

34) $\underline{6}':m'$; 35) $\overline{\underline{4}}\cdot m'$, 36) $\overline{\underline{4}}'\cdot\underline{m}$, 37) $\overline{4}\cdot\underline{m}'$, 38) $\overline{4}'\cdot\underline{m}'$, 39) $\overline{\underline{4}}'\cdot\underline{m}$, 40) $\overline{\underline{4}}\cdot m'$; 41) $\overline{\underline{6}}\cdot m'$,
42) $\overline{6}'\cdot\underline{m}$, 43) $\overline{\underline{6}}\cdot\underline{m}'$, 44) $\overline{6}'\cdot\underline{m}'$, 45) $\overline{\underline{6}}'\cdot\underline{m}$, 46) $\overline{6'}\cdot m'$; 47) $m\cdot\underline{2}:$
$:m'(=\overline{\underline{m}}\cdot\underline{2}:m'=\overline{m'}\cdot 2':\underline{m}=m\cdot\overline{2'}:\underline{m}=\overline{\underline{m}}\cdot\overline{2}':m=m'\cdot\overline{\underline{2'}}:m)$, 48) $m\cdot\underline{2}:\overline{m'}\cdot$
$\cdot(=\underline{m}\cdot\overline{\underline{2}}:\overline{\underline{m}}'=\underline{m}'\cdot\underline{2}':\underline{m}=m\cdot\underline{2}':\underline{m}=\underline{m}\cdot\overline{2'}:\overline{m}=\underline{m}'\cdot 2':\overline{m})$, 49) $m\cdot\overline{2'}:\overline{\underline{m}}'\cdot$
$\cdot(=m'\cdot 2':\underline{m}'=\underline{m}'\cdot\underline{2}':m'=m\cdot\underline{2}':m'=m'\cdot\underline{2}:m=\underline{m}'\cdot\underline{2}\cdot m)$, 50) $\underline{m}\cdot 2':m'\cdot$
$\cdot(=\underline{m}'\cdot 2':m'=m'\cdot\underline{2}':\underline{m}'=\underline{m}\cdot\underline{2}':\underline{m}'=\underline{m}'\cdot\underline{2}:m=m'\cdot\underline{2}:\underline{m})$, 51) $\underline{m}\cdot 2:m'\cdot$
$\cdot(=m'\cdot\underline{2}':\underline{m}=m\cdot\underline{2}':\underline{m})$, 52) $m'\cdot 2:\underline{m}(=\underline{m}\cdot\underline{2}':m'=m'\cdot\underline{2}':m')$, 53) $\underline{m}\cdot 2:\underline{m}'(=$
$=\underline{m}'\cdot 2':\underline{m}=\underline{m}\cdot 2':\underline{m})$, 54) $m'\cdot 2:\underline{m}'(=\underline{m}'\cdot\underline{2}:m'=m'\cdot\underline{2}:m')$, 55) $\underline{m}'\cdot 2:\underline{m}(=$
$=\underline{m}\cdot 2':\underline{m}'=\underline{m}'\cdot 2':\underline{m}')$, 56) $\underline{m}'\cdot 2:m'(=m'\cdot\underline{2}:\underline{m}'=\underline{m}'\cdot\underline{2}:\underline{m}')$, 57) $\underline{m}\cdot 3:m'$,
58) $m'\cdot 3:\underline{m}$, 59) $\underline{m}\cdot 3:\underline{m}'$, 60) $m'\cdot 3:\underline{m}'$, 61) $\underline{m}'\cdot 3:\underline{m}$, 62) $\underline{m}'\cdot 3:m'$;

63) $\underline{m}\cdot 4 : m'$, 64) $m'\cdot 4 : \underline{m}$, 65) $\underline{m}\cdot 4 : \underline{m'}$, 66) $m'\cdot 4 : \underline{m'}$, 67) $\underline{m'}\cdot 4 : \underline{m}$, 68) $\underline{m'}\cdot 4 : m'$, 69) $m\cdot\underline{4} : m' (= \underline{m}\cdot\underline{4} : m')$, 70) $m\cdot 4'\cdot\underline{m} (= m'\cdot 4' : \underline{m})$, 71) $m\cdot\underline{4} : \underline{m'} (= \underline{m}\cdot\underline{4} : \underline{m'})$, 72) $m\cdot 4' : \underline{m'} (= m'\cdot 4' : \underline{m'})$, 73) $m\cdot\underline{4'} : \underline{m} (= \underline{m'}\cdot\underline{4'} : \underline{m})$, 74) $m\cdot\underline{4'} : m' (= \underline{m'}\cdot\underline{4'} : m')$, 75) $m'\cdot\underline{4} : m (= \underline{m'}\cdot\underline{4} : m)$, 76) $\underline{m}\cdot 4' : m (= \underline{m'}\cdot 4' : m)$, 77) $\underline{m}\cdot\underline{4'} : m (= m'\cdot\underline{4'} : m)$, 78) $m'\cdot\underline{4} : \underline{m} (= \underline{m'}\cdot\underline{4} : \underline{m})$, 79) $\underline{m}\cdot 4' : m'\cdot (= \underline{m'}\cdot 4' : m')$, 80) $\underline{m}\cdot\underline{4'} : \underline{m'} (= m'\cdot\underline{4'} : \underline{m'})$, 81) $m'\cdot\underline{4} : m' (= \underline{m'}\cdot\underline{4} : m')$, 82) $\underline{m}\cdot 4' : \underline{m} (= \underline{m'}\cdot 4' : \underline{m})$, 83) $\underline{m'}\cdot\underline{4} : \underline{m'} (= m'\cdot\underline{4} : \underline{m'})$, 84) $\underline{m'}\cdot 4' : \underline{m'} (= \underline{m}\cdot 4' : \underline{m'})$, 85) $\underline{m}\cdot\underline{4'} : \underline{m} (= m'\cdot\underline{4'} : \underline{m})$, 86) $m'\cdot\underline{4'} : \underline{m} (= \underline{m}\cdot\underline{4'} : m')$; 87) $\underline{m}\cdot 6 : m'$, 88) $m'\cdot 6 : \underline{m}$, 89) $\underline{m}\cdot 6 : \underline{m'}$, (90) $m'\cdot 6 : \underline{m'}$, 91) $\underline{m'}\cdot 6 : \underline{m}$, 92) $\underline{m'}\cdot 6 : m'$, 93) $\underline{m}\cdot\underline{6} : m' (= \underline{m}\cdot\underline{6} : m')$, 94) $m\cdot 6' : \underline{m} (= m'\cdot 6' : \underline{m})$, 95) $m\cdot\underline{6} : \underline{m'} (= \underline{m}\cdot\underline{6} : \underline{m'})$, 96) $m\cdot 6' : \underline{m} (= m'\cdot 6' : \underline{m'})$, 97) $m\cdot\underline{6'} : \underline{m} (= \underline{m'}\cdot\underline{6'} : \underline{m})$, 98) $m\cdot\underline{6'} : m' (= \underline{m'}\cdot\underline{6'} : m')$, 99) $m'\cdot\underline{6} : m (= \underline{m'}\cdot\underline{6} : m)$, 100) $\underline{m}\cdot 6' : m (= \underline{m'}\cdot 6' : m)$, 101) $\underline{m}\cdot\underline{6'} : m (= m'\cdot 6' : m)$, 102) $m'\cdot\underline{6} : \underline{m} (= \underline{m'}\cdot\underline{6} : \underline{m})$, 103) $\underline{m}\cdot 6' : m' (= \underline{m'}\cdot 6' : m')$, 104) $\underline{m}\cdot\underline{6'} : \underline{m'} (= m'\cdot\underline{6'} : \underline{m'})$, 105) $m'\cdot\underline{6} : m' (= \underline{m'}\cdot\underline{6} : m')$, 106) $\underline{m}\cdot 6' : \underline{m} (= \underline{m'}\cdot\underline{6} : \underline{m})$: 107) $\underline{m'}\cdot\underline{6} : \underline{m'} (= m'\cdot\underline{6} : \underline{m'})$, 108) $\underline{m'}\cdot 6' : \underline{m'} (= \underline{m}\cdot 6' : \underline{m'})$, 109) $\underline{m}\cdot\underline{6'} : \underline{m} = (\underline{m'}\cdot\underline{6'} : \underline{m})$, 110) $m'\cdot\underline{6'} : m' (= \underline{m}\cdot 6' : m')$; 111) $\underline{\overline{6}}/4'$, 112) $\underline{\overline{6}'}/\underline{4}$, 113) $\underline{\overline{6}}/\underline{4'}$, 114) $\overline{6}'/\underline{4'}$, 115) $\underline{\overline{6}'}/\underline{4'}$, 116) $\underline{\overline{6}'}/\underline{4}$.

The symbol / is used to designate obliquely oriented axes [1].

4. It is natural to extend the concept of antisymmetry further by assigning l + or − signs to each point in l different ways (where l is an arbitrary integer); we then use the following terminology:

a symmetry transformation is an isometric transformation which changes none of the signs;

an antisymmetry transformation of the j-th kind is an isometric transformation which changes only the j-th sign (with j = 1, 2, . . . , l);

an antisymmetry transformation of the (j, k)-th kind is an isometric transformation which changes only the j-th and k-th signs ($1 \leq j \leq k \leq l$); an antisymmetry transformation of the (1, 2 . . l)-th kind is an isometric transformation changing all l signs;

there exist $2^l - 1$ different types of antisymmetries.

The case $l = 1$ has been investigated both for finite and infinite groups [1-5].

The case $l = 2$ has been investigated for finite groups in the thesis of E. I. Sokolov in 1954 at the Kishinev State University; the results of these investigations have been presented above in the present article. At the present time investigations are being performed at the Kishinev State University for this case with infinite space groups (generalized Shubnikov groups); in particular, the 1956 graduates Sh. Tolpalar' and K. Slonovskii have developed the general theory in detail and have investigated the parallel and antiparallel displacement subgroups of various types in the generalized Shubnikov groups (37 essentially new subgroups were found).

Let us consider the case $l = 3$ in more detail; this has been investigated for finite groups by the 1955 graduates of the Kishinev State University E. Dubianskaia and V. Naftalin.

In this case there exist seven different kinds of antisymmetries. If in a set of three anti-identities any one is the product of the other two (in which case each one is a product of the other two), we shall call these anti-identities dependent; if three anti-identities are not so related, we shall call them independent. Similarly, three different kinds of antisymmetries can be called dependent or independent.

The general theory is developed in a similar way, making it possible to classify new groups according to the method by which they are derived from some symmetry group (called the generating group, of which there are 32). All other groups are of the following types: a) major groups of one kind (of which there are 32 of each kind); b) major groups of two (three dependent) kinds (of which there are 32 of each case); c) major groups of three independent (all seven) kinds (of which there are 32); d) minor groups of one kind (of which there are 58 of each kind); e) minor groups of one kind (actually two) and major of another kind (of which there are 58 of each case); f) minor of one kind (actually of four) and major of two (three dependent) kinds (of which there are 58 for each case); g) minor of two (three dependent) kinds (of which there are 116 for each case); h) minor of two (actually of six) kinds and major of one kind independent of these two (of which there are 116 for each case); and i) minor of three independent (all seven) kinds. The derivation of the groups of this last type is the nontrivial part of the further investigation.

Let us extend the notation for the symmetry elements and various types of antisymmetry elements.

$\underline{n}$, n', ${}^{*}n$ represent anti-axes of rotation of kind I, II, and III, respectively, of n-th order;

$\underline{n}'$, ${}^{*}\underline{n}$, ${}^{*}n'$, ${}^{*}\underline{n}'$ represent anti-axes of rotation of kind (1, 2), (1, 3), (2, 3) and (1, 2, 3) of n-th order;

similar notation is used for reflection-rotation anti-axes and reflection antiplanes.

V. Naftalin has given a list of all groups of type i), using the results of E. Umanov (a 1954 graduate of the Kishinev State University) who reformulated A. V. Shubnikov's results in matrix form [1]. We give a brief summary of this listing below.

All such groups are in three families generated by the groups whose forms $m \cdot n : m$ with n = 2, 4, and 6. For n = 4 and n = 6 all the different groups are:

$$\text{a) } m'\cdot\underline{n}:{}^{*}m,\ \text{b) } m'\cdot\underline{n}:{}^{*}\underline{m},\ \text{c) } m'\cdot\underline{n}:{}^{*}m',\ \text{d) } m'\cdot\underline{n}:{}^{*}\underline{m}',\ \text{e) } \underline{m}'\cdot\underline{n}:{}^{*}m',$$
$$\text{f) } {}^{*}\underline{m}'\cdot\underline{n}:\underline{m}',\ \text{g) } \underline{m}\cdot\underline{n}':{}^{*}\underline{m},\ \text{h) } \underline{m}\cdot\underline{n}':{}^{*}m,\ \text{i) } \underline{m}\cdot\underline{n}':{}^{*}\underline{m}',\ \text{j) } {}^{*}m\cdot\underline{n}':\underline{m},$$
$$\text{k) } {}^{*}m\cdot\underline{n}':{}^{*}\underline{m},\ \text{l) } {}^{*}\underline{m}\cdot\underline{n}':\ \underline{m},\ \text{m) } {}^{*}\underline{m}\cdot\underline{n}':{}^{*}m,\ \text{n) } {}^{*}\underline{m}\cdot\underline{n}':{}^{*}\underline{m}',\ \text{o) } \underline{m}\cdot{}^{*}n':{}^{*}m,$$

p) $\underline{m}\cdot{}^{*}\underline{n}' : \underline{m}'$, as well as all groups obtained from groups a)-g), j)-l), o) and p) by all permutations of the symbols —, ', and *, and from groups h), i), m), and n) by all cyclic permutations of these symbols; there are 84 such groups; for n = 2 the groups we obtain are a)-d), f), h), and i), as well as all groups obtainable from a), b), and d) by all permutations of the above symbols and from groups c), f), and i) by all cyclic permutations; there are 28 such groups.

The total number of different groups is $28 + 2 \cdot 84 = 196$.

For $l > 3$, no nontrivial problems exist for finite bodies, since none of the 32 finite crystallographic symmetry groups has a subgroup of index 2^{l} which is an intersection of $2^{l}-1$ subgroups of index 2^{l-1}. In the case of infinite space groups new nontrivial calculations will occur up to $l = 6$, but no further.

LITERATURE CITED

[1] A. V. Shubnikov, Symmetry and Antisymmetry of Finite Bodies [In Russian] (1951).

[2] A. V. Shubnikov, "Recent developments in the science of symmetry and its applications," General Meeting of the AN SSSR, October 14-17, 1944 (M.-L., 1955).

[3] A. V. Shubnikov, "Erratum to Symmetry and Antisymmetry of Finite Bodies (1951)," Tr. Inst. Krist. Akad. Nauk 9, 383, 1954.

[4] A. M. Zamorzaev, "Generalization of Fedorov Groups," Crystallography 2, 1, 15-20 (1957).*

[5] N. V. Belov, N. N. Neronova and T. S. Smirnova, "1651 Shubnikov Groups," Tr. Inst. Krist. Akad. Nauk 11, 33-67 (1955).

Kishinev State University

Received November 4, 1956

---

* [Present issue, translation page 10].

GENERALIZATION OF FEDOROV GROUPS

A. M. Zamorzaev

We give a method, its theoretical basis, and a summary of results for deriving space symmetry and antisymmetry groups (black-white, or Shubnikov groups); the work was performed by the author in 1953 in his candidate's dissertation. Group theory is used to develop the general theory of Shubnikov groups, using a practical method of deriving them from Fedorov groups which has been previously applied by A. V. Shubnikov to the study of the symmetry and antisymmetry of finite bodies. The author has been delayed somewhat in the publication of the list of Shubnikov groups, which has since been published by N. V. Belov [8] who obtained them by a different method in 1954.

1. We shall define a Fedorov group as a group of spatial symmetry transformations (which we shall call homologous) with the following properties: 1) there exists a sphere of sufficiently large radius R such that no matter where it is located in space there lie within it homologous images of any arbitrary previously given point of space (homogeneity) and 2) there is at least one point in the space which has no homologous images arbitrarily close to it (discreteness).

The most important result of Fedorov groups is the periodicity of the space under parallel displacements, which follows from the fundamental theorem [3]. Of no less importance is the association both of the group of "rotations" [3] among the transformations of a given Fedorov group and of the translation subgroup of this latter group (for the corresponding Bravais lattice symmetry) with one of the seven syngonies. The combination of the syngonies of fourteen lattice types with the 32 "rotation" groups leads first to the symmorphic and then to the hemisymmorphic and asymmorphic Fedorov groups.

Let us now assign positive (+) or negative (−) signs to the points of space and define a Shubnikov group as a group of symmetry and antisymmetry transformations, which we shall call homologous and antihomologous, respectively, which fulfills the following requirements: property 1) (homogeneity) is now fulfilled by both homologous and antihomologous images of a point, and property 2) (discreteness) is maintained in its previous form.

2. We indicate the most important theorems in the development of the general theory of Shubnikov groups.

Theorem 1. Any group of symmetry and antisymmetry transformations* has a subgroup of index 2 consisting of symmetry transformations.

Theorem 2. Any group of symmetry and antisymmetry transformations* can be obtained from some group of symmetry transformations either by extending it with all antisymmetry transformations corresponding to its elements, or by replacing all the elements of the coset of one of its subgroups of index 2 by the appropriate antixymmetry transformations.

---

* We are speaking of a group having at least one antisymmetry transformation.

Theorem 3. A group of symmetry and antisymmetry transformations which contains no anti-identity transformation is isomorphic to that group of symmetry transformations from which it is obtained by the second of the above methods.

The set of groups obtainable by the two above methods from a given group of symmetry transformations shall be called the family generated by this group; the groups derived from it by the first or second method will be called major or minor groups of the family, respectively. It is easily seen that different families have no common groups.

Theorem 4. In every family, a major group is the direct product of the generating group and the group consisting of the identity and anti-identity transformations.

Theorem 5. Every Shubnikov group which is not a Fedorov group has a subgroup of index 2 which is a Fedorov group.

Theorem 6 (fundamental). Every Shubnikov group is either a Fedorov group or can be obtained from a Fedorov group either by extending it with all the antihomology transformations corresponding to its elements, or by replacing all the elements of the coset of one of its subgroups of index 2 by the appropriate antihomology transformations.

These theorems do not follow simply from Theorems 1 and 2, since requirements 1) and 2) entering into the definition of a Fedorov group must yet be verified.

Corollary. Every Shubnikov group contains a parallelopiped subgroup of parallel translations and antitranslations which is either a translation subgroup of the generating Fedorov group or can be obtained from it by one of the methods given in Theorem 2.

Theorem 7 (converse). Every group of symmetry and antisymmetry transformations obtainable from a Fedorov group by one of the methods given in Theorem 6 is a Shubnikov group.

It is seen from the above theorems that the family generated by every Fedorov group consists entirely of Shubnikov groups and that Shubnikov groups are naturally separated into three fundamental types:

1) the Shubnikov groups which transform "polar" (single color) spaces and consist only of symmetry transformations (generating groups); these are the already known 230 Fedorov groups (among which 219 are not isomorphic).

2) Shubnikov groups transforming "neutral" (grey) spaces and containing anti-identity transformations (major); each of these is the direct product of one and only one Fedorov group (which is then a subgroup of index 2) by a group of order two generated by an anti-identity transformation; none of these groups are isomorphic to any Fedorov group; there are also 230 of these (among which 219 are not isomorphic).

3) Shubnikov groups which transform spaces of "mixed polarity" (black-white), containing antisymmetry transformations without the anti-identity (minor groups); every such group can be isomorphically mapped onto one and only one Fedorov group, and their common subgroup of index 2 maps onto itself identically, whereas the elements of the coset of this subgroup which map onto each other differ only in an anti-identity transformation.

Every group of type 3) is isomorphic to some group of type 1), so that the number of all Shubnikov subgroups which are not isomorphic to each other is 438.

Let us call Shubnikov groups equal or the same if they are not only isomorphic, but have Fedorov subgroups which map onto each other under isomorphisms of the Shubnikov groups being compared. It is easy to see that only Shubnikov groups of a given family can be equal to each other.

The only nontrivial derivation is that of the minor (that is black-white) Shubnikov groups, and for this derivation the following is sufficient:

1) To derive all possible minor Shubnikov groups by the method given in Theorem 6; this problem can be carried out in practice by replacing some of the symmetry transformations in a finite set of generating elements of each Fedorov group by the corresponding antisymmetry transformations.*

---

* This is essentially the Shubnikov method [1].

2) To find all the equal groups among the Shubnikov groups obtained in this way from each Fedorov group, and to eliminate those which are repetitions.

3) To prove the inequality of all the remaining groups.

In order to simplify this nontrivial problem, we shall break it up into the following steps: a) we shall derive from each "rotation" group all the minor groups, find the equal ones in each family, and eliminate repetitions.

b) We shall do the same with each translation subgroup.

c) We shall derive minor Shubnikov subgroups by families, combining generating translation groups with "minor rotation" and "antirotation" groups, and minor translation and antitranslation groups either with generating "rotation" groups or with minor "rotation" and "antirotation" groups, as this is done with generating translation and "rotation" groups in deriving the generating Fedorov groups [3]; in the process we shall find the equal Shubnikov groups and eliminate repetitions among those found in each family, which will conclude the problem.

3. Step a) has in fact been solved by A. V. Shubnikov. From the 32 generating "rotation" groups 58 minor "rotation" and "antirotation" groups have been obtained [1, 5].

Step b) has been performed in general and published [8], and the present author's results are in complete agreement with those; the author is motivated by differences in the method and notation to publish his results for this step using his own method (which is basically the same as the above-mentioned method of A. V. Shubnikov).

If we consider the family generated by a Fedorov group and the family generated by the translation subgroup of this Fedorov group, we find that not every minor group of the second of these families is a translation and antitranslation subgroup of at least one of the minor groups of the first family. Thus when we speak of eliminating repetitions in step b), we are considering not only those which are repetitions of groups which have been already obtained, but eliminating also those groups which do not play the role of a subgroup in the Shubnikov groups. We shall call this in general elimination of superfluous groups, and must give a practical criterion for performing the elimination in this sense.

According to the general theory, that Shubnikov group, for which the group of parallel translations and antitranslations is a minor group in its family, has a "rotation" group in common with the generating Fedorov group and therefore with their common Fedorov subgroup of index 2 (in this case the group of "rotations" and "antirotations" of the given Shubnikov group is a major group). Therefore the generating Fedorov group and its subgroup of index 2 being considered are related to the same syngony, and their parallel translation subgroups should correspond to the Bravais parallelopiped related to one syngony. Thus in order that a given minor group of a family generated by one of the parallelopiped translation subgroups be one of the ones we are looking for, it is necessary and sufficient that its translation subgroup and generating translation group be related to one syngony.

Let us denote as elementary the parallel translation (or antitranslation) through the smallest possible distance in a given direction, and the vectors corresponding to these elementary translations by a, b, c, ... (or $\underline{a}$, $\underline{b}$, $\underline{c}$, ...).

To the subgroup of parallel translations and antitranslations of a minor Shubnikov group there corresponds an additive group generated by the triad of elementary vectors a (or $\underline{a}$), b (or $\underline{b}$), and c (or $\underline{c}$), which we shall denote [9] by $\{a, b, c,\}$ (or $\{\underline{a}, b, c\}$, $\{a, \underline{b}, c\}$, $\{a, b, \underline{c}\}$, $\{\underline{a}, \underline{b}, c\}$, $\{\underline{a}, b, \underline{c}\}$, $\{a, \underline{b}, \underline{c}\}$, or $\{\underline{a}, \underline{b}, \underline{c}\}$).

Here we have enumerated all the minor groups of the family generated by the group $\{a, b, c\}$; the corresponding translation subgroups in these minor groups are of the form $\{2a, b, c\}$, $\{a, 2b, c\}$, $\{a, b, 2c\}$, $\{2a, a+b, c\}$, $\{2a, b, a+c\}$, $\{a, 2b, b+c\}$ or $\{2a, a+b, a+c\}$.

If we agree to denote the elementary vectors along the edges of the Bravais parallelopiped by a_1, a_2, a_3, the translation groups corresponding to various forms of Bravais parallelopipeds are denoted by

1) $\{a_1, a_2; a_3\}$ (empty Bravais parallelopiped);
2) $\left\{a_1, a_2, \frac{a_1+a_2+a_3}{2}\right\}$ (centered Bravais parallelopiped);
3) $\left\{a_1, \frac{a_1+a_2}{2}, a_3\right\}$ (base-centered Bravais parallelopiped);
4) $\left\{a_1, \frac{a_1+a_2}{2}, \frac{a_1+a_3}{2}\right\}$ (face-centered Bravais parallelopiped);

5) $\{(a_1, a_2)\, a_3\}$(the role of the Bravais parallelopiped is played by a base-centered prism with six faces whose side length is a_3 and whose base has side lengths a_1, a_2 and $a_1 + a_2$).

The solution of the problem we have posed consists of sorting out all minor groups corresponding to the fourteen families (classified according to the syngonies), exhibiting the equal ones among them, and eliminating the superfluous ones according to the above-mentioned criterion.

Let us investigate this process, as an example, for a square syngony, for which the generating translation group is of the form

$$1)\ \{a', a'', a_3\};\quad 2)\ \left\{a', a'', \frac{a' + a'' + a_3}{2}\right\}^{*}.$$

Here the sides a' and a" play the same role, but a_3 plays a unique role.

In case 1) the unequal minor groups are $\{\underline{a}', a'', a_3\}$, $\{a', a'', \underline{a}_3\}$, $\{\underline{a}', \underline{a}'', a_3\}$, $\{\underline{a}', a'', \underline{a}_3\}$ and $\{a', \underline{a}'', \underline{a}_3\}$; considering their translation subgroups ($\{2a', a'', a_3\}$, $\{a', a'', 2a_3\}$, $\{2a', a' + a'', a_3\}$, $\{2a', a'', a' + a_3\}$ and $\{2a', a' + a'', a' + a_3\}$) and using the previously mentioned criterion, we see that the groups $\{a', a'', \underline{a}_3\}$ $\{\underline{a}', \underline{a}'', a_3\}$ and $\{\underline{a}', \underline{a}'', \underline{a}_3\}$ are suitable, whereas the rest are superfluous.

In case 2) the different minor groups are $\left\{a'\ a'', \frac{a', + a'' + a_3}{\underline{2}}\right\}$ $\left\{\underline{a}', a'', \frac{a' + a'' + a_3}{2}\right\}$ and $\left\{\underline{a}', \underline{a}'', \frac{a' + a'' + a_3}{2}\right\}$ and they have the translation subgroups $\{a', a'', a_3\}$, $\left\{2a', a'', \frac{a' + a'' + a_3}{2}\right\}$ and $\left\{2a', a' + a'', \frac{a' + a'' + a_3}{2}\right\}$, it is seen from this that only the group $\left\{a', a'', \frac{a' + a'' + a_3}{2}\right\}$ is suitable, and the rest are superfluous.

We now present a list of all possible parallel translation and antitranslation subgroups in minor Shubnikov groups (the parentheses give the corresponding lattices according to Belov, et al. [8]):

Triclinic syngony: $\{a_1, a_2, a_3\}(P)$, $\{a_1, a_2, a_3\}(P_s)$.

Monoclinic syngony: $\{a_1, a_2, a_3\}(P)$, $\{\underline{a}_1, a_2, a_3\}(P_a)$ $\{a_1, a_2, a_3\}(P_c)$, $\{\underline{a}_1, a_2, \underline{a}_3\}(C_a)$; $\left\{ \{a_1, a_2, \frac{a_1 + a_2}{2}\right\}(C)$, $\left\{a_1, a_2, \frac{a_1 + a_2}{\underline{2}}\right\}(P_C)$, $\left\{a_1, \underline{a}_2, \frac{a_1 + a_2}{2}\right\}$ (C_c).

Orthogonal syngony: $\{a_1, a_2, a_3\}(P)$, $\{\underline{a}_1, a_2, a_3\}(P_s)$, $\{\underline{a}_1, \underline{a}_2, a_3\}(C_a)$, $\{\underline{a}_1, \underline{a}_2, \underline{a}_3\}(F_s)$; $\left\{a_1, a_2, \frac{a_1 + a_2 + a_3}{2}\right\}(I)$, $\left\{a_1, a_2, \frac{a_1 + a_2 + a_3}{\underline{2}}\right\}(P_I)$; $\left\{a_1, \frac{a_1 + a_2}{2}\right.$ $\left.a_3\right\}(C)$, $\left\{a_1, \frac{a_1 + a_2}{\underline{2}}, a_3\right\}(P_c)$; $\left\{a_1, \frac{a_1 + a_2}{2}, \underline{a}_3\right\}(C_c)$, $\left\{a_1, \frac{a_1 +}{2}, \underline{a}_3\right\}(I_c)$; $\left\{a_1, \frac{a_1 + a_2}{2}, \frac{a_1 + a_2}{2}\right\}(F)$, $\left\{a_1, \frac{a_1 + a_2}{\underline{2}}, \frac{a_1 + a_2}{2}\right\}(C_A)$.

Rhombohedral syngony: $\{a', a'', a'''\}(R)$, $\{\underline{a}', \underline{a}'', \underline{a}'''\}(R_I)$.

Square syngony: $\{a', a'', a_3\}(P)$, $\{a', a'', \underline{a}_3\}(P_c)$, $\{\underline{a}', \underline{a}'', a_3\}(P_C)$, $\{\underline{a}', \underline{a}'', \underline{a}_3\}(I_c)$; $\left\{a', a'', \frac{a' + a'' + a_3}{2}\right\}(I)$, $\left\{a', a'', \frac{a' + a'' + a_3}{\underline{2}}\right\}(P_I)$.

Cubic syngony: $\{a', a'', a'''\}(P)$, $\{\underline{a}', \underline{a}'', \underline{a}'''\}(F_s)$; $\left\{a', a''. \frac{a' + a'' + a''}{2}\right\}(I)$, $\left\{a', a'', \frac{a' + a'' + a'''}{\underline{2}}\right\}(P_I)$, $\left\{a', \frac{a' + a''}{2}, \frac{a' + a'''}{2}\right\}(F)$.

Hexagonal syngony: $\{(a', a'')\, a_3\}(H)$, $\{(a', a'')\, a_3\}(H_c)$.

---

[*] Letters with upper primes, rather than lower indices, denote translation and antitranslation vectors of equal lengths.

Thus the 14 generating translation groups lead to 22 minor translation and antitranslation groups.

4. Let us now go on to deriving the Shubnikov groups themselves by the method given at the end of section 2.

A symmorphic group is the product of a group of parallel translations by a group of "rotations" about a single point, and every minor group of the family it generates is obtained from it either by replacing the "rotation" group by some minor group in the family it generates, by a similar replacement of the translation group, or by both simultaneously. In order to find the equal groups among the minor ones of a given family, one uses theorems on the relation between symmetry and antisymmetry elements (not listed here) which are equivalent to the theorems given by Belov et al. [8]. The difference between different minor groups of a given family is not obvious when they have the same subgroups of translations and antitranslations (and if antitranslations do not exist, then only when they have the same subgroups of "rotations" and "antirotations").

Let us list, for example, the minor groups of the family generated by $\left\{a', a'', a_3\right\}(4:2)$* (3Os by E. S. Fedorov, and P 42 by N. V. Belov); the brackets give Belov's notation for these groups:

$$\begin{array}{ll}
\{a',a'',a_3\}\ (4:\underline{2})\,(P42'), & \{a',a'',a_3\}\,(\underline{4}:2)\,(P4'2),\\
\{a',a'',a_3\}\,(\underline{4}:\underline{2})\,(P4'2'), & \{a',a'',\underline{a}_3\}\,(4:2)\,(P_C42),\\
\{a',a'',\underline{a}_3\}\ (\underline{4}:2)\,(P_c4_22), & \{\underline{a}',\underline{a},''a_3\}\,(4:2)\,(P_C42),\\
\{a',a'',a_3\}\,(4:\underline{2})\,(P_C42_1), & \{\underline{a}',\underline{a}'',\underline{a}_3\}\,(4:2)\,(I_C42).
\end{array}$$

Altogether there exist 73 generating, 73 major, and 386 minor generalized symmorphic groups.

A hemisymmorphic and asymmorphic group can be written as the product of its translation subgroup by the group generated by the transformations into which enter different "rotations." Then the group which is the second factor in this product also contains some translations, which must be borne in mind; therefore first one investigates all minor groups of families generated by these "second factors"; the rest of the method for generalizing hemisymmorphic and asymmorphic groups is the same as that for symmorphic groups.

Of generalized hemisymmorphic groups there are 54 generating, 54 major, and 297 minor groups, and of generalized asymmorphic groups there are 103 generating, 103 major, and 508 minor groups.

The total number of all different Shubnikov groups is 1651, of which 1191 are minor.

In his dissertation, the author [6, 7] has derived 1652 Shubnikov groups of which 509 are minor asymmorphic. Belov et al. [8], in their critical notes, give 15 groups supposedly omitted in the dissertation, and assert that 16 of the groups listed in the dissertation are the same as those previously derived. The last of these 16 groups is indeed superfluous, so that their correction with respect to the total number of Shubnikov groups is correct; the author disagrees, however, with the other corrections suggested by Belov and co-workers.

LITERATURE CITED

[1] A. V. Shubnikov, Symmetry and Antisymmetry of Finite Bodies [In Russian] (1951).

[2] A. V. Shubnikov, "Recent developments in the science of symmetry and its applications," General Meeting of the AN SSSR, October 14-17, 1944 (Moscow-Leningrad, 1945).

[3] B. Delone, N. Padurov, A. Aleksandrov, Mathematical Elements of Crystal Structure Analysis [In Russian] (1934).

[4] S. A. Bogomolov, "Derivation of orthogonal systems by the Fedorov method," 1, (1932); 2 (1934).**

[5] A. V. Shubnikov, "Erratum to Symmetry and Antisymmetry of Finite Bodies (1951);" Tr. Inst. Krist. Akad. Nauk 9, 383, 1954.

[6] A. M. Zamorzaev, Generalization of Fedorov Groups (author's abstract of dissertation) [In Russian] (Leningrad, 1953).

---

* The group is denoted as the product of the translation group $\left\{a', a''\ a_2\right\}$ by the rotation group 4 : 2 (see [1]).

** As in original — Publisher's note.

[7] A. V. Shubnikov, "Antisymmetry of finite bodies," Tr. Inst. Krist. Akad. Nauk 10, 3-5 (1954).

[8] N. V. Belov, N. N. Neronova, T. S. Smirnova, "1651 Shubnikov Groups," Tr. Inst. Krist. Akad. Nauk 11, 33-67 (1955).

[9] A. G. Kurosh, Group Theory [In Russian] (1953).

Kishinev State University

Received November 4, 1956

MOSAICS FOR 46 PLANE (SHUBNIKOV) ANTISYMMETRY GROUPS AND FOR 15 (FEDOROV) COLOR GROUPS

N. V. Belov and E. N. Belova

Mosaics are the clearest representation of the groups corresponding to them, since they do not contain "grey" elements (terminology due to Shubnikov [1]). In the usual schematic representation of plane groups by tetrahedra or triangles of two colors [2] all the "empty" space between triangles is "grey." The symmetry of groups is represented best by mosaics in which all the elementary figures of various colors are geometrically the same and sufficiently simple, particularly if their coutlines contain no curves. This condition is relatively easily fulfilled for groups with very high orders of symmetry, and less easily, perhaps even never, for groups with poor symmetry.

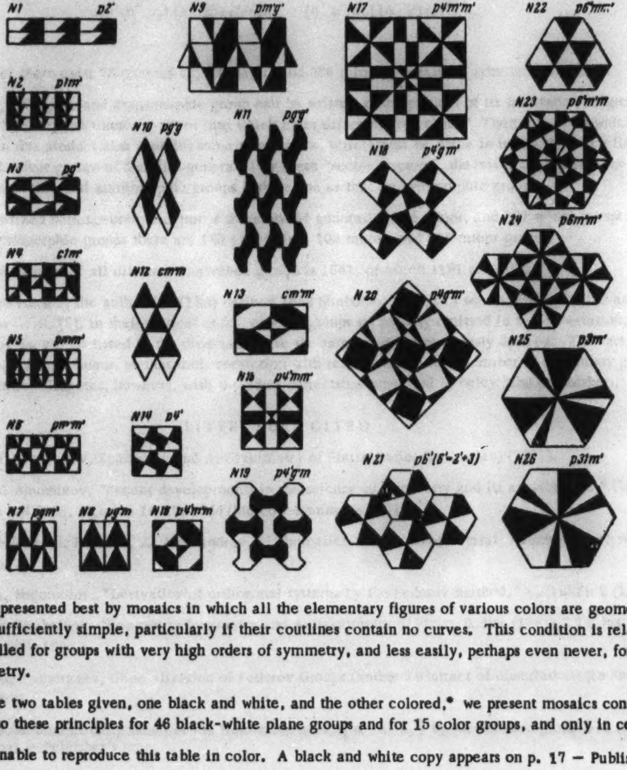
N1 p2'
N2 p1m'
N3 pg'
N4 c1m'
N5 pmm'
N6 pm'm'
N7 pgm'
N8 pg'm
N9 pm'g'
N10 pg'g
N11 pg'g'
N12 cmm
N13 cm'm'
N14 p4'
N15 p4'mm'
N16 p4'm'm
N17 p4m'm'
N18 p4'gm'
N19 p4'g'm
N20 p4g'm'
N21 p6'(6'=2'+3)
N22 p6'mm'
N23 p6'm'm
N24 p6m'm'
N25 p3m'
N26 p31m'

In the two tables given, one black and white, and the other colored,* we present mosaics constructed according to these principles for 46 black-white plane groups and for 15 color groups, and only in certain

---

* [We are unable to reproduce this table in color. A black and white copy appears on p. 17 – Publisher].

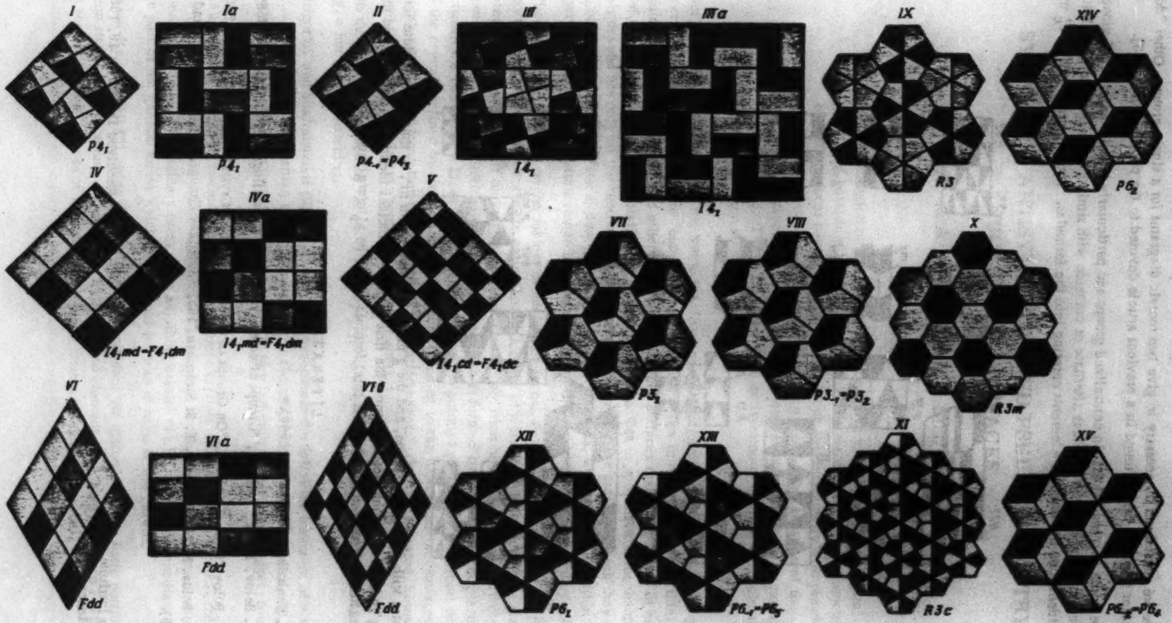
I
$p4_1$
Ia
$p4_1$
II
$p4_{-1}=p4_3$
III
$I4_1$
IIIa
$I4_1$
IX
$R3$
XIV
$P6_2$
IV
$I4_1md-F4_1dm$
IVa
$I4_1md-F4_1dm$
V
$I4_1cd-F4_1dc$
VII
$P3_1$
VIII
$P3_{-1}=P3_2$
X
$R3m$
VI
Fdd
VIa
Fdd
VIб
Fdd
XII
$P6_1$
XIII
$P6_{-1}=P6_5$
XI
$R3c$
XV
$P6_{-2}=P6_4$

special cases have we considered it necessary to give two mosaic diagrams for a single group. Other "doubtlets," particularly for color mosaics, can be found in a previous article devoted to the present problem [3].

It should be borne in mind [4] that in centralized groups and particularly in color centralized groups the symmetry elements entering into the formulas alternate or coincide with similar elements, and these latter may be even more evident than the standard elements entering into the formulas. Thus, in group No. 41 P_c' mg, the

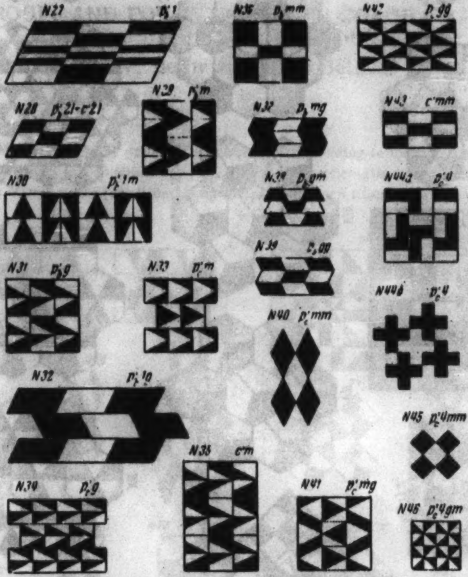
N27 $p_b'1$
N36 $p_b'mm$
N42 $p_c'gg$
N28 $p_b'21{-}c'21$
N29 $p_b'm$
N37 $p_b'mg$
N43 c'mm
N30 $p_c'1m$
N38 $p_b'gm$
N44a $p_c'4$
N31 $p_b'g$
N33 $p_c'm$
N39 $p_c'gg$
N44б $p_c'4$
N40 $p_c'mm$
N32 $p_c'1g$
N45 $p_c'4mm$
N35 c'm
N34 $p_c'g$
N41 $p_c'mg$
N46 $p_c'4gm$

m plane alternates with the color g' plane, and the g plane alternates with m', so that the complete formula would be $p_c'm(g')g(m')$. In group No. 36 $p_b'mm$, the first m plane coincides identically with g', and the second m plane alternates with m', so that the total formula would be $p_b'm(\equiv g')\,m(m')$.

LITERATURE CITED

[1] A. V. Shubnikov, Symmetry (1940).*

[2] N. V. Belov, T. M. Tarkhova, "Groups of color symmetry," Crystallography 1, 1, 4-13 (1956).

[3] N. V. Belov, T. M. Tarkhova, "On Groups of color symmetry," Crystallography 1, 6, 619-620 (1956).

[4] N. V. Belov, N. N. Neronova, T. S. Smirnova,"1651 Shubnikov Groups," Tr. Inst. Krist. Akad. Nauk 11, 33-67 (1955).

Crystallography Institute
Academy of Sciences, USSR

Received December 18, 1956

---

* In Russian.

SYMMETRY, ANTISYMMETRY AND PSEUDOSYMMETRY OF NUCLEATION SURFACES

V. A. Mokievskii and I. I. Shafranovskii

Nucleation surfaces have been studied in variously oriented crystal growths of potassium aluminum alums. The symmetries and antisymmetries of these surfaces have been studied. Cases of pseudosymmetry with pseudoaxes of the sixth and eighth order have been noted. The question of the symmetry, antisymmetry and pseudosymmetry of induction faces in general has been raised. The importance of an antisymmetry concept for nucleation surfaces has been noted.

Nucleation surfaces arising at the boundary of two or more adjoining crystals as a result of their simultaneous crystallization are widespread both in nature (mineral grains in rocks) and in artificial formations (salt sediments, metals, cements and others). The study of such surfaces makes it possible to establish certain details of the mechanism of polycrystalline aggregate formation. Let us note that the mechanical properties of metals depend not only on the mechanical properties of the crystalline grains of which they are constituted but also on the mechanism by which they grow together. Nevertheless, while paying attention to the mechanical properties of individual crystals researchers usually ignore the mechanism by which they grow together.

There is little literature on the subject of nucleation faces. Fersman [1] was one of the first to point out the importance of nucleation surfaces in nature and as a result of a study of the structures of graphic granite formulated the following law of mutual nucleation "The demarcation of two simultaneously crystallizing substances is defined by a cylindrically curved surface which is formed by the periodic displacement of the edge between the two possible faces of either substance at the point of contact... The most important possible faces of the crystal, defined by simple indices and corresponding to the most important surfaces of the space lattice play a part in the formation of such mutual nucleation edges." (It must be noted, however, that nucleation surfaces do not always approach cylindrical ones).

On the surfaces bounded by the faces of icthyoglypt quartzes A. E. Fersman finds pseudofaces with fine hatching, a nucleation hatching.

Grigor'ev and Shafranovskii [2] feel it necessary to separate the following elements of a nucleation surface: a) pseudofaces (a Fersman term), b) pesudoedges (boundary between two pseudofaces), c) nucleation faces (individual flat portions covering the pseudoface in step fashion), d) nucleation edges (boundaries between two nucleation faces).

As a result of a study of nucleation surfaces of quartz crystals that had grown together, the above-mentioned authors showed that a number of the nucleation faces correspond to the usual forms of quartz and that the others correspond to the imprint of ordinary faces of an adjoining crystal or else occupy intermediate positions. All three are part of the general zones which are rational for both crystals in the growth.

Frank-Kamenetskii [3], using a barite crystal, confirmed the matching of the basic portion of the nucleation steps of one element with the steps of the second element (step correspondence law). However, between the nucleation surfaces of the adhering crystals there are many free spaces.

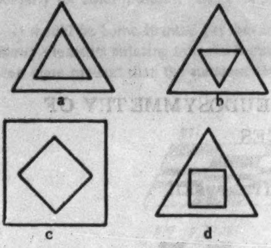

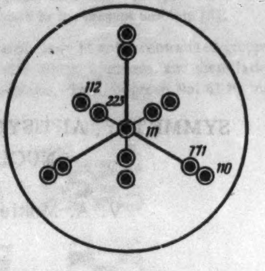

Fig. 1. Mutual orientation of adjoining faces of four types of potassium aluminum alum crystal growths.

Fig. 2. Light star and the projection of the nucleation faces on a growth of the first type.
White circles are nucleation faces of the upper crystal; black dots of the lower crystal. Radius of the projection circle: 45°.

This paper presents the results of a study of artificially produced nucleation surfaces on growths of potassium aluminum alum crystals.

The crystal growth was carried out in ordinary crystallizing dishes by a static method in weak supersaturated solutions at room temperature. The crystals in the growth were oriented by placing one crystal on the other more or less precisely. Usually the smaller crystal was placed on the face of the large crystal in a corresponding orientation. As a result a stepped depression in the shape of a crater was formed on the bottom crystal and a corresponding convex pyramid on the upper crystal. After the crystals had grown together, their mutual orientation was checked on a two-circled Fedorov goniometer. The adjoining surfaces of both crystals after separation were likewise goniometrically studied. A brief description of the following four types of oriented growths is given below.

1. The vertical third order axes of both crystals are parallel. Contours of the adjoining octahedral faces are truly parallel (Fig. 1,a). The conventional designation for such growths is $L_3 \parallel L_3'$, $[1\bar{1}0] \uparrow\uparrow [1\bar{1}0]'$. Both crystals in this position form together a spinel twin.

2. The vertical third order axes of both crystals are parallel. Adjoining octahedral faces are in an antiparallel position (Fig. 1,b) $L_3 \parallel L_3'$, $[1\bar{1}0] \downarrow\uparrow [\overline{11}0]'$. Both crystals in this position form a parallel growth.

3. The vertical "fourth order"* axes are parallel.

The adjoining faces of the cube are rotated relative to each other at a 45° angle around "L_4" (Fig. 1,c). "L_4" $\parallel$ "L_4'," $[1\bar{1}0]:[1\bar{1}0]' = 45°$.

4. The vertical 3-fold axis of one crystal is parallel to the vertical "4-fold" axis of the other crystal. Adjoining faces of the cube and the octahedron are placed as shown in Fig. 1,d) : $L_3 \parallel$ "L_4'", $[1\bar{1}0] \parallel [1\bar{1}0]'$.

Growths of type $L_3 \parallel L_3'$, $[1\bar{1}0] \uparrow\uparrow [\bar{1}10]'$ (first type). Both nucleation surfaces produce reflections on the goniometer in the shape of a star with a clear triple symmetry (Fig. 2). When the three sharper and brighter rays are prolonged, the trigonal-trioctahedral series appears. Outstanding in signal brilliance are $\{771\}$ and also a rhombododecahedron. Three other rays lying on the other side of L_3 differ from the first by their diffuseness. The tetragonal-trioctahedral series is found on their extension, of which $\{223\}$ and $\{112\}$ are outstanding (Fig. 2). The angles of the normals to all these forms with the vertical L_3 are shown in Table 1. The nucleation surfaces have the shape of a triangular crater for the bottom crystal and a triangular convex surface for the upper crystal. On both the surfaces identical forms are seen as nucleation faces, touching each other. Reflections from the concave and the convex surface appear more or less alike.

---

* For the sake of simplicity of didodecahedral symmetry of potassium aluminum alums is considered as a hexoctahedral symmetry.

TABLE 1

Rays	Symbol	Angle with L_3
Bright ray	771	29½°
Bright ray	110	35½°
Diffuse ray	223	11½°
Diffuse ray	112	19½°

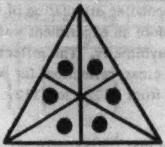

Fig. 3. Figure with m • 3 : m A.V. Shubnikov antisymmetry.

Separately studied nucleation surfaces of both the crystals as well as the reflections coming from them correspond to the trigonal-pyramidal symmetry L_3 3P (3 • m). At the same time such surfaces studied as a unit possess antisymmetry corresponding to the m • 3 : m Shubnikov group [4] (Fig. 3).

Growths of type $L_3 \parallel L_3'\,[1\bar{1}0] \parallel [\bar{1}10]'$ (second type). Due to the antiparallel application of adjoining octahedral faces, the nucleation tetragonal-trioctahedrons of one element coincide with the trigonal-trioctahedrons of the second element and vice versa. The reflections from the nucleation surfaces of both crystals form aroung L_3 a six pointed star all of whose rays appear equal (Fig. 4). The pseudo-symmetry of such formations also has an effect on the nucleation faces, whose signals correspond with the rays of the above mentioned star. This is also shown in Table 2 (the symbols and the angles with L_3 of the corresponding faces of both crystals are given in the same horizontal line).

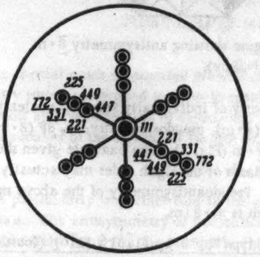

Fig. 4. Light star and projection of nucleation face on a second type growth.
Symbols for the nucleation faces of the bottom crystals are underlined.

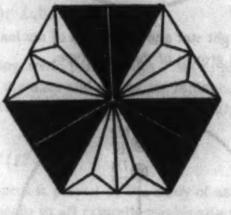

Fig. 5. A figure showing antisymmetry $\underline{\bar{6}}$ • m (A. V. Shubnikov).

Of course the symmetry of the two separately considered nucleation faces remains as before: trigonal-pyramidal L_3 3p (3 • m). However, due to mutual nucleation, there is a definite tendency for the symmetry to increase up to the pseudosymmetry L_6 6P (6 • m). The antisymmetry of both surfaces taken together corresponds to the $\underline{\bar{6}}$ • m group (Fig. 5). If one does not take into account the difference for equally inclined trigonal-trioctahedrons and tetragonal-trioctahedrons, i.e., if one starts with pseudosymmetry, "pseudoantisymmetry" of the m • 6 • $\underline{m}$ group type will be obtained.

TABLE 2

Bottom crystal		Upper crystal	
symbol	angle with L_3	symbol	angle with L_3
221	16	447	16
331	22	449	22.5
772	24	225	25
447	16	221	16
449	22.5	331	22
225	25	772	24

TABLE 3

Bottom crystal			Upper crystal		
symbol	φ	ρ	symbol	φ	ρ
102	0°	26.5°	113	45°	25°
113	45°	25°	102	0°	26.5°

Growth of type "L_4" ‖ "L_4'," $[1\bar{1}0]:[1\bar{1}0]$ = 45° (third type). A study of growths of the second type showed that with a corresponding orientation of the crystals the symmetry of the nucleation surfaces may be artificially increased. Therefore an experiment was carried out on the formation of nucleation surfaces with an eight dimensional pseudosymmetry. The reflections for both the nucleation surfaces show an eight pointed star (Fig. 6). Individual, fairly clear, reflections for both surfaces corresponded to $\{102\}$ faces. Also a series of light bands were noted going from $\{102\}$ to $\{113\}$. Polar distances for both these forms are close (ρ_{102} = 26°34', ρ_{113} = = 25°14').

It is evident that nucleation faces $\{102\}$ of one crystal brought about the formation of the more or less corresponding faces $\{113\}$ on the other crystal (Fig. 8 and Table 3).

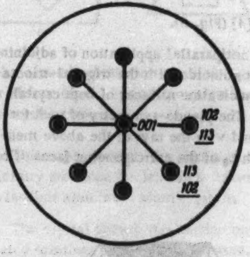

Fig. 6. Light star and projection of nucleation faces on a growth of the third type.

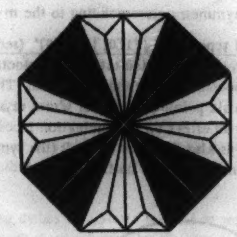

Fig. 7. Figure showing antisymmetry $\bar{\underline{8}}\cdot m$ (A. V. Shubnikov).

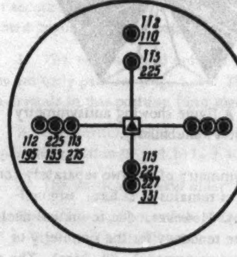

Fig. 8. Light star and projection of nucleation faces on inter-growths of the fourth type.

The symmetry of individually selected nucleation surfaces is $L_4\,4P$ ($4\cdot m$), pseudosymmetry: $L_8\,8P$ ($8\cdot m$), antisymmetry: $\bar{\underline{8}}\cdot m$ (Fig. 7). The example given shows that a mirror antiaxis of the eighth order may actually exist in crystals. Pseudoantisymmetry of the above mentioned intergrowth is $m\cdot 8:m$.

Growths of type '"L_4" ‖ L_3, $[1\bar{1}0]$ ‖ $[1\bar{1}0]$' (fourth type). Superposition of quadruple symmetry on to triple symmetry, when a common symmetry plane exists in both crystals, caused the appearance of two mutually perpendicular zones on the nucleation surface (Fig. 8 and Table 4). For the crystal with a vertical "4-fold" axis, these are the two zones $[\bar{1}10]$ and for the crystal with a vertical 3-fold axis they are the zones $[\bar{1}10]$ and $[\bar{1}12]$. The formation of two mutually perpendicular zones shows the predominant influence of the "4-fold" axis, which affected also the nucleation surface of the crystal with a vertical 3-fold axis. At the same time the latter influenced in its turn the quadruple symmetry of the upper crystal, since for both mutually perpendicular zones the symbols of the nucleation faces were not completely identical. The symmetry form here is P(m). In view of the fact that the coinciding faces of the bottom and top crystal differ in various symbols, there is no point of talking here of pseudosymmetry. In this particular case only ordinary symmetry exists.

From a study of the nucleation surfaces of alums it follows that the adjoining nucleation faces, as a rule, are the faces with rational symbols. In some cases the correspondence of nucleation faces is not ideal and in this case wedge shaped spaces and free spaces appear between them. The more numerous the free spaces the weaker will be the growth. The number of free spaces depends on the mutual orientation of the growing crystals.

TABLE 4

Bottom crystal (vertical axis L_3)		Upper crystal (vertical axis "L_4")	
symbol	angle with L_3	symbol	ρ
First ray ρ = 90°			
221	16°	115	16°
331	22°	227	22°
225	26°	$\bar{1}\bar{1}3$	25.5°
110	35°	$\bar{1}\bar{1}2$	35°
Second ray ρ = 0°			
275	25°	113	25°
153	29°	225	29.5°
195	33°	112	35°

The experimental data given above show the importance of symmetry, antisymmetry and pseudosymmetry on the properties of nucleation surfaces. The symmetry of such individual surfaces (convex and concave) corresponds to the symmetry of one sided rosettes (Shubnikov [5]). The symmetry of "crystallographic rosettes" corresponds to the 10 point groups (primitive and planar)

$$L_1\,(1);\;\; L_2\,(2);\;\; L_3\,(3);\;\; L_4\,(4);\;\; L_6\,(6);$$
$$P\,(m);\; L_2 2P\,(2\cdot m);\; L_3 3P\,(3\cdot m);\; L_4 4P\,(4\cdot m);\;\; L_6 6P\,(6\cdot m).$$

In special cases of oriented growths one must add to these crystallographic point groups cases of pseudosymmetry which correspond to a, so to speak, doubled symmetry. Here the axes and planes are replaced by pseudoaxes and pseudoplanes of symmetry. In addition to the above listed point groups we have here groups with pseudoaxes of the eighth and twelfth orders

$$L_8\,(8);\;\; L_{12}\,(12);\;\; L_8 8P\,(8\cdot m),\;\; L_{12} 12P\,(12\cdot m).$$

A particularly important role in the description of nucleation surfaces is played by the study of antisymmetry of crystals. The antisymmetry of nucleation surfaces apparently corresponds to all crystallographically possible groups of antisymmetry of the terminal figures calculated by Shubnikov [4]. The orders of the antiaxes and mirror antiaxes correspond crystallographically and may, as has been mentioned above, also show the doubled value.

Nucleation surfaces are a good example of antisymmetry in crystals.

LITERATURE CITED

[1] A. E. Fersman, "Elements of demarcation between two simultaneously crystallizing substances," Doklady Akad. Nauk SSSR 7-8 (1922).

[2] D. P. Grigor'ev and I. I. Shafranovskii, "On adjoining surfaces of individual crystals," Zapiski Vsesoiuz. Mineral. Obshchestva 3, 185-193 (1948).

[3] V. A. Frank-Kamenetskii, "Surface structure in barite crystal growths," Zapiski Vsesoiuz. Mineral. Obshchestva 3, 3, 194-200 (1948).

[4] A. V. Shubnikov, Symmetry and Antisymmetry of Terminal Figures [In Russian] (1951).

[5] A. V. Shubnikov, Symmetry [In Russian] (1940).

Leningrad Mining Institute

Received July 9, 1956

ON THE THEORY OF THE RADIAL DISTRIBUTION METHOD

B. K. Vainshtein

The Fourier integral is used to consider the properties of the radial distribution function. A new method of normalization is proposed, making it possible to use the intensity curve as a whole, rather than just its furthest regions, for this purpose.

It is shown that in order to analyze the peaks in the radial distribution function one need know only the relative atomic weights K_i, rather than the absolute ones (as, for instance, in electron units in x-ray diffraction studies). The dependence of the weights of the peaks on the atomic number is clarified for x-ray and electron diffraction studies. In electron diffraction studies $K_i \sim Z^{0.75}$.

1. General Remarks

In investigating amorphous substances, liquids, or gases the method of constructing the radial distribution curve on the basis of the intensity curve obtained from x-ray or electron diffraction patterns is widely used; one then makes use of the formula

$$4\pi r^2 u(r) + 4\pi r^2 u_0 = \frac{2r}{\pi}\int_0^\infty si(s)\sin sr\,ds. \qquad (1)$$

Let us briefly describe the elements of this method, which has been developed elsewhere [1] (see also Porai-Koshits [2]), using the theory of Fourier integrals, which is the most natural way of describing scattering phenomena. In Equation (1), u(r) is a modified form of the atomic distance function P(r) in the object being investigated. The interatomic distance function

$$P(\mathbf{r}) = \int \rho(\mathbf{r}')\rho(\mathbf{r}'+\mathbf{r})\,dv_{r'} = \widehat{\rho\rho^*}(\mathbf{r}) \qquad (2)$$

is the convolution of the density distribution $\rho(\mathbf{r})$ of scattering substance in the object with the inversion through the center of symmetry $\rho^*(\mathbf{r}) = \rho(-\mathbf{r})$ of this same density distribution. The Fourier integral of P(r) determines the scattering intensity I(s)

$$I(\mathbf{s}) = \int P(\mathbf{r})\,e^{i(\mathbf{sr})}\,dv_r, \qquad (3)$$

and its Fourier transform makes it possible to find P(r) from experiment by the formula

$$P(\mathbf{r}) = \frac{1}{8\pi^3}\int I(\mathbf{s})\,e^{-i(\mathbf{sr})}\,dv_s. \qquad (4)$$

Now $\rho(\mathbf{r})$ is composed of a set of atoms ρ_i whose centers are located at the points $\mathbf{r}_i$, so that

$$\rho(\mathbf{r}) = \sum_i \rho_i(\mathbf{r} - \mathbf{r}_i). \tag{5}$$

Substituting (5) in (2) we obtain

$$P(\mathbf{r}) = \int \sum_i \rho(\mathbf{r}' - \mathbf{r}_i) \sum_j \rho(\mathbf{r}' - \mathbf{r}_i + \mathbf{r})\, dv_{\mathbf{r}}, \tag{6}$$

which, after replacing $\mathbf{r}' - \mathbf{r}_i$ by $\mathbf{r}''$ becomes

$$P(\mathbf{r}) = \sum_{i=j} \widehat{\rho_i \rho_i^*}(\mathbf{r}) + \sum_{i \neq j} \widehat{\rho_i \rho_j^*}(\mathbf{r} - [\mathbf{r}_j - \mathbf{r}_i]). \tag{7a}$$

Thus $P(\mathbf{r})$ consists of separate peaks $\widehat{\rho_i \rho_j^*}$ whose weights are proportional to the weights of the atoms responsible for these peaks, and whose distances from the origin are equal to the interatomic distances $[\mathbf{r}_j - \mathbf{r}_i]$ in the object. The set of these peaks can also be interpreted in a different way, writing Equation (2), after inserting (5), in the form

$$P(\mathbf{r}) = \sum_i \widehat{\rho_i(\mathbf{r} - \mathbf{r}_i)\, \rho^*}(\mathbf{r}). \tag{7b}$$

It is seen from this that $P(\mathbf{r})$ is a sum of convolutions for each atom ρ_i with ρ^* for all atoms, or represents the superposition of the distribution function about each atom (taking into account its weight) of all the other atoms.

In studying crystals $I(\mathbf{s})$ decomposes into a set of structure factors, and the integral (4) becomes the Patterson series [3].

In studying amorphous substances, liquids, or gases, $I(\mathbf{s})$ is continuous in reciprocal space. As a result of averaging all possible orientations of atomic pairs over the volume and time of experiment in these cases, which leads to statistically spherical microsymmetry of the object, and therefore also of the scattering intensity, the Fourier integral of Equation (4) can be integrated over the angles and written

$$P(r) = \frac{1}{2\pi^2} \int_0^\infty I(s)\, s^2 \frac{\sin sr}{sr}\, ds \tag{8}$$

in spherical coordinates, and the interatomic distances lose their vector character (which they have in the Patterson series).

The transition from $P(\mathbf{r})$ of Equation (8) to $u(r)$ of Equation (1) is based on the following procedure. Instead of the (normalized) experimental intensity of coherent scattering $I_n(s)$, one uses the function

$$i(s) = \frac{I_n(s) - \sum_{i=1}^{n} f_i^2(s)}{f_{un}^2(s)}, \tag{9}$$

where f_i is the atomic scattering factor.

Since the Fourier transform of each of the peaks $\widehat{\rho_i \rho_j^*}$ entering into (7a) is $f_i f_j^*$, subtracting $\sum_{i=1}^{n} f_i^2(s)$

from the numerator of (9) removes the trivial peaks of P(r) given by the first sum in (7a) with i = j, for which $[r_i - r_j] = 0$ (the distance from an atom "to itself").

Division by a specially-chosen unitary f_{un}^2 -curve eliminates, as is known, the decrease of the I(s) function which is due to the "shape" of the atoms $\rho_i(r)$ (in x-ray scattering $\rho_i(r)$ is the electron density, and in electron scattering it is the atomic potential). Instead of (7) and (8) we obtain the function

$$u(r) = \sum_i \sum_j \delta_{ij}(r - r_{ij}), \tag{10a}$$

so that $4\pi r^2 u(r)$ gives the radial density of distances δ_{ij} between "point" atoms* (each δ_{ij} has "weight," see Section 3). Since it is experimentally impossible to measure the zero order scattering (that is in the neighborhood of s = 0) this region of I(s) is neglected in using Equation (9). Instead of this one introduces the mean density of interatomic distances,** which determines the zero order scattering as well as the equivalent quantity u_0, into Equation (1).

2. Normalization of the Instensity Curve

Since it is impossible in practice to measure the absolute scattering intensity, the experimental I(s) curve is normalized to one calculated for the number of atoms n entering the chemical formula. One then makes use of the damping of oscillations of I(s) for large s, when

$$I_n(s) \approx \sum_{i=1}^{n} f_i^2(s). \tag{11}$$

The absolute values of I(s) for these values of s are small, so that the relative error is increased, showing therefore a disadvantage of this method.

It is possible, however, to normalize the I(s) curve as a whole. The function $\rho(\mathbf{r})$ and its Fourier transform $f(\mathbf{s})$ satisfy a relation connecting their mean square values (obtained from (2) and (4) with r = 0). In the three-dimensional case

$$\int \rho^2(\mathbf{r})\, dv_r = \frac{1}{8\pi^3} \int |f(\mathbf{s})|^2\, dv_s. \tag{12a}$$

The Fourier transform of ρ_i is the atomic factor f_i. For a single atom in spherical coordinates (12a) becomes

$$4\pi \int_0^\infty \rho_i^2(r)\, r^2\, dr = \frac{1}{2\pi^2} \int_0^\infty f_i^2(s)\, s^2\, ds = G_i. \tag{12b}$$

---

* The function $f_{un}^2(s)$ is usually chosen as the curve for an atom at rest. Therefore division by this function eliminates the "proper" spread of the electron density (or potential) of the atom; the "point" atom so obtained, however, still has some spread due to thermal motion. By including a temperature factor f_T, that is dividing by $(f_{un} \cdot f_T)^2$, one can go over to a "strictly point" atom. Such additional "sharpening of the peaks" of P(r) is hardly reasonable, since this strengthens the unfavorable influence of the cut-off in I(s).

** We shall not go into a detailed consideration of how the shape of the object affects the results, considering the scattering volume sufficiently large (see, for instance, Filipovich [4]).

Bearing in mind that $\rho(\mathbf{r})$ represents a set of atoms such as that of Equation (5) (and takes on large values only at the atomic positions), the left side of (12a) can be written

$$\int \rho^2(\mathbf{r})\,dv_r = \sum_i \int \rho_i^2(\mathbf{r})\,dv_r. \tag{13}$$

Noting that in (12a) $|f(\mathbf{s})|^2$ for the object as a whole is just the intensity I(s), and expressing (12a) in spherical coordinates using (12b) and (13), we obtain

$$\int_0^\infty I_n(s)\,s^2\,ds = \sum_{i=1}^n \int_0^\infty f_i^2(s)\,s^2\,ds = 2\pi^2 \sum_{i=1}^n G_i. \tag{14}$$

This is the normalization condition, since the sum on the right can be calculated. The physical meaning of (14) is that the interference which takes place for a certain relative distribution of the atoms cannot change the total scattering intensity from these atoms, but gives only a redistribution of the intensity (we are speaking, of course, of coherent scattering; incoherent scattering shall be treated later). This means that the $I_n(s)\,s^2$ curve oscillates about $\sum_{i=1}^n f_i^2(s)\,s^2$, and that the areas under these curves are equal, as are the areas bounded by these curves above and below the $\sum_{i=1}^n f_i^2(s)\,s^2$ curve (Fig. 1).

It also follows from (14) that for a sufficiently wide interval (s_1, s_2) we have on the average

$$\overline{I_n(s)\,s^2} = \overline{\sum_{i=1}^n f_i^2(s)\,s^2} \tag{15}$$

and less rigorously,

$$\overline{I_n(s)} = \overline{\sum_{i=1}^n f_i^2(s)}, \tag{16}$$

which gives Equation (11) for large $\underline{s}$, when the oscillation of I(s) is small. Statistical relations of a similar type occur in the structural analysis of crystals [5, 6], but in the present case they are generalized to continuous intensity distributions.

In practice (14) may be applied not for the ideal limits s = 0 and s = ∞, but for some small s' ≈ 0 and some upper limit s" (see Fig. 1). For this it is sufficient to find (by numerical or graphical integration) the right side of (14) using the theoretical f_i-curves, to find the left side from the experimental (unnormalized) values of I(s) in the same way, and to equate these two values.

Equation (14) does not include the incoherent scattering I_H. When it is taken into consideration, we obtain

$$\int_0^\infty (I_K + I_H)_n\,s^2\,ds = 2\pi^2 \sum_{i=1}^n G_i + \sum_{i=1}^n \int_0^\infty I_{H_i}\,s^2\,ds. \tag{17}$$

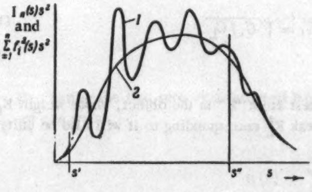

Fig. 1. Oscillation of (1), the $I_n(s)\,s^2$ curve, about (2), the $\sum_{i=1}^n f_i^2(s)\,s^2$ curve.

By calculating I_{H_i} in a well known way (in the same units, of course, as the coherent components I_{K_i}) one can again normalize the intensity and then subtract from it the part due to coherent scattering of Equation (14). In electron diffraction studies I_H is small and can often be neglected.

We note finally that the G_i entering into (14) and (17) are constant for a given kind of atom. The author has shown previously that for x-ray [6] and electron [7] diffraction studies there exists a relation of the form

$$G_i = kZ^{\alpha} q, \tag{18a}$$

where $\underline{k}$ and α are coefficients which depend on the parameter B of thermal motion, Z is the atomic number, and $\underline{q}$ accounts for the cutoff.

Thus if one bears in mind the thermal motion and uses earlier data [6, 7], the normalization of Equation (14) can be performed without calculating integrals such as (12b). If one does not account for thermal motion (see the footnote on p. 26), then the integrals of (12b) converge slowly and they must be calculated by integration to some upper limit s''. In this case the G_i remain proportional to Z^{α}, and for x-ray and electron diffraction studies α is

$$\alpha_X = 2.60, \ \alpha_{el} = 1.50. \tag{18b}$$

When thermal motion is taken into account, the values of α decrease somewhat [6, 7].

3. The Weights of the Peaks in the Radial Distribution Function in X-Ray and Electron Analysis

In constructing u(r) in Equation (1), when analyzing objects composed of different kinds of atoms by x-ray diffraction, electron units are used, which means that f_{un}^2 in Equation (9) is taken as the scattering curve for a single electron [1]. Then if one assumes (an approximation necessary for analysis), that the atoms are of similar shapes, their weights are determined by the "effective numbers" K_i of electrons in them, and the weights of the peaks in the radial distribution function are proportional to the products $K_iK_j(\mathrm{el}^2)$ of the weights of the "point atoms." It should be emphasized immediately, however, that the choice of "electron" units or any others is not required, since the function of Equation (1) can be analyzed by knowing only the ratios of the K_i for the atoms in the object and the relation of these quantities to the $f_{un}^2(s)$ curve chosen.

The ratio of the squares K_i^2 is found from the ratio of the mean scattering factors averaged over the whole $\underline{s}$ interval, that is from the f_i^2-curves. The average must be taken bearing in mind the following point, which is usually ignored. Although experiment gives I(s), on going over to P(r) of Equation (8) and to u(r) of Equation (1) the quantity $I(s)\,s^2$ enters the calculations and this very naturally reflects the three-dimensionality of the intensity distribution in reciprocal space by equal values of I(s) in a spherical band of volume $4\pi s^2 ds$. Therefore the contribution of the atoms to the total intensity taken from all the reciprocal space as given by (14) is due to the quantities $G_i \sim \int f_i^2(s)\,s^2 ds$ (12b).

Thus the relative weights K_i of the atoms are given by the relations

$$K_i^2 = \frac{\int_0^{s''} f_i^2(s)\,s^2\,ds}{\int_0^{s''} f_L^2(s)\,s^2\,ds} = \frac{G_i}{G_L}; \quad K_i = \sqrt{G_i/G_L}. \tag{19}$$

It is simpler to take as the measure of K_i its value for the lightest atom "L" in the object, whose weight K_L will be equal to unity according to (19), just as the weight of the peak K_L^2 corresponding to it will also be unity in u(r) of (10a).

From (18b) and (19) it follows that

$$\text{for x-ray diffraction } K_i = (Z_i/Z_L)^{1.3}, \tag{20a}$$

$$\text{for electron diffraction } K_i = (Z_i/Z_L)^{0.75}. \tag{20b}$$

These relations are sufficiently accurate; for light atoms, however, which sometimes have individual singularities in the f curves, there may be deviations from these relations which are easily established by using the general form of (19). The difference in the exponents of (20a) and (20b) reflects the fact that the atomic potentials (responsible for electron scattering) depend less strongly on the atomic number Z than on their electron densities (responsible for x-ray scattering).

Knowing K_i, one easily finds the unit curve

$$f^2_{\mathrm{un}}(s) = \frac{\sum\limits_{i=1}^{n} f_i^2(s)}{\sum\limits_{i=1}^{n} K_i^2}. \tag{21}$$

This would be exactly the same as $f^2_L(s)$ if the atoms, and therefore the f-curves, were similar (actually the difference between f^2_{un} and f^2_L is not large). Now substituting (21) in (9) will in general eliminate the intermediate calculation of f^2_{un} so that one immediately obtains i(s) by

$$i(s) = \sum_{i=1}^{n} K_i^2 \left(\frac{I_n(s)}{\sum\limits_{i=1}^{n} f_i^2(s)} - 1 \right). \tag{22}$$

Thus in order to analyze the weights of the peaks in u(r) the following is sufficient: 1) to normalize I(s) to $\sum\limits_{i=1}^{n} f_i^2(s)$ taken in arbitrary units, and to divide $I_n(s)$ in (22) by this same curve; 2) to take arbitrary relative values of K_i in (22), and to calculate the weights of the peaks of u(r) in terms of these values (see Equation (27) below). As has already been mentioned, it is most convenient to choose $K_L = 1$, thus obtaining for the other atoms small K_i values of the order of unity, and correspondingly small products K_iK_j.

4. Interpretation of the Peaks and Some Properties of the Radial Distribution Function

The object of constructing the $4\pi r^2 u(r)$ curve is to find the distance and number of neighbors of a given atom. Let us investigate the meaning for this of normalizing I(s) to scattering by the n atoms entering into the chemical formula (molecule) of the given substance. Actually the object contains a large number N of atoms, so that the function P(r) of (7a) contains N^2 terms, and the first sum in (7a) contains N terms. Thus in going over to u(r) by (10a), we have N(N −1) terms remaining. By normalizing I(s) to n atoms, we decrease this quantity, as well as P(r) of Equation (8) and u(r) of (10a), by a factor of N/n, so that we obtain the function

$$u(r) = \frac{n}{N} \sum_{i \neq j}^{N} \sum^{N} \delta_{ij}(r - r_{ij}). \tag{10b}$$

Decreasing the first sum by a factor of N/n and accounting also for the fact that each δ_{ij} peak has weight K_iK_j, we can write

$$u(r) = \sum_{i=1}^{n} \sum_{j=1}^{N} K_i K_j u_{ij}(r - r_{ij}) \tag{10c}$$

and say that now u(r) contains n(N −1) peaks u_{ij}, or is a superposition of the distributions, about each of the n chosen atoms, of all the other N−1 atoms. Comparing (10b) and (10c) shows that each u_{ij} contains a set of "point" peaks δ_{ij}, which means that it characterizes the distribution of crystallochemically equivalent distances about certain mean values r_{ij}. Due to the normalization condition, after the factor K_iK_j is taken out the weight of u_{ij} is equal to unity, and a calculation of the weights of the peaks of the radial distribution function makes it possible finally to evaluate the number of neighbors in one or another coordination sphere.

In the case of scattering by gas molecules, only the distances within the molecules are significant; so that u(r) of (10c) in fact contains n(n −1) peaks and the remaining n(N −n) distances between the atoms of different molecules are not given by u(r). This follows from the fact that gas molecules scatter independently.

Thus, due to the variation of the interatomic distances in amorphous substances and liquids, the peaks u_{ij} which compose u(r) and correspond to the distances between "point" atoms are nevertheless spread out. Since in this case any order is only approximate, the spreading increases with the increase in r, and u(r) becomes damped and approaches u_0. Corresponding to this, as follows from the properties of the Fourier integral, as s increases i(s) is damped, which causes u(r) of Equation (1) to be hardly sensitive to a cutoff in i(s) to some value $s = s''$ by which the upper limit $s = \infty$ is actually replaced in Equation (1) (Fig. 2a). For free gas molecules the distances between the atoms change only due to thermal motion, and in this case the peaks of u(r) are much sharper. This causes a slow decrease in i(s) Fig. 2b) and u(r) becomes more sensitive to the cutoff, as a result of which one must either move the upper limit experimentally (sectoral method in electron diffraction studies of gas molecules), or make use of an artificial temperature factor which would decrease the oscillation of i(s) for large s causing spreading (broadening) of the peaks of u(r).* A sharp cutoff may alter the positions of the true peaks and cause the appearance of false ones [4].

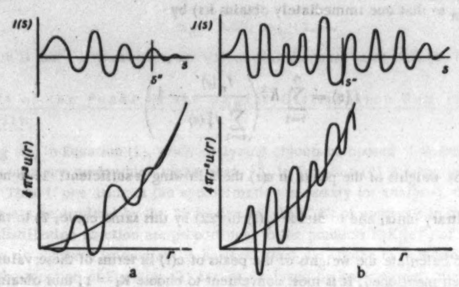

a b

Fig. 2. The character of the i(s) curves and the corresponding $4\pi r^2u(r)$ curves for condensed systems (a) and gases (b).

Returning to the question of the interpretation of the peaks of u(r), let us separate the n atoms entering into the chemical formula according to their types. If there are p types of atoms, then

$$n = n_1 + n_2 + \ldots + n_p \tag{23a}$$

and

$$\sum_{i=1}^{n} K_i^2 = \sum_{a=1}^{p} n_a K_a. \tag{23b}$$

In the normalized radial distribution function of (10c) one may, accounting for the weights K_i, separate out the distributions u_{ab} for the crystallochemically equivalent pairs of atoms

---

* Various artificial methods for changing the roles of the distant and close regions of the intensity curve by means of multiplying I(s) by s or s^2 make the peaks sharper, but increase the disadvantageous effects of the cutoff.

$$u(r) = \sum_{a=1}^{p} n_a K_a \sum_{b} K_b u_{ab}(r - r_{ab}), \tag{10d}$$

which means that the second sum (over $\underline{b}$) is taken over the coordination spheres so that the number m_{ab} of neighbors of type $\underline{b}$ about an atom of type a in this sphere is given by the area under the peak $4\pi r^2 u_{ab}(r - r_{ab})$:

$$m_{ab} = \int_{r'}^{r''} 4\pi r^2 u_{ab}(r - r_{ab})\, dr \,/\, 2n_a K_a K_b, \tag{24}$$

where the integral is taken with the limits r', r" (Fig. 3). The factor 2 in the denominator is due to the fact that in each such peak both the distances ab and ba appear to an equal extent, so that the integral of (24) is equal to $n_a m_{ab} K_a K_b + n_b m_{ba} K_b K_a$. In view of stoichiometry $n_a m_{ab} = n_b m_{ba}$, however, and this latter sum can be replaced by $2m_{ab} n_a K_a K_b$ which gives (24), or equivalently by $2m_{ba} n_b K_a K_b$; in this case interchanging n_a and n_b in (24) gives m_{ba}.

In order to calculate u_0, the second sum in (10d) should be replaced by the mean density of the atoms (assumed weight). The density of matter $\underline{d}$ is used together with the known molecular weight M to find the volume occupied by the $\underline{n}$ atoms of a molecule (molecular unit)

$$V_n = \frac{M \cdot m_H}{d}, \tag{25}$$

where m_H is the mass of the hydrogen atom, $1.65 \cdot 10^{-24}$ g. By dropping the factor 10^{-24} and taking $\underline{b}$ in g per cm³, we obtain V_n in A³. In the assumed units, this volume has the "weight" $\sum_{i=1}^{n} K_i = \sum_{b=1}^{p} n_b K_b$. Thus the mean density of these units is $\sum_{b=1}^{p} n_b K_b \cdot V_n^{-1}$, and the term u_0 can be written

$$\sum_{a=1}^{p} n_a K_a \sum_{b=1}^{p} n_b K_b \cdot V_n^{-1} = \left(\sum_{a=1}^{p} n_a K_a\right)^2 V_n^{-1}. \tag{26}$$

Finally, the radial distribution formula, according to (8), (10d), (22), and (26) is of the form

$$\begin{gathered} 4\pi r^2 u(r) = 4\pi r^2 \sum_{a=1}^{p} n_a K_a K_b \sum_{b} u_{ab}(r - r_{ab}) = 4\pi r^2 \left(\sum_{a=1}^{p} n_a K_a\right)^2 V_n^{-1} + \\ + \sum_{a=1}^{p} n_a K_a^2 \frac{2r}{\pi} \int_0^{\infty} s \left(\frac{I_n(s)}{\sum_{a=1}^{p} n_a f_a^2(s)} - 1\right) \sin srds. \end{gathered} \tag{27}$$

This formula, originally given for x-rays, is valid also for electrons and neutrons. In all three cases the weights of the atoms K_a can be chosen, according to (19), as arbitrary relative quantities; it is most convenient to choose $K_L = 1$.

The choice of electron units in x-ray studies, and therefore the choice of the f_{un}^2-curves for a single electron is not necessary; this choice causes the quantities entering into (27) to have high numerical values, although the final result, the number of neighbors according to (24), obviously remains invariant. In the case of neutron diffraction, when the atoms (nuclei) scatter as points and the atomic scattering curve drops only due to thermal motion, the artificial step of dividing by f_{un}^2 as given by Equation (9) drops out.

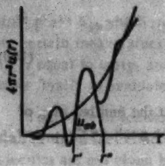

Fig. 3. A separate peak on the $4\pi r^2 u(r)$ curve.

In the electron diffraction laboratory of the Crystallography Institute of the Academy of Sciences U.S.S.R., the above method of normalizing the intensity curve and analyzing the radial distribution curve was applied by L. I. Tatarinova in the electron diffraction study of amorphous antimony sulfide. As opposed to what takes place in the crystalline Sb_2S_3, it was found that in the amorphous phase the Sb atom has approximately six nearest S neighbors, and correspondingly the S atom has four Sb neighbors (at a distance of 2.33 A). From the data obtained one may assume that this phase has a somewhat loosened close packing structure of S atoms, in which two thirds of the octahedral spaces contain Sb atoms. The detailed results of this investigation will be published separately.

In conclusion, let us briefly consider the possibilities of this method. It gives unique results in the case of objects composed of one kind of atom [9, 10]* when the interpretation of the u(r) peaks does not necessitate any particular choice of the combinations $K_a K_b$ in Equation (27), $n = 1$, and there exists only one $K = 1 = K^2$. For two types of atoms, there are three combinations possible K_1^2, $K_1 K_2$, K_2^2. As the number of kinds of atoms increases it is impossible to avoid overlapping of the common peaks of the various combinations. It is then impossible to arrive at unique conclusions from the u(r) curve without additional crystallochemical data. Together, however, with the data on the radii of the atoms, etc., the u(r) function can provide interesting data on the approximate order, which determines many properties of this type of substance.

The quality of the diffraction pattern corresponds to the degree of order of the object. A crystal gives a rich diffraction pattern with an orderly arrangement of a large number of images in the three dimensions of reciprocal space; it can be used to obtain accurate data on the mutual arrangement of the atoms. The diffuse pattern from an amorphous or liquid substance reflects only the statistical approximate order in such objects, and it is impossible to obtain more detailed data from it.

LITERATURE CITED

[1] B. E. Warren, H. Krutter and O. Morningstar, Fourier analysis of x-ray patterns of vitreous SiO_2 and B_2O_3, J. Am. Ceram. Soc. 19, 202-206, 1936.

[2] E. A. Porai-Koshits, "X-ray study of glasslike substances," Usp. Khimii 13, 116-126 (1944).

[3] A. L. Patterson, A direct method for the determination of the components of the interatomic distances in crystals, Z. Krist. 90, 517-542, 1934.

[4] V. N. Filipovich, "Theory of x-ray scattering by gases, liquids, amorphous solids, polycrystals," J. Tech. Phys. (USSR) 25, 1604-1638 (1955).

[5] A. J. G. Wilson, The probability distribution of x-ray intensities, Acta Cryst. 2, 318-321, 1949.

[6] B. K. Vainshtein, "Normalization of Fourier series for electron densities," Doklady Akad. Nauk SSSR 83, 821-823 (1953).

[7] V. K. Vainshtein, "Accuracy of Fourier potential series in electronography," Crystallography 1, 5, 495-501 (1956).

[8] V. N. Danilov, X-ray Scattering by Liquids [in Russian] (1935).

[9] L. I. Tatarinova, "Electronographic study of amorphous antimony," Trudy Inst. Krist. Akad. Nauk 11, 104-114 (1955).

Crystallography Institute
Academy of Sciences, USSR

Received November 29, 1956

---

* As in original — Publisher's note.

X-RAY EXAMINATION OF CAPTAX (2-MERCAPTOBENZOTHIAZOLE)

Iu. Tashpulatov, Z. V. Zvonkova and G. S. Zhdanov

The crystal structure of Captax, $C_7H_5NS_2$, is determined by x-ray analysis. The dimensions of the axes of the monoclinic cell are: a = 7.99, b = 5.99, c = 15.98 A and β = 109°10'. The number of molecules in the unit cell is Z = 4. The space group is $C_{2h}^5 - P2_1/c$. In the work $F^2(hkl)$-series were used chiefly. For refinement of the structure there were also constructed fractional projections of electron density ($^1/_2$ and $^1/_4$ cell along axis c) and a differential projection ($^1/_4$ cell), and also linear sections of electron density. Coordinates are determined for all atoms of the structure and calculations made for interatomic distances and valence angles. The crystallochemical analysis of the structure of Captax is given.

Crystallochemical examinations of heterocyclic compounds are of considerable theoretical interest; however, the structure of these compounds has been studied very little up to the present. Captax and its derivatives have wide application in industry [1, 2] as accelerators in the vulcanization of rubber.

For elucidation of some peculiarities in the structure of Captax, an x-ray examination was conducted. Single crystals of Captax suitable for structure analysis were obtained by recrystallization from solution in a mixture of xylenediol and chloroform, in the ratio 1 : 1. The results of the determination of crystal system, unit cell, number of molecules in the cell, density and space group of Captax crystals are given in Table 1.

TABLE 1

Formula	Crystal system	a in A	b in A	c in A	β	σ_X	σ_{II}	Z	Space group
$C_7H_5NS_2$	Monoclinic	7.99	5.99	15.98	109°10'	1.52	1.50	4	$C_{2h}^5 - P2_1/c$

On the basis of the projection of the interatomic vector functions on plane (010) (Fig. 1) some conclusions may be drawn as to the position of molecules in the unit cell of Captax. In the projection, clearly defined maxima of the function P(xoz) are observed with heights equal to 52 and 71. Analysis of this projection showed that these maxima correspond to the vectors $S_2^I - S_2^{II}$ and $S_1^I - S_1^{II}$, respectively. Hence it follows that the approximate distances between the atoms of sulfur in different molecules, $S_2^I - S_2^{II}$ and $S_1^I - S_1^{II}$, are equal to 1.76 and 4.77 A, respectively. On the basis of these data it may be concluded that the plane of a molecule of Captax (Scheme I)

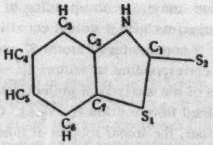

Scheme I

is nearly parallel to the Y axis and makes a small angle with the X axis. However the molecule is not packed longitudinally along axis a, and therefore it is necessary to propose that the direction of the bond $C_1 = S_2$ also forms an angle with plane (010). Coordinates of the atoms obtained from projection P(xoz) are: $x_{S_1^{II}} = 0.410$, $z_{S_1^{II}} = 0.374$, $x_{S_2^{II}} = 0.580$ and $z_{S_2^{II}} = 0.293$.

From the projection of the interatomic vector functions on plane (100), the following conclusions may be drawn as to the position of sulfur atoms. The y coordinates of atoms S_2^I and S_1^{II} differ approximately by $\frac{1}{2}$b.

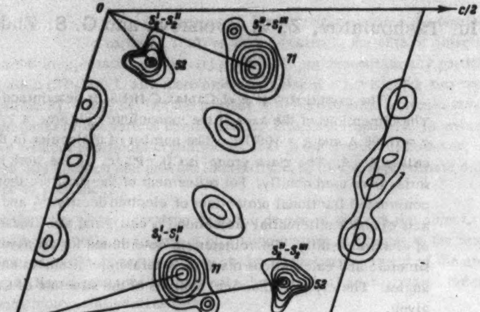

Fig. 1.

The y coordinates of atoms S_1^{II} and S_1^{III} are approximately the same, $\Delta y = y_{S_1^{II}} - y_{S_1^{III}} \approx 0$. Hence it follows that the sulfur atoms S_2^I and S_1^I in the molecule differ little in the value of the y coordinate, that is, to a first approximation $y_{S_2^I} - y_{S_1^I} \approx 0$. Such a distribution of atoms S_2^I and S_1^I is possible only in the case where the molecule is inclined to the plane (010), such that the bond $C_1 = S_2$ in the molecule forms an angle with the plane (010) approximately equal to 20°.

The structure of a five-membered heterocyclic ring which includes sulfur and nitrogen atoms has been studied very little up to the present time. It was therefore first necessary to set up a model of the molecule under study, specifically to model a five-membered ring. For this purpose the interatomic vector function $P(x\frac{1}{2}z)$ [3] was first calculated, which, along with the presence in the crystal of second-order screw axes allows the coordinates of atoms differing among themselves by $\Delta y = \frac{1}{2}b$ to be determined.

In the construction of these maps, the authors have used in all 672 reflections obtained by exposure of the crystals along axes b and c with Cu-emission in x-ray goniometer RGNS designed by M. M. Umanskii. Of this number of reflections 572 were obtained by exposure along axis b and 100 separate reflections by exposure along axis c.

Maxima observed in the section of function $P(x\frac{1}{2}z)$ correspond to the distribution of atoms the coordinates of which differ by $\frac{1}{2}$b (Fig. 2). In addition, maxima corresponding to vectors $S_2^I - S_2^{II}$ and $S_1^I - S_1^{II}$ have a weight equalling respectively 142 and 137, and maxima with a weight equalling 144 correspond to the interatomic vectors $S_1^I - S_2^{II}$. Hence it follows that the y coordinates of atoms S_1^I and S_2^{II} differ among themselves approximately by $\Delta y \approx \frac{1}{2}b$. The absence of maxima corresponding to vectors $S_1^{II} - S_1^{III}$ indicates that $y_{S_1^{II}} - y_{S_1^{III}} \approx 0$. Therefore derivations made earlier on the basis of the analysis of projections of the interatomic vector function on planes (010) and (100) confirm data obtained from section $P(x\frac{1}{2}z)$. Coordinates of atoms S_2^{II} and S_1^{II} obtained in this section are given in Table 2. Further, the linear section of function $P(0\ y\frac{1}{2})$ was calculated. If the crystal has a glide reflection plane, perpendicular to axis b with displacement equal to c/2, then equivalent

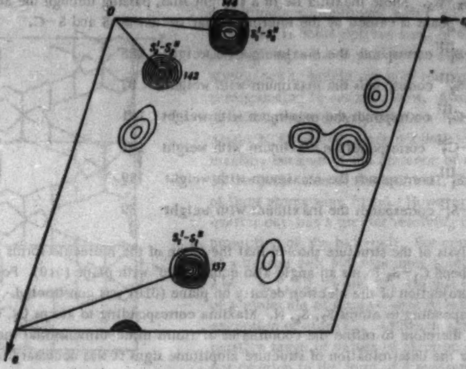

Fig. 2.

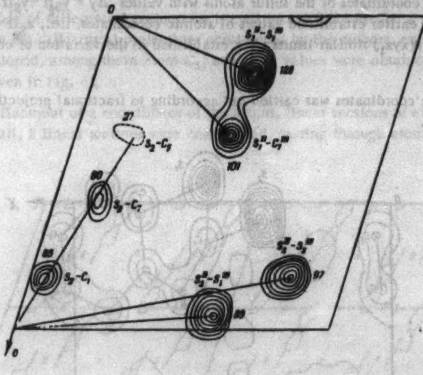

Fig. 3.

TABLE 2

Atoms	x	z
S_2^{II}	0.585	0.295
S_1^{II}	0.400	0.370

points have coordinates (x, y, z) and (x, $\frac{1}{2}$ −y, z + c/2). In addition, maxima of function P(x, y, z), corresponding to vectors between these atoms, have coordinates ± (0, $\frac{1}{2}$ −2y, c/2). According to the maxima of this function, the distribution of atoms can be found from the glide plane, equal to $\frac{1}{2}$ y_i, where y_i are coordinates of the corresponding maxima.

In section P(0 y$\frac{1}{2}$) there is the maximum of greatest weight with y_i = $\frac{1}{2}$ b. Hence it follows that $\frac{1}{2}$ −2y = = $\frac{1}{2}$; y ≈ 0, that is sulfur atoms occur in the coordinate plane $y_{S_1} \approx y_{S_2} \approx 0$. Further, for finding the distribution of the molecule in the unit cell, a section of the three-dimensional function P(x 0 z) (Fig. 3) was constructed, in which are shown separate maxima corresponding to the intramolecular distribution. Thus, the maximum with weight 86 corresponds to vector S_2-C_1, the maximum with weight 60 to vector S_2-C_7 and the maximum with weight 27 to vector $S_2 - C_8$. These maxima lie in a straight line, passing through the acute angle of the cell. The presence of other peaks is caused by the intermolecular vectors S−S and S−C.

To vector $S_1^{II} - S_1^{III}$ corresponds the maximum with weight 128

To vector $S_2^{II} - S_2^{III}$ corresponds the maximum with weight 97

To vector $S_1^{II} - C_7^{III}$ corresponds the maximum with weight 101

To vector $S_1^{III} - C_7^{II}$ corresponds the maximum with weight 101

To vector $S_2^{II} - S_1^{III}$ corresponds the maximum with weight 89

To vector $S_2^{III} - S_1^{II}$ corresponds the maximum with weight 89

Geometric analysis of the structure showed that the plane of the molecule forms an angle equal to 20° with plane (001), and the bond $C_1 - S_2$ forms an angle also equal to 20° with plane (010). For further refinement of the molecular model, a projection of the electron density on plane (010) was constructed. On this projection maxima were developed corresponding to atoms S_2, S_1, N. Maxima corresponding to atoms C_2, C_7 and C_4, C_6 overlap on the given projection; therefore to refine the coordinates of atoms three-dimensional maps of electron density were constructed. For the determination of structure amplitude signs it was necessary to refine the y coordinates of atoms S_2 and S_1. With this intention, we first constructed sections of the three-dimensional function $P(x_1yz)$ and $P(xyz_1)$ for $x_1 = x_{S_2}^{II} - x_{S_2}^{I}$ and $z_1 = z_{S_1}^{II} - z_{S_2}^{I}$. The calculation of function $P(x_1yz)$ permitted limiting the range of variations in the y coordinates of the sulfur atoms with values $\Delta y = y_{S_2}^{II} - y_{S_1}^{II} \approx 0.10-0.15$ ($y_{S_2}^{II} \approx 0.55$, $y_{S_1}^{II} \approx 0.45$) and confirmed earlier established values of atomic coordinates, i.e., $z_{S_2}^{II} = 0.295$, $z_{S_1}^{II} = 0.378$. In the calculation of function $P(xyz_1)$ similar limits were established in the variation of coordinates of atoms $y_{S_2}^{II}$ and $y_{S_1}^{II}$.

Refinement of atomic coordinates was carried out according to fractional projections [4] and linear sections of electron density.

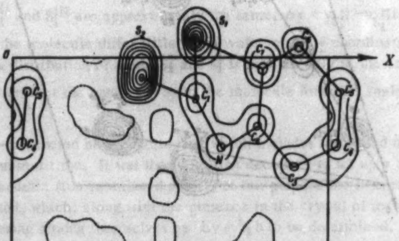

Fig. 4.

In the case of fractional projection of the half cell along axis c, the limits of integration can be taken from − c/4 to + c/4 or from 0 to + c/2. The first limits of integration are convenient for the structure of Captax, since in this case two molecules are isolated, connected by a center of symmetry. In addition, the sulfur atoms S_2 and S_1 of the first molecule will be superimposed correspondingly on atoms S_1 and S_2 of the fourth molecule. Therefore the authors have taken the limits of integration from 0 to c/2. In this case the sulfur atoms of two molecules connected by the screw axis are separated by ½ b, that is atoms S_2 and S_1 of the first molecule are removed by ½ b from atoms S_2 and S_1 of the second molecule.

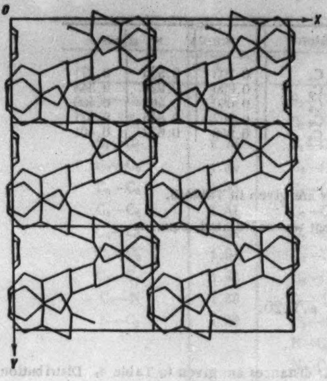

Fig. 5.

In the construction of the projection of the half cell only structure amplitudes with $l = 1, 3, 5, \ldots, 2n + 1$ were used, that is 386 amplitudes out of 672. On this projection, although superfluous peaks were absent, a considerable divergence in height ratios of maxima was observed, corresponding to carbon atoms. Atoms S_2, S_1, C_7, C_3, C_4, C_5 and C_2 were clearly developed on the projection. Atoms N, C_1 and C_6 were not developed in the form of maxima because of the presence of a swamping effect. By the projection of the half cell, coordinates of the series of light atoms were found. However, the projection of a quarter cell has a greater resolving capacity than the projection of the half-cell. For constructing the projection of a quarter cell 599 structures amplitudes were used with $l \neq$ 4, 8, 12, 16 and 20. On this projection all the atoms of a molecule of Captax were developed (Fig. 4), with the exception of atom C_1. Although atom C_1 falls in the positive range of values of electron density, yet it does not develop in the form of a separate maximum, apparently because of the effect of swamping from the heavy sulfur atoms S_1 and S_2.

At present the method of differential projections is used successfully for the x-ray determination of the position of light atoms. In the differential projections constructed by the authors, excluding sulfur atoms, all the light atoms were developed, among them atom C_1, and close values were obtained for heights of maxima of carbon atoms (atom C_1 given in Fig. 4).

For the proof and refinement of $\underline{z}$ coordinates of the atoms, linear sections of electron density parallel to the Z axis were used. In all, 8 linear sections were constructed, passing through atoms S_1, S_2, C_1, C_2, C_3, C_5, C_7 and N. As a result, it was established that atoms C_2, C_3, C_5 and C_7 are coplanar. Deviation of these atoms from the plane of the benzene ring amounts to a maximum ± 0.02 A. Therefore the calculation of the linear sections for atoms C_4 and C_6 was not carried out, and their $\underline{z}$ coordinates were found from the plane equation. Small deviations of the coordinates of the carbon atoms from the plane of the benzene ring lie within the limits of precision for the determination of interatomic distances in the structure of Captax, equal to ± 0.01-0.02 A. Atoms of the heterocyclic ring deviate from the plane of the benzene ring and their distances from the plane equal: N −0.15, S_1 −0.42, C_1 −0.17 and S_2 −0.25 A. The deviation of the atoms of the heterocyclic ring from coplanarity is also increased by the degree of removal from the center of the benzene ring.

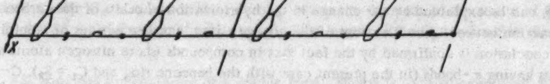

Fig. 6.

TABLE 3

Atom	x	y	z	Atom	x	y	z
S_2	0.591	0.563	0.300	C_7	0.203	0.533	0.371
C_1	0.418	0.654	0.318	C_3	0.090	0.920	0.343
N	0.340	0.842	0.315	C_6	0.080	0.468	0.406
S_1	0.407	0.412	0.377	C_4	0.962	0.845	0.371
C_2	0.207	0.758	0.345	C_5	0.956	0.622	0.401

The final coordinates of atoms in the structure of Captax are given in Table 3.

According to these coordinates, the Reliability Coefficient was calculated, equal to

$$R = \frac{\sum ||F_o| - |F_c||}{\sum |F_o|} = 0.20.$$

Interatomic distances, valence angles and intermolecular distances are given in Table 4. Distribution of the molecules in the Captax crystal is shown in Fig. 5 and 6.

Analysis of interatomic distances in the molecule of Captax (Scheme II) indicates that in this compound there are no C−N bonds which would be simple σ-bonds. The fact that the distance C_2-N and C_1-N proved to be considerably less than the distance C−N, characteristic for single bonds in compounds of the aliphatic series (1.47 A), can be explained by the change in the hybridization of orbits of the carbon atom (sp^2 instead of sp^3) and the reaction between free electrons of the nitrogen atom and p-electrons of adjoining carbon atoms C_2 and C_1. This conclusion is confirmed by the fact that in compounds where nitrogen atoms are connected with groups of atoms having π-bonds (in the present case with the benzene ring and $C_1 = S_2$), C−N distances vary over considerable limits, but always turn out to be less than 1.47 A [5]. In the x-ray examination of piazothiole [6, 7], benzofurazan [6] and isatin [8], in which the nitrogen atom is joined to the benzene ring, it was established that the distances of C−N bonds equal, respectively, 1.34, 1.35, and 1.38 A. Distances C_1-N and C_2-N in the Captax molecule equal, respectively, 1.29 and 1.39 A. The shortening of bond C_1-N 1.29 A in comparison with C_2-N 1.39 A indicates that the free electrons of the nitrogen atom interact more strongly with the p-electron of atom C_1 than with atom C_2. The difference in distances C_1-N and C_2-N in the Captax molecule is also confirmed by data of the literature. Thus, for example, in the examination of the structure of acetanilide [12] it was established that the nitrogen atom of the imino-group −NH− occurs at a distance of 1.426 A from the carbon atom of the benzene ring and at a distance of 1.330 A from the carbon atom of the acetyl group $-C{\overset{O}{\nwarrow}}$.

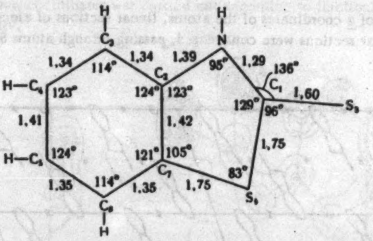

Scheme II

TABLE 4

Bonds	Interatomic distances in A	Bonds	Valence angles	Bonds	Intermolecular distances in A
$S_2—C_1$	1.60	$S_2—C_1—S_1$	96°	$S_2^I—S_2^{II}$	3.48
$C_1—S_1$	1.75	$C_1—S_1—C_7$	83°	$C_1^I—S_2^{II}$	3.08
$S_1—C_7$	1.78	$S_1—C_7—C_2$	105°	$S_2^I—S_1^{II}$	3.53
$C_7—C_6$	1.35	$C_2—C_7—C_6$	121°	$S_2^I—C_7^{II}$	4.60
$C_6—C_5$	1.35	$C_7—C_6—C_5$	114°	$S_2^I—N^{II}$	5.12
$C_5—C_4$	1.41	$C_6—C_5—C_4$	124°	$S_2^I—C_1^{II}$	3.57
$C_4—C_3$	1.34	$C_5—C_4—C_3$	123°	$S_2^{II}—N^I$	2.48
$C_3—C_2$	1.34	$C_4—C_3—C_2$	114°	$S_2^{II}—C_5^{II}$	2.89
$C_2—C_7$	1.42	$C_3—C_2—C_7$	124°	$S_2^{II}—C_4^{II}$	3.28
$C_2—N$	1.39	$C_7—C_2—N$	123°	$C_5^{II}—C_5^{III}$	3.38
$N—C_1$	1.29	$C_2—N—C_1$	95°	$C_4^{II}—C_4^{III}$	5.59
		$N—C_1—S_1$	129°	$C_6^{II}—C_6^{III}$	3.69
		$N—C_1—S_2$	136°	$S_1^{II}—S_1^{III}$	3.87
				$S_1^{II}—S_2^{III}$	5.14
				$C_6^I—C_3^I$	3.37

In structures of compounds in which the nitrogen atom of the amino-group is joined to a carbon atom having a double bond with a sulfur atom, >C = S, for example in dithioxamide [9] 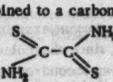, there is also found a shorter distance for C−N (1.308 A). For the nitrogen atom of the imino group, joined with two C = O groups, in saxinamide [10] there were also found short distances for C−N (1.27 and 1.26 A). For atoms of the imino group, joined with two benzene rings, for example in acridine [10], the C−N distance is 1.342 and 1.347 A, and in phenazine [11] it equals 1.342 and 1.345 A. In the structure of Captax, in the case of the nitrogen atom joined to the benzene ring, the distance C−N is increased compared with data from the literature to 1.39 A; for the nitrogen atom joined to the carbon atom with a double bond >C = S, the distance C−N is somewhat diminished (to 1.29 A). Crystallochemical analysis indicates that the interatomic distance C−N shortens with the degree of π-interaction in the side C=S bond.

Distances C_1-S_1 and $C-S_1$ in the Captax molecule equal respectively 1.75 and 1.78 A. For C−S bonds the interaction with part of the free electrons of the sulfur atom is considerable less than in the case of C−N bonds. The mean distance of the single bond ⋟C−S equals 1.81 A, according to the literature [13]. In the Captax molecule the distance S_1-C_7, equal to 1.78 A, corresponds to the decrease in the radius of the carbon atom with the change in the sp^3-hybridization of orbits to sp^2. The length of the $C_1=S_2$ bond in the Captax molecule equals 1.60 A.

Therefore the $C_1=S_2$ bond has the character of a double bond. Hence it may be concluded that in the crystalline state of the Captax molecule the hydrogen atom is covalently bonded with the nitrogen atom, and not with the S_2 sulfur atom.

Valence angles in a five-membered heterocyclic ring equal: $\measuredangle C_2NC_1 = 95°$ and $\measuredangle C_1S_1C_7 = 83°$. Owing to the strong interaction of the free electrons of the nitrogen atom with the C_1 carbon atom, the valence angle NC_1S_2 increases to 136°.

Valence angles in the benzene ring of the Captax molecule are distorted. It is known that in compounds which contain five-membered heterocyclic rings with benzene rings joined to them, the valence angles in these rings can be deformed.

In the structure of Captax the plane of the benzene ring forms a 21° angle with plane (001) and the $C_1=S_2$ bond forms a 23° angle with plane (010).

The results of the present examination repudiate earlier notions assumed in the chemical literature that the thiazole grouping is contained in the Captax molecule:

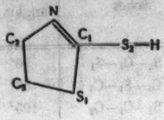

and confirm data obtained from infrared absorption spectra of Captax by Gur'ianova and Shigorin [14], which established the presence of strong hydrogen bonds.

Jeffrey indicated on the basis of preliminary x-ray examination that two molecules in the crystal of Captax are connected by a center of symmetry and form dimers [15]:

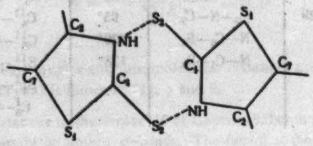

In the present examination it has been shown that the structural model of Captax proposed by Jeffrey is incorrect, since the molecules are connected by hydrogen bonds S...H–N not in dimers but in chains directed along second-order screw axes. Only by the projection of the structure along axis b are the second-order screw axes transformed into centers of symmetry, and consequently the chains of the molecule are projected in the form of dimers. In the structure of Captax the nitrogen atom is found at a distance of 2.48 A from the S_2 sulfur atom of the adjoining molecule. Therefore in Captax there are stronger intermolecular hydrogen bonds N–H...S than in the structure of thiopyridone, where the distance S...H–N equals 3.26 A [16]. The great diminution in intermolecular distance N–H... S is explained by the fact that the intermolecular radius of the S_2 atom along the double bond $C_1=S_2$ is considerably less than in the case of the single C–S bond.

For a molecule of thiopyridone the distance S–C (1.68 A) was obtained, increased in comparison with distance C_1-S_2 in the Captax molecule. In the structure of Captax the intermolecular distance between atoms of different molecules $C_5^{II}-S_2^{II}$ equals 2.89 A and angle $C_5S_2C_1$ equals 129°. Hence it may also be concluded that the intermolecular radius of the sulfur atom in the double bond C=S is considerably shortened in comparison with the intermolecular radius of the sulfur atom in the single C–S bond, which according to data in the literature equals 1.85 A.

The present work has further developed the hypotheses concerning intermolecular radii of nonspherical form and the dependence of intermolecular radii on the direction of σ- and π-covalent bonds in the molecule, established by the work of Zhdanov, Kitaigorodskii and others [17, 18].

LITERATURE CITED

[1] S. G. Bogomolov, I. Ia. Postovskii and Iu. N. Sheinker, "Infrared spectra and structure of thiosemicarbazone," Doklady Akad. Nauk SSSR 91, 5, 1111 (1953).

[2] B. A. Dogadkin, Chemistry and Physics of Rubber [In Russian] (1947) p. 346.

[3] N. V. Belov and V. I. Makeeva, "Application of methods of harmonic analysis for determining parameters of crystal structures by standard powder x-ray photographs," Trudy Inst. Krist. 5, 13 (1949).

[4] N. V. Belov and R. G. Matveeva, "Determination of parameters of beryl by partial projections method," Trudy Inst. Krist. 6, 70 (1951).

[5] S. Abrahams, "The crystal structure of p-nitroaniline $NO_2 \cdot C_6H_4 \cdot NH_2$," Acta Cryst. 1, 252 (1948).

[6] V. Luzzati, "Structure crystalline de piasélenol, piazthiol et benzofurazane," Acta Cryst. 4, 193 (1951).

[7] V. Luzzati, "Structure crystalline piazthiol," Compt. rend. 227, 210 (1948).

[8] G. Goldschmidt, "The crystalline structure of isatin," Acta Cryst. 3, 294 (1950).

[9] B. Long, P. Markey and P. J. Wheatley, "The crystal structure of dithiooxamide," Acta Cryst. 7, 140, (1954).

[10] D. C. Phillips, "The crystal structure of acridine III," Acta Cryst. 9, 237 (1956).

[11] F. H. Herbstein and G. M. J. Schmidt, "The crystal and molecular structures of heterocyclic compounds II. P - Phenazine," Acta Cryst. 8, 406 (1955).

[12] C. Brown and D. Corbridge, "The crystal structure of acetanilide," Acta Cryst. 2, 711 (1954).

[13] E. Cox and G. Jeffrey, "Order length relationships of π-bonds in heteronuclear molecules," Proc. Roy. Soc. 207, 110 (1951).

[14] V. N. Vasil'eva and E. N. Gur'ianova, "The structure of 2-mercaptobenzothiazole and some of its derivatives," Zhur. Fiz. Khim. 28, 7 (1954).

[15] H. P. Koch, "Absorption spectra and structure of sulfur compounds. Vulcanization accelerators and related compounds," J. Chem. Soc. 2, 401-408 (1949).

[16] B. Penfold, "The crystal structure of α- thiopyridone," Acta Cryst. 6, 707 (1953).

[17] G. S. Zhdanov and Z. V. Zvonkova, "Development of crystallochemical hypotheses concerning the nature of intermolecular reactions and molecular radii based on x-ray analysis," Trudy Inst. Krist. 10, 30 (1954).

[18] A. I. Kitaigorodskii, T. L. Khotsianova and Iu. T. Struchkov, "The crystal structure of iodine," Zhur. Fiz. Khim. 27, 780 (1953).

L. Ia. Karpov Institute of Physical Chemistry Received November 19, 1956

METALLOGRAPHIC AND X-RAY DIFFRACTION STUDY OF ALLOYS IN THE ANTIMONY-IRIDIUM SYSTEM

R. N. Kuz'min, G. S. Zhdanov and N. N. Zhuravlev

X-ray and metallographic studies of a series of alloys in the Sb−Ir system have established the existence of two compounds, $IrSb_3$ and $IrSb_2$. The unit cell of $IrSb_2$ has been determined with: $a = 6.5 \pm 0.2$; $b = 6.5 \pm 0.2$; $c = 6.7 \pm 0.2$ A; $\beta = 115° \pm 1°$.

Preparation of Alloys

No data on the system antimony-iridium have been found in literature. The alloys were prepared from chemically pure metals. Samples were placed in argon-filled quartz capsules and melted either in a resistance furnace or in an oxygen flame. Alloys with high melting points were prepared by the powder method. For this purpose, powders of the components were carefully mixed and pressed (in a specially made press). They were melted in argon-filled quartz capsules under small positive pressure.

Melting points were determined from cooling curves recorded by automatic electronic potentiometer EPP-0.9 and also by the method of drop formation. On the basis of melting points and metallographic and x-ray diffraction data obtained from some of the alloys, the probable phase diagram of the Sb−Ir system was outlined (Fig. 1). The peritectic curve of formation of $IrSb_3$ crystals in the temperature range 800-950°C was obtained by quenching the melts at different temperatures and subsequent x-ray determination of the phases present.

Metallographic and x-ray Study of Alloys

Slowly cooled melts with a high content of Sb (up to the composition $IrSb_3$ − 34.59% Ir by weight) consist of the eutectic ($IrSb_3$ + Sb) and crystals of $IrSb_3$. Fine crystals of $IrSb_3$ were separated from the alloy by dissolving antimony in a mixture of HNO_3 and HCl. The microscope showed these crystals to be cubes and cubes modified by the rhombic dodecahedron (Fig. 2,a). Tempered $IrSb_3$ alloys are single-phased and consist of $IrSb_3$ compound. Normally cooled alloys are heterogeneous. The peritectic reaction of crystallization of $IrSb_3$ is not completed under normal conditions of cooling.

Both quickly and slowly cooled $IrSb_2$ alloys are homogeneous compounds containing 44.11% of Ir by weight. Identical powder photographs were obtained from quickly and slowly cooled crystals of $IrSb_2$, indicating that the $IrSb_2$ compound is not polymorphic.

Slowly and quickly cooled alloys of the composition IrSb (61.22% Ir by weight) appear to be heterogeneous under the microscope and consist of crystals of $IrSb_2$ and iridium. Polished sections of these alloys show light-colored iridium crystals in a ground mass of $IrSb_2$ crystals. Calculations and indexing of the powder photographs of the slowly cooled IrSb alloy show that it consists of two phases, crystals of $IrSb_2$ and iridium; no period change was observed in the lattice of iridium. Alloys with a higher content of iridium were not studied because of their high melting points.

Density and Microhardness of the Alloys

The densities of the alloys σ_{hydr} were determined on a hydrostatic balance [1] in carbon tetrachloride. Table 1 gives σ_{hydr} and σ_x, computed on the basis of the x-ray data obtained at room temperature. The

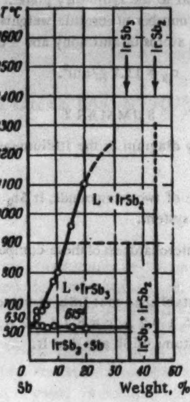

Fig. 1.

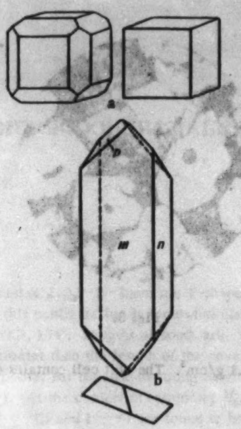

Fig. 2.

TABLE 1

Compound	σ_{hydr}, g/cm^3	σ_x, g/cm^3	Average microhardness, kg/mm^2	Scatter of microhardness, kg/mm^2
Sb	6.6-6.65	6.69	130	120-140
IrSb$_3$	8.9	9.41	770	700-800
IrSb$_2$	10.85	11.1	1130	1100-1150
Ir	22.4-22.5	22.65	655	500-680

densities of Ir and Sb are given according to reference [2]. The microhardness of the alloys was determined on the PMT-3 instrument with constant load of 10 g on the iridenter. Determinations were made on several samples from different melts, and also on crystals of IrSb$_3$ and IrSb$_2$ separated from the alloys. The results were averaged. Table 1 gives average microhardness and the range of its variation.

X-ray Study of the Alloys

The structure of IrSb$_3$ was determined earlier from powder photographs [3]. The compound IrSb$_3$ crystallizes in the isometric system with a = 9.230 ± .002 kX and is isostructural with the mineral skutterudite CoAs$_3$ [4].

Crystals of IrSb$_2$ were grown in the melts and separated by dissolving antimony with an HCl + HNO$_3$ mixture. Figure 3 is a photomicrograph of such an alloy with 28% Ir by weight, cured at a temperature of 1000°C and then cooled quickly. It shows light-colored polyhedral crystals of IrSb$_2$ in the etched eutectic ground-mass. The crystals of IrSb$_2$ have the habit shown in Fig. 2,b, as well as some other forms produced by twinning. Crystal faces have ideal reflectivity.

Measurements on a goniometer and on Laue photographs show that crystals of IrSb$_2$ are monoclinic. Regular twinning on [100] was observed on a number of crystals. Oscillation photographs obtained with Cu radiation by the RKOP camera gave the following dimensions of the unit cell:

$$a = 6.6 \pm 0.2\ \text{A};\ b = 6.5 \pm 0.2\ \text{A},\ c = 6.7 \pm 0.2\ \text{A}.$$

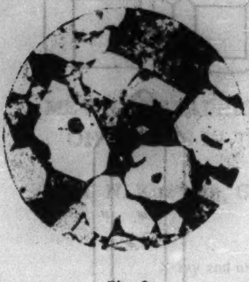

Fig. 3.

The monoclinic angle $\beta = 115° \pm 1°$ was determined from a Laue photograph taken normal to the symmetry plane. With $\sigma_{hydr} = 10.85$ g/cm^3 and the number of formula weights $z = 4$, the unit cell of $IrSb_2$ contains 8 atoms of antimony and 4 of iridium;

$$\sigma_x = 11.1 \text{ g/cm}^3.$$

SUMMARY

1. A preliminary diagram of the iridium-antimony system has been obtained.

2. The existence of two compounds, $IrSb_2$ and $IrSb_3$ has been discovered in the system.

3. Density and microhardness of these compounds have been determined.

4. It has been established that $IrSb_2$ is monoclinic with $a = 6.6 \pm 0.2$ A, $b = 6.5 \pm 0.2$ A; $c = 6.7 \pm 0.2$ A; $\beta = 115° \pm 1°$; $\sigma_x = 11.1$ g/cm^3. The unit cell contains 4 formula weights, i.e., 8 atoms of Sb and 4 of Ir.

LITERATURE CITED

[1] E. M. Bronshtedt-Kupletskaya, in the book: Determination of Specific Gravity of Minerals,* 43-55 (1951).

[2] M. P. Slavinskii, in the book: Physicochemical Properties of Elements,* (1952).

[3] N. N. Zhuravlev and G. S. Zhdanov, "X-ray determination of the structure of $CoSb_3$, $RhSb_3$ and $IrSb_3$," Crystallography 1, 3 (1956).

[4] J. Oftedel, Die Kristallostruktur von Skutterudit und speiskobalt-chloanthit. Z. f. Krist. 66, Hf. 5/6, 1927/28.

M. V. Lomonosov State University of Moscow

Received October 17, 1956

---

* In Russian.

THE CRYSTAL STRUCTURES OF DIPHENYLIODONIUM HALIDES

T. L. Khotsianova

The chloride and iodide of diphenyliodonium – $(C_6H_5)_2I-Cl$ and $(C_6H_5)_2I-I$ – have the T-shaped configuration characteristic of trivalent iodine. Owing to steric hindrance this configuration is somewhat distorted, for example for $(C_6H_5)_2I-Cl$: $< C_1-I-C_1'$, 9.8°; $< C_1-I-Cl$, 87°; $< C_1'I-Cl$, 174°. Lengths of bonds are: C–C, 1.40 A and C–I, 2.08 A. Distance I–Cl, 3.08 A, is considerably greater than the length of the covalent bond I–Cl (2.32-2.35 A). Atoms C_1, I, C_1' and Cl lie practically in one plane, but because of strong steric hindrance the benzene rings are brought out of it by a turn round the bond C–I. At the centers of symmetry ¼, ¼, 0 the molecules join in pairs. In addition the intermolecular distances I – – – Cl and I – – – I are found to be greatly diminished (3.20 A for I – – – Cl and 3.34 A for I – – – I).

The determination of the structures of the chloride $(C_6H_5)_2I-Cl$ and the iodide $(C_6H_5)_2I-I$ of diphenyliodonium has been described in a report [1]. Crystals of these two compounds were found to be completely isomorphic, and therefore only one of them is examined in detail below, the structure of the chloride, and in the iodide only the distribution of the heavy atoms is analyzed.

TABLE 1

Intermolecular Distances and Structures of Diphenyliodonium Chlorides

Atoms	Bonds between molecules	Distances in A	Atoms	Bonds between molecules	Distances in A
$C_4(I) - C_3(IV)$	$2_1\left[\frac{1}{4}\, y\, -\frac{1}{4}\right]$	3.55	$(I) - (III)$	$\bar{1}\ (-\frac{1}{4}\ -\frac{1}{4}\ 0)$	4.24
$C_4(I) - C_3(IV)$	» »	3.82	$(I) - Cl(III)$	» »	3.20
$C_4(I) - C_2(IV)$	» »	(4.01)	$Cl(III) - C'(I)$	»	3.47
$C_3(I) - C_4(IV)$	» »	3.87	$Cl(III) - C_6'(I)$	» »	(3.77)
$C_3(I) - C_4(IV)$	» »	(3.82)	$Cl(III) - C_5'(I)$	» »	3.82
$C_3(I) - C_3(IV)$	» »	4.21	$Cl(III) - C_3'(I)$	» »	(4.04)
$H_4(I) - H_3(IV)$	» »	3.21	$Cl(III) - C_2(I)$	» »	(4.14)
$H_4(I) - H_3(IV)$	» »	(3.30)	$Cl(III) - H_6'(I)'$	» »	(2.69)
$C_4(I) - H_3(IV)$	» »	3.01	$Cl(III) - H_2'(I)$	» »	3.61
$C_4(I) - H_3(IV)$	» »	(4.30)	$C_6'(I) - C_4'(II)$	$\bar{1}$ (000)	3.66
$C_3(I) - H_4(IV)$	» »	2.88	$C_6'(I) - C_5'(II)$	» »	3.68
$C_3(I) - H_4(IV)$	» »	(4.23)	$C_5'(I) - C_6'(II)$	» »	3.80
$C_5(I) - C_4'(V)$	$2\left[0\, y\, -\frac{1}{4}\right]$	3.55	$C_6'(I) - H_5'(II)$	» »	3.94
$C_5(I) - C_4'(V)$	» »	(4.94)	$C_5'(I) - H_6'(II)$	» »	(4.10)
$C_5(I) - C_5'(V)$	» »	4.25	$H_6'(I) - H_5'(II)$		(3.40)
$C_5(I) - C_5(V)$	» »	(3.96)	$H_5'(I) - H_6'(II)$		(3.42)
$C_5(I) - H_4(V)$	» »	2.90	$Cl(III) - H_5'(II)$	$\frac{1}{2}(\vec{a}+\vec{b})$	3.30
$C_4'(V) - H_1(I)$	» »	2.54	$Cl(III) - G_4'(II)$	» »	3.93
$H_4'(V) - H_5(I)$	» »	2.16	$H_4'(II) - H_2(III)$	» »	3.07
$H_5'(V) - H_5(I)$	» »	(2.29)			

The projection of the structure of diphenyliodonium chloride on face ac is presented in Fig. 1. Here the numeration of atoms and the shortest intermolecular distances are indicated. At the top of the figure the skeletal scheme is given, and below the packing of molecules, "framed" by means of intermolecular radii.

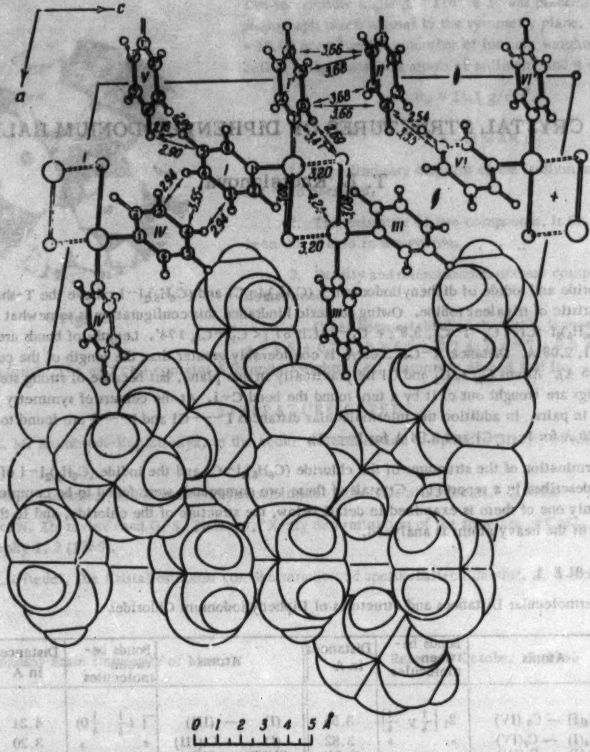

Fig. 1. Projection of structure of diphenyliodonium chloride on face ac (with indication of the shortest intermolecular distances).

Values of all distances corresponding to intermolecular contacts (or somewhat greater) are presented in Table 1. In parentheses are given distances between atoms, one of which is derived from the original with a necessary translation along axis b.

It is convenient to regard the packing of molecules in the crystal as a single layer in a plane parallel to ac. Close superposition of layers is achieved by screw axes 2_1 with contacts C---C (3.55 A) and C-----H (2.94 A). Contacts that are achieved in a layer are as follows: C----C (3.55 A), H----H (2.16 and 2.29 A) and C----H (2.54 A). The latter distance is substantially diminished (by 0.37 A) in comparison with the sum of the intermolecular radii.

The intermolecular radii calculated according to the distances in the structure in question are as follows: I –2.12 A, C –1.79 A and H –1.12 A. These values agree well with the standard (I –2.10 A, C –1.80A, H – 1.17 A).

The heavy atoms grouped by fours at the centers of symmetry $1/4$, $1/4$, 0. This group of four atoms of iodine and chlorine is located practically in one plane, forming a tetragon, close to a square with angles Cl---I–Cl = = 94° 58' and I---Cl–I = 84° 50' and sides 3.08 and 3.20 A. In the structure such tetragons form columns along

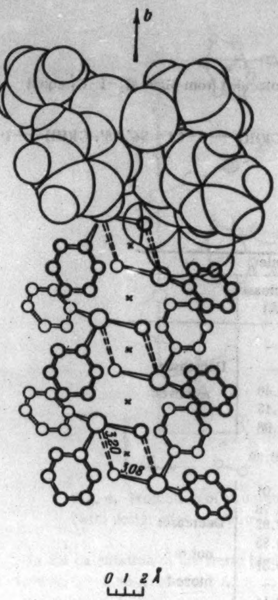

Fig. 2. Column of tetragons of heavy atoms in structures of diphenyliodonium halides.

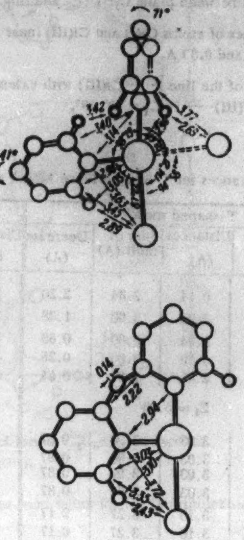

Fig. 3. Molecule of diphenyliiodonium chloride.
Top – configuration according to the results of the present examination;
Bottom - coplanar T-shaped configuration.

direction b, "framed" by phenyl groups connected by valence bonds with iodine atoms (Fig. 2).

The model found for the molecule is given in Fig. 3, with all interatomic distances indicated. Lengths of bonds are C–C = 1.40, C–I = 2.08, I–Cl = 3.08 A; thus, bonds C–C and C–I have the usual length established in other structures. The molecule has a T-shaped configuration; valence angles are $C_1-I-C_1' = 98°\ 19'$, $C_1-I-Cl = 87°\ 22'$, $C_1'-I-Cl = 174°\ 27'$. The deviation of the I–C bonds from the diagonals of the benzene rings[*] $I-C_1-C_4 = 3°\ 41'$ (angle of bond $I-C_1$ with plane of ring, 1° 03'); $I-C_1'-C_4' = 14°\ 20'$ (angle of bond $I-C_1'$ with plane of ring, 11° 49').

Equations of planes of benzene rings[**]

$$\text{ring I}\quad 0.645x + 0.584y - 0.493z - 1.994 = 0,$$
$$\text{ring I}'\quad 0.087x - 0.359y - 0.929z + 7.614 = 0.$$

Equation of plane C_1-I-C_1':

$$-0.0134x + 0.7666y - 0.6420z + 4.9810 = 0.$$

The benzene rings do not lie in the plane C_1-I-C_1'; they are brought out of the coplanar disposition by a turn round bonds C–I (Fig. 3):

---

[*] The deviation of the $I-C_1$ and $I-C_1'$ bonds from the diagonals of the benzene rings and the distortion of normal (120°) valence angles of "key" carbon atoms is explained by the steric factors and in magnitude do not exceed analogous alterations in other structures.

[**] Equations of planes are given in orthogonal coordinates *abc.

angle between planes of benzene rings 72° 16';
angle between plane C_1-I-C_1' and ring I: 40° 55';
angle between plane C_1-I-C_1' and ring I': 71° 20';

The distances of atoms Cl(I) and Cl(III) (near atom of adjoining molecule) from plane C_1-I-C_1' equal respectively 0.17 and 0.33 A.

The angles of the line I---Cl(III) with valence bonds of atom I: Cl(III)---I−Cl = 94° 58'; Cl(III)---I−C = 172° 34'; Cl'(III)---$I-C_1'$ = 79° 03'.

TABLE 2

Steric Hindrances for T-Shaped Plane Model and Real Molecule

Atoms	T-shaped model			Real molecule			
	Distances (A)	Sum of radii (A)	Decrease (A)	Distances (A)	Sum of radii (A)	Decrease (A)	
H_6-H_2'	0.14	2.34	2.20	3.42	2.34	—	Decreases removed
C_6-C_2'	2.22	3.60	1.38	3.95	3.60	—	
C_1-C_1'	2.94	3.60	0.66	3.14	3.60	0.46	
$Cl-C_2$	3.35	3.60	0.25	3.45	3.60	0.15	
$Cl-H_2$	2.43	2.97	0.54	2.89	2.97	0.08	
	$\Sigma_1 = 5{,}03$					$\Sigma_1' = 0.69$	
$C_2'-I$	3.03	3.90	0.87	2.89	3.90	1.01	Decreases not removed
C_6-I	3.03	3.90	0.87	3.14	3.90	0.76	
C_2-I	3.03	3.90	0.87	2.98	3.90	0.92	
$C_6'-I$	3.03	3.90	0.87	3.05	3.90	0.85	
$H_6'-I$	3.10	3.27	0.17	2.96	3.27	0.31	
H_6-I	3.10	3.27	0.17	3.31	3.27	—	
$H_2'-I$	3.10	3;27	0.17	3.16	3.27	0.11	
H_2-I	3.10	3.27	0.17	3.03	3.27	0.24	
	$\Sigma_2 = 4.16$					$\Sigma_2' = 4.20$	
	$\Sigma_1 + \Sigma_2 = 9.19$					$\Sigma_1' + \Sigma_2' = 4.89$	

The plane model of a molecule of diphenyliodonium chloride with an ideal T-shaped configuration (i.e., with angles C_1-I-Cl and C_1-I-C_1' = 90° and angle $C_1'-I-Cl$ = 180°) is shown in Fig. 3. In such a molecule there are very great steric hindrances (Table 2): the sum of the decreases of all intramolecular distances from their normal values is equal to 9.19 A (5.03 A may be removed from them by changing the valence angles, so that 4.16 A remains). In the real model a large part of the steric hindrances is removed or considerably decreased by means of the above-indicated turns of the benzene rings round the bonds C−I and some alteration of the valence angles C_1-I-C_1', C_1-I-Cl and $C_1'-I-Cl$. The sum of the steric hindtances is thereby decreased to 4.89 A, only 0.69 A being removed from them.

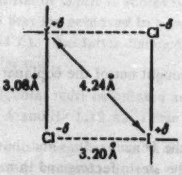

Scheme I

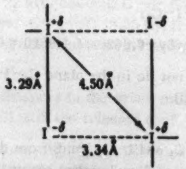

Scheme 2

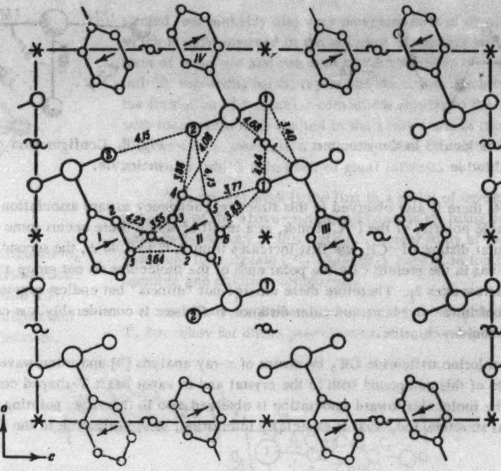

Fig. 4. Projection of structure of benzene iododichloride $C_6H_5ICl_2$ on face ac (with designation of shortest intermolecular distances).

In the calculation of the steric hindrances standard values were taken for the intermolecular radii I −2.10 A; Cl −1.80 A; C − 1.80 A; H −1.17 A.

The most interesting feature of the structure is the pairing of molecules at the centers of symmetry of the type $1/4$, $1/4$, 0 with the unusually small "intermolecular" distance I−−−−Cl = 3.20 A (instead of the sum of intermolecular radii 2.12 + 1.79 = 3.91 A). This distance exceeds by only 0.12 A the intramolecular distance I−Cl = 3.08 A and characterizes the singular "dimerization" of the molecules in the crystal. Undoubtedly, the bond I − Cl in the molecule $(C_6H_5)_2I{-}Cl$ is strongly polar. Actually, in the case of the covalent bond the distance I−Cl should work out to 2.32-2.35 A. Considering the strong polarization of the bond I−Cl, the "dimer" complex can be viewed as having a certain analogy to the hydrogen bond (for example, in dimers of organic acids, see Scheme 1).

A tendency toward a similar dimerization in a crystal* is manifest in the substantial change in the intramolecular and intermolecular distance I−Cl. The first increases and the second decreases, the increase and decrease being practically the same (0.7-0.8A). One of the obstacles to a complete equality of both distances is the steric hindrance between the chlorine atom of the adjoining molecule and the benzene ring (distance Cl(III)−−−H_6'(I) = 2.69 A, decrease by 0.22 A).

In the structure of diphenyliodonium iodide the formation of a "quadrupole" is accompanied by still greater equalization of the intra- and intermolecular distance. The first increases from 2.66 to 3.29 A, the second decreases from 4.2 to 3.34 A. Both distances are found to be practically equal, which is to be expected since in this case the quadrupole is formed by atoms of one sort (see Scheme 2).

The T-shaped valence configuration of the iodine atom with valence angles close to 90° and 180° was established earlier [2] in the crystal of phenyliodochloride [benzene iododichloride (iodobenzene-chlorine complex)] $C_6H_5ICl_2$ (Fig. 4). The molecule of benzene iododichloride is plane with angles Cl−C−I = 86° and length of bond I − Cl = 2.45 A.

---

* Dimerization apparently may also be observed in solution. In this connection the determination of molecular weight of diphenyliodonium halides in different solvents would be of great interest.

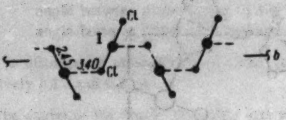

Fig. 5. Segment of molecules in the structure of benzene iododichloride .

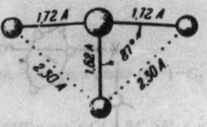

Fig. 6. Configuration of ClF_3 molecule.

As seen in Fig. 4, there is also observed in this structure a tendency toward association in the crystal by virtue of the considerable polarity of the I−Cl bonds, as a result of which there occurs some equalization of the intra- and intermolecular distance I−Cl: the first increases from 2.32 to 2.45 A, the second decreases from 3.90 to 3.40 A. However, in the present case the polar ends of the molecules do not group at the centers of symmetry, but at the screw axes 2_1. Therefore there emerge not "dimers" but endless segments of molecules (Fig. 5). Equalization of intra- and intermolecular distance I−Cl here is considerably less complete than in the structure of diphenyliodonium chloride.

Examination of chlorine trifluoride ClF_3 by means of x-ray analysis [3] and microwave spectroscopy [4] showed that a molecule of this compound both in the crystal and in vapor has a T-shaped configuration (Fig. 6). A strong tendency of the molecules toward association is observed also in this case, pointing to the lamellar character of the crystal structure and, what is especially interesting, to dimerization in the liquid and even in the gaseous state.

It is customary to derive the valence configuration of trivalent iodine, bromide and chlorine [2, 3] and also tetravalent selenium and tellurium from a trigonal bipyramid (Fig. 7); three (or four) electrons form hybrid bonds sp^3d, and one or two points to the pyramid "remain occupied by unpaired electrons.". We think that such a derivation is rather lacking in rigor and needs corroboration by quantum mechanical calculation.

In conclusion it is expedient to dwell on the valence configuration of pentavalent iodine. The structures of n-chloriodoxybenzene [5] [p-chloroiodobenzene dioxide] [para−chlor−iodoxy−benzene (ref. [5])]

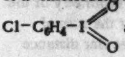

$Cl{-}C_6H_4{-}I\begin{smallmatrix}\nearrow O\\ \searrow O\end{smallmatrix}$ and periodic acid [6] have been examined in detail.

From the standpoint of quantum chemistry the iodine atom in these compounds is only formally pentavalent; it is more correct to consider it as trivalent doubly-ionized iodine with electronic configuration. As in

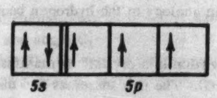

the case of trivalent iodine, here there are three σ-bonds; only one of them is covalent, and two are semi-polar (doubly disconnected). However in contrast to trivalent iodine these bonds will form only on account of the p-electrons, which also will bring about a valence configuration of the trigonal pyramid with valence angles of iodine equal to 90°. Actually in the anion IO_3^- the valence angles O−I−O equal 96.98 and 101°, i.e., some deviate from 90° to the plus side on account of mutual repulsion of the oxygen atoms, and the bonds I−O have a length of 1.80, 1.81 and 1.89 A.

In the molecule of p-chloroiodobenzene dioxide (Fig. 7) the valence angle O−I−O equal 103°, and valence angle C−I−O amount to 94 and 95°. The deviation of angle O−I−O from 90° is well explained by the interaction between atoms I and O of different molecules; actually, the corresponding distances I------O amount to 2.62 A (instead of 3.3-3.4 A, corresponding to the sum of the intermolecular radii), i.e., here also there is observed a tendency toward association in the crystal with the formation of infinite segments (as in the structure of benzene iododichloride).

The tendency of the molecule toward association in the crystal is not confined to iodo-organic compounds. Until now the case studied in most detail was association due to formation of hydrogen bonds. We wish to note, also, the much less studied, but probably also very prevalent case of dipole-dipole association, which is duly observed in the presence of strongly polar bonds and a suitable form of molecule and can lead to the formation of not only dimers, but infinite segments, bands, layers and skeletons. Such association can cause the formation of molecular compounds similar to the complexes of coumarin with mercuric halides studied in the x-ray analysis laboratory of this institute [7]. As a rule, association is accompanied by substantial deformation of molecules, which is in itself of great interest.

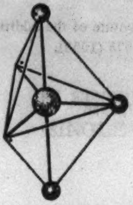

Fig. 7. Valence configuration, corresponding to hybridization sp^3d, and the derivation from it of a T-shaped configuration with two unpaired electrons.

The present work is the first in a series of investigations of the crystal structures of the above-mentioned compounds being conducted in the x-ray analysis laboratory of this institute. Under study at present is diphenyliodonium fluoroborate $[(C_6H_5)_2I][BF_4]$, having an ionic structure, and some bromine and chlorine compounds.

In conslusion I consider it my pleasant duty to express thanks to Iu. T. Struchkov for direct participation in conducting the investigation and to the laboratory director A. I. Kitaigorodskii for constant interest and attention.

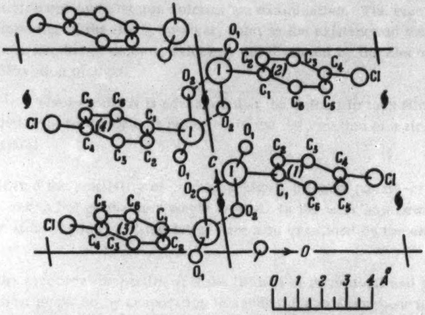

Fig. 8. Projection of structure of p-chloroiodobenzene dioxide on face ac.
Decreased intermolecular distances I---O, between molecules, connected by axes 2_1, are indicated by a broken line.

LITERATURE CITED

[1] T. L. Khotsianova, "Determining the structures of diphenyliodonium chloride and iodide," Kristallografiia 1, 5, 524 (1956).

[2] E. M. Archer and T. G. D. van Schalkwyk, "The crystal structure of benzene iododichloride," Acta Cryst. 6, 88 (1953).

[3] R. D. Burbank and F. N. Bensey, "The structures of the interhalogen compounds I. Chlorine trifluoride at −120°C," J. Chem. Phys. 21, 602 (1953).

[4] D. F. Smith, "The microwave spectrum and structure of chlorine trifluoride," J. Chem. Phys. 21, 609 (1953).

[5] E. M. Archer, "The crystal structure of para−chlor−iodoxy−benzene," Acta Cryst. 1, 2, 64 (1948).

[6] M. T. Rogers and L. Helmholtz, "The crystal structure of iodic acid," J. Am. Chem. Soc. 63, 278 (1941).

[7] Iu. T. Struchkov, A. I. Kitaigorodskii and T. L. Khotsianova, "The crystal structure of the addition compounds $HgCl_2$ • coumarin (I) and $HgBr_2$ • coumarin (II)," Doklady Akad. Nauk 93, 4, 675 (1953).

Institute of Elemento-organic Compounds
Acad. Sci. USSR

Received October 17, 1956

ELECTRICAL PROPERTIES AND REAL STRUCTURE OF SINGLE-CRYSTAL GERMANIUM FILMS PRODUCED BY EVAPORATION IN VACUUM

G. A. Kurov, S. A. Semiletov and Z. G. Pinsker

A study has been made of the electrical properties and structure of single-crystal germanium films produced by evaporation in vacuum on surfaces of germanium single crystals. The single-crystal character of the films, found by electron diffraction analysis, is confirmed by microscope and electron-microscope examination. The electrical properties of the films, however, point to the existence in them of a large number of defects, evidently not disclosed by the electron diffraction method.

The hypothesis is advanced that the defects in such films are analogous to the defects produced in the deformation of a single crystal.

Previous work [1] indicated the possibility of producing highly oriented (single-crystal) germanium films by evaporation in a vacuum onto a hot germanium single crystal. In the work now described, electrical measurements were made on similar films, and the latter were also examined by the electron diffraction method and microscopically.

The investigation of the electrical properties of these films is of theoretical and practical interest. It is known that germanium films, produced by evaporation in vacuum on an amorphous support (glass, quartz, etc.) consist of very small crystals about 10^{-5}-10^{-6} cm in size. Such finely crystalline films have relatively high electrical conductivity and the type of their conductivity (hole type) does not depend upon the type of conductivity of the evaporated material. The mobility of the charge carriers in such films is considerably less than in compact specimens. The above-mentioned difference between the electrical properties of evaporated germanium films and those of compact specimens is explained in the literature [2] as being due to the influence of acceptor surface levels, which are of decisive significance in finely crystalline films. If the dimensions of the small crystals in the film are increased, however, the part played by the surface levels ought rapidly to diminish. At the same time, one would expect the electrical conductivity of the film to diminish and the sign of the charge carriers in it to be determined by the type of conductivity of the evaporated material. With increase in size of the small crystals, the mobility of the carriers ought also to increase. Judging by the data given in the literature, the influence of the surface levels ought not to count at crystal dimensions of about 10^{-3} cm.

The study of single-crystal germanium films is also of interest from the point of view of their technical application.

In the work described in Reference [1], the supports employed were single crystals of germanium, etched after polishing and heated to a temperature of about 900°C. The thickness of the films in [1] did not exceed 2μ. In the present work, thicker films (up to 20-30μ, area $\sim 10 \times 4$ mm^2) were obtained by evaporating in vacuum pieces of (n and p) germanium having a specific resistance of from 2 to 30 ohm · cm, which were placed in a tungsten or graphite holder and heated by electron bombardment. Evaporation was either onto a surface of germanium single

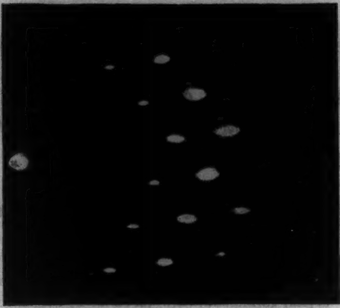

Fig. 1. Electron diffraction pattern from a germanium film produced by evaporation on to a crystal heated to 550°C.

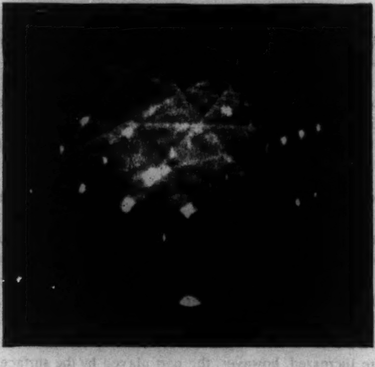

Fig. 2. Electron diffraction pattern with Kikuchi lines and bands from a single-crystal germanium film, produced by evaporation on to a crystal heated to 900°C.

crystals, preliminarily etched in boiling hydrogen peroxide for from 5-10 minutes, or on to a cleavage face of these single crystals.

As the result of numerous experiments, it was found that in order to produce films with a sufficiently perfect structure (for film thicknesses of up to 20-30 μ), evaporation had to be carried out on to single crystals heated to above 750-800°C, the structure of the films being more nearly perfect, the higher the temperature of the support. With supports at lower temperatures (500-700°C) the films formed have a quite imperfect structure. The electron diffraction patterns of such films show many spots arranged in the form of a regular network (Fig. 1). This is evidence of the mosaic structure of the films, i.e., of the presence in them of individual blocks, rotated through angles of about 2-3° relatively to each other. A substantially different picture is obtained by evaporating on to single crystals heated above 750-800°C. The electron diffraction patterns obtained from such films (Fig. 2) show fairly sharp Kikuchi lines and bands, characteristic of single crystals with perfect structure of the surface layer [3]. This indicates that a film formed by evaporation on to single crystals is a single-crystal film.

Electrical measurements of the films were also made at the same time as the structure investigations. The specific resistance, Hall emf and thermo-emf were measured. The film thickness was determined by weighing. The material of the supports consisted of plates of n and p type germanium having a specific resistance of from 2-30 ohm•cm. The mobility of the charge carriers in such plates, as determined from the ratio of the Hall constant to the specific resistance, was $1\text{-}2.5 \cdot 10^3$ cm²/v•sec at room temperature.

Fig. 3. Photograph of etched surface of germanium drop (× 1012.5).

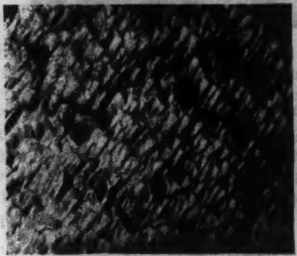

Fig. 4. Photograph of a germanium film produced on the polished surface of a single crystal heated to 550°C (× 300).

In the present work, films were also evaporated on to glass and polished corundum (at support temperatures of, respectively, 450-550°C and 750-900°C). The films on glass at room temperature had a specific resistance of $2\text{-}7 \cdot 10^{-2}$ ohm•cm; the mobility of the charge carriers (holes) in such films was within the limits of 70-250 cm²/v•sec. The films of corundum had a specific resistance of about $1\text{-}5 \cdot 10^{-1}$ ohm••cm; the carrier mobility was 300-450 cm²/v•sec. It should be pointed out that when the germanium films were annealed at temperatures of 500-900°C for 6-12 hours, their electrical properties were only slightly altered. For example, such annealing caused the specific resistance to be increased by 10-20%.

The films on a single-crystal support were subjected to further investigation. It could be assumed that the electrical properties of the highly oriented (single-crystal) film would not differ substantially from the properties of the compact specimen, since such a film ought to continue the single-crystal lattice. Furthermore, the grown-on layer of a thickness of about 10^{-3} cm ought not to influence appreciably the properties of the single crystal as a whole. A rather unexpected result, however, was obtained. It was found that a film of a thickness of several microns shunts the single crystal of thickness of about 1 mm. For example, in one of the experiments, a film of thickness 18.5 μ was formed at 550°C on a germanium crystal of thickness 0.7 mm and specific resistance $\rho = 10.5$ ohm•cm. The result was that the effective specific resistance of the entire specimen (film + single crystal) was diminished to 0.83 ohm•cm. For the film it was $2.2 \cdot 10^{-2}$ ohm•cm.

It should be remarked that the evaporated film adhered permanently to the crystal and it was found impossible to detach it. Measurements of the films were therefore made while taking into account the shunting effect of the support. The mobility of the charge carriers and their concentration in the film evaporated on the crystal were estimated as follows. The Hall emf of the crystal support was about 10^{-1} v, but after the evaporation of the film, it was about 10^{-3} v. The ratio of the resistances of crystal and film (in the direction in which the Hall emf was measured) was approximately 10. The Hall emf of the specimen, during the evaporation of

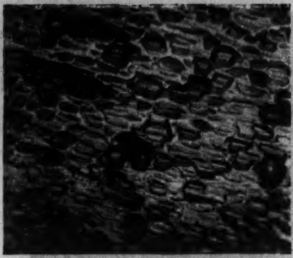

Fig. 5. Photograph of a germanium film produced on the polished surface of a single crystal, heated to 900°C (× 300).

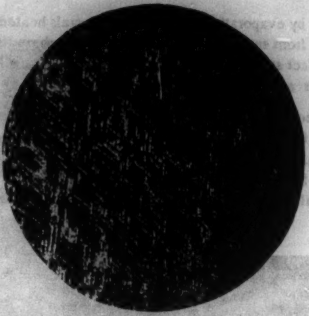

Fig. 6. Photograph of germanium film produced on the cleavage surface of a single crystal (× 405, dark field illumination), heated to 900°C.

the film, diminished rapidly, since the film shunted the crystal. It follows from this that the Hall emf in the film did not exceed about 10^{-3} v. It was therefore possible to determine the lower limit of the possible values of the carrier concentration and (from the product of Hall constant and conductivity) the upper limit of the values of charge carrier mobility in the film.

The measurements showed that the Hall constant and mobility in films evaporated on to a crystal are even lower than in the finely crystalline films evaporated on to corundum. Analogous results were obtained for films produced on the cleavage face of a single crystal. At the same time, no substantial difference was observed in the electrical properties of films produced on supports at temperatures of 550°C and 750-900°C. In all cases of the evaporation of a film on to a single crystal, the effective specific resistance of the specimen was sharply diminished, the Hall constant fell (by approximately 2 orders), and the mobility diminished sharply. In one case, for example, the Hall constant of the film was no more than about 3 cm^3/coul, specific resistance was 0.02 ohm·cm, and the carrier (hole) mobility did not exceed $1.5 \cdot 10^2$ $cm^2/v \cdot sec$.

It should be observed that all the films investigated possessed hole conductivity, regardless of the type of conductivity of the evaporated material and support (determination was made from the sign of the Hall constant and the thermal emf). Annealing the films did not materially affect their electrical properties. If electron-conducting germanium was used as support, heating to above 500°C followed by rapid cooling transformed the specimen into hole-conducting germanium (the well-known influence of thermal acceptors). On long-continued annealing at 500°C, the crystal again assumed electron conductivity. A film on such a crystal invariably retained hole conductivity. Thus, for films evaporated on to the surface of a germanium single crystal, the values of electrical conductivity, Hall constant and carrier mobility obtained at room temperature were approximately of the same order or even less than for the finely-crystalline films produced on corundum.

The following experiment was carried out to examine the possibility of contamination of the films during evaporation. By evaporating n-type germanium on to corundum, we obtained as usual a film with p-type conductivity. This film was then melted. In melting, the film was destroyed and a few small droplets of germanium were formed on the support. After long-continued annealing of the solidified droplets at a temperature of 500°C, it was found that the germanium had been transformed into electron-conducting germanium and its specific resistance had sharply increased, i.e., the germanium had acquired the properties of the evaporated material. Etching one of the drops showed that it was a single crystal (Fig. 3). Thus, the hypothesis of the decisive role played by impurities getting into the film during the evaporation process must be rejected. For this reason, we came to the conclusion that the properties of the single-crystal films we had produced were due to defects formed in their structure during the evaporation process and possibly during the subsequent cooling.

In addition to what has been described, the single-crystal films were subjected to microscopic examination. In the case of evaporation on to an etched surface of a single crystal, the picture, obtained depended

Fig. 7. Photograph of germanium film produced on the cleavage surface of a single crystal, heated to 900°C (× 9900).

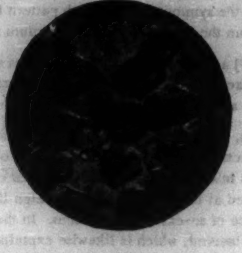

Fig. 8. Photograph of cleavage surface of germanium single crystal (× 9900).

substantially upon the orientation of that surface. Figure 4 shows the photograph of the surface of a germanium film having a thickness of about 20 μ (× 300). The parallel orientation of the grown elevations (or depressions), bounded by the important crystallographic planes, is clearly to be seen. The dimension of the elevations attains 50 μ in cross section. Such a picture, together with electron diffraction data, points to the single-crystal character of the grown layer. The layer evidently continues the lattice of the crystal support. Figure 5 shows a photograph of a germanium film having a thickness of 18 μ (× 300), evaporated on to the etched surface of a single crystal, heated to about 900°C. Here again, the parallel orientation of the grown elevations can be observed. In this case, the crystal was polished so that the growth of the layer occurred along the fourth order axis (the etch figures show this). The size of the elevations is here of the order of 20-30 μ.

As was pointed out above, germanium films were evaporated on to cleavage faces of single crystals, heated to 800-900°C. In one case, evaporation was carried out in such a way that only the central part of the cleavage surface was exposed to the germanium vapor, the edges being screened. The specimen obtained permitted simultaneous observation of the surface of the film (thickness 10 μ) and the cleavage face on which no film was produced. To reveal the finer structure of the film, the specimen was etched slightly with hydrogen peroxide. Figure 6 shows a photograph of the etched surface of the film (× 405, in dark field illumination). The etch figures are here arranged along portions of straight lines, forming an almost continuous regular network, with meshes of rhombic form having angles of 60 and 120°. It should be noted that the etch figures on the cleavage face, on which the film was formed, are disposed in disorderly fashion over its surface (see below).

At our request, L. Aleksandrov of the electron microscope laboratory of the IGEM of the Academy of Sciences, USSR, obtained photographs of the surface of this specimen under the electron microscope. Collodion replicas of the film and cleavage surface were obtained and then shadowed with chromium. Figure 7 is a reproduction of the photograph of the film replica and Fig. 8 that of the etched cleavage surface (× 9900). As will be seen from Fig. 7, the etch figures on the film are regular hexagons with the same orientation, spaced at equal distances apart and arranged along the boundaries of a rhombus, which is the growth figure. The etch figure of the cleavage face (Fig. 8) likewise have a regular orientation, but are arranged in disorderly fashion over the surface.

It is well known that the arrangement of etch figures reflects the structure of the crystal surface, since etching usually commences at points of lattice defects (grain boundaries, accumulations of impurities, steps, etc.) The picture we have obtained (Fig. 7) discloses the so-called substructure of the single crystal. Evidently, the layer consists of individual blocks, separated from each other by narrow regions with distorted lattices, or micro-cracks. Electron diffraction and microscopic examinations show that the size of these blocks is fairly large, of the order of tens of μ. From data on the electrical properties of the films it is, however, possible to draw the conclusion that each of these blocks evidently also has a "fine structure" [4], i.e., in its turn consists of many smaller blocks.

The foregoing also relates to films produced on the polished surface of a single crystal. It should be noted that the symmetry of the etch pattern in Fig. 6 agrees with the symmetry of the pattern obtained in Ref. [5] from the (111) face of a germanium single crystal bent around the [110] direction.

In [6] a germanium single crystal was subjected to uneven cooling. This resulted in a deformed specimen, the (111) face of which revealed an etch pattern similar to ours. In [6] it is shown that in such a specimen, slip occurs along the faces an octahedron, the etch figures being arranged along the traces of the slip planes.

Thus, in the single-crystal film obtained by us on the (111) cleavage face, the symmetry of arrangement of the defects coincides with the symmetry of the slip lines. This evidently points to the common nature of the defects in the film and in the deformed single crystal. It should be noted that in the theory of plasticity as developed at the present time in foreign literature, the block structure of single crystals is associated with the presence of so-called dislocations. In the deformation of a single crystal, a change in its electrical properties is observed, which is likewise explained by the occurrence of dislocation. For example, in [5], a change in the electrical conductivity and concentration and mobility of the charge carriers was observed during the bending of an n-type germanium single crystal about the [110] direction, the carrier mobility diminishing. In our films, the concentration of the defects is much greater than in a bent single crystal. This explains the low mobility of the charge carriers in a film in comparison with a compact crystal. The defects mentioned are evidently not revealed by the electron diffraction method. The anomalous electrical properties of the films as investigated by us are thus not due to the small dimensions of the small crystals, as is observed in the case of films produced by evaporation on to glass or corundum, but to defects in their real structure.

LITERATURE CITED

[1] S. A. Semiletov, "Electron diffraction study of germanium films produced by evaporation in vacuum," Kristallografiia 1, 5, 542-545 (1956).

[2] Ia. E. Pokrovskii, "Influence of surface levels on the electrical properties of fine-grain films of germanium, silicon, and tellurium," J. Tech. Phys. (USSR) 24, 7, 1229-1243 (1954).

[3] S. A. Semiletov and Z. G. Pinsker, "Electron diffraction study of the degree of perfection of germanium single crystals," Kristallografiia 1, 2, 209-214 (1956).

[4] E. Votava, W. Dekeyser, S. Amelinckx and G. Vandermeerssche, "Fine structure lines on (111) faces of ZnS," Naturwissenschaften 40, 18, 479-480 (1953).

[5] G. L. Pearson, W. T. Read and F. J. Morin, "Dislocations in plastically deformed germanium," Phys. Rev. 93, 4, 666-667 (1954).

[6] E. Billig, "Some defects in crystals grown from the melt. I. Defects caused by thermal stresses," Proc. Roy. Soc. 235 A, 1200, 37-55 (1956).

Institute of Crystallography

NEUTRON DIFFRACTION STUDY OF IRON–NICKEL ALLOYS OF THE PERMALLOY CLASS

B. G. Liashchenko, D. F. Litvin, I. M. Puzei and Iu. G. Abov

Single crystals of Fe–Ni alloys (50, 70, 75, 80% permalloys) and alloys containing Mo, Cr, Cu (Mo-permalloy, supermalloy, 74% permalloy with Cr and 75% permalloy with Cu) have been studied by means of a single-crystal neutron spectrometer. The concentration region of the existence of the superlattice has been defined on the basis of the experimental data. The temperature-dependence of the intensity of the superlattice reflection has been measured and the dimensions of the long-range order regions in the ordered alloy of stoichiometric composition Ni_3Fe have been estimated. Certain peculiarities of the ordering of the ternary solid solution containing chromium have been discovered.

The work was carried out using the experimental physical heavy water reactor of the Academy of Sciences of the USSR.

Many peculiarities of the iron–nickel alloys, of considerable interest on account of their magnetic properties, are very closely related to the atomic structure of these alloys. The existence of a superlattice, established for the stoichiometric composition Ni_3Fe by direct x-ray diffraction studies [1] and more recently by neutron diffraction studies, has enabled a qualitative explanation to be given for the physical and technological anomalies of the properties of permalloys, apparent during their treatment and alloying and which, in fact, have been one of the principal causes giving rise to the entire problem of magnetically soft alloys of this series.

At the same time, however, this problem is far from being completely solved from the theoretical aspect. In this connection the most important point appears to be the question of the nature of the ordering in iron–nickel solid solutions, the components of which are characterized by very close values of the atomic radii and similar chemical properties. The question of the stimulus which causes the ordered arrangement of the atoms of Ni and Fe among the lattice points of the solid solution is common to a number of systems of metals of the transition groups, and essentially is one of the least studied subjects of solid state physics.

The phenomena occurring in alloyed permalloys (ternary alloys with additions of Mo, Cr, Cu and other elements) differ still further by their greater complexity and confliction. This relates above all to those anomalous states of the solid solution (called the "K–states"), which were discovered recently in Mo-permalloy [3, 4] and Cr-permalloy [5] when the electrical resistance, volume and some other characteristics of the alloys were measured. The concept of the formation, within the solid solution, of a special close-range order and local distortions of the crystal lattice, associated with the atoms of the alloying element, like other less probable views of the nature of these anomalous states, are nowadays unfortunately no more than a hypothesis. At the same time, it must be assumed that a fairly wide special class of single-phase solid solutions is involved here, since similar special states have been observed by a number of investigators in very different alloys containing elements of the transition groups.

With the availability of nuclear reactors, it has become possible to apply the methods of neutron diffraction to the solution of these problems. These methods make it possible not only to overcome a certain limitation in the x-ray diffraction analysis of the superlattice, due to the monotonic dependence of the scattering amplitudes upon the atomic number of the element, but also to obtain valuable data regarding the magnetic moments of the atoms of components in alloys of transition metals.

EXPERIMENTAL METHOD*

The method employed was that of neutron diffraction analysis of single-crystal specimens without preliminary monochromatization of the radiation [7]. This method ensured greater radiation intensity, and a sensitivity in the analysis of the permalloy superlattice of one order higher than the method of neutron diffraction analysis using polycrystalline specimens on the Debye-Scherrer principle [2]. The neutron source was the experimental physical heavy water reactor of the Academy of Sciences of U.S.S.R. [8]. The apparatus was based on the neutron crystal spectrometer of the Academy of Sciences of U.S.S.R. [9]. Figure 1 shows a diagram of the apparatus.

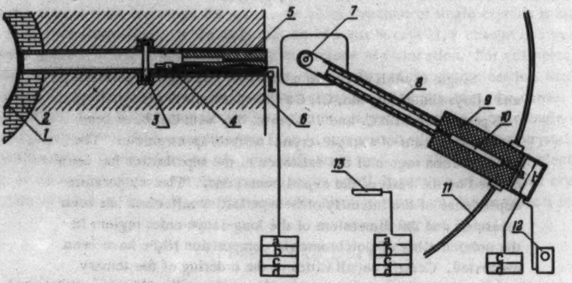

Fig. 1. Diagram of apparatus.
1) Tank wall; 2) graphite lining; 3) slide; 4) fission chamber and preamplifier; 5) plug; 6) protective wall of reactor; 7) single-crystal specimen; 8) screening box; 9) protection of spectrometer detector; 10) spectrometer detector; 11) spectrometer rails; 12) oscillograph; 13) room background detector; a) detector supply; b) linear amplifier and pulse discriminator; c) scaler; d) pulse number counter.

The polished single-crystal specimens in the form of spheres 8-11 mm in diameter [10] were mounted in a special crystal holder, terminating in an x-ray type of goniometric head. All the adjustments of the specimen position in the crystal holder and their check in the microscope were carried out on a separate adjusting table, whereupon the crystal holder with the specimen was transferred to the spectrometer. The accuracy of orientation of the axis of the crystallographic zone of the crystal, on which were located the exits of third and fourth order axes by means of a magnetic anisometer, was also checked on this table. The final adjustment to the maximum of the diffraction reflections was made by further adjustment of the crystal position in the holder according to intensity measurements of the reflected neutron beam. Figure 2 is a general view of the crystal holder mounted on the adjusting table.

Notwithstanding the fact that the shape of the reflection curves was incorrect in a number of cases because some specimens had a defective structure [11], perfect reproducibility of the results of the diffraction reflection intensity measurements was obtained when the specimen was remounted on the spectrometer after going through the complete cycle of adjusting operations.

The degree of long-range order was estimated from the difference in intensities of the neutron flux scattered in all orders from the (010) planes for an alloy which had been subjected to a 600-hour stepped

---

* A more detailed description of the method and apparatus employed will be found in [6].

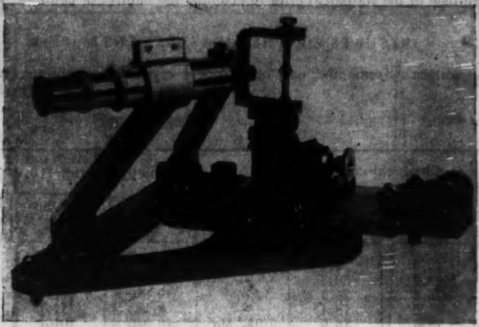

Fig. 2. Crystal holder with adjusting table.

TABLE 1

Element	X-rays [12]		Nuclear scattering [12]		Magnetic scattering [2]	
	Amplitude $f \times 10^{12}$ ($\sin\theta/\lambda = 0.5$)	$\frac{f_{Ni} - f_{Fe}}{3f_{Ni} + f_{Fe}}$	Amplitude $f \times 10^{12}$	$\frac{f_{Ni} - f_{Fe}}{3f_{Ni} + f_{Fe}}$	Amplitude $f \times 10^{12}$ ($\sin\theta/\lambda = 0,05$)	$\frac{f_{Fe} - f_{Ni}}{3f_{Ni} + f_{Fe}}$
Fe	3.27	0.02	0.96	0.02	~0.20	~0.43
Ni	3.58		1.03		~0.05	

annealing in the temperature range 600-300°C (heat treatment R_2) and an alloy quenched from 600°C, a temperature above the critical point (heat treatment R_1). In the latter case, the intensity of the higher orders of reflection was measured for a normal face-centered cubic lattice. The main contribution is in this case provided by the second order, i.e., the (020) reflection. The intensity of this reflection is determined almost entirely by scattering of neutrons at the nickel and iron nuclei and therefore represents the background (independent of the degree of order of the solid solution), on which are superimposed the diffraction reflections from the ferromagnetic superlattice of the permalloy. Such a picture of the diffraction of neutrons at an iron-nickel alloy crystal follows from a consideration of Table 1, which gives the values of the amplitudes of neutron scattering by the nickel and iron atoms (alloy of the composition Ni_3Fe) and the ratio of the structure amplitudes for the Ni_3Fe superlattice and the normal face-centered lattice. For purposes of comparison, the table also gives the corresponding data for x-ray scattering.

The highly mosaic character of the single crystals studied means that specimens having a diameter of about 10 mm behave with regard to the diffraction of neutron radiation mainly like "thin" crystals [13]. Specially conducted experiments confirmed this [11].

All the measurements of the intensity of the superlattice (010) reflection (as well as higher orders) were accompanied by a measurement of the (111) reflection intensity, which in the case of the face-centered cubic lattice does not depend upon the degree of atomic order in the alloy. It was therefore possible to use the (111) reflections as standard, with which the results of the intensity measurements of the superlattice reflections were compared. In order to avoid additional errors, these two reflections were photographed with the detector stationary (2θ = const). In this case, the (010) reflection with a wavelength $\lambda_{010} = 1.08$ A, situated close to the maximum of the Maxwell spectrum of the reactor neutrons [9] corresponds to the (111) reflection with a wavelength $\lambda_{111} = \gamma_{010}/\sqrt{3}$.

The accuracy of the measurements of the relative magnitude of the (010) reflection intensities, being dependent upon the magnitude of the statistical error in counting the number of neutrons, was about ±2%.*

RESULTS OF THE MEASUREMENTS

The chemical composition and some other data of the single-crystal specimens are given in Table 2.

TABLE 2

Specimen number	Chemical composition in at. %			Diameter of sphere in mm	Axis of easiest magnetization [10, 14]	
	Ni	Fe	Alloying additions		After quenching from 600°C	In equilibrium condition at room temp.
1	49.3	50.7	—	9.690	[010]	[010]
2	69.7	30.3	—	11.344	[010]	[111]
3	75.5	24.5	—	9.310	[111]	[111]
4	81.6	18.4	—	8.583	[111]	[111]
5	78.8	18.9	2.3% Mo	10.340	[010]	[111]
6	79.4	17.2	3.4% Mo	8.940	[010]	[111]
7	73.4	23.6	3.0% Cr	11.104	[010]	[111]
8	74.6	21.7	3.7% Cr	11.058	[111]	[111]

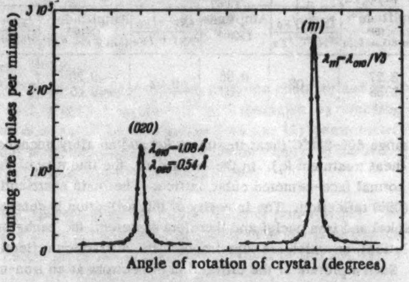

Fig. 3. Reflection for specimen No. 1 after heat treatment R_1 (crosses) and R_2 (circles).

Figure 3 shows the reflection curves for specimen No. 1 after heat treatments R_1 and R_2. The figure shows that the superlattice is absent in this alloy. In Fig. 4 the effect of the Ni_3Fe superlattice (specimen No. 3) is clearly to be seen.

It is noteworthy that this effect for specimen No. 3 (as well as for specimen No. 2) is much greater than was to be expected from calculations based on the results given in [2].

Comparison of the intensities of the superlattice reflections from specimens No. 1-4, which had been subjected to identical heat treatments R_1 and R_2, shows the existence of a pronounced asymmetry in the curve of the "order – disorder" phase transformation, as regards the stoichiometric composition Ni_3Fe. Since the intensity of the (020) reflection varies only slightly with the concentration of the solid solution (see Table 1),

---

* Along with the neutron diffraction analysis of the superlattice, an investigation was also made on the same specimen of the dependence of the magnitic anisotropy constant upon the heat treatment. The results of these measurements are discussed in [14]. They will here be considered merely to the extent to which they relate to the fundamental object of the present investigation.

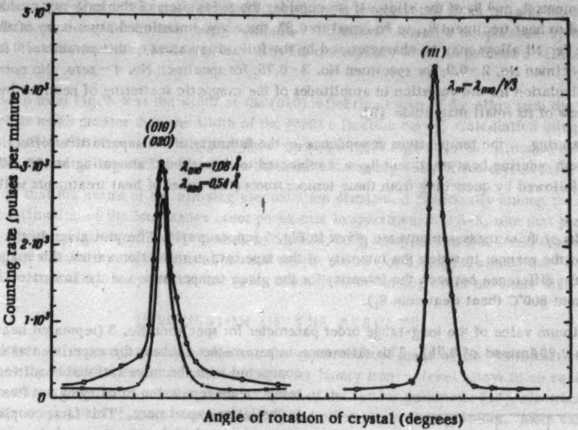

Fig. 4. Reflection curves for specimen No. 3.

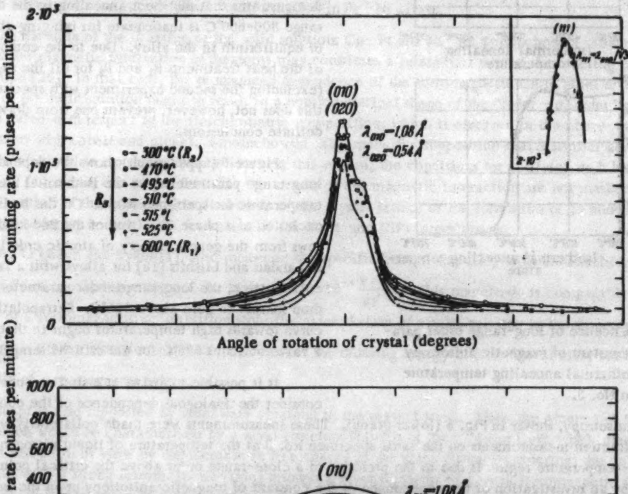

Fig. 5. Temperature dependence of the intensity of superstructure reflection from specimen No. 3.
The symbols Δ, O, □ and Δ, the scale of which correspond to the magnitude of the experimental error in measuring the counting rate, denote on the lower graph the positions at which the respective curves merge with the background.

the degree of long-range order may be estimated from the ratio of the areas of the reflection curves, obtained after heat treatments R_1 and R_2 of the alloy. If we consider the parameters of the long-range order for specimen No. 2, subjected to heat treatment R_2, to be equal to 0.9* the above-mentioned asymmetry of the transition phase curve in binary Fe–Ni alloys may be characterized by the following values of this parameter: for specimen No. 1 – zero; for specimen No. 2 –0.9; for specimen No. 3 –0.75; for specimen No. 4 – zero. No correction has been made in the calculation for the variation in amplitudes of the magnetic scattering of neutrons by the atoms of the alloys in view of its small magnitude [2].

For measuring the temperature dependence of the intensity of the superlattice reflection, specimen No. 3 after a fresh ordering heat treatment R_2, was subjected to three-hours' annealing at 470, 495, 510, 515, 525 and 600°C followed by quenching from these temperatures (this series of heat treatments will be referred to as R_3).

The results of these measurements are given in Fig. 5 (upper graph). The plot given in the lower part of this figure shows the manner in which the intensity of the superlattice reflection varies, this magnitude being determined as the difference between the intensity for the given temperature and the intensity after quenching the specimen from 600°C (heat treatment R_1).

The maximum value of the long-range order parameter for specimen No. 3 (repreated heat treatment R_2) was found to be 0.80 (instead of 0.75). This difference in parameters exceeds the experimental error and is connected with the more rational conditions and better temperature regulation in carrying out heat treatment R_2 in the latter experiment. This fact, coupled with the circumstance that the long-range order parameter in the alloy with 69.7% Ni (specimen No. 2) was found to be higher than in the alloy of stoichiometric composition Ni_3Fe, demonstrates that 600-hour annealing in the temperature range 300-600°C is inadequate for bringing about a state of equilibrium in the alloy. Due to the complete identity of the heat treatments R_1 and R_2 for all the specimens (excluding the second experiment with specimen No. 3), this does not, however, prevent one from drawing quite definite conclusions.

Figure 6 (upper graph) shows the dependence of the long-range parameter upon the isothermal annealing temperature for specimen No. 3. On the basis of the exclusion of a phase transition of the 2nd kind, which follows from the general theory of atomic ordering according to Landau and Lifshits [15] for alloys with a face-centered cubic lattice, the long-range order parameters should drop sharply to zero above 525°C. Extrapolation of the curve towards high temperatures ought in that case to give a value of about 530°C for the critical temperature.

It is possible to arrive at a similar conclusion if we consider the analogous dependence of the constant of magnetic anisotropy, shown in Fig. 6 (lower graph). These measurements were made collaterally with the neutron diffraction measurements on the same specimen No. 3 at the temperature of liquid nitrogen. The "tail" in the high-temperature region is due to the presence of a close-range order above the critical point. This was confirmed by an investigation of the dependence of the constant of magnetic anisotropy upon the isothermal annealing temperature of specimen No. 1 and some others [14], where according to neutron diffraction data, superlattice is absent.

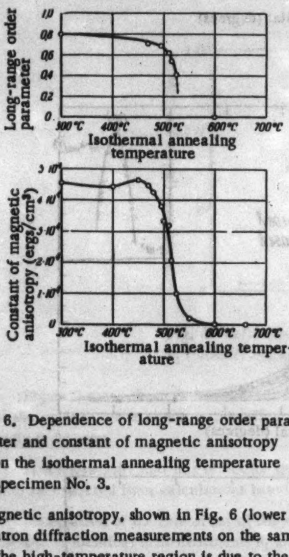

Fig 6. Dependence of long-range order parameter and constant of magnetic anisotropy upon the isothermal annealing temperature of specimen No. 3.

---

* Despite the fact that there is some foundation for this choice (incomplete saturation of the properties, concentration disordering) the figure 0.9 is to some extent quite arbitrary.

It has also been found [14] that in the case of the reverse sequence of the heat treatment R_3 for specimen No. 3 (transition from the disordered to the ordered state) there is a substantial shift, towards lower temperatures, of the curve of the dependence of the anisotropy constant. This is evidence of a temperature hysteresis of the transformation in this alloy and may be connected with the discrepancy found in published values for the critical point.

It will be seen from Fig. 5 that the width of the (010) reflection curve of the alloy with the stoichiometric composition Ni_3Fe is much greater than the width of the (020) reflection curve. Calculation using the Seliakov – Scherrer formula enables the linear dimensions of the long-range order regions to be estimated at approximately 30 A. Such regions contain altogether only about a thousand elementary cells of the crystal lattice.

If we assume that the atoms of the alloying elements are distributed chaotically among the lattice points of permalloy, an estimation of the long-range order parameter in specimens Nos 5-8, like that performed for the first four specimens, gives zero for specimens Nos. 5 and 6, 0.75 for specimen No. 7 and 0.3 for specimen No. 8. The preferred distribution of the chromium and copper atoms (for example, among the "iron" points of the lattice of the ordered alloy) may reduce this value somewhat, but in any event not more than by 1%.

DISCUSSION OF THE RESULTS

For some time now, investigators have observed the asymmetrical shape of the "composition – property" curves in respect to the stoichiometric composition Ni_3Fe for binary iron – nickel alloys in an equilibrium condition. These effects have been noted in measurements of the lattice parameter [16], electrical resistance [17], magnetic anisotropy [10, 18], magnetostriction [18] and other physical magnitudes. More direct data indicating assymetry of the curve of the "order – disorder" transition phase in these alloys were obtained in the work described in [19], in which the transmission of polycrystalline specimens was measured in white neutron irradiation. The result obtained in the work described in the present paper indicates that the enumerated effects are in fact due to peculiarities of the phase transformation in Fe–Ni alloys.

Analyzing the data of the ordering of the solid solutions Co–Pt and Ni–Pt, Smoluchowski advanced the hypothesis that the magnetic interaction of the atoms may constitute a substantial part of the ordering energy of a solid solution [20]. In that case, the pronounced dependence of the ferromagnetic Curie point upon the concentration of the solid solution ought to result in a nonsymmetrical shape of the "order – disorder" phase transformation curve with respect to the stoichiometric composition, which is observed in the above-mentioned alloys of platinum with cobalt and nickel. Smoluchowski also made the supposition that a similar asymmetry ought also to be observed in iron and nickel alloys. In this system, the conditions for verifying such hypotheses were particularly favorable, due to the fact that the effects of the magnetic interaction are not masked in this case by the relaxation of the large elastic distortions of the crystal lattice or the formation of an additional ion bond, which evidently occurs in the formation of the CoPt and NiPt superlattice.

According to Leech and Sykes [1], who measured the specific heat of the alloy with the stoichiometric composition Ni_3Fe, the ordering energy of the latter $Q < 5 \cdot 10^{-3} \frac{ev}{at}$. This magnitude is comparable with the energy change of a ferromagnetic on transition from the ordered state of a solid solution to the disordered state: $\Delta E < 10^{-3} \frac{ev}{spin}$*. Such a situation suggests the idea that the ordering energy of iron-nickel alloy solid solutions is fundamentally of ferromagnetic origin.

This concept is also supported by other data obtained in the present work. Thus, the absence of the NiFe superlattice, which would be characterized by a layer structure (lattice of the CuAu or CuPt type), may be explained from this point of view by the increase in free energy of the alloy during its ordering, due to the interaction of the atoms of a strong ferromagnetic (iron) through a layer of atoms of a weak ferromagnetic (nickel). In the limit case, in the presence of a nonferromagnetic component in the ferromagnetic alloy, the formation of a superlattice of the CuAu type would result in two-dimensional ferromagnetism, which is thermodynamically disadvantageous. From this point of view, the close-range order region, which in Fe–Ni alloys evidently extends as far as the stoichiometric composition NiFe [19, 10, 18, 17], should be connected not with the NiFe superlattice, but with the Ni$_3$Fe superlattice.

---

* The estimation of ΔE as the difference of $\frac{k\theta}{2}$ for the ordered and disordered state (θ is the ferromagnetic Curie point) leads to a low result, since the experimental value of θ for the ordered phase [21] is always found to be lower than it is in actual fact, due to partial disordering in the process of heating the specimen.

On the other hand, additions of chromium and copper in the alloy of Ni$_3$Fe stoichiometric composition have a different influence on the formation of the superstructure. In this alloy, chromium atoms evidently possess a considerable magnetic moment [2] and enter into antiferromagnetic coupling with their surroundings. This antiferromagnetic coupling must evidently be regarded as the cause of the sharp drop in saturation magnetization when nickel atoms in the alloy are replaced by chromium atoms. Thus, according to data [10], the alloy with 76.7 (at.) % Ni and 23.3 (at.) % Fe has J_s = 900 gauss at room temperature, while the alloy with 73.4 + 3.0 (at.) % (Ni + Cr) and 23.6 (at.) % Fe has J_s = 780 gauss. If the chromium atoms in the alloy had no magnetic moment, the replacement of such a small portion of the nickel by chromium would not lead to such a considerable drop in saturation. It must be assumed that, due to this antiferromagnetic coupling, chromium atoms, as distinct from copper atoms, actively participate in the formation of a three-component Ni$_3$ (Fe, Cr) superlattice.

The possibility is not excluded that there is a continuous transition from the Ni$_3$Fe superlattice to those special states which have recently been observed in the alloy with the stoichiometric composition Ni$_3$Cr [22], possessing a structure that is isomorphous with Ni$_3$Fe. In this connection, it is logical to suppose that Ni$_3$Cr is an antiferromagnetic. The formation of the "K-state" in Cr-permalloy, in agreement with the most prevailing concepts [4, 5], may be ascribed to the special close-range order which chromium atoms form within the Ni$_3$ (Fe, Cr) superlattice.

The ferromagnetic nature of the ordering energy does not, of course, contradict the requirement of the theory of Landau and Lifshits [15] for the necessity of a phase transition of the 1st kind in the ordering of Fe–Ni alloys. The small dimensions of the regions of long-range order in the ordered alloy are, in this case, due not merely to the sluggishness of the diffusion processes [23], but mainly to the competition between the gain in free energy on the appearance of a new phase and the loss due to the work of formation of a surface of separation. If we consider that supercooling is equal to a temperature hysteresis of transformation, which is observed experimentally, while the equilibrium crystal nucleus of the ordered phase has a mean dimension of 30 A, since quantitatively, the ordered phase in the alloy increases only at the expense of the appearance of fresh nuclei, then according to Gibbs phase theory, the coefficient of surface tension should not exceed tenths of an erg per square centimeter. This value is two or three orders less than the known values of the coefficient, characterizing crystallization from a melt or the condensation of vapor.

Two-dimensional ferromagnetism, if it exists at all, ought in that case to contribute to a coefficient of surface tension less than the indicated value.

The final solution of the problem of the part played by ferromagnetic energy in the ordering of solid solutions and furthermore, the extension of the concepts set forth above to other systems (including antiferromagnetics) will only be possible when a sufficiently large amount of experimental data has been analyzed. In this connection, further neutron diffraction and magnetic studies of Fe–Ni alloys, as well as of alloys such as Fe–Co, Co–Ni, Ni–Mn, Ni–Cr and a number of others, ought to shed sufficient light on these problems.

The authors wish to take this opportunity of expressing their profound gratitude to Academicians G. V. Kurdiumov and A. I. Alikhanov for fruitful discussions and advice in the course of the work.

LITERATURE CITED

1. P. Leech and C. Sykes, "The evidence for a superlattice in the nickel-iron alloy Ni$_3$Fe," Phil. Mag. 27, 185, 742 (1939).

[2] C. G. Shull and M. K. Wilkinson, "Neutron diffraction studies of the magnetic structure of alloys of transition elements," Phys. Rev. 97, 2, 304 (1955).

[3] F. Assmus and F. Pfeifer, Widerstandsanomalien einer hochpermeablem Nickel–Eisen–Molybdän–Legierung Z. Metallk. 42, 10, 294 (1951).

[4] B. G. Lifshits and M. P. Ravdel'. "Electrical resistance of alloys containing molybdenum." Doklady Akad. Nauk SSSR 6, 1033 (1953).

[5] Ia. P. Selisskii and M. P. Ravdel'. Report of the Institute of Precision Alloys of the Central Scientific Research Institute for Ferrous Metallurgy No. 808. "Study of ordering processes in magnetic alloys with the object of improving the magnetic characteristics and eliminating brittleness," Part III (1955).*

[6] B. G. Liashchenko, D. F. Litvin, I. M. Puzei and Iu. G. Abov, "Neutron diffraction study of the iron-nickel alloys of the permalloy class," In the 5th Symposium of the Institute of Metallography and Physics of Metals of the Central Scientific Research Institute for Ferrous Metallurgy "Problems of Metallography and Physics of Metals," (1957).*

[7] R. D. Lowd, "Single-crystal neutron diffraction analysis," Nature 167, 4241, 243 (1951).

[8] A. I. Alikhanov, V. V. Vladimirskii, S. Ia. Nikitin, A. D. Galanin, S. A. Gavrilov and N. A. Burgov, "Experimental physical heavy water reactor," in Reactor Construction and Reactor Theory (Papers ready by members of the Soviet Delegation to the International Conference on the Peaceful Uses of Atomic Energy, Geneva, 1955).*

[9] Iu. G. Abov, "Neutron crystal spectrometer with bent single crystal of quartz," Session of the Academy of Sciences of the U.S.S.R. on the Peaceful Uses of Atomic Energy (Meeting of the Section of Physico-Mathematical Sciences, 1955). *

[10] I. M. Puzei, "Constant of the magnetic antisotropy of alloys of the permalloy class," Izv. AN SSSR, Ser. Fiz. 16, 5, 549 (1952).

[11] B. G. Liashchenko, D. F. Litvin, I. M. Puzei, Iu. G. Abov and V. S. Golovkin, Report of the Institute of Metallography and Physics of Metals of the Central Scientific Research Institute for Ferrous Metallurgy No. 1097. "Study of metals and alloys by the method of neutron diffraction analysis," (1956). *

[12] G. E. Bacon and K. Lonsdale,' "Neutron diffraction," Repts. Progr. in Phys. 16, 1 (1953).

[13] G. E. Bacon, "The diffraction of thermal neutrons by single crystals," Proc. Roy. Soc. 209, 1098, 397 (1951).

[14] I. M. Puzei, "Ordering and temperature dependence of the energy of magnetic anisotropy of alloys," Izv. AN SSSR, Ser. Fiz. 1957 (in press).

[15] L. D. Landau and E. M. Lifshits, Statistical Physics (1951);* E. M. Lifshits, "Theory of phase transitions of the second kind (parts I, II)," J. Exptl.-Theoret. Phys. (U.S.S.R.) 11, 2-3, 255-281 (1941).

[16] A. J. Bradly, A. H. Jay and A. Taylor, "The lattice spacing of iron-nickel alloys," Phil. Mag. 23, 155, 545 (1937).

[17] S. Kaya, "The formation of a superlattice in Ni-Fe alloys and the permalloy problem," J. Fac. Sci. Hokkaido Univ. (Sapporo) 2, 29 (1938).

[18] R. M. Bozorth, "The permalloy problem," Rev. Mod. Phys. 25, 1, 42 (1953).

[19] F. C. Nix, H. G. Beyer and R. Dunning, "Neutron studies of order in Fe-Ni alloys," Phys. Rev. 58, 12, 1031 (1940).

[20] R. Smoluchowski , "Influence of order of magnetic properties," J. Phys. Rad. 12, 3, 389 (1951).

[21] E. Josso, "Relations entre l'etat structural et les proprietés magnetiques des alliages fer-nickel voisins de Ni$_3$Fe, J. Phys. Radium 12, 3, 399 (1951).

[22] I. I. Kornilov, Iron Alloys, Vol. 3 (1956).*

[23] M. B. Neiman and A. Ia. Shiniaev, "Study of the diffusion of iron into iron-nickel alloys," Doklady Akad. Nauk, SSSR 102, 969 (1955).

Central Scientific Research Institute for
Ferrous Metallurgy

Received November 13, 1956

---

* In Russian.

THE STATE OF FIXATION OF THE CATIONS OF METHYLENE BLUE ON THE CRYSTALS OF MONTMORILLONITE AND THE CAPACITY OF THE LATTER TO FORM ORIENTED AGGREGATES

N. E. Vedeneeva and L. I. Tsukerman

The doublet adsorption of methylene blue on montmorillonite clays is related to the formation of oriented aggregates. Because of their relatively large ionic potentials, the cations of Na^+, Ca^{2+}, Mg^{2+} which are present in montmorillonite clays aid in the formation of film-like oriented aggregates. The presence of cations with small ionic potentials, such as K^+ and NH_4^+, interferes with the formation of films.

A very sensitive new method is given for the determination of cations in montmorillonite clays; this should simplify the identification of clay minerals.

In investigation of the mineralogical composition of clays with the aid of dyes [1] an important diagnostic feature, is the change in the spectrum of methylene blue (M. B.) adsorbed on montmorillonite clays, caused by the introduction of potassium ions into the clay suspension. An explanation of the mechanism of this phenomenon was given by one of the authors [2]. It was based on the hypothesis of doublet (two-point) fixation of the cations of methylene blue on the basal pinacoids (001) of montmorillonite crystals. Doublet adsorption requires geometric order and, above all, the preservation of interatomic distances on these faces. These conditions can be fulfilled only by montmorillonite particles with sufficiently extensive (001) faces.

The hypothesis of doublet adsorption together with electron microscope data for montmorillonite with introduced ions of Na^+, Ca^{2+} and H_3O^+ [3] led to the supposition [2] that the change of M.B. spectrum is influenced by the ionic potentials Z/r of the cations [4] (Z - charge, r - ionic radius). Cations with relatively high ionic potentials aid in edge to edge aggregation of the highly disperse crystals of montmorillonite which forms large, pseudomonocrystalline scales [3]* with smoothed out defects along the edges and thus creates favorable conditions for doublet adsorption of M.B. Cations with smaller ionic potentials have the opposite effect.

This explanation makes it clear why in the presence of Na^+, Ca^{2+}, Mg^{2+} or Pb^{2+} ions the adsorption band of M.B. adsorbed on montmorillonite lies in the 560-580 mμ region, while K^+, NH_4^+, Cs^+ and other ions with small Z/r shift it toward the red end of the spectrum and the spectral curve has the usual ionic maximum.

The data in [1] are insufficient to serve as a firm basis for the hypothesis. Moreover, it is desirable to have a simpler, more easily controlled method for judging the character of aggregation of montmorillonite crystals.

One of the diagnostic features of montmorillonite particles under the electron microscope is the presence of characteristic "spikes" [5] whose nature is not clear at present. We believe that these spikes are actually rolled up edges of the extremely thin films formed as the result of edge to edge aggregation of the particles and that the well known property of montmorillonite suspensions to form durable thin films on drying is due to the same cause. It is to be expected that Na^+, Ca^{2+}, and Mg^{2+} will not prevent formation of such films while K^+ will.

---

* Formation of oriented aggregates of hexagonal crystals of aluminum hydroxide is clearly seen on electron micrographs.

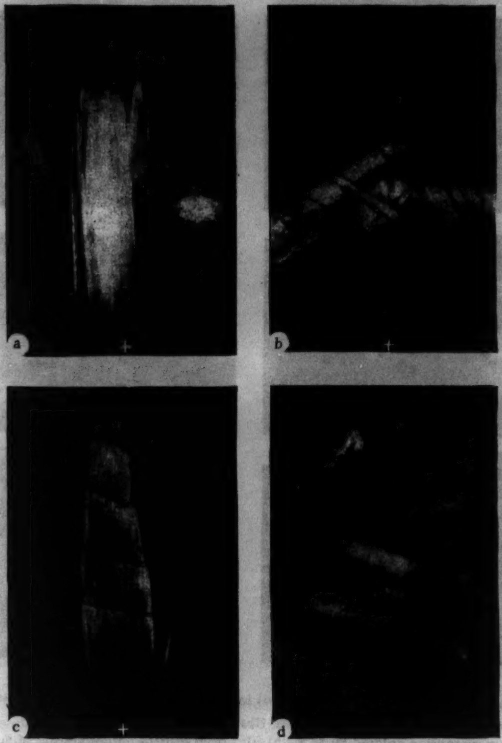

Fig. 1. Photomicrographs of typical montmorillonite films.
a, b, c) Films obtained from undyed suspensions; d) film from a suspension dyed by benzidine (plus sign indicates ability to form doublet adsorption).

Bearing these points in mind, we attempted to observe under the microscope the appearance of "oriented aggregates" of clay particles whose fragments were recommended by Vikulova [6] for determination of the refractive indices of clay minerals.

The method of obtaining these preparations is described at the end of the article.

Figure 1 shows four photomicrographs of typical montmorillonite aggregates or films photographed in oblique reflected light. These thin films (Fig. 1, a and b) are perfect. Usually they have the shape of scrolls or twisted ribbons. In Fig. 1, photographs a, b, and c were obtained from undyed suspensions and the plus sign indicates that these supensions are colored violet by M.B., i.e., that the latter forms doublet adsorption on the clay particles. The suspension of Fig. 1, d was dyed by benzidine.

Seeking an answer to the question which interested us, we investigated in detail two samples of montmorillonite, one of which was obtained from V. V. Petrov (Tsikhis-Uban' locality, from the depth of 130 m) and the other from I. I. Ginzburg (weathered mantle, Kazakhstan).

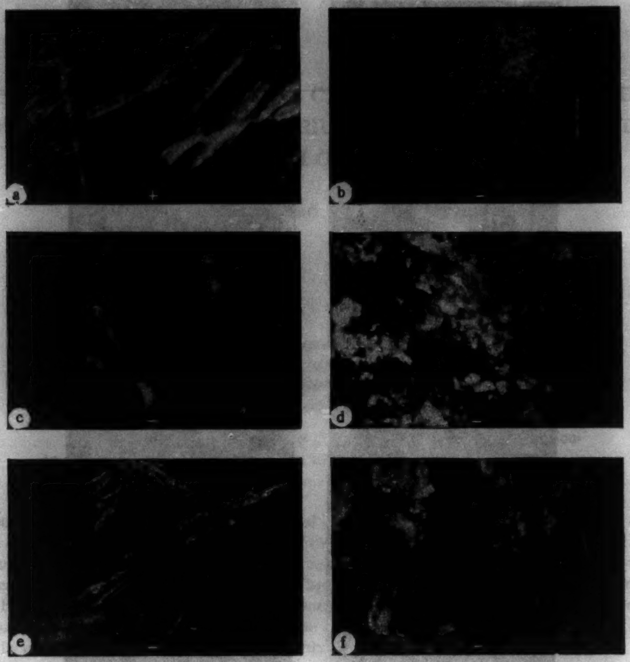

Fig. 2. Photographs illustrating the action of ions and heating on montmorillonite clay suspensions. Montmorillonite from Tsikhis-Uban' locality:
a) film from suspension colored by M.B.; b) film from suspension colored by M.B. with KCl added; c) film from suspension colored by M.B. with KOH added; d) film from suspension colored by benzidine with KCl added; e) film from a heated suspension colored by M.B.: f) film from a heated suspension colored by M.B. with KCl added.
Sign - indicates susceptibility to doublet adsorption.

Figure 2 shows the effect of introduction of K^+ into a suspension made from the first sample and dyed by M.B. An aggregate in the form of a thin scroll (Fig. 2, a) was obtained from this suspension. Evidently M.B., like benzidine, does not prevent the formation of a film.

Addition to the suspension of a few drops of a saturated solution of KCl (which destroys the doublet maximum on the spectral curve of the adsorbed M.B. [2]) has a strong effect on the shape of the aggregates, and clots of montmorillonite form instead of a film (Fig. 2, b). The minus sign on the photograph indicates that doublet adsorption is absent.

The destructive effect on the film must be ascribed not to the chlorine ions or the undissociated KCl molecule but to the K^+ ion. Indeed, an analogous effect is obtained when KOH is used instead of KCl (Fig. 2, b).

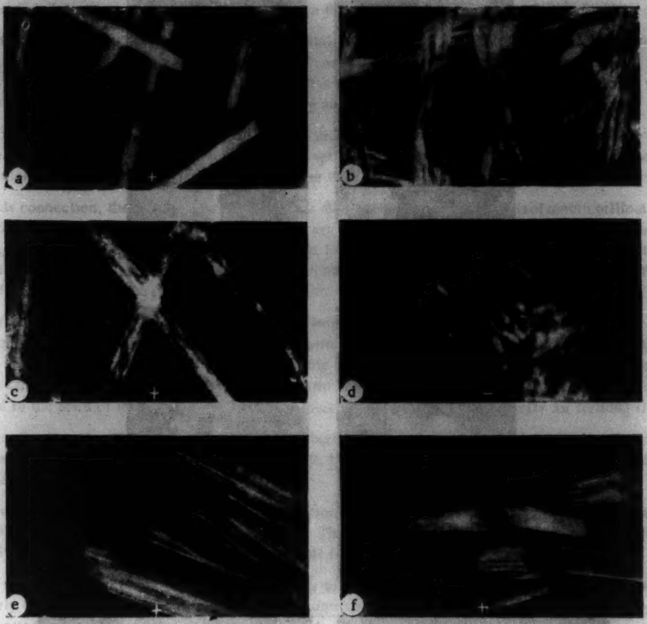

Fig. 3. Photomicrographs illustrating the effect on Z/r on suspension of montmorillonite clays.
Montmorillonite from Kazakhstan: a) film from suspension with NaOH added; b) film from suspension with KOH added
Montmorillonite from Tsikhis-Uban': c) film from suspension colored by M.B.; d) film from suspension colored by M.B. with KCl added; e) film from an undyed suspension with $CaCl_2$ added; f) film from suspension dyed by M.B. with $CaCl_2$ added.

Methylene blue does not play an active part in destroying the capacity for film formation. Thus, if the suspension is colored by benzidine instead of M.B., and KCl is added, the resulting aggregates (Fig. 2,d) look exactly like those in Fig. 2,b, i.e., they consist of clots. Benzidine (Fig. 1,d) does not destroy the film-forming capacity. The destruction of this capacity in this case also is due to the K^+ ion.

The effect of the ionic potential of the cations Na^+ and Ca^{2+} introduced into the suspensions, on one hand, and the K^+, on the other, is shown in Fig. 3.

The photomicrographs (Fig. 3,a and b) are of montmorillonite from Kazakhstan, which gives a very perfect thin film (Fig. 1,a and b). Addition of a small amount of NaOH (Fig. 3,a) does not impair this property; rolls of thin, transparent film show clearly in the photograph. This film will not form if a cation with a lower ionic potential is introduced, for example, if KOH is substituted for NaOH (Fig. 3,b). As for the color of the suspensions, in the first case (Na), it is violet, in the second (K), bluish-green.

The same phenomena were observed with montmorillonite from Tsikhis-Uban'.

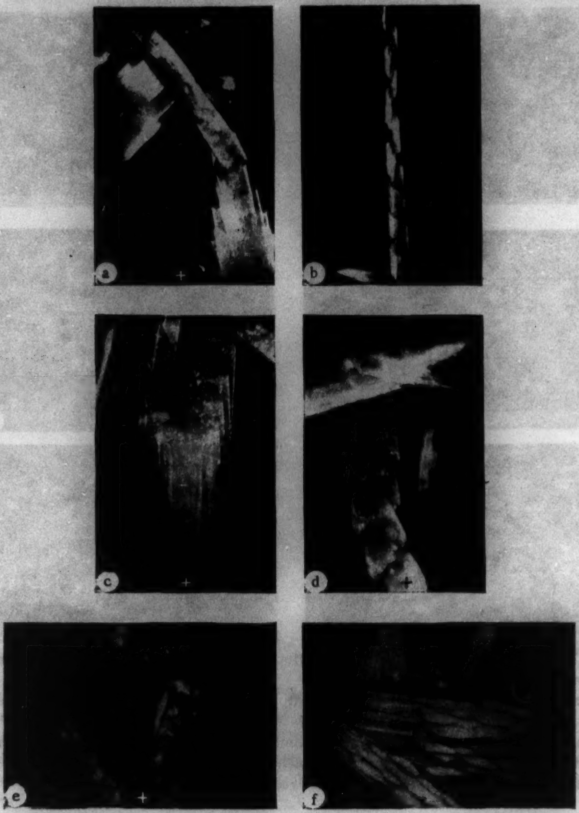

Fig. 4. Photomicrographs illustrating introduction of cations into the montmorillonite lattice.
a, b) films from suspensions saturated with Na; c, d) films from suspensions saturated with Mg^{2}; e) film from suspension saturated with Ca^{2+}; f) film from suspension saturated with K.

That the difference in the effect of NaOH and KOH must be ascribed to the difference in the values of the ionic potential of the Na^+ and K^+ ions is convincingly shown by the aggregates from an undyed suspension of Tsikhis-Uban' montmorillonite to which 2 or 3 drops of $CaCl_2$ solution were added, thus introducing into it the Ca^{2+} ion with a larger ionic potential than that of Na^+. These films are more perfect in structure than those of the Kazakhstan montmorillonite. If $CaCl_2$ is added to a previously dyed suspension, the same effect is observed (Fig. 3,a). In experiments with other clays, we observed that Mg^{2+} behaves in the same way as Na^+ and Ca^{2+}.

Suspensions which form films are always colored violet; M.B. has doublet adsorption on the particles of these suspensions (plus signs on the photographs). When the film does not form, there is not doublet adsorption.

In investigation [2] it was shown that on the crystals of a montmorillonite sample, saturated after electrolysis with ions of Na$^+$, Mg^{2+}, and Ca^{2+}, methylene blue has doublet fixation. If, however, K$^+$ ion is introduced the "doublet" maximum on the spectral curve is absent. The form of the curve indicates that the action of K$^+$ introduced into the lattice is not as strong as when KCl is added to the suspension.

Figure 4 shows montmorillonite clay aggregates saturated with these ions. Photographs a and b show aggregates with Na$^+$ and Mg^{2+} forming tightly twisted spirals. The aggregate saturated with Ca^{2+} (the suspension is colored violet by M.B.) is a rough opaque film unlike the thin transparent film shown in Fig. 3,e and f.

In this connection, the authors of article [3] note that the pseudo-monocrystals of montmorillonite are visible under the electron microscope only when they are not completely saturated with Ca^{2+}. Saturation produces a solid coagulated mass in the form of a thick film shown in Fig. 4,e. Experiments show that the doublet fixation of M.B. is possible on this film also. This film differs from the aggregates shown in Fig. 4,f (for K) and in Figs. 2,c and 3,b (for KOH).

In article [2] spectral curves are given for dyed suspensions which were heated in boiling water and which lack the doublet maximum also (but which differ in form from the curves obtained from identical suspensions with KCl). In this connection, it is supposed that heating of suspensions with adsorbed M.B. destroys the initial "monocrystalline" aggregates and that their reaggregation after cooling is not as orderly as the initial one. This is reflected in the form of the spectral curves, and , therefore, must affect the capacity for forming films.

Figure 2,e is a photomicrograph of aggregates obtained from a heated suspension of a sample from Tsikhis-Uban'. They are unlike the aggregates shown in Fig. 2, b and d or the aggregates from a heated dyed suspension with KCl (Fig. 2, f).

It should be noted that the aggregates obtained from suspensions with KOH (Fig. 2, c; Fig. 3, b and d) are also unlike those obtained from suspensions with KCl. They appear to be somewhat better ordered, which can be logically ascribed to the stabilizing effect of the OH ion.

The results obtained by us give a positive answer to the question posed in the beginning since they show convincingly that the doublet adsorption of M.B. on montmorillonite takes place only in those cases when the highly dispersed crystals are capable of forming thin films.

These results are very important for the study of clays by the staining technique and have also an independent interest since they furnish a new method for the study of clay minerals and clays.

Preparation and Investigation of Mounts. For the preparation of mounts we used a method recommended by Vikulova [7] modifying it slightly to suit our purpose. A 0.25-0.30 g sample of clay was moistened with water and ground in a porcelain mortar. After a thorough six-minute grinding, the mortar was filled with 20 cm^3 of water, the mixture was well stirrer and poured into a test tube. After 2-3 hours, the upper part of the suspension (to the depth of 7 cm) was carefully transferred by a pipette into a small shallow evaporating dish and placed in a drying oven with temperature of 37°C. Evaporation lasted 6-8 hours producing a thin, dense layer of dry clay. To make a suitable microscopic mount this layer was cut into very thin slices with a fragment of a safety razor blade. The slices were placed on object glasses, in a drop of kerosene, and covered with cover glasses.

If dyed aggregates were studied, staining was done immediately after preparation of suspensions, which were allowed to stand for 2 to 3 hours. To some suspensions 2 to 3 drops of NaOH or KOH (0.1 N) or of the saturated solution of KCl were added. All of the aggregates illustrated in the photomicrographs, Figs. 1, 2, and 3, were made from deflocculated suspensions.

The mounts were studied and photographed by oblique reflected light obtained by means of a parabolic mirror attached to the microscope stand. This type of illumination discloses the most important morphological characters of montmorillonite aggregates, which are invisible in transmitted light. The rolls of thin, transparent films, for example (Fig. 1, a, b, c, 2, a, 3, a, etc.) are very well seen against a dark field, and under oblique illumination have an almost three-dimensional appearance. The texture of partly transparent films becomes visible, etc. Photography was done with objectives × 8 and × 10, and oculars × 5 and × 10 on 35 mm panchromatic film with the photomicrographic camera constructed by the Institute of Crystallography, Acad. Sci. USSR.

LITERATURE CITED

[1] N. E. Vedeneeva, Methods of Investigation of Clay Minerals with the Aid of Dyes and Its Application to Lithology (1952)[In Russian].

[2] N. E. Vedeneeva, "Relation between the spectra of thiazine dyes and the state of their fixation on crystalline surfaces," Doklady Akad. Nauk S.S.S.R. 98, 4 (1954).

[3] Mathieux-Sicaud, I. Mering and I. Perrin-Bonnet, "Etude au mikroskope elektronique del'ectorite saturées par differents cations," Bull. soc. franc. mineral. et crist. 74, 7 (1951). *

[4] V. K. Semenchenko, "Solubility and surface tension," Uspekhi Khimii 3, 5 (1934).

[5] M. F. Vikulova, "The newest methods of investigation of clay minerals," Proc. of the All-Union Conference of Workers in Mineralo-Petrographic Laboratories [In Russian] (1955) pp. 20-48.

[6] V. Kargin, "Adsorption of electrolytes on silica, sesquioxides and their mixed gels," Pochvovedenie 11, 1 (1939).

[7] M. F. Vikulova, "Determination of the mineralogical composition of clay particles smaller than 0.001 mm with the aid of immersion liquids," Collection: The Weathered Mantle [In Russian] (1952) 1, 190-192 (1952).

Crystallography Institute AN SSSR

Received November 15, 1956

---

* As in original — Publisher's note.

ANOMALOUS BISECTRIX DISPERSION IN ORGANIC PIGMENT CRYSTALS

N. M. Melankholin

A quantitative study of bisectrix dispersion in crystals of three pigments showed that this dispersion is anomalous. When the dispersion curve was compared to the previously studied absorption spectra of the same crystals, a relationship was established between the anomalous dispersion and the absorption bands of the crystals, but not, as a rule, with absorption bands due to those vibrations whose directions cause dispersion. Extinction dispersion was largest in the diagonally oriented crystals.

As is well known, the crystals of monoclinic and triclinic crystal systems show bisectrix dispersion, i.e., dispersion of the principal axes of the optical indicatrix. In the case of monoclinic crystals one axis and the indicatrix symmetry plane perpendicular to it remain nondispersive; in triclinic crystals all three indicatrix axes may cause dispersion [1].

Dispersion is usually characteristic of all optical constants of a substance, and in case of highly absorbing substances an anomalous dispersion behavior has been found and studied for a series of constants in different parts of the spectrum. The theory and experimental study of the anomalous dispersion of certain constants (index of refraction, rotation of polarization plane) show that the dispersion is anomalous only within strong absorption bands. It would be natural to assume that the bisectrix dispersion would likewise be occasionally anomalous. However, to date, there are no experimental or theoretical papers dealing with this question.

We have studied the absorption spectra of crystals of various organic pigments for definite polarizations of light vibrations. We had to pay special attention to the fact that the directions of the oscillations in a crystal often change considerably along the spectrum, which indicates a considerable bisectrix dispersion. The bisectrix dispersion was further quantitatively studied by measuring the dispersion of the angles of extinction in crystals of three pigments of the thiazine group: methylene green, neomethylene blue and thionine blue. The crystals were obtained by means of slow evaporation of a drop of pigment in water solution placed on a glass plate. These crystals have not been studied as yet crystallographically, but apparently all of them belong to the monoclinic group (or are very close to monoclinics). This is confirmed by the fact that in crossed Nicols, in every preparation some of the crystals show a sharp total extinction, and others considerable extinction dispersion. Although the conoscopic figures of these crystals are not very clear they nevertheless make it possible to distinguish between the crystals oriented in one of the indicatrix planes of symmetry approximately parallel to the glass and those which are diagonally oriented. For the measurement of curves of extinction dispersion we chose crystals whose dispersion was as great as possible. The measurements were carried out by means of a polarizing microscope. The crystal chosen was mounted for extinction with a consecutive introduction of various monochromatic interference light filters, and the position of extinction was read off on the graduated circle of the microscope table. The curves for extinction dispersion were drawn from these calculations.

As can be seen from these curves, the bisectrix dispersion is anomalous in all the crystals studied, i.e., with the consecutive change in the wavelength, the indicatrix axes rotate first in one direction, then in the opposite direction, and then again in the original direction. A dispersion of this nature is observed for example in crystals

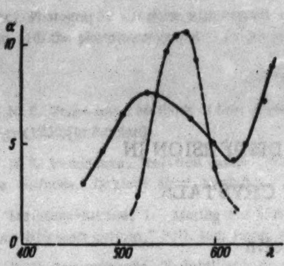

Fig. 1. Curve for the bisectrix dispersion in a crystal of neomethylene blue.
(Dashed line shows the position of the absorption band).

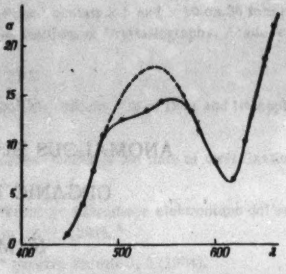

Fig. 2. Curve for the extinction dispersion in a diagonally oriented crystal of neomethylene blue.

of neomethylene blue when their orientation corresponds to dichroism from blue to deep-violet. The extinction dispersion curve for these crystals (Fig. 1) resembles the well known curve of the anomalous dispersion of the index of refraction. It is natural to assume, therefore, that the anomalous bisectrix dispersion is also related to the absorption bands. As the absorption spectra of differently oriented crystals of the above-mentioned pigments had been already studied [2] it was possible to compare them with the curves of extinction dispersion which had been measured with definite orientations of the crystals.

The curve shown in Fig. 1 refers to the dispersion of axes n_g and n_p of the indicatrix; the absorption spectrum of vibrations parallel to these axes is characterized by intense bands at 605 and around 640 mμ. If the bisectrix dispersion is considered normal in the middle section of the curve and anomalous at the ends, then the latter band may be related to the right branch of the curve, but there is no appreciable band for its left branch in the absorption spectrum of neomethylene blue. If the bisectrix dispersion is considered anomalous in the middle section of the curve, which seems more natural judging by its general appearance, then the dispersion anomaly is not connected with the absorption bands arising from vibrations causing dispersion (along the n_g and n_p axes). However in the absorption spectrum of the crystal there is one intense band at 567 mμ, i.e., coinciding exactly with the middle section of the dispersion curve (in Fig. 1 this band is shown by a dashed line) but this band belongs to the absorption spectrum for vibrations parallel to the n_m axis. Apparently only this band can be related to the anomalous bisectrix dispersion of crystals. If this is true, then the dispersion of the n_g and n_p axes is due to the absorption vibrations perpendicular and not parallel to these axes. Such an unexpected result seems quite incomprehensible and so far has not been explained.

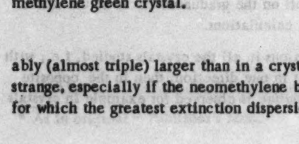

Fig. 3. Curve of bisectrix dispersion in a methylene green crystal.

Similar curves for the dispersion have been obtained for several crystals, more or less similarly oriented. For a crystal whose n_gn_p plane was inclined in relation to the glass, a more complicated dispersion curve was obtained (Fig. 2), with a depression in place of the peak in the first curve. This depression may be due to another absorption band (in the 500-520 mμ region), appearing only in the absorption spectra of diagonally oriented crystals, and therefore, related to the absorption of those vibrations which, in this case, cause dispersion. Thus with a certain orientation of the crystal, anomalous extinction dispersion may be due simultaneously to the absorption of dispersive vibrations and vibrations which are approximately perpendicular to them.

A comparison of the two given curves shows also that the extinction dispersion of a diagonally oriented crystal is considerably (almost triple) larger than in a crystal whose n_gn_p plane is oriented parallel to the glass. This seems very strange, especially if the neomethylene blue crystals are classified as belonging to a monoclinic crystal group, for which the greatest extinction dispersion should be observed in one of the symmetry planes of the indicatrix.

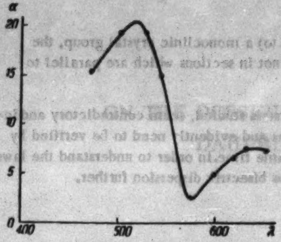

Fig. 4. Curve of extinction dispersion for a diagonally oriented crystal of thionine blue.

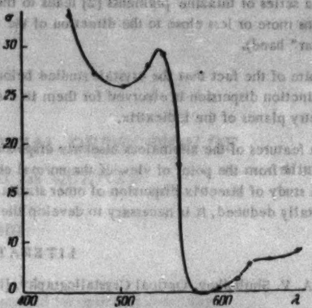

Fig. 5. Curve of extinction dispersion for a thionine crystal with a different orientation.

For crystals of methylene green the measurements of extinction dispersion were also carried out largely in the n_gn_p plane or in planes slightly diverging from it. The dispersion curves obtained for these crystals have a more complex form (Fig. 3) than for the crystals of neomethylene blue; such a curve shape can not be, obviously, due to a single absorption band. Absorption spectra of the crystal with the orientation which was chosen for the measurement of extinction dispersion is characterized by one very intense band at 590 mμ and another, weaker one, at 455 mμ. As the extinction dispersion curve had a peak at 590 mμ it is evident that the more intense band has no connection with the anomalous dispersion. Taking this into consideration and also taking into account the absence of a completely appropriate band for the short wave portion of the curve, it must be apparently assumed that the dispersion is anomalous in the middle section of the curve, which also agrees better with its shape. In this case only the intense band at 560 mμ, observed in the absorption spectra of a methylene green crystal, may be considered as responsible for the anomalous dispersion. However this band is very weak in the absorption spectrum of vibrations causing dispersion and arises apparently from the absorption of vibrations approximately perpendicular to them.

Thus the anomalous bisectrix dispersion for methylene green crystal apparently obeys the same laws as for the crystal of neomethylene blue. The distortion of the dispersion curve in the long wave region of the spectrum may be due to the intense absorption band at 610 mμ, observed with a certain diagonal orientation of the crystal [2].

With a certain inclination of the n_gn_p plane of the indicatrix in relation to the glass, the dispersion curve on the whole keeps its form, but around 640 mμ a definite peak appears. Quantitatively the extinction dispersion increases rapidly (more than twice) as in the case of the above observed effect for crystals of neomethylene blue.

In thionine blue crystals curves of extinction dispersion were measured only for diagonal orientations. The curves obtained sometimes have the regular form of an anomalous dispersion curve (Fig. 4), sometimes they are distorted at both ends. The dispersion is, apparently, anomalous in the middle section of the curve, i.e., practically in the same region of the spectrum as in the case of the first two pigments. However the absorption band around 558 mμ, which brings about the anomaly, belongs, in the case of thionine blue crystals, to the absorption spectrum of the vibrations causing dispersion. The other curve, measured for a somewhat differently oriented crystal, is slightly distorted at the ends (Fig. 5) but shows a very great anomalous extinction dispersion, reaching almost 30° in a range of only 40 mμ.

Thus the study of the anomalous bisectrix dispersion in crystals of certain organic pigments showed that in these crystals the dispersion is anomalous. It may be that this is a general characteristic of highly absorbing crystals.

The anomalous bisectrix dispersion, as other previously studied forms of anomalous dispersion, are related to the absorption bands of the crystal studied. In crystals of all three pigments studied, the basic anomaly is due to almost identically placed absorption bands lying in the 558-570 mμ region. The comparison of the absorption spectra of a series of thiazine pigments [2] leads to the conclusion that this band corresponds to the absorption of vibrations more or less close to the direction of the long axes of the pigment molecules in the crystal lattice ("molecular" band).

In spite of the fact that the crystals studied belong (or are very near to) a monoclinic crystal group, the largest extinction dispersion is observed for them in diagonal sections and not in sections which are parallel to the symmetry planes of the indicatrix.

Such features of the anomalous bisectrix dispersion, found in the crystals studied, seem contradictory and incomprehensible from the point of view of the normal crystallo-optical ideas and evidently need to be verified by means of a study of bisectrix dispersion of other similar crystals. At the same time,in order to understand the laws experimentally deduced, it is necessary to develop the theory of anomalous bisectrix dispersion further.

LITERATURE CITED

[1] A. V. Shubnikov, Optical Crystallography, [In Russian] (1950).

[2] N. M. Melankholin, "Absorption spectra of thiazine pigment crystals" Optika i Spektroskopiia (in press).

Institute of Crystallography
Acad. Sci. USSR

Received November 21, 1956

ON THE POSSIBILITY OF OPTICAL DETECTION OF DAUPHINE TWINNING IN QUARTZ

V. L. Indenbom

The practical possibility is discussed for optically detecting Dauphine twinning in stressed quartz crystals. Quantitative analyses are performed for the cases of crystals observed parallel to and perpendicular to the principal optic axis. The possibility of using an electric field in place of an external mechanical stress is discussed.

The Difference in the Optical Indicatrices of the Components of Dauphine Twinning in a Stressed Crystal

It is well known [1] that the two components of Dauphine scattering in quartz are optically equivalent. The symmetry operation corresponding to the Dauphine law (rotation by 180° about the Z axis) changes neither the optical indicatrices nor the direction of rotation of a plane polarized wave. As opposed to Brazil and Japan twinning, whose presence in quartz is easily detected by the bright colored interference patterns which occur when the crystal is inspected between crossed Nicol prisms, the detection of Dauphine twinning necessitates successive grinding and etching of the sample [1-3], which is not only work consuming, but cannot guarantee that twinning does not occur within any chosen piece of the crystal.

It is usually asserted that it is impossible to detect Dauphine twinning in quartz by optical methods, but this refers only to an unstressed crystal. Let us consider the changes in the optical indicatrices of the components of Dauphine twinning in the field of a mechanical strain. For this we may make use of the data of Pockels [4, 5], who measured the optical strain and stress constants for many crystals, and although several mistakes were made in this work [6], those for quartz were all correct. If in an unstressed quartz crystal the equation of an optical indicatrix is

$$\frac{x^2+y^2}{n_0^2}+\frac{z^2}{n_e^2}=1 \tag{1}$$

(where $n_0 = 1.5442$ and $n_e = 1.5533$ are the principal indices of refraction), then when the stress is applied, the indicatrix is given by

$$a_{11}x^2+a_{22}y^2+a_{33}z^2+2a_{23}yz+2a_{31}zx+2a_{12}xy=1, \tag{2}$$

where the a_{lk} are linear functions of the stress tensor σ_{lm} given by

$$a_{11}-\frac{1}{n_0^2}=-\{\pi_{11}\sigma_x+\pi_{12}\sigma_y+\pi_{13}\sigma_z+\pi_{14}\tau_{yz}\},$$

$$a_{22}-\frac{1}{n_0^2}=-\{\pi_{12}\sigma_x+\pi_{11}\sigma_y+\pi_{13}\sigma_z-\pi_{14}\tau_{yz}\},$$

$$\begin{aligned} a_{33}-\frac{1}{n_e^2} &= -\{\pi_{31}(\sigma_x+\sigma_y)+\pi_{33}\sigma_z\}\,, \\ a_{23} &= -\{\pi_{41}(\sigma_x-\sigma_y)+\pi_{44}\tau_{yz}\}\,, \\ a_{31} &= -\{\pi_{44}\tau_{zx}+2\pi_{41}\tau_{xy}\}\,, \\ a_{12} &= -\{\pi_{14}\tau_{zx}+(\pi_{11}-\pi_{12})\,\tau_{xy}\}, \end{aligned} \qquad (3)$$

Here the π_{ik} are the photoelastic constants, and according to Pockels [5] they are

π_{11}	π_{12}	π_{13}	π_{14}	π_{31}	π_{33}	π_{44}	π_{41}
1.06	2.46	1.93	−0.095	2.72	0.18	−0.991	−0.314

(where all quantities are multiplied by 10^7 and given in cm^2/kg).

Let us compare the optical indicatrices of the components of Dauphine twinning in a crystal subjected to a homogeneous stress. The twinning components differ from each other by a rotation of 180° about the Z axis, which corresponds to changing the sign of the X and Y axes. Such a transformation leads to a change in those components of the optical tensor in which the expanded sets of (four) indices contain the indices of the X and Y axes an odd number of times. In the following table of the optical constants we indicate these components:

$$\begin{array}{cccccc} \cline{4-5} \pi_{11} & \pi_{12} & \pi_{13} & \multicolumn{1}{|c}{\pi_{14}} & \multicolumn{1}{c|}{0} & 0 \\ \pi_{21} & \pi_{11} & \pi_{13} & \multicolumn{1}{|c}{-\pi_{14}} & \multicolumn{1}{c|}{0} & 0 \\ \pi_{31} & \pi_{31} & \pi_{33} & \multicolumn{1}{|c}{0} & \multicolumn{1}{c|}{0} & 0 \\ \cline{4-5} \cline{1-3} \cline{6-6} \multicolumn{1}{|c}{\pi_{41}} & -\pi_{41} & \multicolumn{1}{c|}{0} & \pi_{44} & 0 & \multicolumn{1}{|c|}{0} \\ \multicolumn{1}{|c}{0} & 0 & \multicolumn{1}{c|}{0} & 0 & \pi_{44} & \multicolumn{1}{|c|}{2\pi_{41}} \\ \cline{1-3} \cline{6-6} \cline{4-5} 0 & 0 & 0 & \multicolumn{1}{|c}{0} & \multicolumn{1}{c|}{\pi_{14}} & \pi_{11}-\pi_{12} \\ \cline{4-5} \end{array}$$

It follows from this that the difference in the optical indicatrices of the twinning components is determined only by the coefficients π_{14} and π_{41}, whose magnitude is much less than that of the other photoelastic constants. As can be seen from (3), the components of Dauphine twinning are optically equivalent only if $\sigma_x = \sigma_y$ and all the tangential stresses τ_{ij} vanish.

At first sight it may seem that Dauphine twinning could conveniently be detected optically by the same methods as those used by Pockels in determining π_{14} and π_{41}. It is found, however, that in these determinations Pockels made use of complex measurements of the absolute retardation of the rays, and obtained π_{14} and π_{41} only in combination with other constants which are much larger than the desired ones.

For this reason we shall discuss the possibility of detecting twinning in a simpler manner, based on the effect of relative retardation of the rays.

Observation Along the Z Axis

For simplicity let us assume that the only nonzero tangential stress is τ_{yz}. Then the index of refraction ellipse is given by

$$\left(\frac{1}{n_0^2}\mp\pi_{14}\tau_{yz}\right)x^2+\left(\frac{1}{n_0^2}\pm\pi_{14}\tau_{yz}\right)y^2=1, \qquad (4)$$

where the upper sign is used for one component of twinning, and the lower sign for the other. This leads to biaxial crystals with the angle between the axes given by 2Ω, where

$$\sin^2\Omega \cong \frac{2\pi_{14}\tau_{yz}}{\frac{1}{n_0^2}-\frac{1}{n_r^2}}; \tag{5}$$

the plane of the optical axes, however, coincides with the XZ plane in the first case, and with the YZ plane in the second case. In the first approximation we have

$$\Delta = n_x - n_y = \pm n_0^3\pi_{14}\tau_{yz} = \pm 0{,}35\cdot 10^{-7}\tau_{yz} \tag{6}$$

(where τ_{yz} is given in kg/cm²). When $\tau_{yz} = 100$ kg/cm², the twinning according to Equation (6) should lead to double refraction whose magnitude is 35 mμ/cm, but with different signs.

The phenomenon is complicated, however, by the rotation of the plane of polarization. According to the general theory of Voigt [7] there propagate, in optical biaxial elliptically polarizing media, two elliptically polarized waves with similar and mutually perpendicular elliptical vibrations such that the principal axes of the ellipses lie along the directions along which the vibrations would occur if there were no rotation of the plane of polarization (Fig. 1). The difference between the squares of the propagation velocities v_r and v_l of these waves is the geometric mean of the difference between the velocities v_r^0 and v_l^0 of the right and left rotated waves in the monoaxial medium (in the present case the unstressed crystal) and the difference between the squares of the velocities v_x and v_y which would occur without rotation of the plane of polarization;* in other words,

$$v_r^2 - v_l^2 = \sqrt{(v_r^{0^2} - v_l^{0^2})^2 + (v_x^2 - v_y^2)^2}. \tag{7}$$

If the velocities hardly differ, the differences between the squares can be replaced by the differences between the velocities themselves or simply by the differences between the index of refraction, and we arrive at the well known rule for the phase change of waves in doubly refracting media with axes slowly rotating along the ray, which has been recently treated in detail in its application to optical stress analysis (see for instance, [8-10]

$$\Delta' = n_l - n_r = \sqrt{\Delta^2 + \left(\frac{\lambda\rho}{\pi}\right)^2}. \tag{8}$$

Here Δ is the proper birefringence of each layer, λ is the wavelength, and ρ is the rate of rotation of the axes along the ray. In our case $\Delta = n_x - n_y$, ρ is the specific rotation of the plane of polarization and $\frac{\lambda\rho}{\pi} = n_l^0 - n_r^0 = \Delta_\rho$ is the circular birefringence of the crystal.

For any actually attainable stresses, $|\Delta| << |\Delta_\rho|$, and it follows from (6) and (8) that a stress τ_{yz} changes the index of refraction for right and left rotation by the amount

$$\Delta'' = \Delta' - \Delta_\rho \cong \frac{n_0^6\pi_{14}^2\tau_{yz}^2}{2\Delta_\rho}. \tag{9}$$

In particular, for the D line $\Delta_\rho = n_l^0 - n_r^0 = 7.1\cdot 10^{-5}$ [11] and

$$\Delta'' = 1.7\cdot 10^{-11}\,\tau_{yz}^2 \;(\tau_{yz} \text{ in kg/cm}^2). \tag{10}$$

When $\tau_{yz} = 100$ kg/cm² we have $\Delta'' = 1.7\cdot 10^{-7}$, or only 1.7 mμ/cm, which is twenty times less than the value obtained from (6).

---

* To be specific, we shall discuss right circularly polarized quartz ($v_r > v_l$).

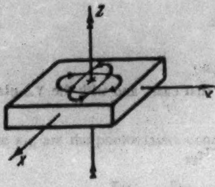

Fig. 1. Splitting of rays parallel to the Z axis in a stressed quartz crystal.

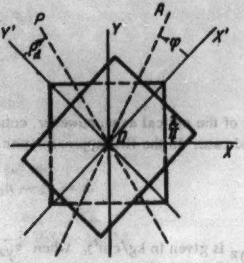

Fig. 2. Diagram of optical detection of Dauphine twinning, observing along the Z axis.
P and A are the polarization planes of the polarizer and analyzer, respectively. The rest of the notation is given in the text.

In other words, one can hardly detect the circular birefringence caused by a stress τ_{yz}. We arrive at exactly the same conclusion in attempting to use a stress τ_{xz} to separate twinning.

Up to this point, however, we have used only the phase difference of the two rays, ignoring their amplitude. In addition, the axial ratio of the ellipse for each elliptically polarized ray also depends on the birefrigence Δ [4]. If $\tau_{yz} > 0$, then in the faster ray the major axis of the ellipse is parallel to the X axis, and the axial ratio κ is given by

$$\varkappa = \sqrt{\frac{\sqrt{\Delta^2 + \Delta_\rho^2} - \Delta}{\sqrt{\Delta^2 + \Delta_\rho^2} + \Delta}} \tag{11}$$

(the notation is simpler than that of Equation (8), and $\Delta > 0$).

Let us consider, following Pockels, optical effects which will be observed if the analyzer is set diagonally with respect to the X and Y axes. As an analyzer, however, we shall use not a wedge compensator, but a quarter wave plate. Let the analyzer be oriented so that the vibrations in the ray leaving the unstressed crystal be along the bisector of the angle XOY (this is done by rotating the polarizer through an angle $\rho_d = \rho \cdot d$ with respect to this angle bisector, where d is the thickness of the crystal along the ray). After leaving the stressed crystal, the vibrations along the X and Y directions in the right and left rotated rays will be given by

$$\begin{aligned} x_r &= \cos \omega t, & x_l &= \varkappa \sin(\omega t - \psi), \\ y_r &= \varkappa \sin \omega t, & y_l &= \cos(\omega t - \psi) \end{aligned} \tag{12}$$

(where ω is the angular frequency of the vibrations, and $\psi = \frac{2\pi}{\lambda} \cdot \Delta' \cdot d$ is the phase difference between the rays). For the vibrations along the axes of the $\lambda/4$ plate (Fig. 2) we then obtain

$$\begin{aligned} x' &= \frac{1}{\sqrt{2}} \cos \frac{\psi}{2} (\cos \omega t + \varkappa \sin \omega t), \\ y' &= \frac{1}{\sqrt{2}} \sin \frac{\psi}{2} (\sin \omega t + \varkappa \cos \omega t). \end{aligned} \tag{13}$$

The plate introduces an additional phase shift of $\pi/2$, and we obtain

$$x' = \frac{1}{\sqrt{2}} \cos \frac{\psi}{2} (\cos \omega t + \varkappa \sin \omega t),$$
$$y' = \frac{1}{\sqrt{2}} \sin \frac{\psi}{2} (\cos \omega t - \varkappa \sin \omega t). \tag{14}$$

In the plane rotated through an angle φ with respect to the X' axis, the square of the amplitude is given by

$$A^2 = \frac{1}{4} [(1 + \varkappa^2) + \cos(\psi - 2\varphi) + \varkappa^2 \cos(\psi + 2\varphi)]. \tag{15}$$

Differentiating (15) by φ, we obtain an equation for finding the extrema, namely

$$\frac{\sin(\psi - 2\varphi)}{\sin(\psi + 2\varphi)} = \varkappa^2. \tag{16}$$

Since $|\psi| \ll 1$, the approximate solution of this equation has the simple form

$$\tan 2\varphi = \psi \cdot \frac{1 - \varkappa^2}{1 + \varkappa^2} = \psi \cdot \frac{\Delta}{\sqrt{\Delta^2 + \Delta_\rho^2}} = \frac{2\pi}{\varkappa} \cdot \Delta \cdot d. \tag{17}$$

The quantity on the right side of (17) has simple physical meaning: it is equal to the phase difference δ between the rays which would occur in the sample in the absence of circular birefringence, namely

$$\delta = \frac{2\pi}{\lambda} \Delta \cdot d. \tag{18}$$

Noting that δ is quite small, we finally find that the angle of rotation of a Nicol prism analyzer placed behind the quarter wave plate gives maximum darkening when it is equal to

$$\varphi = \frac{\delta}{2}, \tag{19}$$

as in ordinary use of a Senarmon compensator [11]. Thus after introducing a quarter wave plate, Dauphine twinning exhibits dark regions, and the angle 2φ between them is numerically equal to the phase difference due to the double refraction Δ in a crystal without rotation of the plane of polarization. Expressing this angle in degrees, we obtain

$$2\varphi \cdot \frac{180^\circ}{\pi} = \frac{360^\circ}{\lambda} \Delta \cdot d = \frac{360^\circ}{\lambda} d n_0^3 \pi_{14} \tau_{yz} \tag{20}$$

which, for $\lambda = 589$ mμ and a twinning thickness $d = 1$ mm, is approximately 2° for each 100 kg/cm^2 of the tangential stress τ_{yz}.

Of the various methods of realizing this method, one should mention rotation of a Z-cut about the X axis (Δ is due to a τ_{yz} stress) or about the Y axis (Δ is due to a τ_{zx} stress), as well as rotation of a sample cut in the form of a prism about the Z axis (Δ is due to a tangential stress $\tau = \sqrt{\tau_{xz}^2 + \tau_{yz}^2}$ acting on the plane of the base).

Observation Perpendicular to the Z Axis

In this case the stressed crystal has a high anisotropy (the initial birefrigence $n_e - n_0 = 0.0092$, or 92 μ/cm), which makes the detection of additional effects due to mechanical stress extremely difficult. It is sufficient to note that according to (3) and (6) a stress τ_{yz} of magnitude 100 kg/cm² changes the birefrigence of quartz only by $3.5 \cdot 10^{-6}$, which is about 0.04%. One can, however, make use of the rotation of the indicatrix due to a load applied perpendicular to the Z axis.

As was shown by Pockels [5] it follows from Equation (3) that if the direction of a pressure p makes an angle φ with the X axis, the indicatrix rotates about an axis whose angle with the X axis is 2φ, this rotation being by an amount

$$\Phi \cong \frac{\pi_{41} p}{\frac{1}{n_0^2} - \frac{1}{n_e^2}}. \tag{21}$$

It is most convenient to observe the effect for $\varphi = 90°$ (pressure along the Y axis, or $p = \sigma_y$). In this case the indicatrix rotates about the X axis, along which the crystal must be illuminated. Inserting the numerical values of the constants into Equation (21), we obtain the expression

$$2\Phi = 0.63 \cdot 10^{-1} \sigma_y, \tag{22}$$

for the angle between the minima of the twinning, which corresponds to an angle of 4.3' for $\sigma_y = 100$ kg/cm².

The effect is found to be much less noticeable than when observing along the Z axis. It should be noted, however, that at a pressure of 500 kg/cm² Pockels actually observed and measured the angle of rotation of the indicatrix in a quartz single crystal, and this angle was found to be 11', as follows from (21). One may hope that the detection of Dauphine twinning by observation along the X axis may be possible also for much lower stresses by fine adjustment of the optics.

Other Methods for Optical Detection of Twinning

The analysis of the effect when observing at an angle to the Z axis now presents no great difficulty. The double refraction one is looking for will obviously be masked both by the linear and circular birefrigence. When the former of these dominates, it is more convenient to detect rotation of the indicatrix, and when the second dominates it is more convenient to use a quarter wave plate. In principle these cases present nothing new, although in practice it may be found convenient to use just such a method of observation (at an angle with respect to the Z axis).

In conclusion we find it interesting to note there exists yet another possibility of detecting Dauphine twinning, this based on the use of an effect entirely similar to the one discussed. We speak now of the electro-optical effect, which involves the distortion of the indicatrix under the action of an electric (rather than mechanical) field.

According to the data of various authors as presented by Kedi [12], the total birefringence which occurs in quartz $\Delta = n_x - n_y$ under the action of an electric field $E_x = 1$ v/cm is about $2.2 \cdot 10^{-10}$. Thus a field $E_x = 16$ kv/cm gives about the same effect as a stress $\tau_{yz} = 100$ kg/cm².

Both in the case of a mechanical stress and an electric field we have not accounted for possible deviations of the field from homogeneity, which must inevitably occur at the boundaries of twinning due to the difference of the elastic and piezoelectric coefficients. This effect, it would seem, may simplify the observation of the twinning boundary.

LITERATURE CITED

[1] A. V. Shubnikov, Quartz and its Uses [In Russian] (1940).

[2] A. W. Schubnikow and E. W. Zinserling, Über die Schlag-und Druckfiguren und über die Quarzzwillinge, Z. Krist. 83, 3-4, 1932.

[3] W. A. Wooster, The Control and Elimination of Electrical (Dauphine) Twinning in Quartz, J. Inst. Electr. Eng. 84, 927-938,(1947).

[4] F. Pockels, Optisches Verhaltung deformierten Kristalle, Ann. d. Phys. und Chimie (Wied. Ann.) 37, 144-172, 269-305, 372-394,(1889).

[5] F. Pockels, Lehrbuch der Kristalloptik,(1906).

[6] S. Bhagavantam, Proc. Ind. Acad. Sci. 16, 359,(1943).

[7] W. Voigt, Theorie des Lichtes für volkommen durchsichtige Medien. Ann. d. Phys. und Chemie (Wied. Ann.), 19, 893,(1883).

[8] D. C. Drucker and R. D. Mindlin, Stress Analysis by Three-Dimensional Photoelastic Methods, J. Appl. Phys. 11, 724-732,(1940).

[9] V. L. Ginzburg, "On optical stress analysis," J. Tech. Phys. (USSR) 14, 3, 181-192 (1944).

[10] V. L. Indenbom, "On surface stresses in glass objects," J. Tech. Phys. (USSR) 26, 2, 370-374 (1956).*

[11] A. V. Shubnikov, Optical Crystallography [In Russian] (1950), pp. 191, 161.

[12] W. Cady, Piezoelectricity and its Practical Uses (1949) p. 661.

Crystallography Institute
Academy of Sciences, USSR

Received November 21, 1956

---

* [Soviet Physics – Technical Physics, p. 362].

SYMMETRY AND PIEZOELECTRIC PROPERTIES OF CRYSTALS AND "TEXTURES"

I. S. Zheludev

This paper shows that piezoelectric polarization in crystals and in textures is associated with special polar directions, either those already present or those arising due to mechanical action. The Curie symmetry principle has been used to classify crystals and textures as possibly piezoelectric; also the change in symmetry due to mechanical action has been studied directly. The paper also shows that under certain conditions piezoelectric polarization can be brought about in crystals belonging to the 3/4 group and in textures of the ∞/∞ group. On this basis it is assumed that the absence of a symmetry center in crystals and in textures may serve as a necessary and sufficient indication for classifying them as possibly piezoelectric.

1. Introduction

The Voigt [1] equations have been used up until now for describing the piezoelectric effect. These equations in tensor form determine the relation between the polar vectors of electric polarization, induction, or electric field on one hand and the mechanical stress or deformation tensor (symmetrical polar tensor of the second rank) on the other. The symmetry condition on the stress (or deformation) tensor results in the fact that a piezoelectric tensor of the third rank in the general case does not have 27 but 18 independent coefficients. Tensor equations, linking for example the polarization vector P and the symmetrical mechanical stress tensor ($t_{ik} = t_{ki}$), may be written in the form of a table

$$\begin{array}{c|cccccc} & t_{11} & t_{22} & t_{33} & t_{23} & t_{31} & t_{12} \\ \hline P_1 & d_{11} & d_{12} & d_{13} & d_{14} & d_{15} & d_{16} \\ P_2 & d_{21} & d_{22} & d_{23} & d_{24} & d_{25} & d_{26} \\ P_3 & d_{31} & d_{32} & d_{33} & d_{34} & d_{35} & d_{36} \end{array}$$

where d_{ilk} are the piezoelectric coefficients.

Crystal symmetry, as is well known, imposes definite limitations on the form of the piezoelectric coefficient tensor; depending on this symmetry a part of the coefficients (or even all other than zero) are found to be equal one to the other, and part (or even all) equal to zero. In accordance with this all crystals are either those in which a piezoelectric effect is possible (possibly piezoelectric) or those in which it is impossible. The crystals which are possibly piezoelectric are those whose piezoelectric tensor has at least one piezoelectric coefficient which is not zero; the crystals in which a piezoelectric effect is impossible are those all of whose

---

* Textures (tekstury) —"homogeneous bodies with non-lattice structures, composed of many particles of any physical nature definitely oriented in space according to the laws of symmetry." Shubnikov [5] — Publisher's note.

piezoelectric coefficients are equal to zero; i.e., such crystals for which the piezoelectric tensor is a zero-tensor. It can be shown analytically [1] that on this basis the crystals which belong to the following 20 point groups (according to A. V. Shubnikov) may be considered as possibly piezoelectric:

$$1;\ 2;\ 3;\ 4;\ 6;\ m;\ 2\cdot m;\ 3\cdot m;\ 4\cdot m;\ 6\cdot m;\ 4;\ \bar{2}:2;$$
$$3:m;\ 3:2;\ \bar{4}\cdot m;\ 4:2;\ 6:2:\ m\cdot 3:m;\ 3/\bar{4};\ 3/2.$$

In order to classify crystals as possibly piezoelectric another method than the one indicated has been occasionally used [2-4], taking into consideration that crystals having no center of symmetry may be considered as possibly piezoelectric. This method, however, is less rigorous, for when it is used one must always make the reservation that even though the crystals belonging to the 3/4 group do not have a center of symmetry they can not be classified as possibly piezoelectric because the piezoelectric tensor for crystals in this group is a zero-tensor.

Crystals are not the only structures to show piezoelectric properties. Shubnikov [5] presents a general study of 'textures' and in particular of piezoelectric textures. The study of textures which belong by symmetry to limiting point groups is especially detailed:

$$\infty;\ \infty\cdot m;\ \infty:2;\ \infty:m;\ m\cdot\infty:m;\ \infty/\infty;\ \infty/\infty\cdot m.$$

Shubnikov showed that for points groups ∞, $\infty\cdot m$, $\infty:2$ the piezoelectric tensor is not zero-valued and that textures of such a symmetry may be classified as possibly piezoelectric (they are called piezoelectric textures). As for the textures which belong to the point group ∞/∞ they too, in spite of an absence of a center of symmetry, have a zero-valued piezoelectric tensor.

To date the piezoelectric textures of Rochelle salt, wood, ceramic barium titanate and others [6] have been thoroughly studied.

2. Application of the Curie Symmetry Principle in Classifying Crystals and Textures as Possibly Piezoelectric

A more objective geometric study of the piezoeffect in crystals and textures can be carried out by means of the Curie symmetry principle.

Studying, for example, the simple piezoeffect we can easily see that the crystal (or the texture) generally changes its symmetry due to some mechanical action. In clarifying questions relating to the piezoeffect the changes of symmetry which are important are not random ones but rather those which are associated with specific polar directions in the crystals and the textures. (By specific polar directions in crystals we understand those directions which remain unchanged under any symmetrical transformations corresponding to the point group of the crystal studied.) The importance of these special polar directions for the piezoelectric effect is due to the fact that only with special polar directions is electric polarization (described by a polar vector) compatible with symmetry. In other words, as long as the very appearance of electric polarization in a certain direction makes this direction a special polar one, in the crystal (or the texture) a piezoelectric polarization will be possible only when a special polar direction arises due to some mechanical action (but not necessarily before). Let us note that a crystal which has been subjected to a mechanical action may have more than one geometrically special polar direction (for example in the case of a decrease in symmetry to the m and 1 point groups). However in these cases, as in the case of a single direction, it is possible to combine an electrically special polar direction (which is the direction coinciding with the direction of the electric polarization vector) with at least one geometrically special polar direction.

Therefore the question whether a certain crystal (or texture) may or may not be classified in the piezoelectric group within the framework of the Voigt theory may be reduced to the question of whether or not it can show special polar directions following mechanical action which is defined by means of a symmetrical tensor of the second rank. This question may be answered both by the study of the symmetry change for a given crystal using a generalized Hooke's law or in a more simple manner by using the Curie symmetry principle. It can be easily seen that the problem indicated is in a certain sense the opposite of the problem we considered with Shuvalov [7] on the determination of changes in symmetry of crystals when electric polarization arises in them. Actually in this latter case a change in symmetry is looked for because electric polarization has appeared in the crystal, whereas in the problem we are now considering we are looking for a change in symmetry due to mechanical action which would bring about electric polarization (this, however, is not always possible).

According to the Curie symmetry principle (particularly well demonstrated with concrete examples by Shubnikov [8]) the symmetry of a crystal subjected to external action is determined as the highest general point subgroup of the external action and the point group of the crystal itself for a given distribution of the elements of both action and crystal symmetry (the principle of superposition). As we shall eventually need to know the symmetry arising from external action as well as the mutual distribution of the elements of both the action and crystal symmetry let us consider these questions.

The external action symmetry may be defined as the symmetry of the tensor which describes it. Thus in the case which interests us, in order to determine the symmetry of mechanical stresses (or deformations) it is necessary to know the symmetry of a symmetrical polar tensor of second rank. This question has been examined in detail by Shubnikov [9], who has shown that a symmetrical polar tensor of the second rank may have its own symmetry, belonging to one of three point groups m · 2 : m, m · ∞ : m, and ∞/∞ · m depending on whether the diagonalyzed tensor has 3, 2 or 1 independent coefficients, respectively. This makes possible the establishment of a well defined action symmetry determined, for example, by the stress components t_{ii} and $t_{ik} = t_{ki}$ as in the Voigt equations. Thus an external action defined by the tensors (tensile or compressive stress) in the form

$$\begin{Vmatrix} t_{11} & 0 & 0 \\ 0 & 0 & 0 \\ 0 & 0 & 0 \end{Vmatrix}, \quad \begin{Vmatrix} 0 & 0 & 0 \\ 0 & t_{22} & 0 \\ 0 & 0 & 0 \end{Vmatrix} \quad \text{or} \quad \begin{Vmatrix} 0 & 0 & 0 \\ 0 & 0 & 0 \\ 0 & 0 & t_{33} \end{Vmatrix}, \tag{1}$$

having two distinct diagonal coefficients, has a m · ∞ : m symmetry.

The symmetry of an action determined by pure displacement stresses ($t_{ik} = t_{ki}$) whose tensor is written down as follows:

$$\begin{Vmatrix} 0 & t_{12} & 0 \\ t_{12} & 0 & 0 \\ 0 & 0 & 0 \end{Vmatrix}, \quad \begin{Vmatrix} 0 & 0 & t_{13} \\ 0 & 0 & 0 \\ t_{13} & 0 & 0 \end{Vmatrix} \quad \text{or} \quad \begin{Vmatrix} 0 & 0 & 0 \\ 0 & 0 & t_{23} \\ 0 & t_{23} & 0 \end{Vmatrix}, \tag{2}$$

may be found as above after tensors of this type have been reduced to diagonal form. This may be done by rotating the tensor 45° about the axis around which the displacement takes place. As a result of such a reduction the tensors (2) will have the form

$$\begin{Vmatrix} t_{11} & 0 & 0 \\ 0 & -t_{11} & 0 \\ 0 & 0 & 0 \end{Vmatrix}, \quad \begin{Vmatrix} t_{11} & 0 & 0 \\ 0 & 0 & 0 \\ 0 & 0 & -t_{11} \end{Vmatrix}, \quad \begin{Vmatrix} 0 & 0 & 0 \\ 0 & t_{22} & 0 \\ 0 & 0 & -t_{22} \end{Vmatrix}, \tag{3}$$

from which it follows that they, having three distinct diagonal coefficients, belong to the m · 2 : m group.

Reciprocal distribution of the elements of both crystal and external action symmetry are defined by their orientation in relation to the crystallophysical coordinate system. It is easy to see that if one assumes (as it is usually done) that the tensors (1) and (2) are written down in the crystallophysical coordinate system, then the axis ∞ of the external action which interests us, determined by the tensors (1), coincides with one of the crystallophysical axes. The external action determined by tensors (2) is oriented in such a way that one of the axes 2 coincides with the axis around which the displacement takes place, whereas the two others lie in a plane perpendicular to this axis, making an angle of 45° with the two crystallophysical axes (Fig. 1).

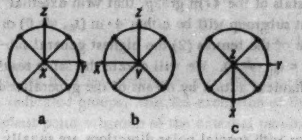

Fig. 1. Orientation of the elements of symmetry in a symmetrical polar stress tensor of a pure displacement referred to the crystallophysical coordinate system.
a) $t_{23} = t_{32} \neq 0$; b) $t_{13} = t_{31} \neq 0$; c) $t_{12} = t_{21} \neq 0$.

Let us consider the direct application of the Curie symmetry principle for the finding of piezoelectric point groups in crystals and textures. First of all let us consider crystals and textures belonging to groups having a center of symmetry. In the case of crystals these groups are

$$\bar{2};\ 2:m;\ \ m\cdot 2:m;\ \ 4:m;\ \ m\cdot 4:m;$$
$$\bar{6};\ \bar{6}\cdot m;\ \ 6:m;\ \ m\cdot 6:m;\ \bar{6}/2,\ \bar{6}/4,$$

and for textures these groups are

$$\infty:m;\ \ m\cdot\infty:m;\ \ \infty/\infty\cdot m.$$

As long as the mechanical force, determined by the symmetrical polar tensor of second order (and likewise any polar tensor of the second order) possesses a center of symmetry, according to the Curie symmetry principle, the upper point group of these crystals (and textures) and the external action will always have, among the elements of symmetry, a center of symmetry. The presence of a center of symmetry in a crystal (or texture) subjected to a mechanical action is incompatible with special polar directions; therefore crystals and textures belonging to the centric point groups can not be classified as possibly piezoelectric. The conclusion arrived at agrees completely with the results obtained by Voigt for centric crystals.

Let us look at crystals and textures having special polar directions. These are the so called pyroelectric crystals and pyroelectric textures which belong to the following point groups:

$$1;\ 2;\ 3;\ 4;\ 6;\ m;\ 2\cdot m;\ 3\cdot m;\ 4\cdot m;$$
$$6\cdot m;\ \infty;\ \infty\cdot m.$$

The application of the Curie symmetry principle to crystals and textures in these point groups shows that the general point subgroup of the external mechanical action, defined by a symmetrical tensor of the second tank, and of the crystal (and texture) will never contain a center of symmetry in this case. Furthermore, a

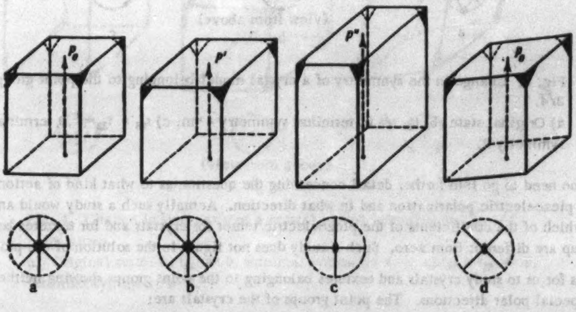

Fig. 2. Piezoelectric polarization in pyroelectric crystals of the 4·m point group arising from a change in the spontaneous polarization vector.
a) Original state of the crystal; b) $t_{33} \neq 0$, piezoelectric polarization along the X axis; c) $t_{22} \neq 0$, piezoelectric polarization along the X_3 axis; d) $t_{12} = t_{21} \neq 0$, no piezoelectric polarization ; P_0) spontaneous polarization, P' and P" changed vectors of spontaneous polarization.

centric force in this case can not eliminate special polar directions from such crystals and textures. Actually, using the Curie symmetry principle we find, for example, for crystals of the 4 · m group, that with external action, defined by one of the tensors (1), the general highest point subgroup will be either 4 · m ($t_{33} \neq 0$) or 2 · m (t_{11} or $t_{22} \neq 0$). When the external action is defined by one of the tensors (2) the highest general subgroup will be either 2 · m ($t_{12} = t_{21} \neq 0$) or m($t_{23} = t_{32} \neq 0$ or $t_{13} = t_{31} \neq 0$). We will obtain the same result if we study the concrete changes in crystal symmetry due to mechanical action by means of the generalized Hooke's law.

Crystals and textures which belong to the pyroelectric groups with special polar directions are usually associated with spontaneous electric polarization. Thus the piezoelectric effect in pyroelectric crystals and pyroelectric textures may be treated as an effect due to a change in size and direction of the spontaneous polarization vector. This effect can be graphically observed in a crystal belonging to the 4 · m group (Fig. 2) which we have studied. It is easy to see on the basis of the above statements why, for example, piezoelectric polarization can not be formed in this crystal with stresses $t_{12} = t_{21} \neq 0$. The fact that the crystal, deformed as above, having a special polar direction (terminal symmetry 2 · m) does not show in this case piezoelectric polarization (for in this case there is no change in either the absolute value or the direction of the vector of spontaneous polarization) does not mean that a crystal belonging to a 4 · m point group cannot be classified as possibly piezoelectric because in order to classify it as a piezoelectric crystal it is sufficient that in at least one case piezoelectric polarization should take place due to the mechanical action defined by symmetrical polar tensors of the second degree. In our case this occurs when $t_{33} \neq 0$.

An analogous study may be carried out for other pyroelectric crystals and textures. It shows that all pyroelectric classes and pyroelectric textures are possibly piezoelectric.

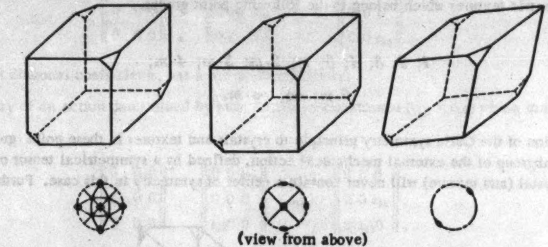

Fig. 3. Change in the symmetry of a crystal model belonging to the point group $3/\bar{4}$.
a) Original state; b) $t_{33} \neq 0$, terminal symmetry $\bar{4} \cdot m$; c) $t_{23} = t_{32} \neq 0$, terminal symmetry 2.

There is no need to go into further detail concerning the question as to what kind of action will or will not bring about piezoelectric polarization and in what direction. Actually such a study would answer the question as to which of the coefficients of the piezoelectric tensor for crystals and for textures belonging to a given point group are different from zero. Such a study does not figure in the solution of our problem.

It remains for us to study crystals and textures belonging to the point groups showing neither a center of symmetry nor special polar directions. The point groups of the crystals are:

$$\bar{4};\ 2:2;\ 3:m;\ 3:2;\ \bar{4}\cdot m;\ 4:2;$$

$$6:2;\ m\cdot 3:m;\ 3/\bar{4};\ 3/2;\ 3/4,$$

and the point groups of the textures are :

$$\infty : 2; \infty/\infty.$$

Using the Curie symmetry principle it can be shown that for all crystals and all textures belonging to the above indicated groups, with the exception of the 3/4 point group for crystals and the ∞/∞ group for textures, the highest point subgroup of the external mechanical action point groups (defined by a symmetrical polar tensor of the second order) and of the crystal itself (or the texture) may contain (with the above mentioned mutual arrangement of the symmetry elements), among the elements of symmetry, either special axes or a special plane (in the case where point group $\underline{m}$ is the subgroup symmetry) or a special volume (in the case where point group 1 is the subgroup symmetry).

Let us consider, as a concrete example by means of the generalized Hooks's law, the simplest and most graphic case when special polar axes are formed within a crystal as a result of an external mechanical action. A change in the symmetry of a crystal belonging to the $3/\bar{4}$ group is shown in Fig. 3. It can be seen from the drawing that the external mechanical action defined by a type (1) tensor lowers the symmetry of the crystal to the point group $\bar{4} \cdot m$. However, as in this case no special polar directions are formed, piezoelectric polarization within the crystal can not take place. However, special polar directions may arise in the crystal due to displacement stresses [tensors of the (2) type]. The crystal symmetry in this case decreases to the symmetry of point group 2 and piezoelectric polarization will be associated with the special polar axis 2.

Thus crystals and textures belonging to point groups showing neither centers of symmetry nor special polar directions are possibly piezoelectric with the exception of the point groups 3/4 and ∞/∞.

3. Piezoelectric Effect in Crystals of the 3/4 Point Group and Textures of the ∞/∞ Point Group

The results that we have obtained so far agree perfectly with those of Voigt. However, we must note in particular that it is impossible to classify crystals as possibly piezoelectric when we consider only the above mentioned mutual arrangement of the elements of symmetry in the crystal and the action (Fig. 4). However, in the case of a general orientation of the action in relation to the crystals of this class it may happen that special polar directions will be present in the crystal after the application of the action (in accordance with the Curie symmetry principle) and in the most general case the crystal may decrease symmetry as far as the symmetry of group 1. Figure 5 shows the case in which action lowers the crystal symmetry of point group 3/4 to the point group having a special polar direction (point group 2 with axis 2 coinciding with one of the previous 4 axes of

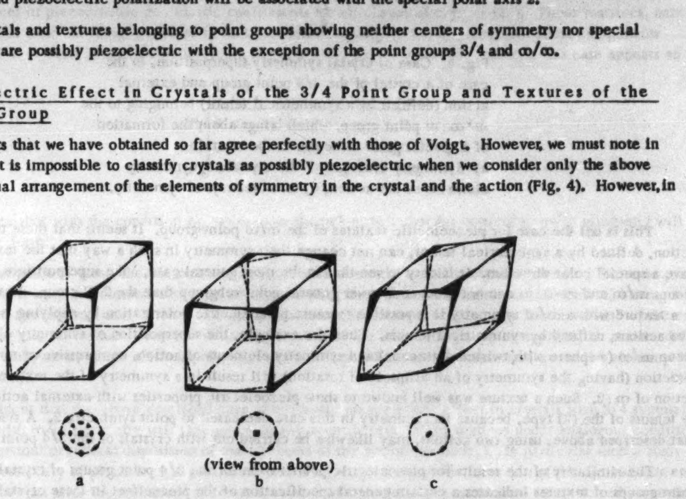

Fig. 4. Change in symmetry of a crystal model belonging to the 3/4 point group.
a) Original state; b) $t_{33} \neq 0$, terminal symmetry 4 : 2; c) $t_{23} = t_{32} \neq 0$, terminal symmetry 2 : 2.

the crystal). Therefore if one proceeds from the more general positions, then the crystals which belong to the 3/4 group must be classified as possibly piezoelectric.

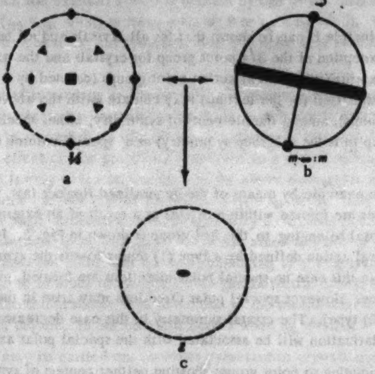

**Fig. 5. Case of crystal symmetry superposition, in the case of a crystal of the 3/4 point group and external action (defined by a symmetrical tensor) belonging to the m·∞:m point group, which brings about the formation of a special polar direction in the crystal.
a) Symmetry elements of the crystal; b) symmetry elements of the action; c) terminal crystal symmetry.**

This is not the case for piezoelectric textures of the ∞/∞ point group. It seems that these textures under action, defined by a symmetrical tensor, can not change their symmetry in such a way that the texture would have a special polar direction. It is easy to see that in the most general case, the superpositions of point groups ∞/∞ and m·2:m can not produce a lower general point subgroup than the 2:2 group. However, even in a texture with a ∞/∞ symmetry it is possible to cause piezoelectric polarization by applying two consecutive actions, defined by symmetrical tensors. Thus, for example, the superposition of symmetry elements of group ∞/∞ (a sphere with twisted diameters) and symmetry elements of action, compressive or tensile in any direction (having the symmetry of an ellipsoid of rotation) will result in a symmetry of the texture following action of ∞:2. Such a texture was well known to show piezoelectric properties with external action, defined by tensors of the (2) type, because its symmetry in this case decreased to point symmetry 2. A study, such as that described above, using two actions, may likewise be carried out with crystals of the 3/4 point group.

The similarity of the results for piezoelectric polarization for the 3/4 point groups of crystals and the ∞/∞ point groups of textures indicates a certain general specification of the piezoeffect in these crystals and textures which distinguishes it from the usually studied piezoeffect. The piezoelectric polarization in this case may be considered to be a result of a previous change in symmetry due to a mechanical action, defined by a symmetrical tensor, followed by a subsequent action on the crystal with a changed symmetry.

Thus this effect is a kind of "quadratic piezoeffect." This in turn indicates that the effect is very small and that the piezoelectric coefficients depend on the degree of the prior "compression." The fact that in the crystals of the 3/4 point group piezoelectric polarization may be produced also by an action defined by a symmetrical tensor (see Fig. 5) is not in contradiction with the conclusion drawn, because such an action, in the crystallophysical system of coordinates, is described by the tensor

$$\begin{Vmatrix} 0 & 0 & 0 \\ 0 & t_{22} & t_{23} \\ 0 & t_{23} & t_{33} \end{Vmatrix}, \tag{4}$$

which can be considered as characteristic of an unequal compression, a tension along the 2 and 3 axes with a simultaneous displacement.

It is interesting to note that the subsequent action, analytically studied above, defined by two symmetrical tensors, may be described as the product of tensors

$$\begin{Vmatrix} 0 & 0 & 0 \\ 0 & 0 & 0 \\ 0 & 0 & t_{33} \end{Vmatrix} \begin{Vmatrix} 0 & 0 & 0 \\ 0 & 0 & t_{23} \\ 0 & t_{22} & 0 \end{Vmatrix} = \begin{Vmatrix} 0 & 0 & 0 \\ 0 & 0 & 0 \\ 0 & t_{23} & 0 \end{Vmatrix}, \tag{5}$$

which, as can be seen, is described by an already nonsymmetrical tensor.

In this connection one should mention the Laval [10] and Raman [11] papers defining the stressed state of a solid body in the general case by a nonsymmetrical tensor ($t_{ik} \neq t_{ki}$). For this case LeCorre obtained, analytically, matrices of piezoelectric and elastic coefficients for all classes of crystals [12]. These matrices, naturally, may differ from the Voigt matrices in that part which belongs to the displacement stress components ($t_{ik} \neq t_{ki}$). For crystals in the 3/4 point group, in particular, the piezoelectric tensor in this case appears as

$$\begin{array}{c|ccccccccc} & t_{11} & t_{22} & t_{33} & t_{23} & t_{31} & t_{12} & t_{32} & t_{13} & t_{21} \\ \hline P_1 & 0 & 0 & 0 & d_{14} & 0 & 0 & -d_{14} & 0 & 0 \\ P_2 & 0 & 0 & 0 & 0 & d_{14} & 0 & 0 & -d_{14} & 0 \\ P_3 & 0 & 0 & 0 & 0 & 0 & d_{14} & 0 & 0 & -d_{14} \end{array}$$

It is easy to see that with the condition $t_{ik} \neq t_{ki}$ the piezoelectric tensor for textures of ∞/∞ symmetry will have the same form.

From our point of view, the piezoelectric polarization due only to this nonsymmetricity of the tensor, may be explained if it may be considered as a polarization arising from action on the crystal (or texture) having a lower symmetry than the original one. Such a change may be brought about not only by prior "compression" of the crystal (or texture) but also (as we have seen in the case of crystals of the 3/4 point group) by applying an action, defined by a symmetrical tensor, whose elements of symmetry are disposed generally with reference to the elements of crystal symmetry.

It is evident that the above described case of quadratic piezoelectric effect in crystals with 3/4 symmetry and textures with ∞/∞ symmetry will take place in any acentric crystals and textures under analogous conditions (prior "compression" or general disposition of the elements of the action symmetry). In particular such a study leads to the possibility of piezoelectric polarization formation in quartz in the direction of the optical axis, etc. It is easy to see that prior "compression" of a centric crystal will not lead to a subsequent formation of piezoelectric polarization by the usual means.

The study that we carried out on the piezoelectric polarization of crystals of the 3/4 point group and textures of the ∞/∞ point group leads to a wider knowledge of the piezoeffect. It seems more expedient to classify (as possibly piezoelectric) crystals and textures in which a piezoelectric polarization is possible due to a mechanical action, which is defined by a polar tensor of the second order (without regard to its symmetry, as long as in the cases that interest us the complete action of the prior "compressed" crystals or textures may be described by a nonsymmetrical polar tensor).

From these data it is possible to classify as possibly piezoelectric not only the crystals already studied but also crystals belonging to the 3/4 point group and textures belonging to the ∞/∞ point group. The general number of piezoelectric groups will then be equal to 21 (instead of 20) for crystals and 4 (instead of 3) for textures.

On the basis of these somewhat enlarged concepts of the piezoeffect, all crystals and textures which lack a center of symmetry may be classified as possibly piezoelectric. In other words, under these conditions a lack of a center of symmetry in crystals and textures is a necessary and sufficient sign for classifying them as possibly piezoelectric.

Let us note, finally, that generally speaking any centric crystal may be brought to an acentric state by means of an external action (electric field, complicated deformation, etc). It is evident that in such a state this crystal may become polarized, being subjected to mechanical action, defined by a centric polar tensor of the second order and may thus become possibly piezoelectric. A more concrete study of such cases does not fall within the limits of our problem.

The author is deeply grateful to Academician A. V. Shubnikov for continued guidance and valuable suggestions during the course of this work.

LITERATURE CITED

[1] W. Voigt, Lehrbuch der Kristallphysik (Leipzig - Berlin, 1910).

[2] A. V. Shubnikov, E. E. Flint and G. B. Bokii, Bases of Crystallography [in Russian] (1940).

[3] W. Cally, Piezoelectricity and its Practical Applications [in Russian] (IL, 1949).

[4] W. Mason, Piezoelectric Crystals and Their Application in Ultraacoustics [in Russian] (IL, 1952).

[5] A. V. Shubnikov, Piezoelectric Textures [in Russian] (1946).

[6] A. V. Shubnikov, I. S. Zheludev, V. P. Konstantinova and I. M. Sil'vestrova, Study of Piezoelectric Textures [in Russian] (1955).

[7] I. S. Zheludev and L. A. Shuvalov, "Ferroelectric phase transitions and crystal symmetry," Kristallografiia 1, 6, 681-688 (1956).

[8] A. V. Shubnikov, "On the Pierre Curie studies in the realm of symmetry," Uspekhi Fiz. Nauk 59, 4, 591-602 (1956).

[9] A. V. Shubnikov, "On the symmetry of vectors and tensors," Izvest. AN SSSR, Ser. Fiz. 13, 3, 347-375 (1949).

[10] I. Laval, Sur l'elasticité du milicu cristallin 1951. L'etat Solide Congress Solvary Bruxelles. Stoops 273, 414-479. *

[11] C. V. Raman and K. Wismanathan, Proc. Indian Acad. Sci. 42, 1, 2 (1955).

[12] Y. Le Corre, "Constantes élastiques et piezoēlectriques cristallines," Bull. Soc. Franc. Minéral.et Crist. 76, 464-479 (1953).

Institute of Crystallography,
Academy of Sciences, USSR

Received November 19, 1956

---

* As in original – Publisher's note.

ON THE SUPERPOSITION OF SYMMETRY GROUPS IN CRYSTAL PHYSICS

V. A. Koptsik

We consider the linear equations relating homogeneous tensor fields in homogeneous anisotropic media. It is shown that the symmetry of a tensor and the number of its independent components are invariant properties of the tensor, and do not depend on the specific form of its matrix in any admissible coordinate system. It is shown that the intersections of symmetry groups of tensors entering into coupling equations always give the same group. Relations are derived which make it possible to determine or evaluate the symmetry of interacting crystallophysical objects.

On the basis of Curie's [1] superposition principle for symmetry groups, which has been considered in detail by Shubnikov [2], the symmetry group of a crystal subjected to any external action is found to be, within certain limits, the largest common subgroup of the symmetry groups of the crystal and of the external action applied to it for the given mutual orientation of the symmetry elements of these groups.

A. V. Shubnikov has suggested finding this subgroup from the symmetry of the composite figure obtained by superposing the geometric figures representing the symmetry groups of the crystals and of the external action. In the same way one solves arbitrary problems related to finding the symmetry of two interacting objects.

Restricting ourselves to the field of phenomenological tensor crystal physics, it can be shown that the "superposition principle" corresponds to a special ("superpositional") property of the relation between homogeneous tensor fields in unbounded homogeneous crystal media; this property, as is well known, is expressed by the set of tensor equations

$$A_{pq\ldots r} = a_{ij\ldots kpq\ldots r} B_{ij\ldots k}\,, \qquad (1)$$

where the $B_{ij\ldots k}$ are the components of the external action tensor, the $A_{pq\ldots r}$ are the components of the tensor of the resulting phenomenon, and the $a_{ij\ldots r}$ are the components of the tensor which describes the given physical properties of the crystal, such as its thermal expansion α_{pq}, piezoelectric deformation d_{ipq}, or elastic coefficients s_{ijpq}, etc.

We note that some of the indices of the crystal tensor components $a_{ij\ldots r}$ are the same as those of the action tensor $B_{ij\ldots k}$, and the others are the same as those of the $A_{pq\ldots r}$, so that these indices can be changed only in the same way. The operation of equating the indices $i, j, \ldots, k$ of the $a\ldots$ and $B\ldots$ tensors, called "contraction," maintains the tensor dimension of both sides of Equation (1). Clearly, "carrying over" the indices of the $A\ldots$ and $B\ldots$ tensors to the $a\ldots$ tensor corresponds to carrying over the symmetry of A and B to a (see Fig. 1).

Restricting our considerations to the symmetries of real tensors only, we note that we mean by the symmetry of a tensor the highest order group of real orthogonal transformations which maintain the matrix of the tensor

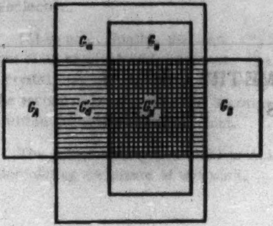

Fig. 1. Illustration of the superposition principle for symmetry groups in crystals physics for the case in which Equations (11) and (12) are fulfilled. G_B and G_A are the symmetry groups of the external action tensor and the resulting phenomenon tensor, related by Equation (1). G_a and $G_a' = (G_A, G_a) = (G_a, G_B)$ are the symmetry groups of the physical property of the crystal before and after application of the external action. G_k and $G_k' = (G_A, G_k) = (G_k, G_B)$ are the symmetry groups of the crystal before and after application of the external action. The following relations correspond to the cases defined and enumerated in the present article:

$$1.\ G_A \ni G_a \ni G_k';\ 2.\ G_a \ni G_a' \ni G_k';\ G_a \ni G_k \ni G_k';\ 3.\ G_B \ni G_a' \ni G_k';\ 4.\ G_k' \in G_k' \in G_a',\ G_k' = (G_A, G_k) = (G_k, G_B);\ 5.\ G_a' = (G_A, G_a) = (G_a, G_B),\ G_k' \in G_a' \in G_a;\ 6.\ G_k' \in G_k \in G_a.$$

invariant [3], and therefore also the number of independent tensor components in any allowable coordinate system. Most convenient is the principal coordinate system, in which this number is given immediately by the "matrix" of the tensor.

Let us prove the equivalence of both definitions for the case of real symmetric tensors of second order. We shall show that the symmetry of the tensor and the number of its independent components are its invariant properties, independent of the specific form of the tensor matrix in any allowable coordinate system.*

Consider any orthogonal rectilinear coordinate system X_1, X_2, X_3 in which a symmetric real tensor is given by the matrix

$$A = \begin{Vmatrix} a_{11} & a_{12} & a_{13} \\ a_{12} & a_{22} & a_{23} \\ a_{13} & a_{23} & a_{33} \end{Vmatrix}$$

In this case, as is well known [4], there exists a real orthogonal matrix

$$C = \begin{Vmatrix} c_{11} & c_{12} & c_{13} \\ c_{21} & c_{22} & c_{23} \\ c_{31} & c_{32} & c_{33} \end{Vmatrix},$$

which will bring the tensor to the diagonal form

$$A' = \begin{Vmatrix} a_{11}' & 0 & 0 \\ 0 & a_{22}' & 0 \\ 0 & 0 & a_{33}' \end{Vmatrix}.$$

The Matrix A' is real when written in the principal axes X_1', X_2', X_3'. The c_{ij} are the direction cosines of these axes $c_{ij} = \cos(X_i, X_j')$. In matrix form, the operation of writing the matrix in terms of the principal coordinate system is

$$C^{-1}AC = A'.$$

The tensor A' possesses the symmetry m · 2 : m. This means that

$$C_x^{-1}A'C_x = A',$$

where C_x is any of the matrices of the representation of the group m · 2 : m, namely

$$(c_{ij})_1 = \begin{pmatrix} 1 & & \\ & 1 & \\ & & 1 \end{pmatrix},\ (c_{ij})_{2 | X_1'} = \begin{pmatrix} 1 & & \\ & 1 & \\ & & 1 \end{pmatrix},\ (c_{ij})_{2 \parallel X_2'} = \begin{pmatrix} -1 & & \\ & 1 & \\ & & -1 \end{pmatrix},$$

---

* This proof is due to A. V. Shubnikov.

$$(c_{ij})_{2\parallel X_3'} = \begin{pmatrix} -1 & & \\ & -1 & \\ & & 1 \end{pmatrix}, \quad (c_{ij})_{\bar{2}} = \begin{pmatrix} -1 & & \\ & -1 & \\ & & -1 \end{pmatrix}, \quad (c_{ij})_{m\perp X_1'} = \begin{pmatrix} -1 & & \\ & 1 & \\ & & 1 \end{pmatrix},$$

$$(c_{ij})_{m\perp X_2'} = \begin{pmatrix} 1 & & \\ & -1 & \\ & & 1 \end{pmatrix}, \quad (c_{ij})_{m\perp X_3} = \begin{pmatrix} 1 & & \\ & 1 & \\ & & -1 \end{pmatrix}.$$

The matrices C_X are written in the principal coordinate system. On going over to the coordinates X_1, X_2, and X_3, they become

$$C_Y = CC_XC^{-1},$$

from which

$$C^{-1}C_Y = C_XC^{-1} \text{ and } C_Y^{-1}C = CC_X^{-1}.$$

Let us show that

$$C_Y^{-1}AC_Y = A.$$

We have $C_X^{-1}A'C_X = A'$, or

$$CC_X^{-1}A'C_XC^{-1} = CA'C^{-1} = A.$$

Replacing C_XC^{-1} and CC_X^{-1} by the expressions given above, we have

$$C_Y^{-1}CA'C^{-1}C_Y = A,$$

or

$$C_Y^{-1}AC_Y = A,$$

which was to be proved. For instance, for the tensor

$$A = \begin{Vmatrix} a_{11} & a_{12} & 0 \\ a_{12} & a_{22} & 0 \\ 0 & 0 & a_{33} \end{Vmatrix}$$

we have the matrix

$$C = \begin{Vmatrix} c & s & 0 \\ -s & c & 0 \\ 0 & 0 & 1 \end{Vmatrix},$$

where $c = \cos(X_1, X_1')$ and $s = \cos(X_1, X_2')$. Calculating C_Y, we obtain a representation of the group $m \cdot 2 : m$ in terms of the X_1, X_2, X_3 axes, namely

$$(c_{ij})_1 = \begin{pmatrix} 1 & & \\ & 1 & \\ & & 1 \end{pmatrix}, \quad (c_{ij})_{2\parallel X_1'} = \begin{pmatrix} c^2 - s^2 & -2sc & 0 \\ -2sc & s^2 - c^2 & 0 \\ 0 & 0 & 1 \end{pmatrix},$$

$$(c_{ij})_{2\parallel X_2'} = \begin{pmatrix} s^2 - c^2 & 2sc & 0 \\ 2sc & c^2 - s^2 & 0 \\ 0 & 0 & -1 \end{pmatrix}, \quad (c_{ij})_{2\parallel X_3'} = \begin{pmatrix} -1 & & \\ & -1 & \\ & & 1 \end{pmatrix}, \quad (c_{ij})_{\bar{2}} = \begin{pmatrix} -1 & & \\ & -1 & \\ & & -1 \end{pmatrix}$$

$$(c_{ij})_{m\perp X_1'} = \begin{pmatrix} s^2 - c^2 & 2sc & 0 \\ 2sc & c^2 - s^2 & 0 \\ 0 & 0 & 1 \end{pmatrix}, \quad (c_{ij})_{m\perp X_2'} =$$

$$= \begin{pmatrix} c^2 - s^2 & -2sc & 0 \\ -2sc & s^2 - c^2 & 0 \\ 0 & 0 & 1 \end{pmatrix}, \quad (c_{ij})_{m\perp X_3'} \begin{pmatrix} 1 & & \\ & 1 & \\ & & -1 \end{pmatrix}$$

It can be shown directly that these matrices leave A invariant.

The above considerations show that it is most convenient to define the symmetry of a tensor by investigating the symmetry of its matrix in the principal coordinate system. They show also that the number of independent tensor components is a tensor invariant, and does not depend on its specific form in any allowable coordinate system. This follows immediately from the existence of an orthogonal matrix C which brings the tensor into diagonal form:

$$C^{-1}AC = A',$$

since this equation provides the necessary number of relations between the components of A. If A' has three independent components, then so does A, since its nine components a_{ij} are related by the six equations

$$a'_{12} = a'_{13} = a'_{21} = a'_{23} = a'_{31} = a'_{32} = 0.$$

This number is reduced to one or two if the tensor A' has one or two independent components, since there will then be one or two additional equations relating the components.*

We now go on to derive certain relations expressing the "superposition principle" between the symmetry groups from relation (1) which couples homogeneous tensor fields in homogeneous anisotropic media.

Let us denote the symmetry groups of the tensors A and B by G_A and G_B, those of the tensor a̲ before and after the external action by G_a and G'_a, and those of the crystal before and after the external action by G_k and G'_k respectively. We shall also use the symbol (G_1, G_2) to denote the largest common subgroup, or intersection, of the groups G_1 and G_2 for a given mutual orientation of the symmetry elements of these groups. With this notation, the "superposition principle" following from Equation (1) can be written, assuming that the inverse effects exist, in the form of the two identities

$$G'_a \ni (G_A, G_a) = (G_a, G_B), \tag{2}$$

$$G'_k \ni (G_A, G_k) = (G_k, G_B). \tag{3}$$

Here the second relation follows from the first in view of the fact that by definition of the tensor a̲, its symmetry is no lower than that of the crystal, which means that

$$G_k \in G_a, \quad G'_k \in G'_a, \tag{4}$$

where the symbol $\in$ indicates that a subgroup is contained in a group.

Actually, from the equation A... = a... B... it follows that

$$G_A \ni (G_a, G_B) \ni (G_k, G_B). \tag{2'}$$

In addition, from the inverse equation B... = b... A... it follows that

$$G_B \ni (G_b, G_A) = (G_a, G_A). \tag{2''}$$

Let us find the intersection of G_a with the groups entering into the above expressions, namely

$$(G_A, G_a) \ni (G_a, (G_a, G_B)) = (G_a, G_B),$$

$$(G_a, G_B) \ni (G_a (G_a, G_A)) = (G_a, G_A).$$

---

* In general, the invariance of the number of independent tensor components follows from Hilbert's theorem on the existence of a finite number of fundamental invariants for a tensor [5].

These relations are consistent, therefore, if $(G_A, G_a) = (G_a, G_B)$, which is what was to be proved.

The restrictions used in the proof are permissible. Since, as is known from thermodynamics, the differential of any thermodynamic potential is a total differential, the inverse effect exists if the direct effect exists. In those cases in which it is difficult to find the matrix of the tensor b..., in terms of the tensor a..., it can in principle be established experimentally. It is found that the tensors a... and b... have the same order, number of independent components, and symmetry Ga... = Gb... .*

From Equations (2-4) follow other conclusions, which we shall consider in the present work (Fig. 1). With their aid one may solve various types of problems involving the exact or approximate determination of G_A, G_a, G_B, G'_k, G'_a, G_k.

We present several specific examples of determining given groups for thermal, piezoelectric, and elastic phenomena in quartz crystal ($G_k = 3:2$).

1. Determination of G_A. Let us write the equations for thermal expansion, the piezoelectric effect, and the generalized Hooke's law for quartz crystals in the matrix form with the crystallophysical designation of the axes

$$\begin{Vmatrix} S_{11} & 0 & 0 \\ 0 & S_{11} & 0 \\ 0 & 0 & S_{33} \end{Vmatrix} = \begin{Vmatrix} \alpha_{11} & 0 & 0 \\ 0 & \alpha_{11} & 0 \\ 0 & 0 & \alpha_{33} \end{Vmatrix} \cdot t, \tag{5}$$

$$\begin{Vmatrix} S_{11} \\ -S_{11} \\ 0 \\ S_{23} \\ S_{23} \\ S_{13} \\ S_{13} \\ S_{12} \\ S_{12} \end{Vmatrix} = \begin{Vmatrix} d_{111} & 0 & 0 \\ -d_{111} & 0 & 0 \\ 0 & 0 & 0 \\ d_{123} & 0 & 0 \\ d_{123} & 0 & 0 \\ 0 & -d_{123} & 0 \\ 0 & -d_{123} & 0 \\ 0 & -2d_{111} & 0 \\ 0 & -2d_{111} & 0 \end{Vmatrix} \begin{Vmatrix} E_1 \\ E_2 \\ E_3 \end{Vmatrix} \tag{6}$$

$$\begin{Vmatrix} S_{11} \\ S_{22} \\ S_{33} \\ S_{23} \\ S_{23} \\ S_{13} \\ S_{13} \\ S_{12} \\ S_{12} \end{Vmatrix} =$$

$$= \begin{Vmatrix} s_{1111} & s_{1122} & s_{1133} & s_{1123} & s_{1123} & 0 & 0 & 0 & 0 \\ s_{1122} & s_{1111} & s_{1133} & -s_{1123} & -s_{1123} & 0 & 0 & 0 & 0 \\ s_{1133} & s_{1133} & s_{3333} & 0 & 0 & 0 & 0 & 0 & 0 \\ s_{1123} & -s_{1123} & 0 & s_{2323} & s_{2323} & 0 & 0 & 0 & 0 \\ s_{1123} & -s_{1123} & 0 & s_{2323} & s_{2323} & 0 & 0 & 0 & 0 \\ 0 & 0 & 0 & 0 & 0 & s_{2323} & s_{2323} & 2s_{1123} & 2s_{1123} \\ 0 & 0 & 0 & 0 & 0 & s_{2323} & s_{2323} & 2s_{1123} & 2s_{1123} \\ 0 & 0 & 0 & 0 & 0 & 2s_{1123} & 2s_{1123} & 2(s_{1111}-s_{1122}) & 2(s_{1111}-s_{1122}) \\ 0 & 0 & 0 & 0 & 0 & 2s_{1123} & 2s_{1123} & 2(s_{1111}-s_{1122}) & 2(s_{1111}-s_{1122}) \end{Vmatrix} \begin{Vmatrix} T_{11} \\ T_{22} \\ T_{33} \\ T_{23} \\ T_{23} \\ T_{13} \\ T_{13} \\ T_{12} \\ T_{12} \end{Vmatrix} \tag{7}$$

---

* By definition $aa^{-1} = e$. Let $Ga = aG$, in which case $Gaa^{-1} = aGa^{-1} = G$ and $Ga^{-1} = a^{-1}G$.

The quantities entering into Equations (5-7) are the components of the mechanical deformation tensor S_{ij}, the mechanical stress T_{ij}, the electric field E_i, and the temperature $\underline{t}$. The symmetry of these tensors, as well as of the tensors α_{pq}, d_{ipq}, s_{ijpq}, is given by examining their corresponding matrices for invariance with respect to one or another transformation group, or by direct comparison with tables of invariant forms of tensors for the given designation of the axes [6]. Since such tables exist for most tensors used in physics, the matrix form of writing the crystallophysical equations is often more useful than the tensor form.

For the matrices on the right sides of Equations (5-7), we have

$$G_a = m\cdot\infty : m, \quad G_t = \infty / \infty\cdot m, \tag{5'}$$
$$G_d = 3 : 2, \qquad G_E = \infty\cdot m, \tag{6'}$$
$$G_S = \overline{6}\cdot m, \qquad G_T = m\cdot 2 : m. \tag{7'}$$

Performing the matrix multiplication, we find the form of the matrices on the left sides of Equations (5-7), which give the symmetry

$$G_S = m\cdot\infty : m, \tag{5''}$$
$$G_S = m\cdot 2 : m, \tag{6''}$$
$$G_S = m\cdot 2 : m; \tag{7''}$$

At the same time, the determination of G_A from Equations (2') gives

$$G_S = (G_a,\ G_t) = m\cdot\infty : m, \quad G_S \ni (G_k,\ G_t) = 3 : 2, \tag{5'''}$$
$$G_S \ni (G_d,\ G_E) = 1, \quad G_S \ni (G_k,\ G_E) = 1, \tag{6'''}$$
$$G_S \ni (G_S,\ G_T) = 2 : m, \quad G_S \ni (G_k,\ G_T) = 2. \tag{7'''}$$

In the same way one may treat special cases of fields B applied to the crystal.

For instance, in the case of the field E_i applied along the X_1 or X_2 axis, the deformation tensor according to Equations (6) becomes

$$\begin{Vmatrix} S_{11} & 0 & 0 \\ 0 & -S_{11} & S_{23} \\ 0 & S_{23} & 0 \end{Vmatrix}, \quad \text{or} \quad \begin{Vmatrix} 0 & S_{12} & S_{13} \\ S_{12} & 0 & 0 \\ S_{13} & 0 & 0 \end{Vmatrix}$$

The fact that we have written $\| S_{pq} \|$ in the form of a three-by-three matrix rather than a column matrix is insignificant, and is used only for convenience in comparing with the tables of invariant tensor forms. In both cases we have $G_S = m\cdot 2 : m$, and as is easily shown

$$G_S \ni (G_d,\ G_{E_1}) = 2, \quad G_S \ni (G_k,\ G_{E_1}) = 2,$$
$$G_S \ni (G_d,\ G_{E_3}) = 1, \quad G_S \ni (G_k,\ G_{E_3}) = 1.$$

These examples show that the symmetry of the interaction depends not only on the symmetry of the electric field E_i but also on the way it is applied to the crystal.

Let us also consider the following cases: a) a set of principal stresses $T_{11} \neq T_{22} \neq T_{33} \neq 0$, $T_{ij} = 0$ for $i \neq j$ is applied to a crystal, b) the crystal is subjected to hydrostatic pressure $T_{11} = T_{22} = T_{33} \neq 0$, $T_{ij} = 0$ for

$i \neq j$, c) a single stress T_{33} is applied along the X_3 axis. For these three cases the deformation tensor as given by Equation (7) is*

$$\begin{Vmatrix} S_{11} & 0 & 0 \\ 0 & S_{22} & S_{23} \\ 0 & S_{23} & S_{33} \end{Vmatrix}, \quad \begin{Vmatrix} S_{11} & 0 & 0 \\ 0 & S_{11} & 0 \\ 0 & 0 & S_{33} \end{Vmatrix}, \quad \begin{Vmatrix} S_{11} & 0 & 0 \\ 0 & S_{11} & 0 \\ 0 & 0 & S_{33} \end{Vmatrix}$$

We have a) $G_S = m \cdot 2 : m$; $G_T = m \cdot 2 : m$; b) $G_S = m \cdot \infty : m$; $G_T = \infty/\infty \cdot m$; c) $G_S = m \cdot \infty : m$; $G_T = m \cdot \infty : m$; and $G_S \ni (G_a, G_B)$; $G_S \dot{\ni} (G_k, G_B)$ in all cases.

We thus see that the symmetry group G_A in all cases is given uniquely by the form of the matrix of the contracted product of $\underline{a}$ and B. At the same time, it follows from Equation (2') in all cases that $G_A \ni (G_a, G_B) \ni$ $\ni (G_k, G_B)$.

2. The determination of G_a can be performed in the same way from the equation

$$a... = A... B^{-1}_{...}. \tag{8}$$

when the inverse tensor exists and the matrix multiplication $A... B^{-1}_{...}$ is possible. If $B^{-1}_{...}$ does not exist, a... can be found from Equation (1) by the method described below for unidirectional external actions. If the symmetry of the crystal is known, then the form of the matrix a... is determined uniquely for a given group G_k from the tensor transformation equations

$$a'_{pq...r} = c_{ip} c_{jq} \cdot \cdot \cdot c_{kr} a_{ij...k}, \tag{9}$$

where $c_{ji} = \cos(X_i, X'_j)$ for the condition $a'_{pq...r} = a_{pq...r}$, or can be found from the relation $G_a \ni' G_k$.

At the same time it is clear that Equations (2) with $G_a = x$ the unknown have no unique solutions of $(G_A, x) = (x, G_B)$, but have either a finite or infinite number of solutions. However, $G_a \ni (G_A, G_B)$.

Examples: In the case of the thermal properties of crystals, $t^{-1} = 1/t$ and the equation $S_{pq} t^{-1}$ gives a diagonal form for the α_{pq} matrix with the symmetry $G_\alpha = m \cdot \infty : m$.

For finding the matrix of the tensor d_{ipq}, let us use the method of unidirectionally applied external action, applying the field E_i to the quartz crystal along each of the X_1, X_2, X_3 axes successively. It then follows uniquely from Equations (6) that

$$d_{111} \neq 0, \quad d_{112} \neq 0, \quad d_{133} = 0, \quad d_{123} \neq 0, \quad d_{131} = 0, \quad d_{112} = 0,$$
$$d_{211} = 0, \quad d_{222} = 0, \quad d_{233} = 0, \quad d_{223} = 0, \quad d_{231} = 0, \quad d_{212} \neq 0,$$
$$d_{311} = 0, \quad d_{322} = 0, \quad d_{333} = 0, \quad d_{323} = 0, \quad d_{331} = 0, \quad d_{312} = 0.$$

From the form of the $\| d_{ipq} \|$ matrix one obtains uniquely $G_d = 3 : 2$.

Both methods can be used to find the $\| s_{ijpq} \|$ matrix, and they lead to the same result, namely $G_s = \bar{6} \cdot m$.

3. The determination of G_B is performed in the same way, from the equation

$$B... = \overset{-1}{a...} A... \quad \text{or} \quad B... = b... A... \tag{10}$$

---

* It follows from the first matrix, by the way, that the principal axes of the S_{ij} tensor do not coincide with the principal axes of the T_{ij} tensor.

If it is known that $a^{-1}_{\cdot\cdot\cdot}$ or $b_{\cdots}$ exists, then its symmetry can be determined without calculating the matrix of the tensor, since by definition of the inverse operation it follows that $G_{a^{-1}} = G_a$.

At the same time, the determination of G_B from Equations (2") gives $G_B \ni (G_A, G_a) \ni (G_k, G_A)$.

Examples: It is easily seen that for the thermal and elastic properties of quartz crystals being discussed, the inverse tensors $\alpha^{-1}_{\cdot\cdot\cdot}$ and $s^{-1}_{\cdot\cdot\cdot}$ exist, so that the determination of $t = \alpha^{-1}_{\cdot\cdot\cdot} S_{\cdots}$ and $T_{\cdots} = s^{-1}_{\cdot\cdot\cdot} S_{\cdots}$ can be performed uniquely. For the case of the piezoelectric properties of crystals, the equation $E = d^{-1}_{\cdot\cdot\cdot} S_{\cdot\cdot}$ is best replaced by $E_i = -h_{ipq}S_{pq}$ ($G_h = G_d$), which leads to a unique definition of the matrix $\| E_i \|$ and symmetry G_E.

4. The determination of G'_k is performed on the basis of Equations (3). If the symmetry of the crystal is reduced by the action of the field as in the cases we have been considering, so that $G'_k \in G_k$, then in addition to the more general expressions (3) we have

$$G_k = (G_A, G_k) = (G_k, G_B). \tag{11}$$

In fact, if we allow G_A or G_B in Equations (11) to run through all symmetry groups from $\underline{1}$ to $\infty/\infty \cdot m$, we find that $G'_k \in G_k$. In particular, we find that the symmetry of the quartz crystal (3 : 2) does not change under thermal expansion (if there does not take place a polymorphous transformation). Under the action of the electric field the symmetry of the crystal changes to 1, 2, and 1 and under the action of the mechanical stresses to 2, 2, 3 : 2 and 3 : 2 for the cases considered in this article.

5. The determination of G'_a is performed on the basis of Equations (2). In our examples

$$G'_a = (G_A, G_a) = (G_a, G_B). \tag{12}$$

As above, when Equation (12) is satisfied $G'_a \in G_a$, but $G'_a \ni G'_k$.

For the cases considered in this article, the symmetry G'_a is $m \cdot \infty : m$, 1, 2 : m, 2, 1, 2 : m, $\bar{6} \cdot m$ and $\bar{6} \cdot m$ respectively. If the symmetry G'_k is known, then G'_a can be obtained by finding the matrix of the tensor $a'_{\cdots}$, invariant with respect to G'_k.

6. Determination of G_k. Condition (4) gives $G_k \in G_a$. In our case for G_k we may have all crystallographic groups except the cubic (for the case of thermal expansion), all subgroups of the groups 3 : 2 (for the case of the piezoelectric effect), and all subgroups of the group $\bar{6} \cdot m$ (for the elastic case). If G_a is not found first, a finite number of solutions for G_k can be obtained by choosing those of Equations (11) in which, if we set $G_k = x$ the unknown, $(G_A, x) = (x, G_B)$ is indefinite. This equation gives for G_k all crystallographic groups except the cubic (for the case of thermal expansion and hydrostatic deformation), all groups without a symmetry center (for the case of the piezoelectric effect), and all crystallographic groups (for the case of general elastic forces).

The group G_k can be found uniquely by investigating the morphological symmetry of the crystal and the crystal properties (for instance, the piezoelectrical properties) for which $G_k = G_a$.

In conclusion we note that the methods described for determining the symmetry of interacting crystallophysical objects indicates in principle the possibility of new effects in crystals subjected to certain definite external forces. The properties of such "stressed" crystals should be described by tensors whose symmetry is $G'_a \ni G'_k$ when the crystal symmetry becomes $G'_k \in G_k$, if Equations (11) and (12), rather than the more general ones (2) and (3), are fulfilled. For the case of (11) and (12), the results of this work can be summarized by the following chain:

$$\begin{array}{ccccc}
 & & G_B & & \\
 & & \rotatebox[origin=c]{90}{$\in$} & & \\
G_A & \ni & G'_a & \ni & G'_k \\
 & & \rotatebox[origin=c]{-90}{$\in$} & & \rotatebox[origin=c]{-90}{$\in$} \\
 & & G_a & \ni & G_k
\end{array} \tag{13}$$

The advantage of the approach based on the superposition principle is that it makes possible a determination of the number of independent components of A... without solving Equation (1). This advantage is most useful on going over to more complex systems of equations (for instance, partial differential equations).

The explicit solution of (1), giving an exact answer to the problem as stated, shows that the superposition principle in general gives only the upper limit to this number.

The author expresses his gratitude to Academician A. V. Shubnikov for his interest in the work and for fruitful discussion of the results.

LITERATURE CITED

[1] P. Curie, Sur la Symètrie dans les phénomenes physiques, symétrie d'un champs électrique et d'un champs magnetique. J. de Phys. (3), 3, 393 (1894). Oeuevres d. P. Curie, 1908, 118.

[2] A. V. Shubnikov, "On the work of Pierre Curie in the field of symmetry," Uspekhi Fiz. Nauk 59, 4, 591-602 (1956).

[3] A. V. Shubnikov, "On symmetry of vectors and tensors," Izv. AN SSSR, ser. fiz. 13, 347-375 (1949).

[4] A. K. Sushkevich, Elements of Higher Algebra [in Russian] (Moscow-Leningrad (1941).

[5] G. B. Gurevich, Elements of the Theory of Albegraic Invariants [in Russian] (Moscow-Leningrad (1948).

[6] A. V. Shubnikov, E. E. Flint and G. B. Bokii, Elements of Crystallography [in Russian] (Moscow-Leningrad (1940).

M. V. Lomonosov Moscow State University

Received November 26, 1956

WOOD AS A PIEZOELECTRIC TEXTURE*

V. A. Bazhenov

We have studied the effect on the piezoelectric properties of wood (considered as a piezoelectric texture) of the cellulose orientation in the cell sheaths of the wood cells, taking their shape and layered structure into consideration.

The piezoelectric properties of wood, discovered by Shubnikov [1], have been quantitatively studied in the USSR [2, 3] and in Japan [4].

Both the Russian and the Japanese studies showed that absolutely dry wood has two piezoelectric moduli d_{14} and d_{25}; their absolute values differ somewhat, as a rule, with $|d_{14}| > |d_{25}|$ in the case where the piezoelectric properties of the wood are described in a coordinate system defined by the main structural directions (Fig. 1).

We [3] have shown that wood as a piezoelectric texture still belongs to the $\infty:2$ point group and that the inequality $|d_{14}| > |d_{25}|$ which often contradicts this symmetry, is a result of the appearance of nonhomogeneity in the morphological structure of the wood.

Another special characteristic of the piezoelectric properties of different types of wood is the discrepancy between the values of their piezoelectric moduli and the cellulose content, the cellulose being the component responsible for the piezoelectric properties of wood. Thus, for example, it has been shown that mastic tree wood and lignum vitae have an insignificant piezoelectric effect, even though they contain an appreciable amount of cellulose and have in general a typical woody morphological structure. Finally, the conclusion (based on a study of piezoelectric properties of various cellulose materials [5]) that for all cellulose materials the elementary units of the piezoelectric textures are the polar molecules of cellulose (or parts of them) whose orientation in piezoelectric textures $\infty:2$ meets the requirements of A. V. Shubnikov's theorem IV ([1], p. 26), cannot be applied to wood without taking into account the well known fact that the cellulose molecules of the cellular sheaths are not oriented parallel to the longitudinal axes of the cells but parallel to the fibrils.

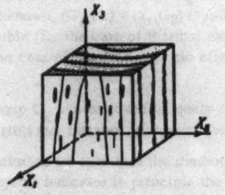

Fig. 1. Coordinate system, defined by the principal structural directions in wood. x_3 is the longitudinal direction, x_2 is the tangential direction, x_1 is the transverse radial direction.

It is shown below that these and other piezoelectric properties of wood can be explained if wood is considered to be a composite piezoelectric texture [1, 6].

In the sheath structure of plant cells, stratification and striation are typical. In the cell walls of woody plants three layers are usually identified (Fig. 2) assuming a finer stratification within the thicker layers. Each layer is characterized by its own typical parallel striation, which is due to a grouping of cellulose molecules into morphological entities called fibrils or elementary filaments. Each layer of the cellular sheath represents a group of fibrils, wound spirally around the longitudinal axis of the cell and the separate layers of the cell sheath are

---

*** See footnote on p. 86 – Publisher.**

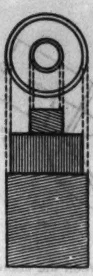

Fig. 2. Diagram of cellular sheath structure, showing its stratification and striation. According to Bailey [10].

distinguished by the magnitude of the angle of inclination of the fibrils to the longitudinal axis of the cell. It should be mentioned here that the hollow cells, whose sheaths show a layered structure, and whose layers show a different orientation of the fibrils, may be, in cross section, not only circular but rectangular, square, pentagonal and hexagonal with a tendency to form regular shapes (see for example [7]).

Studies [8, 9] show that the fibril orientation, seen in a microscope, coincides with the size of the open angle of the interference maximum on an x-ray pattern (Fig. 3). These data, as well as experimental facts [5] prove that both separate fibrils and groups of parallel fibrils may be studied as a fibrous piezoelectric texture of the first order [1, 6] showing $\infty:2$ symmetry. The ∞ axis of this texture lies along a row of parallel groups of fibrils.

As shown by the widely known studies of Bailey [10] the angle of inclination of the fibrils to the longitudinal axis of the cell changes from layer to layer with many modifications and without showing any strict correlation in its changes from layer to layer, but assumes some average value α for each layer. Any layer of parallel fibrils on a flat wall of any cell [for example a hexagonal one (Fig. 4)] may be studied as a piezoelectric texture $\infty:2$, having in its principal coordinate system X_1^{ϕ}, X_2^{ϕ}, X_3^{ϕ} the following piezoelectric moduli:

$$d_{123}^{\phi} = d_{132}^{\phi} = -d_{231}^{\phi} = -d_{213}^{\phi}.$$

Our problem was to express the components of the piezoelectric tensor for a wood cell by means of piezoelectric moduli of the fibrillar textures $\infty:2$ for its separate layers. The solution of this problem is important inasmuch as the cell is a particle of the wood which is a piezoelectric texture.

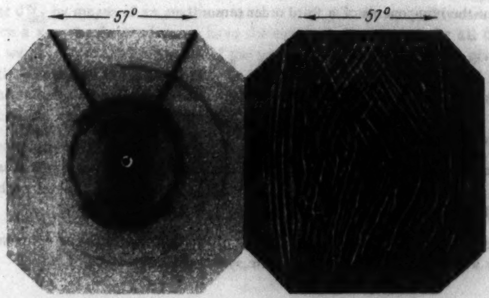

Fig. 3. Agreement of a microscopic picture of fibril orientation with the cellulose orientation as given by an x-ray pattern. According to Sisson [10].

The general method of solving this problem provides first of all for the determination of the components of the piezoelectric tensor for one layer of the cellular sheath and then for the whole sheath, as a sum total of several geometrically similar sheaths. Each layer of the sheath, repeating the shape of the cell, can be generally subdivided into a row of flat walls (Fig. 4). The fibrils of each flat wall form a piezoelectric texture $\infty:2$. The number of such textures, equal to the number of flat walls, depends on the shape of the cell; in a m-gonal cell there will be m such walls and in a cylindrical cell there will obviously be an infinite number of such walls.

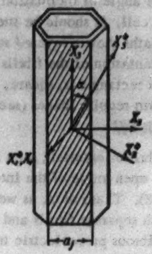

Fig. 4. Relation between the principal coordinate system of a fibrillar texture X_1^ϕ, X_2^ϕ, X_3^ϕ and the coordinate system of an arbitrary flat cell wall X_1, X_2, X_3.

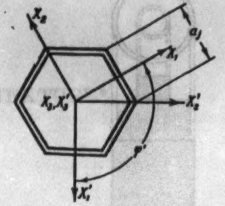

Fig. 5. Relation between the coordinate system of an arbitrary wall X_1, X_2, X_3 and the coordinate system of any wall X_1', X_2', X_3', taken as fixed.

In order to find all components of the piezoelectric tensor for the whole layer, as a single texture d'^{c}_{ikl} in the fixed coordinate system X_1', X_2', X_3' of one of the cell walls, one must transform the piezoelectric moduli of all m fibril textures ∞ : 2 to the same system of coordinates X_1', X_2', X_3' and add like components of the piezoelectric tensors for all the walls. Naturally in this sum one must take into account the degree of development, or relative breadth, of each wall. By relative breadth we mean the ratio of the wall layer breadth a_j (Fig. 4) to the perimeter of the cell $(a_1 + a_2 + \ldots + a_m)$, i.e., $\dfrac{a_j}{a_1 + a_2 + \ldots + a_m}$.

Transformation of the piezoelectric moduli $d_{123}^\phi = d_{132}^\phi = -d_{231}^\phi = -d_{213}^\phi$ of a fibrillar piezoelectric texture to the coordinate system X_1', X_2', X_3' takes place in two stages. First of all the indicated moduli in the coordinate system X_1^ϕ, X_2^ϕ, X_3^ϕ are converted to the coordinate system X_1, X_2, X_3 (Fig. 4) obtained by the rotation of the first system around the X_1^ϕ axis at a fibril inclination angle α. This transformation is brought about by using well known conversion formulas for the components of a third order tensor

$$d_{pqs} = \sum_{m=1}^{3} \sum_{n=1}^{3} \sum_{o=1}^{3} c_{mp} c_{nq} c_{os} d_{mno},$$

where c_{ij} are the direction cosines.

The d_{pqs} components, which have been found, are then converted by means of the same formulas from the coordinate system X_1, X_2, X_3 to the fixed coordinate system X_1', X_2', X_3' (Fig. 5) obtained by a rotation of the first system by an angle φ around the x_3 axis.

As a result of both transformations we obtain by simplification the following components of the piezoelectric tensor for any wall, expressed in the coordinate system X_1', X_2', X_3':

$$\begin{aligned}
d'_{122} &= 2 \sin\alpha \cos\alpha \, d_{123}^{\Phi} (c^3 + cs^2) \\
d'_{133} &= -2 \sin\alpha \cos\alpha \, d_{123}^{\Phi} c \\
d'_{123} &= (\cos^2\alpha - \sin^2\alpha) \, d_{123}^{\Phi} c^2 + \cos^2\alpha \, d_{123}^{\Phi} s^2 \\
d'_{131} &= -\sin^2\alpha \, d_{123}^{\Phi} cs \qquad (1) \\
d'_{112} &= \sin\alpha \cos\alpha \, d_{123}^{\Phi} (c^2 s + s^3) \\
d'_{211} &= -2 \sin\alpha \cos\alpha \, d_{123}^{\Phi} (s^3 + c^2 s)
\end{aligned}$$

(continued on next page)

$$\begin{gathered}
d'_{223} = 2\sin\alpha\cos\alpha\, d^{\Phi}_{123}\, s \\
d'_{233} = \sin^2\alpha\, d^{\Phi}_{123}\, cs \\
d'_{231} = -\cos^2\alpha\, d^{\Phi}_{123}\, c^2 - (\cos^2\alpha - \sin^2\alpha)\, d^{\Phi}_{123}\, s^2 \\
d'_{212} = -\sin\alpha\cos\alpha\, d^{\Phi}_{123}\,(cs^2 + c^3) \\
d'_{311} = 2\sin^2\alpha\, d^{\Phi}_{123}\, cs \\
d'_{322} = -2\sin^2\alpha\, d^{\Phi}_{123}\, cs \\
d'_{333} = -\sin\alpha\cos\alpha d^{\Phi}_{123}\, s \\
d'_{331} = \sin\alpha\ \cos\alpha\, d^{\Phi}_{123}\, c \\
d'_{312} = \sin^2\alpha\, d^{\Phi}_{123}\,(c^2 - s^2)
\end{gathered} \tag{1}$$

(continued)

In these formulas c = cos φ, and s = sin φ.

Given the values of angle φ, by means of the Formulas (1), it is possible to determine the piezoelectric tensor components for any wall in the X'_1, X'_2, X'_3 coordinate system for any wall taken as fixed.

The resulting Formulas (1) form the basis around which is built the method for determining the piezoelectric tensor, first of one layer and then of the entire cell taken as a sum total of several layers.

The components of the piezoelectric tensor for one layer d'^{c}_{ikl} are found as a sum of like components of the piezoelectric tensor for the separate walls of the parts which make up the layer d'_{ikl} taking into account the relative breath of the walls $\frac{a_j}{\Sigma a}$. Thus for example for an m-gonal cell we have

$$d'^{c}_{123} = -2\sin\alpha\cos\alpha\, d^{\Phi}_{123}\,\frac{c_1a_1 + c_2a_2 + \ldots + c_ma_m}{a_1 + a_2 + \ldots + a_m}.$$

Formulas for the remaining components of the desired piezoelectric tensor may be obtained in a similar way. Practically, however, it is more important to show a method of calculating the components of the piezoelectric tensor for layer d'^{c}_{ikl} by means of an auxiliary table (Table 1) made up in this case for a cell with a rectangular cross section a × b. In the top line we have the values of the angles φ for all the walls of the cell, and in the second line we have the relative breadth of the walls. In the left column are given the trigonometric expressions for the angle φ involved in Formulas (1). In the spaces where the columns and lines intersect we have the products of the relative breadth of the walls and the numerical values of the trigonometric expressions, and in the right hand column we have the sum for each line.

Using Table 1 and Formulas (1) we obtain

$$\begin{gathered}
d'^{c}_{123} = \frac{2a\cos'^{c}\alpha - a + b\cos^2\alpha}{a+b}\, d^{\Phi}_{123}\,; \\
d'^{c}_{231}\ \frac{-a\cos^2\alpha - 2b\cos^2\alpha + b}{a+b}\, d^{\Phi}_{123}\,; \\
d'^{c}_{312} = \frac{a\sin^2\alpha - b\sin^2\alpha}{a+b}\, d^{\Phi}_{123}.
\end{gathered} \tag{2}$$

Formulas (2) show that the piezoelectric tensor for a rectangular cell has a 2 : 2 symmetry. When a = b, i.e., the cells are square, we obtain

$$\begin{gathered}
d'^{c}_{123} = \frac{3\cos^2\alpha - 1}{2}\, d^{\Phi}_{123}\,; \\
d'^{c}_{231} = -\frac{3\cos^2\alpha - 1}{2}\, d^{\Phi}_{123}\,; \\
d'^{c}_{312} = 0.
\end{gathered} \tag{3}$$

TABLE 1

φ	0	90	180	270	Σ
	$\frac{a}{2a+2b}$	$\frac{b}{2a+2b}$	$\frac{a}{2a+2b}$	$\frac{b}{2a+2b}$	
c	$\frac{a}{2a+2b}$	0	$-\frac{a}{2a+2b}$	0	0
s	0	$\frac{b}{2a+2b}$	0	$\frac{b}{2a+2b}$	0
cs	0	0	0	0	0
c^2	$\frac{a}{2a+2b}$	0	$\frac{a}{2a+2b}$	0	$\frac{a}{a+b}$
s^2	0	$\frac{b}{2a+2b}$	0	$\frac{b}{2a+2b}$	$\frac{b}{a+b}$
c^2s	0	0	0	0	0
cs^2	0	0	0	0	0
c^3	$\frac{a}{2a+2b}$	0	$-\frac{a}{2a+2b}$	0	0
s^3	0	$\frac{b}{2a+2b}$	0	$\frac{b}{2a+2b}$	0

It is easy to see that Formulas (3) hold for any cell of a regular m-gonal shape, including a circular cyinder for which m = ∞. We shall show this only for a cylindrical cell, for which case the relative breadth of an infinitely small flat wall is equal to $\frac{d\varphi}{2\pi}$ and the angles φ take on all the values from 0 to 2π. Under these conditions the sums of the last column in Table 1 for each line become definite integrals, in particular

$$\frac{1}{2\pi}\int_0^{2\pi} \cos^2\varphi \, d\varphi = \frac{1}{2},$$

$$\frac{1}{2\pi}\int_0^{2\pi} \sin^2\varphi \, d\varphi = \frac{1}{2}.$$

All the other definite integrals are equal to zero. Using this result and Formulas (1) we easily obtain Formulas (3).

Thus the piezoelectric tensor for regular m-gonal and circular cylindrical cells has ∞ : 2 symmetry.

From Formulas (2) and (3) we arrive at the following deductions.

1. When $\alpha = 0$ we obtain everywhere: $d'^{c}_{123} = d^{\phi}_{123}$ and $d'^{c}_{231} = -d^{\phi}_{123}$, because in this case there is only one texture ∞ : 2, made up of parallel fibrils.

2. From Formulas (3) the angle α may be found, for which $3c^2 - 1 = 0$, $\alpha \approx 54°$ 40 minutes. Such a layer may be classified as nonpiezoelectric.

3. When $a > b$ the piezoelectric modulus d'^{c}_{312} has the sign of the piezoelectric modulus d'^{c}_{123}, and when $a < b$ it has the sign of the piezoelectric modulus d'^{c}_{231}, i.e., the opposite sign.

It now remains for us to obtain formulas for the calculation of piezoelectric moduli of the whole cell as a particle composed of m layers. Each layer has its piezoelectric tensor and its relative thickness. Apparently, the addition of like components of piezoelectric tensors must be carried out, taking into account the angle of fibril inclination α, the relative thickness of layers $\frac{s_j}{s}$ and the relative content of cellulose $\frac{q_j}{q}$ according to formulas of the general type

$$d'^{k}_{123} = \frac{[(3\cos^2\alpha_1 - 1)\, s_1 q_1 + \dots + (3\cos^2\alpha_m - 1)\, s_m q_m]\, d^{\Phi}_{123}}{2sq},$$

where $s = s_1 + s_2 + \dots + s_m$ is the thickness of the cell sheath and the layers which make it up, $q = q_1 + q_2 + \dots + q_m$ is the amount of cellulose in the cell and in the layers of which it is composed.

Individual layers have different angles of fibril inclination and therefore are not equal in piezoelectric properties. As a whole the cell may be characterized by a certain average angle of fibril inclination α_Φ.

$$d'^{k}_{123} \frac{3\cos^2\alpha_\Phi - 1}{2}\, d^{\Phi}_{123}. \tag{4}$$

The position we have taken in this article is confirmed not only by the fact that the differences in moduli of various species of wood may be explained by Formulas (2-4) but also by the following experiments with compressed wood.

With plane compression of wood its cells are not infrequently deformed to such an extent that there is no open space between the walls [11]. When compression takes place in the direction of the X_1 axis (Fig. 1) the walls a elongate, and when compression takes place in the direction of the X_2 axis (Fig. 1) the walls b elongate [see formula (2)]. Under these conditions we have found in birch wood, compressed to a density of 0.91 g/cm^3, piezoelectric moduli $d_{36} = d_{312} + d_{321}$, of the order of $0.1 \cdot 10^{-8}$ CGS units, clearly changing their sign depending on the direction of the compression, in accordance with Formulas (2). In the case of noncompressed normal wood $d_{36} = 0$ [3, 4].

As long as the compression is accompanied not only by changes in the shape of the cell, but also by the packing of the wood, we have found in aspen which was radially compressed (along the X_1 axis) an increase in the piezoelectric modulus d_{25} from $0.348 \cdot 10^{-8}$ to $0.740 \cdot 10^{-8}$; this increase is proportional to the increase in density up to a certain limit; changes in the piezoelectric modulus d_{14} are insignificant. A change in the piezoelectric properties of wood on planar compression occurs in connection with changes in the elastic properties of the material which occur at that time. In the case of tangentially compressed wood, when such a compression is possible, it is natural for the piezoelectric modulus d_{14} to increase, but also only up to a certain limit. The existence of such a limit is due to the sudden increase of the moduli of normal elasticity when the walls of the compressed cells come together.

The piezoelectric properties of compressed wood are of interest to the growing technology of compressed wood [12].

It is interesting to note that the practically nonpiezoelectric mastic tree wood shows isotropic mechanical properties [13] due to the degree of its cellulose orientation, an indication of which may be the magnitude of the piezoelectric modulus.

It follows from this study that the piezoelectric moduli of wood serve as indications of the degree of its orientation as an anisotropic material as long as they correlate with the structure of the cell sheaths, are influenced by the nonhomogeneity of the morphological structure of wood and reflect the artificially induced changes in the structure of wood resulting from such actions as compression.

In conclusion let us note that the piezoelectric properties of wood discovered by A. V. Shubnikov and the theory of piezoelectric textures which he developed may be used not only in the study of wood as a technical material but also for the study of cell structure and tissue groupings as biological entities.

LITERATURE CITED

[1] A. V. Shubnikov, Piezoelectric Textures, [In Russian] (1946).

[2] V. A. Bazhenov and V. P. Konstantinova, "Piezoelectric properties of wood," Doklady Akad. Nauk SSSR, 71, 2 (1950).

[3] V. A. Bazhenov, "Piezoelectric effect in wood," TrudyInst. Lesa, AN SSSR 9, 281 (1953).

[4] Fukada Eiichi, Piezoelectricity of Wood, J. Phys. Soc., Japan 10, 2,(1955).

[5] V. A. Bazhenov, "Piezoelectric properties of wood and cellulose materials," Izv. AN SSSR, Ser. Phys. 20, 2 (1956).

[6] A. V. Shubnikov, I. S. Zheludev, V. P. Konstantinova and I. M.Sil'vestrova, Study of Piezoelectric Textures [In Russian] (1955).

[7] V. E. Vikhrov, Diagnostic Features of the Principal Species of Wood in USSR, [In Russian] (1947).

[8] W. A. Sisson, Contribs. Boyce Thompson Inst. 9, 239(1938).

[9] A. I. Kataigorodskii, X-ray Structural Analysis of Fine Crystalline and Amorphous Bodies, [In Russian] (1952).

[10] I. W. Bailey, Contributions to Plant Anatomy USA,(1954).

[11] V. E. Moskaleva, "Study of compressed wood structure in the case of mechanical breakdown," Trudy Inst. Lesa, AN SSSR, IV, 237 (1949).

[12] P. N. Khukhrianskii, Wood as a Metal Substitute [In Russian] (1956).

[13] L. M. Perelygin, Wood of Less Known Species, [In Russian] (1952).

Institute of Forestry, Acad. Sci. USSR

Received November 15, 1956

PIEZOELECTRIC SHEAR MODULUS OF POLARIZED BARIUM TITANATE

S. V. Bogdanov, B. M. Vul, R. Ia. Razbash

The piezoelectric modulus $d_{24} = d_{15}$ of polarized barium titanate ceramic is determined by a static method. We calculate d^*_{33}, d^*_{31} and d^*_{24} for a single crystal from the values obtained on ceramic samples.

The piezoelectric moduli d_{33} and $d_{31} = d_{32}$, which characterize the behavior of polarized barium titanate under tension and compression, have already been measured [1]. For the dynamic state they have been determined by Rzhanov [2, 3] and others [4, 5]. In addition to these two piezoelectric moduli, polycrystalline barium titanate is characterized by $d_{24} = d_{15}$, which is associated with shear. For the static case it can be determined by a method suggested by Shubnikov [6].[1] This method consists of measuring d_{33} and d_{31} on some initial samples (in which the remnant polarization is directed along the axis chosen as the Z axis), and then measuring d'_{33} in samples cut out of the initial ones so that the direction of the remnant polarization makes an angle of 45° with the new Z' axis (Fig. 1). This data is easily used to obtain $d_{24} = d_{15}$.

The method suggested by Shubnikov may be modified so as to reduce the determination of d_{24} to only two measurements (or even one) on a cubic sample in which the polarization is directed at an angle of 45° to a side of the cube. To do this, let us express d'_{33} and d'_{23} in terms of the piezoelectric moduli of the initial samples [7]. We have $d'_{ikl} = \Sigma c_{ji}c_{mk}c_{nl}d_{jmn}$, [Eq. (1)] where $c_{\alpha\beta}$ are the direction cosines indicated in Table 1.

TABLE 1

	X'	Y'	Z'
X	c_{11}	c_{12}	c_{13}
Y	c_{21}	c_{22}	c_{23}
Z	c_{31}	c_{32}	c_{33}

For barium titanate the nonzero components

$$d_{333},\ d_{311} = d_{322},\quad d_{223} = d_{232} = d_{113} = d_{131}, \tag{2}$$

are given in terms of the moduli with two indices by the equation

$$d_{333} = d_{33},\ d_{311} = d_{31},\ d_{322} = d_{32},\ d_{223} + d_{232} = d_{24},\ d_{113} + d_{131} = d_{15}. \tag{2'}$$

Thus Equation (1) becomes

$$\begin{aligned} d'_{ikl} = {} & c_{3i}c_{3k}c_{3l}d_{333} + c_{3i}c_{1k}c_{1l}d_{311} + c_{3i}c_{2k}c_{2l}d_{322} + \\ & + c_{2i}c_{2k}c_{3l}d_{223} + c_{2i}c_{3k}c_{2l}d_{232} + c_{1i}c_{1k}c_{3l}d_{113} + c_{1i}c_{3k}c_{1l}d_{131}. \end{aligned} \tag{3}$$

Bearing in mind (2) and (2'), the desired piezoelectric moduli are given by

$$d'_{33} = d'_{333} = c^3_{33}d_{33} + c_{33}c^2_{13}d_{31} + c_{33}c^2_{23}d_{32} + c_{33}c^2_{23}d_{24} + c_{33}c^2_{13}d_{15}, \tag{4}$$

$$d'_{23} = d'_{233} = c_{32}c^2_{33}d_{33} + c_{32}c^2_{13}d_{31} + c_{32}c^2_{23}d_{32} + c_{22}c_{23}c_{33}d_{24} + c_{12}c_{13}c_{33}d_{15}. \tag{5}$$

---

[1] This method was communicated to us before publication of the book.

In our case (see Fig. 1)

$$c_{11}=1,\ \ c_{22}=c_{32}=c_{33}=\sqrt{2}/2,\ \ c_{23}=-\sqrt{2}/2,\ c_{12}=c_{13}=c_{21}=c_{31}=0,$$

so that (4) and (5) reduce to the much simpler expressions

$$d'_{33}=0.354\,(d_{33}+d_{32}+d_{34}), \tag{6}$$

$$d'_{23}=0.354\,(d_{33}+d_{32}-d_{34}). \tag{7}$$

As is seen from (6) and (7), in order to find d_{34}, we need know, in addition to d_{33} and d_{32} of the original samples, only d'_{33} or d'_{23}; this is seen by writing

$$d_{34}=\frac{d'_{33}}{0.354}-(d_{33}+d_{32}), \tag{8}$$

$$d_{34}=(d_{33}+d_{32})-\frac{d'_{23}}{0.354}. \tag{9}$$

We may also restrict our measurements to d'_{33} and d'_{23}, and obtain the piezoelectric shear modulus from the relation

$$d_{34}=\frac{d'_{33}-d'_{23}}{0.708}. \tag{10}$$

If the areas of the Y and Z faces are equal, then $d'_{33} = Q'_3/F'_{33}$; $d'_{23} = Q'_2/F'_{33}$ and Equation (10) becomes

$$d_{34}=\frac{Q'_3-Q'_2}{0.708\,F'_{33}}, \tag{11}$$

where Q'_3 and Q'_2 are the charges on the Z' and Y' faces, respectively, and F'_3 is the force acting on the Z' face.

It follows from (11) that the determination of d_{34} can be reduced to a single measurement if each electrode makes contact simultaneously with two faces, as is indicated schematically in Fig. 2, since in this case we are obtaining a direct measurement of the algebraic sum of the charges $Q'_3-Q'_2$. (One electrode contacts the faces crossed by the positive Z axis and negative Y axis, and the other one contacts the faces crossed by the positive Y axis and negative Z axis).

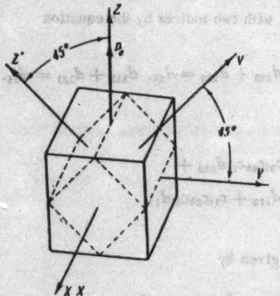

Fig. 1.

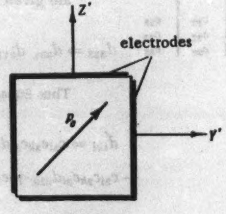

Fig. 2.

TABLE 2

d_{33}	$\frac{d_{31}+d_{32}}{2}$	$\frac{d'_{33}+d'_{22}}{2}$	$\frac{d'_{23}+d'_{32}}{2}$	$\frac{Q'_1-Q'_2}{F'_{33}}$	Calculated according to Equation (8)	(9)	(10)	(11)
$4.0\cdot10^{-6}$	$1.4\cdot10^{-6}$	$2.9\cdot10^{-6}$	$1.1\cdot10^{-6}$	$3.6\cdot10^{-6}$	$5.6\cdot10^{-6}$	$5.7\cdot10^{-6}$	$5.6\cdot10^{-6}$	$5.0\cdot10^{-6}$
3.9 »	1.4 »	2.7 »	1.0 »	3.7 »	5.1 »	5.3 »	5.2 »	5.2 »
4.0 »	1.4 »	2.8 »	1.1 »	3.5 »	5.3 »	5.7 »	5.5 »	4.9 »
4.0 »	1.5 »	2.8 »	1.2 »	3.5 »	5.4 »	5.9 »	5.6 »	4.9 »
4.0 »	1.5 »	2.7 »	1.1 »	3.5 »	5.1 »	5.6 »	5.4 »	4.9 »
4.7 »	1.7 »	3.1 »	1.1 »	3.7 »	5.7 »	6.1 »	5.9 »	5.2 »
Av $4.0\cdot10^{-6}$	$1.5\cdot10^{-6}$	$2.8\cdot10^{-6}$	$1.1\cdot10^{-6}$	$3,6\cdot10^{-6}$	$5.4\cdot10^{-6}$	$5.6\cdot10^{-6}$	$5.5\cdot10^{-6}$	$5.0\cdot10^{-6}$

In the present work the piezoelectric shear modulus was determined by using Expressions (8), (9), and (10), as well as directly by (11). The results of the measurements and calculations for d_{24} (in cgs electrostatic units) are presented in Table 2. In performing the calculations one must bear in mind the fact that d_{32} and d'_{23} have signs opposite to those of d_{33} and d'_{33}. In the calculations we used $0.5\,(d_{31} + d_{32})$, $0.5\,(d'_{33} + d'_{22})$ and $0.5(d'_{23} + d'_{32})$ in order to eliminate chance deviations from the equalities $d_{31} = d_{32}$, $d'_{33} = d'_{22}$, $d'_{23} = d'_{32}$. In the measurements, the stresses σ_{33}, σ_{22}, σ'_{33} and σ'_{22} were no greater than 20 kg/cm^2 so as to avoid "fatigue" of the samples.

It is seen that (10) is the arithmetic mean of (8) and (9), so that the value of d_{24} it gives may be considered more accurate. At the same time, the piezoelectric modulus obtained by (11) is found to be somewhat higher (by about 10%). This can be explained by the fact that when applying the electrodes, as can be seen from Fig. 2, it is necessary to leave a small gap near the edges in order to avoid contact between the oppositely charged electrodes. In our case the face width was 4.5 mm, and a gap of only 0.2-0.3 mm is sufficient to cause this error. Thus this method can be used for finding d_{24} only if the area of the remaining gap is negligible compared to the area of the face.

From the table it is seen that the piezoelectric shear modulus d_{24} of polarized polycrystalline barium titanate is of the order of $5.5\cdot10^{-6}$ and is greater than d_{33}. Measurement of d_{15} in the dynamic state, which was performed by Rzhanov on other samples [3] also showed that d_{15} is greater than d_{33} by a factor of about 1.5.

The effective piezoelectric moduli d_{kl} of a polarized polycrystalline sample are related to those of a single crystal d^*_{mn} by [8, 9]:

$$d_{33} = \frac{1}{4}(1+\cos\theta)\,[d^*_{33}(1+\cos^2\theta) + (d^*_{31}+d^*_{15})\sin^2\theta];$$

$$d_{31} = \frac{1}{8}(1+\cos\theta)\,[(d^*_{33}-d^*_{15})\sin^2\theta + (4-\sin^2\theta)d^*_{31}];$$

$$d_{15} = \frac{1}{4}(1+\cos\theta)\,[(d^*_{33}-d^*_{31})\sin^2\theta + d^*_{15}(1+\cos^2\theta)],$$

where θ is the limiting angle between the direction of a polarizing electric field and the spontaneous polarization in a single crystal.

On the assumption that $\theta = 90°$, we have

$$d_{33} = 0.25\,(d^*_{33} + d^*_{31} + d^*_{15});$$

$$d_{31} = 0.125\,(d^*_{33} + 3d^*_{31} - d^*_{15});$$

$$d_{15} = 0.25\,(d^*_{33} - d^*_{31} + d^*_{15}).$$

Inserting the average values

$$d_{33} = 4.0 \cdot 10^{-6};\; d_{31} = -1.5 \cdot 10^{-6};\; d_{15} = 5.5 \cdot 10^{-6},$$

into these expressions, we obtain

$$d_{33}^{*} \approx 8.0 \cdot 10^{-6};\quad d_{3}^{*} \approx -3.0 \cdot 10^{-6};\quad d_{15}^{*} \approx 11.0 \cdot 10^{-6}.$$

This result is in satisfactory agreement with data obtained directly on single crystals [10], namely

$$d_{33}^{*} = 9.5 \cdot 10^{-6};\quad d_{31}^{*} = -3.1 \cdot 10^{-6}.$$

If we assume that $\theta = 55°$, we have

$$d_{33} = 0.52\; d_{33}^{*} + 0.26\; d_{31}^{*} + 0.26\; d_{15}^{*};$$

$$d_{31} = 0.13\; d_{33}^{*} + 0.65\; d_{31}^{*} - 0.13\; d_{15}^{*};$$

$$d_{15} = 0.26\; d_{33}^{*} - 0.26\; d_{31}^{*} + 0.52\; d_{15}^{*}.$$

Then $d^{*}_{33} \approx 5.1 \cdot 10^{-6}$; $d^{*}_{31} \approx -1.9 \cdot 10^{-6}$ and $d^{*}_{15} \approx 7.0 \cdot 10^{-6}$ which differs greatly from the results presented above for direct measurements on single crystals.

Thus this result may be considered indirect verification of the fact that polarization of a ceramic causes predominant reorientation of the domains by 180°, or that the maximum angle θ is more likely to be 90° than 55°.

LITERATURE CITED

[1] B. M. Vul and co-workers, Report: "Piezoelectric and elastic properties of piezoelectrics made of semicrystalline barium titanate" (FIAN, 1950).

[2] A. V. Rzhanov, "Piezoelectric effect of barium titanate, " J. Exptl. Theoret. Phys. (USSR) 19, 6 502-506 (1949).

[3] A. V. Rzhanov, Report: "Dynamic experiments on the piezoelectric and elastic properties of polarized barium titanate samples," (FIAN, 1950).

[4] M. L. Cherry and R. Adler, Phys. Rev. 72, 981 (1947).

[5] W. Mason, Electrostrictive effect in barium titanate ceramics, Phys. Rev. 74, 1134 (1948).

[6] A. V. Shubnikov, I. S. Zheludev, V. P. Konstantinova and I. M. Sil'vestrova, Investigations of Piezoelectric Structures [In Russian] (1955).

[7] W. Cady, Piezoelectricity and its Practical Uses* (IL, 1949).

[8] B. M. Vul, Report: "Piezoelectric ceramics," (FIAN, 1950).

[9] M. Ia. Shirobokov and L. P. Kholodenko, Report: "On the theory of the ferroelectric properties of $BaTiO_3$ ceramics," (GIFTI,** 1951).

[10] W. L. Bond, W. Mason and N. J. McScimin, Phys. Rev. 82, 442 (1951).

P. N. Lebedev Physical Institute

Received November 21, 1956

---

* Russian translation.

** Gorkii Research Institute of Physics and Technology.

DIELECTRIC AND PIEZOELECTRIC PROPERTIES OF POLARIZED CERAMIC $BaTiO_3$ IN ITS VARIOUS FERROELECTRIC PHASES*

L. A. Shuvalov

The relationship between polarization, piezomoduli and permittivity of polarized ceramic $BaTiO_3$ and the same properties of monocrystals, of which this ceramic consists, is obtained for all ferroelectric phases. Dependence on the polarizing field and on various allowed domain rotations of the changes in the above properties of the ceramic at phase transitions is discussed. The effectiveness of polarization of the ceramic $BaTiO_3$ under various conditions is estimated.

1. Introduction

Just as Rochelle (Seignette) salt was the first representative of a now very extensive class of ferroelectric crystals, so texture obtained on melting of Rochelle salt was the first representative of piezoelectric textures discovered by Shubnikov [1].

Polycrystalline ceramics of the barium titanate-type ferroelectric crystals, which have been used in recent years for a great variety of purposes, also possess piezoelectric texture in the polarized state [2].

Expressions which relate the piezoelectric, dielectric and other constants of polarized ceramic barium titanate to the constants of component crystals are of great interest. Such expressions make it possible to compare properties of ceramics and monocrystals, to estimate the effectiveness of polarization of ceramics, to discuss changes in the constants of ceramics on phase transitions and to make other deductions.

The study these expressions in the first approximation we may use the method employed by Shubnikov in his study of the Rochelle salt texture [1]. In the case of polarized ceramic $BaTiO_3$ the problem is more complex than the Rochelle salt texture due to a greater variety of crystallite orientations as well as due to the presence of three ferroelectric phases in $BaTiO_3$, compared with one in Rochelle salt, which belong to different crystallographic classes and in each of them several domain orientations are possible because there are several ferroelectric axes in barium titanate crystals [3].

The present paper deals with the first approximation to the relationship between properties of polarized ceramic $BaTiO_3$ and the crystals of which it consists, in all three ferroelectric phases, as well as with certain conclusions from the expressions obtained.

2. Ferroelectric ceramic texture

In a ceramic crystallites are distributed and oriented chaotically i.e., statistically uniformly in all (arbitrary) directions. Each of the crystallites of a ferroelectric ceramic in a ferroelectric phase consists of domains (in the general case each crystallite is polydomain). When the ceramic is not polarized polar Z-axes in the domains of crystallites are distributed statistically (on the average) uniformly along all allowed directions of the spontaneous polarization vector P_s (the number and orientation of such directions are rigidly fixed for each crystallite and change only on transition to another ferroelectric phase [3]). Thus in the ceramic as a whole the axes Z of the domains are also distributed uniformly along all directions. Such a ceramic has isotropic nonpiezoelectric texture of the symmetry group ∞/∞ or $\infty/\infty \cdot m$.

---

* The main part of the present communication was reported at the First Conference on Ferroelectricity held in Leningrad in June 1956.

Barium titanate in the cubic phase belongs to the $\bar{6}/4$ class while in the ferroelectric phases a monodomain crystal (or a single domain) of $BaTiO_3$ belongs to the classes $4 \cdot m$, $2 \cdot m$ or $3 \cdot m$. Consequently the $BaTiO_3$ ceramic in the cubic phase, or in the ferroelectric phases when it is not polarized, has texture of $\infty/\infty \cdot m$ symmetry, since it consists of crystallites (domains) with longitudinal planes of symmetry.

On polarization of the ceramic the crystallite domains acquire a predominant orientation and are eventually aligned with their Z-axes along those allowed directions of P_s in crystallites which are closest to the direction of the polarizing field and are most favorable for energy reasons. Almost all the crystallites then become monodomain, the exception being those which possess two or more permissible directions of spontaneous polarization each of which is equally close to the direction of the polarized field.

In contrast to ferromagnetics, in ferroelectric crystals it is not possible to have a continuous rotation, relative to the crystals, of the direction of the spontaneous polarization vector P_s (or the Z-axis) of domains or alignment of this direction along the applied field, if the field has an arbitrary direction which does not coincide with one of the allowed directions of P_s for the crystal. Therefore in polarization of the $BaTiO_3$ ceramic the domains cannot align their Z-axes strictly along the polarizing field and these Z-axes lie in a certain solid angle θ about the direction of the field – the so-called Z^c-axis of the ceramic. This angle θ depends on the magnitude of the polarizing field, on conditions of polarization, degree of departure from cubicity of individual cells etc., but the minimum possible angle of distribution θ_{lim}, which corresponds to the state of maximum polarization, is determined only by the allowed rotations of domains by fixed angles (for details see below).

As a result of polarization the $BaTiO_3$ ceramic acquires polar piezoelectric texture with $\infty \cdot m$ symmetry [2] in any one of the three ferroelectric phases (since in each phase the $4 \cdot m$, $2 \cdot m$, or $3 \cdot m$ domains possess a longitudinal plane of symmetry). Thus the symmetry of the polarized $BaTiO_3$ ceramic does not change when its component crystallites undergo phase transformations with changes of temperature.

3. Deduction of formulas relating constants of the polarized ceramic with constants of the component monocrystals*

Before deduction of formulas relating constants of the polarized $BaTiO_3$ ceramic with those of the component monocrystals, a number of simplifying assumptions must be made. We shall disregard interaction between crystallites (and domains) as well as imperfections of the ceramic (vacancies, binder and so on). It shall be assumed that internal mechanical stresses produced in the ceramic on firing are not affected by external influences and that only the field applied to the ceramic acts on each crystallite (domain). The distribution of the Z-axes of domains in a solid angle θ is assumed to be uniform. We should note also that, on application of the formulas given below to finding the relationships between various piezo-coefficients (d, e, g or h) or various dielectric constants of the ceramic and of monocrystals, we may obtain different results. It is very difficult to prove theoretically the correctness of averaging out the properties corresponding to tensors of the same rank [4] and this correctness should be checked by comparison, under various conditions, of calculated results with experiment.

The formulas given velow for the relationships of properties of the ceramic with those of its component monodomain crystallites (or simply domains) are necessarily approximate and should be used with caution. These formulas do, nevertheless, permit qualitative conclusions to be drawn and even produce fair agreement with experiment. This was shown by calculations of the relationship between piezomoduli d_{ij}^c of the ceramic and d_{ij} of monocrystals of the tetragonal $BaTiO_3$ carried out by Vul, Bogdanov, Razbash and Timonin [5], which supported the correctness of averaging of d_{ij}.

We shall now deal with deduction of formulas. The complex details are omitted and only the general plan of calculations is given.

A system of coordinates X, Y, Z, fixed in a crystallite (domain), is related to a fixed system of coordinates of the ceramic X^c, Y^c, Z^c, in the general case, by three Euler angles θ, ψ and φ, where θ is the angle between the Z and Z^c-axes, ψ is the angle of rotation of the X, Y, and Z system about the Z^c-axis and φ is the angle of rotation about the Z-axis (see, for example, [6], § 52). The angles ψ and φ may vary from 0 to 2π, the angle θ – from 0 to π for nonpolarized ceramics and from 0 to θ for polarized ceramics (on polarization of a ceramic only the angle θ changes, as shown earlier). By means of the usual tensor transformations we write down the components of tensors d_{ij}, ε_i, etc. of a monodomain crystal (they are different for each ferroelectric phase) in the coordinate system X^c, Y^c, Z^c of the ceramic, we integrate for all possible angles of orientation of a single crystallite (domain) and then we average out the expression obtained for each tensor component. As a result of these operations we obtain, following the symmetry of a polarized ceramic, formulas expressing piezomoduli d_{ij}^c of the ceramic in terms of piezomoduli d_{ij} of a single crystallite (domain).

---

* For the $BaTiO_3$ ceramic in the tetragonal phase these formulas were obtained earlier by B. M. Vul, S. V. Bodganov and A. M. Timonin and discussed in their paper read at the First Conference on Ferroelectricity in June 1956 (see [5]).

For the tetragonal phase (4 • m)

$$\begin{aligned} d_{15}^c &= \frac{1}{4}(1+\cos\theta)\,[(1+\cos^2\theta)\,d_{15} + \sin^2\theta\,(d_{33}-d_{31})], \\ d_{31}^c &= \frac{1}{8}(1+\cos\theta)\,[(4-\sin^2\theta)\,d_{31} + \sin^2\theta\,(d_{33}-d_{15})], \\ d_{33}^c &= \frac{1}{4}(1+\cos\theta)\,[(1+\cos^2\theta)\,d_{33} + \sin^2\theta\,(d_{15}+d_{31})]; \end{aligned} \tag{1}$$

for the rhombic phase (2 • m)

$$\begin{aligned} d_{15}^c &= \frac{1}{4}(1+\cos\theta)\left[(1+\cos^2\theta)\,\frac{d_{15}+d_{24}}{2} + \sin^2\theta\left(d_{33}-\frac{d_{31}+d_{32}}{2}\right)\right], \\ d_{31}^c &= \frac{1}{8}(1+\cos\theta)\left[(4-\sin^2\theta)\,\frac{d_{31}+d_{32}}{2} + \sin^2\theta\left(d_{33}-\frac{d_{15}+d_{24}}{2}\right)\right], \\ d_{33}^c &= \frac{1}{4}(1+\cos\theta)\left[(1+\cos^2\theta)\,d_{33} + \sin^2\theta\left(\frac{d_{15}+d_{24}}{2}+\frac{d_{31}+d_{32}}{2}\right)\right]; \end{aligned} \tag{2}$$

and for the rhombohedral phase (3 • m) the formulas are identical with those for the tetragonal phase given by Eq. (1).

Calculations of polarization P^c of the ceramic give the same formula for all ferroelectric phases, which has been obtained by Rzhanov [7]:

$$P^c = \frac{1+\cos\theta}{2}\,P_S, \tag{3}$$

where P_s is the spontaneous polarization of a single domain.

Calculations of dielectric permittivities of the ceramic ε_1^c and ε_3^c yield the formulas given below. For the tetragonal phase

$$\begin{aligned} \varepsilon_1^c &= \frac{1}{6}\left[(4+\cos\theta+\cos^2\theta)\,\varepsilon_1 + (2-\cos\theta-\cos^2\theta)\,\varepsilon_3\right], \\ \varepsilon_3^c &= \frac{1}{3}\left[(2-\cos\theta-\cos^2\theta)\,\varepsilon_1 + (1+\cos\theta+\cos^2\theta)\,\varepsilon_3\right]; \end{aligned} \tag{4}$$

for the rhombic phase

$$\begin{aligned} \varepsilon_1^c &= \frac{1}{6}\left[(4+\cos\theta+\cos^2\theta)\,\frac{\varepsilon_1+\varepsilon_2}{2} + (2-\cos\theta-\cos^2\theta)\,\varepsilon_3\right], \\ \varepsilon_3^c &= \frac{1}{3}\left[(2-\cos\theta-\cos^2\theta)\,\frac{\varepsilon_1+\varepsilon_2}{2} + (1+\cos\theta+\cos\theta)\,\varepsilon_3\right]; \end{aligned} \tag{5}$$

and for the rhombohedral phase the formulas are identical with those for the tetragonal phase given by Eq. (4).

The formulas (1)-(5) hold only within the limits of the polarized ceramic model, i.e., at sufficiently small applied fields which cannot reverse polarization of the ceramic with consequent effects due to re-orientation of domains.

The formulas (1) - (5) allow us to find, from P_s, d_{ij} and ϵ_i for a monodomain crystal, the quantities P^c, d^c_{ij} and ϵ^c_i for the ceramic. The converse solution is always permissible for P_s, but to find all d_{ij} and ϵ_i from the properties of the ceramic, the number of components of tensor of the ceramic must be identical with the number of such components for a monocrystal. This condition is obeyed in the tetragonal phase. For the rhombic phase we can find (from the ceramic properties) only

$$d_{33},\quad \frac{d_{31}+d_{32}}{2}\ \text{and}\ \frac{d_{15}+d_{24}}{2},\quad \varepsilon_3\ \text{and}\ \frac{\varepsilon_1+\varepsilon_2}{2}\,.$$

For the rhombohedral phase we can find only ϵ_i and moduli d_{15}, d_{31}, d_{33}; modulus d_{21} of a monocrystal does not occur in the formulas of Eq. (1) and consequently its value does not affect the values of d^c_{ij} of the ceramic. All these calculations are possible only when the angle of distribution θ is known, since it occurs in all the formulas of Eqs. (1) - (5).

4. Differences in the domain angle of distribution θ at various allowed rotations of domains

It was shown above that minimum (limiting) angle of distribution of the Z axes of domains, which corresponds to the maximum of polarization of the $BaTiO_3$ ceramic, is determined only by the allowed domain rotations of fixed angles whose values are different in different ferroelectric phases and which are, in their turn, determined by the allowed directions of P_s (Z-axes of domains) in a crystal of the given phase.

We shall consider the tetragonal phase of $BaTiO_3$. In a polydomain tetragonal $BaTiO_3$ crystal the domain orientations are possible only along edges of the original cubic crystal, that is domain rotations by 180° (from an antiparallel position) and by 90° (from a normal position). It is of no importance to us that these rotations may in fact occur indirectly due to motion of domain boundaries. If in crystals forming the ceramic only the 180° rotations are allowed, then at the maximum polarization of the ceramic the domains oriented furthest away from the polarizing field direction (the Z^c-axis of the ceramic) have their Z-axes at 90° to Z^c. Therefore $\theta_{lim} = 90°$. If in addition to the 180° rotations also 90° ones are allowed, then at the maximum of polarization the domains oriented furthest away from the field direction are those for which the Z^c-axis of the ceramic lies along the space (internal) diagonal, i.e., those for which the angle $ZZ^c = 54°\,44'08''$, and therefore in this case $\theta_{lim} = 54°\,44'08''$. When tetragonality of the domain is taken into account the minimum angle becomes $\theta_{lim} = \arctan\dfrac{\sqrt{2}\,a}{c} = 54°\,36'$; in further discussion such a difference in the third place is neglected for all phases.

In a polydomain $BaTiO_3$ crystal in the rhombic phase the domains are oriented with their Z-axes along diagonals of the faces of the original cubic crystal and consequently 180°, 90°, 120° and 60° rotations are possible. If in the crystals of which the ceramic is composed only the 180° domain rotations are allowed, then $\theta_{lim} = 90°$; if the 180° and 90° rotations are allowed, then $\theta_{lim} = 60°$; if all the domain rotations (180°, 90°, 60° and 120°) are allowed, then $\theta_{lim} = 45°$.

In a polydomain $BaTiO_3$ crystal in the rhombohedral phase the domains are oriented with their Z-axes along the space diagonals of the original cubic crystal; consequently 180°, ~55° and ~109° domain rotations are possible. If in the component crystals of the ceramic only the 180° domain rotations are allowed then $\theta_{lim} = 90°$; if the 180° and ~55° (and ~109°) rotations are allowed, then $\theta_{lim} = 54°\,44'$.

It follows that, depending on which of the possible domain rotations take place on polarization of the ceramic, the values of θ_{lim}, and consequently the values of P^c, ϵ^c_i and d^c_{ij}, may differ considerably.

Knowing P^c and P_s or the corresponding values of constants for the polarized ceramic and monodomain monocrystals of $BaTiO_3$ in a given ferroelectric phase, we can find from the formulas (1) - (5) the angle of distribution θ and deduce which domain rotations are predominant in the given phase and the given ceramic.

The possibility of such calculations for the tetragonal BaTiO$_3$ ceramic was first pointed out by Vul, Bogdanov and Timonin [5].

5. Variation of d_{ij}^c, P^c and ϵ_i^c with change of the angle of distribution θ and the polarizing field

Properties of the BaTiO$_3$ ceramic described by tensors of odd and even rank vary in different ways with variation of the angle of distribution θ in polarization of the ceramic. The odd-rank tensors (P^c and d_{ij}^c) are equal to zero in a nonpolarized BaTiO$_3$ ceramic ($\theta = 180°$), since such a ceramic belongs to the $\infty/\infty \cdot m$ symmetry group, it possesses a center of symmetry, and consequently, following Neumann's principle, it cannot have physical properties describable by tensors of lower symmetry (tensors of odd rank do not possess a center of symmetry). On application of the polarizing field.components of the odd-rank tensors rise monotonically and reach a maximum value when the Z-axes of all domains are aligned parallel to the field, i.e., when $\theta = 0$ (a purely theoretical case). The even-rank tensors (for example ϵ_i and S_{ijkl}) do not become zero at any value of θ but the number of independent components of tensors at $\theta \neq 180°$ increases, since the ceramic changes from isotropic $\infty/\infty \cdot m$ to anisotropic (transversely isotropic) $\infty \cdot m$ texture.

To discuss the dependence of d_{ij}^c on θ, given by Eqs. (1)-(2), we must know numerical values of d_{ij}. Unfortunately there are no published values of all moduli d_{ij} for BaTiO$_3$ monocrystals even in one phase. The author suggests a different approach. It was reported in a number of papers (see Table 2 below) that in the polarized tetragonal BaTiO$_3$ ceramic free from impurities the following relationship is well obeyed

$$d_{33}^c - d_{31}^c = d_{15}^c \,. \tag{6}$$

We may assume that the above empirical relationship holds also for moduli d_{ij}, i. e.,

$$d_{33} - d_{31} = d_{15}. \tag{6'}$$

[We may note here that Eq. (6) follows from Eq. (6')]. The formulas in Eq. (1) now become identical and assume the form

$$d_{ij}^c = \frac{1 + \cos\theta}{2} d_{ij}. \tag{7}$$

The ceramic piezomoduli d_{ij}^c now have the same dependence on θ (Fig. 1) and consequently proportionality between them is conserved at all values of the polarized field. The maximum possible values of moduli d_{ij}^c of the tetragonal ceramic are equal to 0.79 d_{ij} (when the 180° and 90° domain rotations are allowed, i.e., when $\theta_{\lim} = 54° 44'$). We may assume a qualitatively similar dependence of d_{ij}^c on θ for the rhombic and rhombohedral BaTiO$_3$ ceramics.

Comparison of Formulas (3) and (7) shows that dependence of polarization of the ceramic P^c on θ is identical with dependence of d_{ij}^c on θ, and Fig. 1 represents both these dependences.* This is to be expected in view of what was said earlier on behavior of the odd-rank tensors.

The curve showing dependences of d_{ij}^c and P^c on θ (Fig. 1) is very similar to the experimental curves showing dependences of d_{ij}^c and P^c on the polarizing field (the latter two curves are of identical nature) [14]. Consequently we may assume that the angle of distribution θ is a linear function of the polarizing field intensity E, i.e., decrease of the angle θ is proportional to increase of the field intensity E up to a value of E_{max} which corresponds to the state of maximum polarization of the ceramic (for given allowed domain rotations) and with further increase of E the angle θ remains unchanged.

Thus we may assume that

$$\theta = -kE + \pi \text{ (for } E \le E_{max}\text{)}, \; \theta = \text{const (for } E \ge E_{max}\text{)}. \tag{8}$$

---

* The limiting value of P^c for the tetragonal ceramic (when the 180° and 90° domain rotations are allowed) calculated by Rzhanov [7] and used in literature is inexact and should be equal to ≈0.79 P_s, not to ≈0.78 P_s.

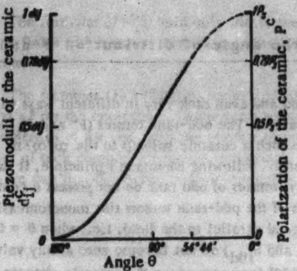

Fig. 1. Dependence of piezomoduli d^c_{ij} and polarization P^c of the tetragonal $BaTiO_3$ ceramic on θ, the angle of distribution of the Z-axes of domains.

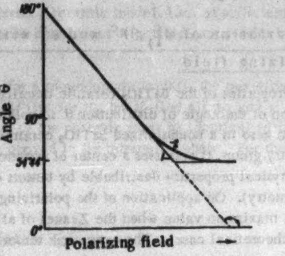

Fig. 2. Dependence of the angle of distribution θ on the polarizing field intensity.

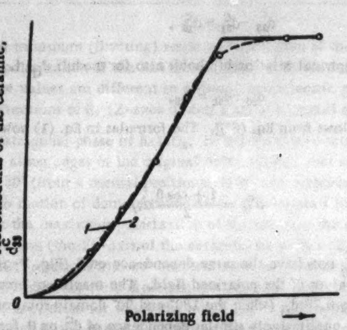

Fig. 3. Dependence of d^c_{33} of the $BaTiO_3$ ceramic on the polarizing field intensity.
1) The experimental curve ($d^c_{33\,max} = 42 \cdot 10^{-7}$ c.g.s. units, E_{max} = 2 kv/mm, t = 2 hours), 2) the theoretical curve.

Here k = a constant which gives "polarizability" of the ceramic (the higher value of k, the lower E_{max}). Such a dependence of θ on E is shown by curve 1 in Fig. 2.

If, assuming the relationships given by Eq. (8), a theoretical dependence of d^c_{ij} on E is drawn on the basis on Fig. 1, and it is compared on a suitable scale with a typical experimental curve of $d^c_{ij} = f(E)$ [14], good agreement is obtained (Fig. 3) up to the values of E, close to E_{max}, where the experimental curve is smooth and the theoretical curve shows a break. A similar behavior is exhibited by the theoretical and experimental curves $P^c = f(E)$. Such an agreement supports the assumptions of Eq. (8) and the real dependence of θ on E, with the difference between the curves of Fig. 3 taken into account, should have the form of curve 2 in Fig. 2.

The process of polarization of the ceramic can be thus represented, in a first approximation, as decrease of the angle of distribution θ of the Z-axes of domains which is proportional to the field intensity, i.e., a "rotation" of domains proportional to the field. When not only the 180° but also other possible domain rotations take place the effective values of d^c_{ij} are always increased.

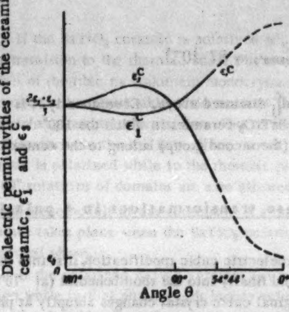

Fig. 4. Dependence of dielectric permittivities ϵ_1^C and ϵ_3^C of the ceramic on the angle of distribution θ.

Dependence of ϵ_i^C (an even-rank tensor) on θ should be quite different. Starting from $\epsilon_1 >> \epsilon_3$, we obtain curves of $\epsilon_1^C = f(\theta)$ and $\epsilon_3^C = f(\theta)$ given in Fig. 4. We may assume that dependences of ϵ_i^C on E are qualitatively similar. From Fig. 4 we can see that, if only the 180° domain rotations are allowed, at E_{max} (when θ = 90°) the ceramic has the same permittivities as in the unpolarized state. Anisotropy of ϵ_i^C at E_{max} shows that other than the 180° domain rotations also occur.

We used the Formulas (1)-(5) which hold for a uniform distribution of the Z-axes of domains, although at field intensities lower than E_{max} this distribution is not uniform, even when the 90° rotations take place after the 180° rotations are complete. Thus, although useful in a descriptive way, the angle $\theta < \theta_{lim}$ is a somewhat formal (theoretical) quantity.

6. Comparison of values of d_{ij}^C and d_{ij} of the tetragonal phase of BaTiO$_3$

Comparison of d_{ij}^C and d_{ij} using the Formulas (1) and (2) is difficult because for BaTiO$_3$ monocrystals only d_{33} and d_{31} have been measured and only in the tetragonal phase [8]. Vul, Bogdanov, Razbash and Timonin [5], who calculated from their experimental values of d_{ij}^C of the tetragonal BaTiO$_3$ ceramic the values of d_{ij} for a monodomain monocrystal, obtained good agreement with experiments when θ = 90° (see Table 1). They concluded that in the ceramic measured by them the 180° domain rotations predominate.

TABLE 1

	d_{33}	d_{31}	d_{15}
Experimental values of $d_{ij}^C \times 10^7$ c.g.s. units [5]	40	−15	55
Experimental values of $d_{ij}^C \times 10^7$ c.g.s. units [8]	95	−31	–
Theoretical values of $d_{ij} \times 10^7$ c.g.s. units at θ = 90° [5]	80	−30	100
Theoretical values of $d_{ij} \times 10^7$ c.g.s. units at θ = 54° 44' [5]	51	−19	70

TABLE 2

Piezomodulus	Work cited						
	[7]	[9]	[10]	[11]	[12]	[5]	[13]
$d_{15}^C \cdot 10^7$ c.g.s. units	—	—	—	81	78	55	—
$d_{31}^C \cdot 10^7$ c.g.s. units	−14	−22.5	—	−23.7	−23.5	−15	−13
$d_{33}^C \cdot 10^7$ c.g.s. units	32	54	32–43	57.3	57.5	40	35

Values of piezomoduli d_{ij}^C of the polarized tetragonal BaTiO$_3$ ceramic measured by various authors differ considerably (see Table 2). These values can be, however, easily divided into two groups:

First – $d_{33}^C = 32 \div 43 \cdot 10^{-7}$, $d_{31}^C = -13 \div -15 \cdot 10^{-7}$; $d_{15}^C = 55 \cdot 10^{-7}$ c.g.s. units.
Second – $d_{33}^C = 54 \div 57.5 \cdot 10^{-7}$; $d_{31}^C = -22.5 \div -24 \cdot 10^{-7}$; $d_{15}^C = 78 \div 81 \cdot 10^{-7}$ c.g.s. units.

From Eq. (7) or Fig. 1 we can easily find the relationship between $d_{ij\,180°}^C$ when the 180° rotations only are allowed and $d_{ij\,90°}^C$ when the 90° rotations are also allowed

$$d_{ij\,90°}^C = 1.58\, d_{ij\,180°}^C \, . \qquad (9)$$

As $d^C_{ij\,180°}$ we may use, following [5], the values of d^C_{ij} from Table 1 (these values belong to the first group of d^C_{ij} obtained by various authors; see text above). From Eq. (9) we now find

$$d^C_{33(90°)} = 63 \cdot 10^{-7}, \quad d^C_{31(90°)} = -24 \cdot 10^{-7}, \quad d^C_{15(90°)} = 87 \cdot 10^{-7}.$$

This new set of values is very close to the second group of values of d^C_{ij} discussed above. Consequently it is suggested that the first group of values of d^C_{ij} refers to the tetragonal $BaTiO_3$ ceramics in which the 180° domain rotations predominate in polarization, while the higher values of d^C_{ij} (the second group) belong to the ceramics in which also the 90° rotations of domains take place.

7. Variation of the angle of distribution θ on phase transformations in a polarized ceramic

On lowering of temperature $BaTiO_3$ transforms from the nonferroelectric cubic modification, first into the ferroelectric tetragonal (at 120°C), then into the rhombic (at 10°C) and finally into the rhombohedral (at −70°C) modification. The direction of P_s of domains with respect to the original cubic crystal changes abruptly at phase transformations. These changes will also occur at appropriate temperatures, in crystallites of which the polarized $BaTiO_3$ ceramic is composed.

Nine cases (see Table 3) are theoretically possible, but in practice only the cases 1, 2, 4 and 5 are of interest.

TABLE 3

No.	Region of polarization of the ceramic	Region of application of the ceramic
1	Tetragonal	Tetragonal
2	Tetragonal	Rhombic
3	Tetragonal	Rhombohedral
4	Rhombic	Tetragonal
5	Rhombic	Rhombic
6	Rhombic	Rhombohedral
7	Rhombohedral	Tetragonal
8	Rhombohedral	Rhombic
9	Rhombohedral	Rhombohedral

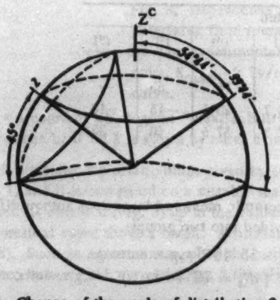

Fig. 5. Change of the angle of distribution θ on transition of the ceramic, polarized in the tetragonal phase, from the tetragonal to the rhombic phase.
(On polarization both the 180° and 90° rotations of domains take place).

On transition of $BaTiO_3$ from the tetragonal to the rhombic phase in each domain the Z-axis (direction of P_s) is rotated by 45° about the X-axis. In the polarized ceramic along every direction in the solid angle of distribution θ lie Z-axes of the domains which have arbitrary directions of the X- and Y-axes (the angle φ varies from 0 to 2π). After transition of the polarized ceramic from the tetragonal to the rhombic phase the domains, previously oriented with their Z-axes along one straight line, now form, with their Z-axes, a cone of 45° semi-angle around that straight line (Fig. 5). The angle θ, therefore, increases by 45° in this phase transformation. The relationship between the absolute values of d^C_{ij} in the tetragonal and rhombic phases does not depend on the relationship between d_{ij} in these phases. The ratio d^C_{ij}/d_{ij} (the relative effectiveness of piezomoduli of the ceramic) decreases on phase transformation. (In the rhombic phase by d_{ij} we mean d_{33} or $\frac{d_{31}+d_{32}}{2}$, or $\frac{d_{15}+d_{24}}{2}$).

On transition of $BaTiO_3$ from the rhombic to the rhombohedral phase the Z-axis of each domain is rotated by 35°16'. Consequently in this transition of the polarized $BaTiO_3$ ceramic the angle θ increases by ~35°.

If the $BaTiO_3$ ceramic is polarized while in the tetragonal phase, then $d^C_{ij\,180°} = 0.5\ d_{ij}$, $d^C_{ij\,90°} = 0.79\ d_{ij}$; after transition to the rhombic phase this ceramic possesses the following moduli, related now to the piezomoduli of rhombic monodomain monocrystals, $d^C_{ij} = 0.15\ d_{ij}$ and $d^C_{ij} = 0.4\ d_{ij}$, respectively. (The latter values were obtained without taking into account the nonuniformity of the domain distribution arising in a polarized ceramic at phase transformations. Due to that nonuniformity the effective increase of the angle is smaller and the differences in the relative effectiveness of piezomoduli of the ceramic are not so appreciable.) If the ceramic is polarized while in the rhombic phase, then we obtain $d^C_{ij\,180°} = 0.5\ d_{ij}$, $d^C_{ij\,90°} = 0.75\ d_{ij}$ and, when the 60° rotations of domains are also allowed, $d^C_{ij\,60°} = 0.85\ d_{ij}$ (which is the maximum possible relative effectiveness of piezomoduli of the ceramic). A similar decrease of the relative effectiveness of piezomoduli of the ceramic takes place when the $BaTiO_3$ ceramic is polarized while in the rhombic phase and used while in the tetragonal phase.

If the polarized $BaTiO_3$ ceramic is used at temperatures corresponding to the rhombic phase, then polarization while in that phase yields higher values of piezomoduli than polarization while in the tetragonal phase (if in the rhombic phase the same rotations, in the limit, take place as in the tetragonal phase). If the polarized ceramic is used both in the tetragonal and rhombic phases, and polarization while in the rhombic phase produces the 60° domain rotations, it may be useful to polarize such a ceramic while in the rhombic phase. (These conclusions hold assuming a sufficiently high electric breakdown strength of samples.)

This theoretical discussion of dielectric and piezoelectric properties of the polarized $BaTiO_3$ ceramic, including domain orientation, shows that, although the formulas (1)-(5), which relate the values of constants of the polarized ceramic with the values of the same constants of monocrystals (domains) of which the ceramic consists should be used with caution, they make it possible to estimate the effectiveness of the process of polarization of the $BaTiO_3$ ceramic, to study the changes in parameters of the polarized ceramic on phase transformations, as well as to give a physical picture of the processes of polarization of the ceramic.

In conclusion the author thanks I. S. Zheludev for directing this work and S. V. Bogdanov for valuable advice.

LITERATURE CITED

[1] A. V. Shubnikov, Piezoelectric Textures [in Russian] (1946).

[2] A. V. Shubnikov, I. S. Zheludev, V. P. Konstantinova and I. M. Sil'vestrova, Investigation of Piezoelectric Textures [in Russian] (1955).

[3] I. S. Zheludev and L. A. Shuvalov, "Ferroelectric phase transformations and crystal symmetry," Kristallografiia 1, 6, 681-8 (1956).

[4] A. F. Devonshire, "The theory of the barium titanate II." Phil. Mag. 42, 1065-1079 (1951).

[5] B. M. Vul, S. V. Bogdanov and A. M. Timonin, "On the relationship between dielectric, piezoelectric and elastic properties of polycrystalline ceramics and monocrystals," Izv. AN SSSR, Ser. fiz. 3 (1957).

[6] S. V. Bogdanov, B. M. Vul and R. Ia. Razbash, "Piezoelectric shear modulus of polarized barium titanate," Kristallografiia 2, 1, 115-118 (1957).*

[6] ** W. G. Cady, Piezoelectricity and its Practical Applications (Russian translation), (1949).

[7] A. V. Rzhanov, "Piezoeffect in barium titanate," J. Exptl.-Theoret. Phys. (USSR) 19, 3, 502-6 (1949).

[8] W. L. Bond, W. P. Mason and H. I. McScimin, "Elastic and electromechanical coupling coefficients of single-crystal barium titanate," Phys. Rev. 82, 3, 442-443 (1951).

[9] H. Jaffe, "Titanate ceramics for electromechanical purposes," Ind. Eng. Chem. 42, 264-268 (1950).

---

* This issue, page 111.

** Erroneous duplication as in original.

[10] L. Egertone and S. E. Koonce, "Effect of firing cycle on structure and some dielectric and piezoelectric properties of barium titanate ceramics," J. Am.Ceram. Soc. 38, 11, 413-418 (1955).

[11] R. Bechman, "Elastic, piezoelectric and dielectric constants of polarized barium titanate ceramics and some applications of the piezoelectric equations," J. Acoust. Soc. Am. 28, 3, 347-350 (1956).

[12] D. Berlincourt, "Recent developments in ferroelectric transducer materials," I.R.E. Trans. Ultrasonic Eng. 4, 53-65 (1956).

[13] N. A. Rol, "Dielectric and piezoelectric properties of solid solutions (Ba, Sr)TiO_3, Ba(Ti, Sn)O_3 and Ba(Ti, Zr)O_3," Acoustics J. (USSR) 2, 1, 62-70 (1956) [Soviet Physics – Acoustics, p. 80].

[14] B. M. Vul and co-workers, Report of FIAN(1951).

Institute of Crystallography, AN SSSR Received December 25, 1956

ELECTROPHOTOGRAPHY ON PHOTOELECTRETS

V. M. Fridkin

A method is described for producing images on photoelectrets of polycrystalline sulfur and single crystals of sulfur and anthracene. Reproductions are given of the first photographs on photoelectrets of polycrystalline sulfur. A sensitometric method of investigating the photoelectret state is proposed.

In previous work, we studied the photoelectret state in polycrystalline sulfur [1, 2]. It was shown, in full agreement with [3], that the persistence of a polycrystalline specimen in the polarized state was much longer than the time during which polarization is retained in a single crystal. At the same time, a photoelectret of polycrystalline sulfur was regarded as a polar texture with the symmetry ∞ · m (according to A. V. Shubnikov).

Together with A. I. Froiman and E. L. Nemirovskii, we predicted the possibility of producing images on the surface of this type of polar texture [4]. This was based on the supposition of the local character of the space-charge distribution, due to the polarization of the photoelectret. The work described in the present paper is an experimental confirmation of this supposition.

The method we employed for producing images on the surface of a photoelectret was as follows.

A thin layer of sulfur, evaporated in a vacuum on to an aluminum or zinc plate, was polarized with continuous illumination and applied voltage. The semitransparent electrode used was a quartz plate with an evaporated film of gold or silver. On completion of polarization, illumination was discontinued and the voltage cut off from the electrodes.

The charge on the surface of the photoelectret produced in this way was measured by means of a dynamic electrometer, the circuit of which is shown in Fig. 1. A vibrating electrode E, connected to the input of a cathode follower, was placed above the surface of the photoelectret. The output voltage from the cathode follower was applied to the deflecting plates of a cathode ray oscillograph. The amplitude of the signal was measured on the oscillograph screen directly in volts.

A transparency of any kind (for example a raster) was placed on the surface of the photoelectret and the latter was reilluminated through it. The illuminated portions of the photoelectret were now fully depolarized, while the unilluminated portions (those covered by elements of the image) retained their polarization. This exposure produced a latent image, formed by the portions of the photoelectret which had retained their polarization.

A triboelectric effect was used for developing the latent image. Asphalt powder was mixed with particles of sand or common salt, the sand or salt particles becoming negatively charged and the particles of asphalt positively charged. The mixture of the two powders was scattered on the surface of the exposed layer and according to the sign of the charge on the photoelectret surface, the latent image was developed by particles of asphalt or sand, which adhered only to those portions where the polarization had been retained.

Figure 2 shows reproductions of such electrophotographs produced on the surface of a photoelectret of polycrystalline sulfur.

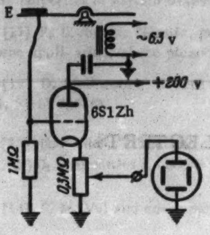

Fig. 1. Circuit of dynamic electrometer. [6 S 1 Zh≡955 (Acorn)].

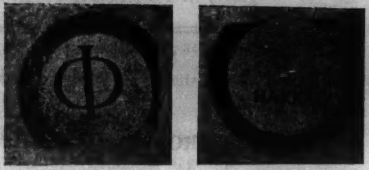

Fig. 2. Specimens of electrophotographs on a photoelectret of polycrystalline sulfur.

The layer of polycrystalline sulfur was polarized for 2-5 minutes at a voltage of 1.7 kv, with illumination by a PRK-2 mercury quartz lamp (the illumination of the surface layer was 10^{-3} v/cm^2). To eliminate the occurrence of a homogeneous charge, due to the transfer of charges from the semitransparent electrode to the photoelectret, a thin glass plate was placed between the sulfur layer and the semitransparent electrode. For producing the latent image, the photoelectret was depolarized by illuminating it through a transparency for 1 minute using the same illumination.

Since the photoelectret state persists in a polycrystalline specimen for a relatively long time, the images produced on the photoelectret could be reproduced many times. A photoelectret of polycrystalline sulfur was kept in the dark with short-circuited cover plates, and the latent images was repeatedly developed, although its intensity diminished in the course of several days. Just as the term "electret" was introduced by Heaviside to denote the electrostatic analogue to the magnet, the phenomenon described is analogous to magnetic recording.

It may be assumed that the density of the powder developing the latent image on the surface of the photoelectret is proportional to the density of the surface charge of the photoelectret. We have investigated the variation in density of the powder on the photoelectret surface with the time during which the photoelectret was retained in the dark with short-circuited cover plates. The surface of the photoelectret was periodically developed by the method described above, and the optical density of the powder was measured on a specific portion of the layer. For this purpose, the coefficient of reflection of the developed portion was measured by means of an FT-2 photometer (constructed by the All-Union Institute of Scientific Instrument Construction). Assuming the optical density of the developed portion to be proportional to the density of surface charge of the photoelectret, we obtained in this way the time-dependence of the charge, investigated previously by us directly by means of an electrometer [1]. Figure 3 shows the dependence of the optical density of a developed portion of a photoelectret on the time elapsing from the moment of completion of polarization, which characterizes the variation in the charge of the photoelectret with time. The results given were obtained for layers of polycrystalline sulfur and for the above-mentioned polarization conditions.

This method was applied to a study of the photoelectret state in single crystals of sulfur and anthracene.

Sulfur plates of an area of about 1 cm^2 and thickness 1 mm were cut perpendicularly to the acute bisectrix of the optical axes and polished on silk, moistened with kerosene. These specimens were polarized by the method described above, both visible and ultraviolet light being used for illumination. The polarizing voltage was 1.7 kv and the polarizing time 2-5 minutes. On completion of polarization, "development" of the photoelectret surfaces was carried out as described above, using a mixture of sand and asphalt. The results was that one surface of the polarized plate was covered uniformly with asphalt and the other with sand, this corresponding to the direction of the polarization produced.

The decay of polarization with time was studied by plotting the dependence of optical density on the time elapsing from the moment of completion of polarization. The results confirm the deduction previously made [1, 3] that the persistence of polarization in single crystals is much less than the persistence of polarization in a polycrystalline specimen.

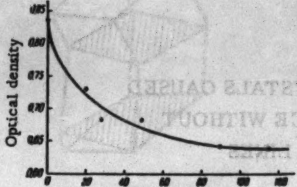

Fig. 3. Dependence of optical density of the developed portion of a photoelectret on the time elapsing from the moment of completion of polarization.

Similar results were obtained for anthracene plates cut perpendicularly to the b axis.

It must be assumed that the sensitometric method as employed by us, in view of its clarity and simplicity, can be used in studying the photoelectret state. The virtue of the method is not merely that it provides a qualitative notion of the variation of photoelectret polarization with time, but that the field distribution on the surface of a polar texture is obtained directly by its means. This method serves as additional evidence of the local character of the polarization produced in a photoelectret and provides a visible representation of the distribution of this polarization. The possibility of applying the well-developed methods of sensitometric measurements to the study of photoelectrets is also important.

We also consider that electrophotography on photoelectrets, as proposed in the present article, is of practical interest as being analogous to magnetic recording. This once more confirms the fruitfulness of approaching the phenomena of polarization in photoconductivity from the viewpoint of the investigation of the electret state, as was first pointed out by G. Nadzhakov.

Iu. N. Martyshev and A. I. Delova assisted in carrying out this work.

The author expresses his sincere gratitude to Academician A. V. Shubnikov and I. S. Zheludev for their guidance in the present work, and also to L. M. Beliaev for kindly letting us have single crystals of anthracene.

LITERATURE CITED

[1] V. M. Fridkin, "Some results of the study of the photoelectret state of single crystals of sulfur," Kristallografiia 1, 5, 557-563 (1956).

[2] V. M. Fridkin, "Depolarization of photopolarized single crystals of sulfur at different temperatures," Kristallografiia 1, 6, 692-695 (1956).

[3] G. Nadzhakov and N. T. Kashukeev, Study of photoelectrets. Bull. Bulg. Acad. Sci. Phys. Ser. 2, 321-337 (1951).

[4] V. M. Fridkin, A. I. Froiman, E. L. Nemirovskii, Author's Certificate No. 103649, 57d, 10, 1955.

Institute of Crystallography
of the Academy of Sciences,
USSR

Received December 16, 1956

PLASTIC DEFORMATION OF CRYSTALS CAUSED BY ROTATION OF THE LATTICE WITHOUT FORMATION OF GLIDE LINES

M. V. Klassen-Nekliudova and A. A. Urusovskaia

Evidence is presented that dislocation layers may be produced by rotation of crystal lattice without formation of glide lines.

According to the modern concepts, plastic deformation of crystal takes place by gliding. The prevailing opinion is that the other type of residual deformation, twinning (classical), changes the form of a crystal considerably less and that its role is subordinate. A different point of view was advances in 1935 by Brilliantov and Obreimov [1, 2]. Their investigations showed that during compression of a rock salt crystal reorientations of large regions occur within the crystal as in mechanically induced twinning. However, in contradistinction to classical twinning, these regions do not form contact with the initial crystal along rational crystallographic surfaces; moreover, the angle through which these regions are turned is not constant [1-4]. N. A. Brilliantov and I. V. Obreimov named this phenomenon "twinning on irrational faces." They pointed out [1] that the reality of deformation by gliding (according to Mügge and Poliani this deformation is translation of a part of a crystal through a distance which is a multiple of the period of the lattice) needs to be confirmed experimentally.

Klassen-Nekliudova [4], in studying the deformation of rock salt under elevated temperatures (400-600°C), observed the appearance of regions in which the lattice was turned relative to the original position through various angles (up to 38°). In her paper she suggested that the classical twins and twins on irrational faces are special cases of a more general phenomenon, asymmetrical reorientation of the lattice.

Formation of large rotated regions in rock salt crystals under tension was observed by A. V. Stepanov [5]. These regions had the form of interlayers or plates.

Deformation accompanied by appearance in interlayers with asymmetrically rotated lattice was called lamination by Stepanov.

Asymmetrically reoriented regions in crystals had been described by Lehman [6] and Mügge [7]. Mügge observed this phenomenon during deformation of a number of crystals and called it bends, breaks or dislocations (Knickungen). Figure 1 shows the formation of dislocations in calcite according to Mügge. He supposed that it may be explained by a complication of either gliding or twinning process.

In the last 15 years metallurgists have shown much interest in dislocations which form during plastic deformation of single crystals and crystal aggregates of metals. It is supposed that dislocations result from gliding accompanied by bending of the glide plane.

We have investigated the conditions of formation of dislocations and their structure in transparent crystals of TlBr−TlI, CsI and CsBr, using optical and x-ray methods [8-10]. These investigations showed that the displaced layers consist of a series of wedge-shaped laminae rotated with respect to each other. The angle of rotation in the layer increases with the degree of deformation. The orientation of the lattice in the wedges relative to the original position, in general, does not correspond to the position of twinning (although in some displaced layers of CsI, Kolontsova and others [11] discovered that the mutually rotated lattices were in contact according to the law of irrational twinning).

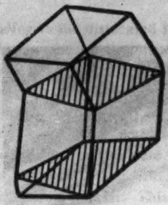

Fig. 1. Bending of the regions adjacent to the ends of a cut prism of calcite under compression.

Fig. 2. Laue photograph of an area with a dislocated layer of a specimen of TlBr-TlI.

In all crystals of TlBr-TlI, CsI and CsBr investigated by us up to now, signs of gliding were found which agree with the concepts of the foreign metallurgists (Orowan, Barrett, Hess, Gilman, Read and others). In order to check the hypotheses of Brilliantov and Obreimova [1, 2], and those of Stepanov [11] and Klassen-Nekliudova [4], we tried to separate the process of rotational deformation of the lattice from the process of gliding by the use of a motion picture camera [12]. However, because of the rapidity of dislocation we could not separate the process of rotation from that of gliding with a camera speed of 24 frames per second. If reorientation occurs as rapidly as twinning (10^{-4} sec.) high speed photography is necessary. This paper described experiments designed to distinguish reorientation of the lattice from gliding by using definitely oriented crystals.

Irrational twins in rock salt crystals were obtained by Brilliantov and Obreimov by squeezing cleavage plates 5-10 times as broad and as long as they were thick in a press. Within the rotated regions of the plates more or less pronounced signs of gliding must always appear, for it is practically impossible to select an orientation of samples such that gliding would be excluded along all gliding directions (at room temperature the glide planes are $\{110\}$, glide lines – $< 110 >$).

Unlike NaCl crystals, the crystals of CsI, CsBr, TlBr-TlI, having analogous glide surfaces $\{110\}$, have glide directions $< 100 >$. If the crystals of cesium and thallium halides are compressed in the direction of cube edge [100], then no gliding can occur in the other two directions $< 100 >$, which are normal to the axis of compression. If crystals of CsI and CsBr are compressed in the direction of gliding [100] dislocation bands form but always with glide lines within [12]. This is evidently due to a very low resistance of these crystals to gliding and possibly to the presence of an additional glide system.

We succeeded in separating the two phenomena, rotation and gliding, by compressing samples of TlBr-TlI crystals of a definite orientation. Ten prisms from 4 by 4 to 2 by 3 mm in cross section and 20-25 mm high were subjected to compression. The main axis of the prisms was parallel to the direction of gliding (precision of orientation was from 30' to 1°); in some specimens the direction of gliding was at some angle to the principal axis but not in excess of 10°. The side surfaces of the prisms were carefully polished [9].

Before the experiment the specimens were heated to 280°C. The result of heating was checked by examination in polarized light. The specimens were compressed by means of a lever press. Especially good dislocated layers were obtained by using a common metal-working vise. The deformed specimens were carefully examined under a microscope in parallel polarized light. It was found that all ten specimens had regions with a rotated lattice and that within these regions, in spite of the considerable angle of rotation, glide lines were absent. In a previous article [10] a photograph was given of a part of one of these specimens (Fig. 6,c [10]). The rotation of the lattice in this specimen was discovered by means of percussion figures. The angle of rotation was so great that an octahedral plane of the dislocated layer came into coincidence with the dodecahedral plane of the undeformed crystal.

In order to find out whether this layer was not a twinning lamella (classical or irrational) the indices of the boundary between the original crystal and the rotated part were determined. This was done by taking a Laue photograph in the direction normal to the surface containing the boundary. This photograph is reproduced in Fig. 2. It shows two types of spots: round, corresponding to the undeformed part of the crystal, and elongated,

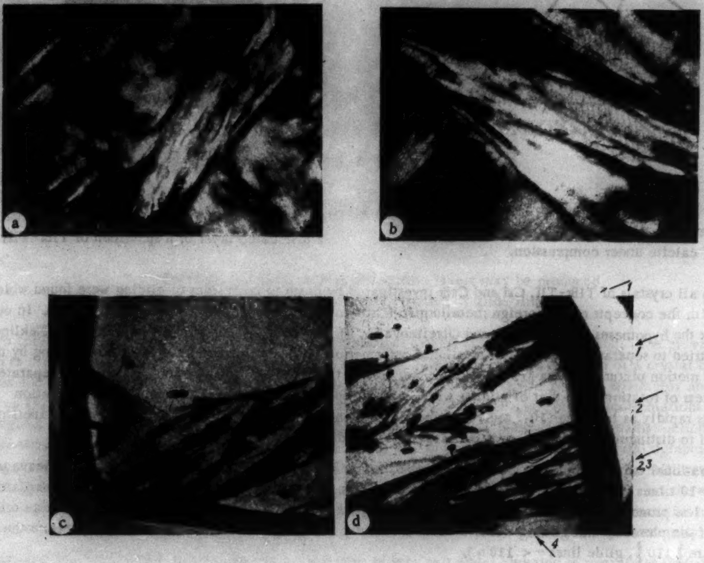

Fig. 3. Areas with dislocation layers produced by compression in three specimens of TlBr-TlI. Photographs a and b were taken in transmitted polarized light; photographs c and d, in transmitted plain light.

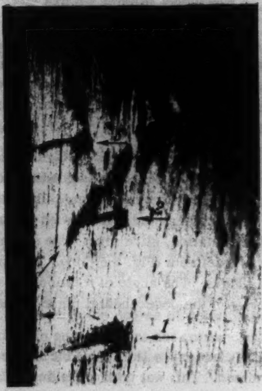

Fig. 4. Photograph taken by reflected light of the surface of a TlBr-TlI specimen in which percussion figures disclosed the formation of several rotated regions of different sizes.

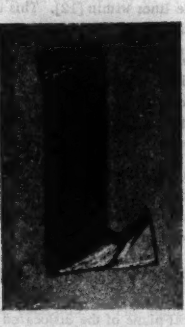

Fig. 5. A specimen of TlBr-TlI showing 13% shortening produced by compression along [100].

corresponding to the dislocated layer. A few round spots are superimposed on the elongated ones, indicating coincidence between some directions of the undeformed and the rotated lattices. After the photograph was indexed (in indexing of spots on a gnomonosterographic projection it was taken into consideration that the center of projection of the undeformed part of the crystal was the direction [110] and the center of projection of the rotated part was the direction [111]), it was found that both parts had the direction $[1\bar{1}0]$ in common, which therefore was the axis of rotation. Besides this the following directions corresponding respectively to the original and the rotated parts of the crystal were found: [20.20.13] and $[\bar{4}13]$, $[73.\bar{1}.46]$ and $[14\bar{3}]$, $[\bar{3}16]$ and $[1\bar{3}3]$. All of these directions lay in one plane with the index (241) with respect to the undeformed lattice and (17.17.10) with respect to the rotated part. This plane made an angle of 13° with the surface of the crystal plate and passed through the boundary of the displaced layer which could be observed directly. Differences in the indices of the boundary shows that it is not a symmetry plane of the lattices in contact. The dislocated layer in this specimen is not a twinning lamella. This type of deformation may be called an asymmetrical reorientation of the crystal lattice relative to the initial position.*

Figure 3, a, b, c, d are photographs of the dislocated layers in a number of specimens of TlBr-TlI taken in parallel polarized light. Specimens whose compression was stopped immediately upon the appearance of the first signs of dislocation layers are shown in Fig. 3, a and b. Such layers are still quite transparent and fractured only in some areas (mainly in the areas of the greatest deformation). The photographs show that there are no lines of gliding** either within or near the layer. In both cases the dislocation layers were formed by pure rotation of the lattice. With the aid of percussion figures the angles of rotation of these layers were determined. The layer shown in Fig. 3,a was rotated through about 21°, and that in Fig. 3,b, through about 15°.

Figures 3,c and d are photographs of two areas corresponding to the ends of dislocation layers formed in a specimen of TlBr-TlI under strong pressure directed exactly along [100]. Under such pressure, several adjacent dislocation layers were formed. The outlines of the deformed specimen are also seen in the photographs. The boundaries of the individual dislocation layers are indicated by arrows (1−1, 2−2, 3−3). Between the layers 1−1 and 2−2 there is an undisturbed region. In the middle of this region dislocation 4 was formed. The layer 2−2 can be distinguished from layer 3−3 by the fracture in the edge of the specimen. In order to estimate the amount of rotation of the lattice, percussion figures were made by pricking the specimen with a needle. Figure 3,c shows that the percussion figure have axes of two-fold symmetry (with a slight deviation). From the position of the longer axis of a percussion figure which is parallel to [110], it is possible to judge the character of reorientation of the lattice and even to estimate the angles of rotation. Thus, for example, the angle of rotation of the lattice in relation to the original orientation of the specimen (fixed by the uppermost percussion figure) is nearly 26°. The lattice of the undisturbed region 1−2, judging by the position of the percussion figures, is slightly turned with respect to the initial orientation. Measurement of the angle between the longer axes of the percussion figures and one of the sharp boundaries of the layer 1−1 shows that this boundary makes an angle of 7° with the original crystal and an angle of 9° with the region of the crystal adjacent to the dislocation layer, i.e., the boundary of the layer is not a plane of symmetry and the rotated regions do not always occupy twinning positions. None of the layers in this specimen shows signs of gliding. That they are absent can be seen from Fig. 3, taken in polarized light. Thus a detailed investigation of this specimen once more confirms the conclusion that the dislocation layers form as the result of rotational (reorientation) of the lattice under mechanical stress.

So far as the size of the reoriented regions is concerned, they vary widely and may be several millimeters in width.

We feared [9] that the appearance of such large monocrystalline reorientations in the crystals of TlBr-TlI was due to coalescence of smaller regions after the deformed specimens had been kept for a long time (i.e., to recrystallization at room temperature). Control experiments have shown that this is not so. A photograph taken by reflected light of a portion of a specimen with a broad dislocation layer in the middle (photographed immediately after deformation) is shown in Fig. 4. Three percussion figures were made of this layer (1, 2, 3). The lower two figures (1, 2) were made on the undeformed part of the specimen and fix the orientation of the undeformed crystal. The plane of the drawing is near (100), a slight deviation of the specimen from (100) is indicated by the fact that only one branch of a cruciform percussion figure can be seen. The upper percussion figure, 3, is in the middle of the dislocation layer. The boundary of the layer is a little above percussion figure 2, and does not show up well in the photograph (its position is indicated by a cross). Figure 3 shows two legs of the cross. This indicates that it was made in a region which had been rotated through a certain angle relative to the original crystal. Examination of this specimen in transmitted polarized light shows clearly that the depression made by the needle, the entire left quadrant of the figure and the lower part of its vertical leg lie in the monocrystalline region which was rotated as a whole in the process of deformation. The upper part of the vertical branch of figure 3 extends into the region of the specimen which consists of many narrow, long areas rotated through a small angle. The presence of these areas affected the relief of the surface of the upper part of percussion figure 3. This part of the figure is crossed by narrow stripes corresponding to the boundaries of the rotated regions of the specimen. Thus in deformation of crystals TlBr-TlI very large regions are reoriented and their size is not due to recrystallization.

---

* From this specimen we obtained a proof of possibility of determining the orientation of adjacent rotated regions not only by means of the Laue photographs but also by percussion figures. In further investigations of lattice rotation this method was used exclusively.

** These lines are visible in polarized light because of local internal stresses, and in ordinary light because of local change in refractive index.

As has already been mentioned, in twinning the general deformation is very slight. We observed the shortening of a specimen of TlBr-TlI under compression along [100] by 10-15% (Fig. 5). In this case dislocation layers developed on both ends. No signs of gliding were discovered in the specimen by examination in polarized light. The regions of dislocation became nontransparent and acquired numerous cracks. This experiment shows that formation of dislocation layers may be accompanied by a considerable plastic deformation of a crystal. Whether the great shortening of the crystal was produced by mere rotation of the lattice and displacement of parts of the crystal along cracks which appeared along the boundaries of the rotated region is hard to say at present. In such a great deformation the possibility is not excluded of a secondary gliding in the areas into which the layer is broken.

SUMMARY

1. It has been shown that dislocation layers form as the result of reorientation of regions within the crystal lattice under mechanical stress. If the crystal is so oriented as to exclude plastic deformation by gliding, this reorientation may occur without the formation of glide lines, but entirely by rotation of the lattice.

2. It has been confirmed that the dislocation layers consist of a series of regions rotated through various angles. The surface of separation between adjacent rotated regions may have asymmetrical position with respect to the lattices of these regions.

3. It has been shown that the formation of dislocation layers in case of compression may cause a considerable plastic deformation of the crystal (up to 10-15%).

LITERATURE CITED

[1] N. A. Brilliantov and I. V. Obreimov, "Plastic deformation in rock salt, III," J. Exptl.-Theoret. Phys. (USSR) 5, 3-4, 330-339 (1935).

[2] N. A. Brilliantov and I. V. Obreimov, "Plastic deformation, IV," J. Exptl. Theoret. Phys. (USSR) 7, 8, 978-986 (1937).

[3] V. I. Startsev, "Investigation of rotation of crystal lattice during plastic deformation," J. Exptl.-Theoret. Phys. (USSR) 10, 6, 703 (1940).

[4] M. V. Klassen-Nekliudova, "Mechanical twinning in rock salt crystals according to the spinel law," J. Exptl.-Theoret. Phys. (USSR) 12, 9, 349-357 (1942).

[5] A. V. Stepanov and A. V. Donskoi, "A new mechanism of plastic deformation of crystals," J. Tech. Phys. (USSR) 24, 2, 161 (1954).

[6] O. Lehman, "Mikrokristallographische Undersuchungen," Z. Krist. 10, 321 (1885).

[7] O. Mügge, "Über Translation und verwandte Erscheinungen in Kristallen," Neues. Jahr. Mineral. 1, 71-158 (1898).

[8] A. B. Zemtsov, M. V. Klassen-Nekliudova and A. A. Urusovskaia, "On the complex manifestation of plastic deformation in single crystals," Doklady Akad. Nauk, SSSR 91, 4, 813-816 (1953).

[9] M. V. Klassen-Nekliudova and A. A. Urusovskaia, "The effect of nonuniform stress on the mechanism of plastic deformation of halides of thallium and cesium," Crystallography, 1, 4, 410-418 (1956).

[10] M. V. Klassen-Nekliudova and A. A. Urusovskaia, "Investigation of the structure of dislocation bands in the crystals of the thallium halides," Crystallography 1, 5, 564-571 (1956).

[11] E. V. Kolontsova, I. V. Telegina and G. M. Plavnik, "The structure of dislocation bands in some ionic crystals," Crystallography 1, 4, 419-424 (1956).

[12] A. A. Urusovskaia, A Study of Complex Phenomena of Plastic Deformation of Crystals (Dissertation), Institute of Crystallography, Acad. Sci. USSR(Moscow, 1955) [In Russian].

[13] J. J. Gilman, "Mechanism of ortho kink-band formation in compressed zinc monocrystals," J. Metals, Sec. 2, 6, 5, 621-629 (1954).

[14] J. Washburn and E. Parker," Kinking in zinc single crystal tension specimens," J. Metals 4, 10, 1076-1078 (1952).

Institute of Crystallography,
Academy of Science of the USSR

Received November 14, 1956

PROPAGATION OF ELASTIC SHEAR WAVES IN A CRYSTAL BENT AROUND A SPECIFIC DIRECTION

K. S. Aleksandrov

The case is considered of the propagation of elastic shear waves in an anisotropic medium subjected to torsional deformation around a direction along which purely shear waves could be propagated prior to deformation.

It is shown that the phenomenon of the rotation of the polarization plane of the elastic shear wave, previously found experimentally, is a special case of the phenomenon of the elliptical double refraction of elastic shear waves in a medium possessing linear and circular double refraction.

As stated in a previous communication [1], the oscillation plane of an elastic shear wave propagated in a sodium chloride crystal in the [110] direction, which is the axis of twist of the specimen, is rotated through an angle approximately equal to the angle of twist of the specimen, and in the direction in which the deformation has been effected. We called this phenomenon, in analogy to optics, the rotation of the plane of polarization of elastic shear waves. The same paper [1] emphasized the analogy between the discovered phenomenon and the phenomenon of the rotation of the plane of polarization in liquid nematic crystals.

The object of the present paper is to solve the equation for the propagation of elastic waves along a specific direction in an anisotropic medium, subjected to torsional deformation around the direction of propagation of the waves, and to establish a quantitative analogy of the rotation of the plane of polarization of the elastic shear waves with another optical phenomenon, i.e., the rotation of the plane of polarization of light in stressed specimens (this theory has recently been developed in papers on photoelasticity [4, 5]). It is assumed that, as a first approximation, in the plastic torsional deformation of a crystal, its cross sections merely rotate relatively to each other and do not undergo any other deformation.

The specific direction of propagation of elastic waves in a crystal is characterized by the fact that all three waves (compressional wave and the two shear waves) are pure waves. In other words, the directions of displacement of the particles in the shear waves under consideration are perpendicular to the direction of propagation. The directions of displacement of particles in shear waves, propagated along a specific direction, are defined crystallographically [2].

The equations of motion of the elastic medium in the one-dimensional case have the form

$$\frac{\partial t'_{ik}}{\partial x'_i} = \rho \frac{\partial^2 U'_k}{\partial t^2}, \quad i,k = 1,2,3 \qquad (1)$$

where t'_{ik}, x'_i, U'_k are, respectively, the stress, coordinate and displacement at the given point and ρ is the density of the medium.

We select a system of coordinates such that the X' axis coincides with a specific direction in the crystal, and the Y' and Z' axes coincide with the mutually perpendicular directions of displacement in shear waves propagated along X'. The origin of the coordinates is situated on the surface of the crystal. Assume the crystal to be twisted around the X' axis according to the law

$$\varphi = A \cdot x', \tag{2}$$

where A is a constant and φ is the angle through which a cross section situated at a distance x' from the origin is rotated with respect to the zero cross section.

A solution of an analogous problem was given in papers [4, 5]. As shown in [5], a monochromatic, linearly polarized light beam, passing through a medium possessing linear and circular double refraction, emerges from the specimen elliptically polarized. The character of the polarization of the transmitted light (ratio of the axes of the ellipse) depends upon the ratio of the intensities of the linear and circular double refraction. It will be shown below that in certain conditions elastic waves behave in a similar manner.

We select a moving system of coordinates (X, Y, Z) with the same origin, such that X ∥ X', and in each cross section the directions of the Y and Z axes coincide with the permitted directions of displacement in the shear waves, while for x = x' = 0, the Y axis is parallel to the Y' axis. Then, for any cross section of the crystal, the relationships

$$\begin{aligned} t_{xy} &= c^{*}_{66}\left(\frac{\partial U_y}{\partial x} - AU_z\right), \\ t_{xz} &= c^{*}_{55}\left(\frac{\partial U_z}{\partial x} + AU_y\right), \end{aligned} \tag{3}$$

are valid. In these expressions c^{*}_{66} and c^{*}_{55} are the effective elastic shear moduli for the given direction X, connected with the principal moduli c_{ik} by known relationships [3].

Equations (1) are written in a stationary coordinate system. In order to transfer them to the moving system, X, Y, Z, we use the transform equations

$$t'_{ik} = l_{pi}\, l_{qk}\, t_{pq}, \tag{4}$$

$$U'_i = l_{ik} U_k, \tag{5}$$

where l_{pi}, l_{qk} and l_{ik} are the cosines of the angles between the old and new axes. In the case under consideration, Equations (4, 5) are written in the form

$$\begin{aligned} t'_{xy} &= t_{xy}\cos\varphi(x) - t_{xz}\sin\varphi(x), \\ t'_{xz} &= t_{xy}\sin\varphi(x) + t_{xz}\cos\varphi(x), \end{aligned} \tag{4'}$$

$$\begin{aligned} U'_y &= U_y\cos\varphi(x) - U_z\sin\varphi(x), \\ U'_z &= U_y\sin\varphi(x) + U_z\cos\varphi(x). \end{aligned} \tag{5'}$$

We now substitute (3, 4', 5') in (1) and shall seek the solution in the form of the monochromatic wave

$$U_{y,z}(x,t) = U_{y,z}(x)\,e^{j\omega t}. \tag{6}$$

Then taking into account Condition (2), we get

$$\begin{aligned} B\Big(\frac{d^2U_y}{dx^2}\cos Ax - A\frac{dU_z}{dx}\cos Ax - A\frac{dU_y}{dx}\sin Ax + A^2U_z\sin Ax\Big) + \\ + U_y\cos Ax - C\Big(\frac{d^2U_z}{dx^2}\sin Ax + A\frac{dU_y}{dx}\sin Ax + \\ + A\frac{dU_z}{dx}\cos Ax - A^2U_z\cos Ax\Big) - U_z\sin Ax = 0, \end{aligned}$$

$$B\left(\frac{d^2U_y}{dx^2}\sin Ax - A\frac{dU_z}{dx}\sin Ax + A\frac{dU_y}{dx}\cos Ax - A^2U_z\cos Ax\right) +$$

$$+ U_y \sin Ax + C\left(\frac{d^2U_z}{dx^2}\cos Ax + A\frac{dU_y}{dx}\cos Ax -\right.$$

$$\left. - A\frac{dU_z}{dx}\sin Ax - A^2U_y\sin Ax\right) + U_z\cos Ax = 0,$$

where

$$B = \frac{\overset{\bullet}{c}_{66}}{\rho\omega^2}; \quad C = \frac{\overset{\bullet}{c}_{55}}{\rho\omega^2}.$$

It is thus necessary to solve a system of differential equations with variable coefficients, written in the moving system of coordinates X, Y, Z. To eliminate the variable coefficients, we multiply the first equations on system (7) by sin Ax and the second by cos Ax and subtract one equation from the other.

We get

$$(1 - A^2C)U_y + B\frac{d^2U_y}{dx^2} - (B + C)\frac{dU_z}{dx} = 0. \tag{8}$$

Similarly, we get a second equation

$$(1 - A^2B)U_z + C\frac{d^2U_z}{dx^2} + A(B + C)\frac{dU_y}{dx} = 0. \tag{8'}$$

We seek a solution of the system of Equations (8) and (8') in the form

$$U_{y,z}(x) = U_{y,z}e^{jkx}. \tag{9}$$

Then, after transformations, the Systems (8) and (8') assume the form

$$\begin{gathered}\left(k_y^2 - k^2 - A^2\frac{k_y^2}{k_z^2}\right)U_z - jkA\left(1 + \frac{k_y^2}{k_z^2}\right)U_z = 0,\\ jkA\left(1 + \frac{k_z^2}{k_y^2}\right)U_y + \left(k_z^2 - k^2 - A^2\frac{k_z^2}{k_y^2}\right)U_z = 0,\end{gathered} \tag{10}$$

where k_y and k_z are the wave numbers of the shear waves propagated in the undeformed crystal.

A condition for the existence of nonzero solutions of Equation (10) gives a biquadratic equation for the determination of k

$$k^4 - (k_y^2 + k_z^2 + 2A^2)k^2 + [k_y^2k_z^2 - A^2(k_y^2 + k_z^2) + A^4] = 0. \tag{11}$$

The solutions of Equation (11) may be written in the form

$$k_{1,2}^2 = \frac{1}{2}\{(k_y^2 + k_z^2 + 2A^2) \pm [(k_y^2 - k_z^2)^2 + 8A^2(k_y^2 + k_y^2)]^{1/2}\}. \tag{12}$$

The further solution of the problem and the assessment of the results obtained are carried out as in the case discussed in [5]. For given values of the double refraction of the crystal ($k_y^2 - k_z^2$) and specific rotation A, the value of k must be determined from (12) and then the ratio between the displacement components from (10).

As will be seen from (10), for any value of $\underline{k}$ different from k_y and k_z, the waves propagated in the crystal will be elliptically polarized. The ratio of the semi-axes of the ellipse in each wave is determined by the wavelength, the double refraction of the crystal and the specific rotation.

We shall estimate the quantities involved in Formulas (10) and (12) for the case of the propagation of shear waves of frequency 1.67 Mc/sec in the [110] direction of a sodium chloride crystal, twisted through 90° around [110], for a crystal length of 100 mm[1]. The velocity of the shear waves propagated along [110] is determined by the moduli

$$c^{*}_{55} = c_{44} \text{ and } c^{*}_{66} = (c^{*}_{11} - c_{12})/2.$$

In Equation (12), $(k_y^2 - k_z^2) >> 8A^2(k_y^2 + k_z^2)$, and its approximate solution has the form

$$\frac{k_1^2}{k_y^2} \simeq 1 - A^2 \frac{1 + 3\frac{k_z^2}{k_y^2}}{k_y^2 - k_z^2};$$

$$\frac{k_2^2}{k_z^2} \simeq 1 + A^2 \frac{1 + 3\frac{k_y^2}{k_z^2}}{k_y^2 - k_z^2}. \tag{13}$$

The second term in the right-hand part of each equation is equal to $\sim 10^{-4}$, and consequently the speeds of propagation of the elastic waves in the deformed crystal differ from the speeds in the undeformed crystal by an amount much less than the sensitivity of the speed determination. For $A = 0$, k_1 corresponds to a wave with a displacement along Y and k_2 to a wave with displacement along Z. Substituting k_1 and k_2 from (13) in (10), we get the ratio of the axes of the two elliptically polarized waves

for $\qquad k_1 \simeq k_y,\ U_y/U_z \simeq 30,$

for $\qquad k_2 \simeq k_z,\ U_z/U_y \simeq 80.$

Thus, for the propagation of elastic waves along specific directions possessing considerable double refraction in comparison with the specific rotation, there is practically complete entrainment of the polarization plane of the elastic wave in consequence of the rotation of the permitted directions of displacement, as has also been found experimentally [1]. From the variation in the ratio between the magnitude of the linear double refraction $k_y^2 - k_z^2$ and the magnitude of the circular double refraction (specific rotation of the axes), for example on varying the frequency of the elastic wave, it is possible to produce an elastic wave of any polarization: from practically linear polarization, as in the case considered, to circular polarization in the case of low frequencies.

We shall now consider those specific directions in which there is no double refraction, i.e., $k_y = k_z = k_0$.

From Equation (12) we get

$$k_{1,2}^2 = k_0^2 + A^2 \pm 2k_0 A. \tag{14}$$

In the absence of torsional deformation (for $A = 0$), Equations (10) identically become zero. For $A\lambda << 1$, Equations (10) give a solution in the form of two circularly polarized waves propagated at the same speed. Thus, for the propagation of an elastic wave along a specific direction without double refraction, there is no rotation of the polarization plane of the elastic wave. This conclusion is also in agreement with the experimental results [1].

The phenomenon of the elliptical double refraction of elastic waves, as this discussion shows, is produced in the propagation of elastic waves along specific directions in crystals. The case of the propagation of an elastic wave along an arbitrary direction in an anisotropic medium subjected to torsional deformation around that axis is mathematically more complex.

The authors express his thanks to V. L. Indenbom and V. Ia. Khaimov-Mal'kov for assistance and valuable advice.

LITERATURE CITED

[1] K. S. Aleksandrov and V. Ia. Khaimov-Mal'kov, "Rotation of the polarization plane of elastic shear waves," Kristallografiia 1, 3, 373-374 (1956).

[2] F. E. Borgnis, "Specific directions of longitudinal wave propagation in anisotropic media," Phys. Rev. 98, 4, 1000-1005 (1955).

[3] A. Liav, Mathematical Theory of Elasticity [In Russian] (1935).

[4] V. L. Ginzburg, "Stress analysis by the optical method," J. Tech. Phys. (USSR) 14, 3, 181-192 (1944).

[5] D. C. Drucker and R. D. Mindlin, "Stress analysis by three-dimensional photoelastic methods," J. Appl. Phys. 11, 11, 724-732 (1940).

Institute of Crystallography
Academy of Sciences, USSR

Received October 20, 1956

PHASE TRANSITIONS AND CRITICAL PHENOMENA IN ANISOTROPIC PHASES

V. K. Semenchenko

The possibility of application of the general principles of thermodynamic theory of critical and supracritical transitions to anisotropic media is discussed. The possibility of a new type of transitions with abrupt changes in thermodynamic coordinates (entropy, deformation, magnetic and electric induction) in only some of the components of a given tensor is considered. Experimental material shows that in anisotropic media (quartz) transitions of supracritical and even critical type are possible.

The possibility of critical transition from crystal or liquid to a saturated vapor has been discussed many times [1-5]. Most investigators considered these transitions impossible [2, 3], but a few inclined to the opposite point of view [4, 5]. The possibility of critical transition of a crystal from one crystal system to another, so far as we know, has never been discussed. This paper reviews the thermodynamic theory of polymorphic transitions, the possibility of critical and supracritical transitions of this type, and also the experimental data which confirm their existence. The existence of such transitions points also to the probability of critical transitions between anisotropic and fluid phases since, because of the increased amplitude of vibration of atoms in the lattices, the difference in their positions in two anisotropic phases which can continuously change one into the other is hardly greater than in an anisotropic and a fluid phase at sufficiently high temperatures and pressures.

1. On Regions of Existence and Coexistence of Phases.

Experimental and theoretical study of phase transitions near the critical point made it necessary to change somewhat the traditional concepts of phase transitions and of phases themselves [6, 7]. We believe that for every pair of conjugate phases there are two regions, one in which the phases can both exist and coexist and the other in which the phases can exist but not coexist. For some substances (for example, for most complex molecular compounds), only the second region exists; for some high pressure crystal modifications, the region of coexistence of the crystal-vapor phases is not realized. In the region of coexistence of two phases, the field of each phase is bounded on any of the $X_i - x_i$ diagrams by the curve of stability limit (spinodal). The spinodal is the geometric locus of the extremes of the generalized forces X_i, for instance pressure on the p-V diagram, and is defined by the equation

$$\left(\frac{\partial X_i}{\partial x_i}\right)_{x_j} = 0, \qquad (1)$$

where X_i may be temperature (T), pressure (p), chemical potential (μ), and intensity of electric (E) or magnetic (H) field, and x_i may be entropy (S), volume (V), number of molecules or moles (N), and electrostatic (D) or magnetic (B) induction.

Within the field bounded by the spinodal the phase is unstable and cannot exist. The presence of a region of instability is related to the form of the isotherms on the p-V diagram or analogous lines on other $X_i - x_i$

diagrams (for example, isobars on the T-S diagram) which, as was shown long ago by Thompson [8], must necessarily pass through a maximum and a minimum which coincide in the critical point. The presence of a region of instability causes every phase transition between two coexisting phases to be accompanied by finite changes in all thermodynamic coordinates x_i and requires the expenditure of work $X_i \Delta x_i$.

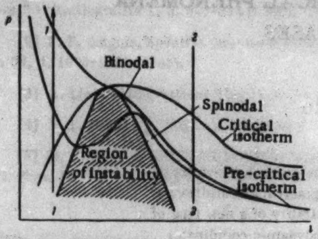

Fig. 1. p-V diagram.
1-1) Direction of isochore transformation in the region of existence of the low temperature phase.
2-2) Direction of isochore transformation in the region of the high temperature phase.

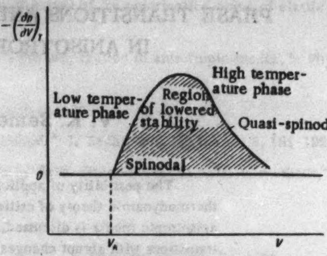
$-\left(\frac{\partial p}{\partial V}\right)_T$
High temperature phase
Low temperature phase
Region of lowered stability
Quasi-spinodal
Spinodal
0
V_k
V

Fig. 2. Diagram $\left(\frac{\partial p}{\partial V_k}\right)_T$ -V in the supracritical region.
V_k – critical volume.

However, it is easily seen that in isochore transformation on the p-V diagram (Fig. 1) from the region of stability of the liquid phase (or any other low temperature phase) into the region of high pressures and temperatures, the substance does not anywhere experience abrupt changes of properties, and therefore there is no reason to speak of its transition into another phase. The same can be said of the isochore transformation of the high temperature phase into the low temperature region. However, the transition in the supracritical region from a point corresponding to the low temperature phase on axis V to the point on the same axis corresponding to the high temperature phase will be accompanied by sharper changes in the properties of the substance and besides, as is shown by experiments, by the passage of all coefficients of stability $\left(\frac{\partial X_i}{\partial x_i}\right)_{X_j}$ through extreme values. This will be called the supracritical transition.

The supracritical region differs from the infracritical region in that in it the substance is stable, i.e., $\left(\frac{\partial p}{\partial V}\right)_T < 0$ everywhere. However, there is within it an area of lowered stability along whose boundaries the coefficients of stability $\left(\frac{\partial X_i}{\partial x_i}\right)_{X_j}$ pass through the extreme values just as in the infracritical region the generalized forces X_i pass through extreme values on the boundaries of the region of instability. The boundaries of this region of lowered stability are determined by a curve, which we shall call quasi-spinodal and which is defined by the equation

$$\left(\frac{\partial^2 X_i}{\partial x_i^2}\right)_{x_j} = 0 \text{ where } \left(\frac{\partial X_i}{\partial x_i}\right)_{x_j} \neq 0. \tag{2}$$

In the infracritical region the coexistence of the phases depends on the presence between them on the diagram of a region of complete instability separating the two phases. In the supracritical region the latter does not exist; there is only the area of lowered stability bounded by the quasi-spinodal (Fig. 2). In passing through it, stability decreases rapidly and then increases again. It does not follow from this, however, that within it the phases can exist in the state of the usual thermodynamic equilibrium. The properties of the phases are determined by the values of the thermodynamic coordinates x_i = S, V, N, and if these are equal the phases are macroscopically homogeneous and indistinguishable from each other.

Infracritical equilibrium is related to the existence of a surface of separation between the phases on which all thermodynamic coordinates x_i vary abruptly. This surface is of finite thickness and work must be expended for its formation which equals $\sigma\omega$ where ω is the area of the surface and σ is surface tension.

In the supracritical region all x_i vary continuously, and for this reason the transition from one phase to the other is continuous also and occurs within a finite range of temperature, pressure, and other generalized forces X_i. The surface of separation and surface tension depend on the presence of finite differences in the values of the generalized coordinates x_i, but since these change continuously they cannot come into existence.

Statistical mechanics makes it possible to understand the supracritical transitions and their characteristics. It can be shown that $\left(\frac{\partial X_i}{\partial x_i}\right)_{X_j}$, the coefficients of stability, are always inversely proportional to the fluctuations. For example, the coefficient of thermal stability $\left(\frac{\partial T}{\partial S}\right)_p$ is inversely proportional to the fluctuations of energy, and the coefficient of concentration stability $\left(\frac{\partial \mu_i}{\partial c_i}\right)_{T,p}$ is inversely proportional to the concentration fluctuations, i.e.,

$$\left(\frac{\partial T}{\partial S}\right)_p = \frac{kT^2}{\overline{E^2} - \overline{E}^2}; \quad \left(\frac{\partial \mu_i}{\partial c_i}\right)_{Tp} = \frac{kT}{\overline{c^2} - \overline{c}^2}. \tag{3}$$

On the binodal all coefficients of stability are finite and greater than zero, both phases are stable, the energy received by the system is expended in changing one phase into the other, and therefore during the process of transition all generalized forces X_i have constant values. As the critical point is approached the values of the coefficients of stability decrease, the width of the region of instability decreases and the fluctuations which are inversely proportional to the coefficients increase. The work of the phase transition $X_i \, \Delta x_i$ decreases with the decreasing width of the region of instability. Let us consider the heat of transition Q. Near the critical point it will decrease as the difference of entropies of the phases $S'' - S' = \Delta S$, while the energy of fluctuations, $\sqrt{\overline{\Delta\epsilon^2}} = \sqrt{kT^2 c_v}$ will increase. When the latter has the same sign as the heat of transition, nuclei of the other phase will come into existence and therefore the phase transition will occur partly at the expense of the energy of the system itself.

It is necessary to distinguish the fluctuational nuclei of the phase from the equilibrium nuclei. The difference between them becomes clear if the significance of the thickness of the surface layer δ of the nucleus is considered. There may exist within the nucleus a region possessing the properties of the macrophase only if its size exceeds 2δ (in the case of a drop). For a crystal nucleus the thickness of the surface layer is different for different faces and for this reason the dimensions of the critical nucleus will also differ in different directions. With approach to the critical point the thickness of the surface layer grows, approaching infinity at the critical point, and formation of equilibrium nuclei becomes impossible. However, the nonequilibrium nuclei appear continuously and are destroyed, and because of their considerable size, which is due to the great thickness of the surface layer, the duration of their existence also increases. This formation of nonequilibrium (macroscopically) nuclei continues beyond the critical point. There exists here, the external forces X_i being constant, an equilibrium between the nuclei formed and those destroyed. Since these nuclei are not phases (in the usual sense of the word), we shall call such systems microheterogeneous. The development of microheterogeneity is one of the most characteristic features of the critical and near-critical states; outwardly it is manifested first of all in critical opalescence.

In the supracritical region the system is in a microheterogeneous state, but to the left of the quasi-spinodal, nuclei of the low temperature phase prevail. Here a more intensive development of fluctuations occurs, microheterogeneity increases, and the values proportional to the fluctuations $\frac{C_p}{T}$, $\left(\frac{\partial V}{\partial p}\right)_T$, ϵ, etc., reach their maximum values. Then the fluctuations and microheterogeneity decrease and the system reaches maximum stability and the purest (so far as the presence of nuclei of the other phase is concerned) composition. Therefore, supracritical transitions occur in a certain range of the generalized forces (temperature, pressure, etc.) and consist in a continuous change in the number of nuclei of both phases. When quasi-phases differ in certain properties (for example, have different refractive indices) the presence of microheterogeneity can be easily discovered experimentally (see below, Fig. 3).

From the thermodynamic point of view supracritical transitions will be manifested by the passage of all derivatives of the generalized forces through the extremes along the corresponding coordinates. Let us enumerate the most important of these:

$$\left(\frac{\partial T}{\partial S}\right)_p = \frac{T}{C_p}, \quad \left(\frac{\partial p}{\partial V}\right)_{T}, \quad \left(\frac{\partial \rho}{\partial p}\right)_T, \tag{4}$$

the derivatives of deformational stresses $\left(\frac{\partial \sigma_{ik}}{\partial r_{ik}}\right)_T$ (or their reciprocals)

$$\left(\frac{\partial \bar{E}}{\partial D}\right)_{Tp} = \frac{1}{\varepsilon_i}, \quad \left(\frac{\partial \vec{H}}{\partial B}\right)_{Tp} = \frac{1}{\mu_i} \tag{5}$$

(ϵ_{ik} dielectric and μ_{ik} magnetic permeability). Besides this in transition from the region of decreased stability the crystalline structure must change continuously.

2. Tensorial Phase Transition*

Classical thermodynamics developed largely from investigations of fluid phases and therefore the possibility of vectorial phase transitions is completely foreign to it. Investigation of phase transitions between two crystalline phases indicates the possibility of other types. Let us consider two monocrystals of different crystal systems existing at different temperatures and stresses. Let us assume further that T and σ_{ik} change in such a way that for certain values of these variables not all r_{ik} in each crystal become equal. Since T and σ_{ik} are equal, the crystals are in thermodynamic equilibrium. All of their thermodynamic coordinates are also equal with the exception of S and some r_{ik}. The spinodals therefore exist only on the T-S diagrams and on some σ_{ik}-r_{ik} diagrams, and also, of course, on the $E_i - D_i$ diagrams if the substance is a dielectric and on $H_i - B_i$ diagram if it is magnetic. During phase transition the properties of the crystal will change only for some components of deformation, and dielectric and magnetic permeability; for this reason this type of transition may be called tensorial. If by an appropriate change of external forces it is possible to effect a continuous transition of two such phases, we shall have a critical tensorial transition if it occurs at fixed values of the generalized forces, or supracritical if it occurs in a certain range of the generalized forces.

3. A Review of Experimental Material

The above discussion shows the possibility of phase transitions of a new type. Experimental data pertaining to the α-β transition in quartz and the transition from the tetragonal to the cubic modification of $BaTiO_3$ confirm the possibility of tensorial phase transitions and at the same time of tensorial transitions of the critical type. Let us consider the α-β transition in quartz, which has been studied in detail by the Soviet investigators. As far back as 1933, Jay [9] studied thermal expansion of quartz by means of x-rays and came to the conclusion that the α-β transition occurs without volume change but that the direction of the curve V−T at the inversion point changes abruptly, i.e., the transition is accompanied by a finite change in the derivative $\left(\frac{\partial V}{\partial T}\right)_p$. Jay's results are given in Fig. 3, which shows that his measurements were made at such large temperature intervals that no definite conclusions can be made concerning the character of change of $\left(\frac{\partial l}{\partial T}\right)_p$ near transition point. In our opinion this change may be either a jump or a very sharp maximum. Strelkov, Kosourov and Samoilov [10] measured thermal expansion of quartz in the interval between 20 and 925° by means of a very sensitive quartz dilatometer constructed by P. G. Strelkov. The results of this work [10] are shown in Figs. 4 and 5. The curves of relative elongation parallel and normal to the axis (Fig. 4) show breaks at the point of transition

---

* This term was suggested by V. A. Koptsik.

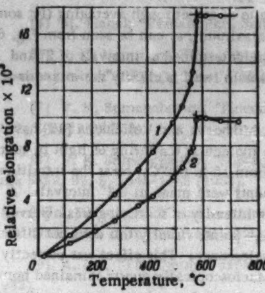

Fig. 3. Relative elongation of quartz $\Delta l/l$ with temperature referred to its dimensions at 18°C [9].
Curve 1) Along optic axis, 2) normal to optic axis.

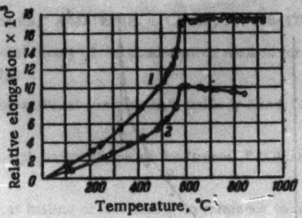

Fig. 4. Relative elongation of quartz $\Delta l/l$ with rise in temperature [10].
Curve 1) Along optic axis, 2) normal to it.

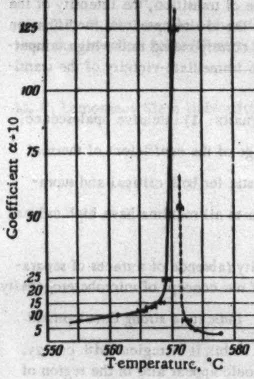

Fig. 5. Change of coefficient of expansion of α-quartz in the region of α-β transition [10].
Horizontal bars give temperature intervals in which measurements were made.

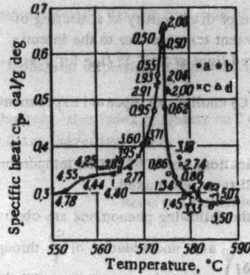

Fig. 6. Change in specific heat near α-β transition [11].
Figures are values of temperature intervals in which specific heat was determined,
a) first, b) second, c) third determinations,
d) values calculated from two preceding and two following experimentally determined points.

analogous to that noted by Jay, whose data [9] agree with those of the Soviet authors [10]. The variation of the coefficient of expansion with temperature (Fig. 5) shows what the authors call a break but what may equally well be regarded as a sharp maximum. The agreement of the results of [9] and [10] obtained by entirely different methods indicates their correctness.

Specific heat of quartz was determined by Sinel'nikov [11] in a vacuum calorimeter in the interval from 30 to 700°C. The results of this work near the transition point are shown in Fig. 6. Unfortunately no tabulations of values of c_p were given in [10] and [11] and it was impossible to calculate the entropy change c_p/T, which has maxima in the critical and the pseudocritical points. For quartz, since its temperature of transition is high, the difference between curves for specific heat and entropy change should be small, although the actual value

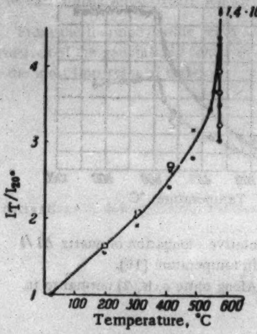

Fig. 7. Ratio of the intensity of scattering of light at different temperatures to the intensity of scattered light at 20°C $I_T/I_{20°}$ for quartz [12].
●) heating, O) cooling, ×) repeated experiment.

of the former is approximately 1000 times the value of the latter. In spite of rather rough averaging (for some points near the maximum, as can be seen from Fig. 6, values of c_p were determined at intervals of 2° and more), the maximum itself is clearly shown and is very sharp.

Iakovlev, Mikheeva and Velichkina [12] have investigated the molecular scattering of light in quartz in the interval from 15 to 600°C. Near the transition point measurements were made at 0.1° intervals. A sharp increase in intensity of scattering was observed near the transition point; visually this does not differ from critical opalescence. This effect was perfectly reproducible. Macroscopically quartz remained homogeneous. The results of these observations are given in Fig. 7.

Very interesting results were obtained by Baranskii [13], who studied the variation of the refractive index of quartz near the transition point (both modifications of quartz are doubly refracting). Here Baranskii observed four rays corresponding to four refractive indices. Up to the temperature of transition, the intensity of the rays corresponding to the low temperature modification was greater than that corresponding to the high temperature modification; above transition temperature the reverse was true. In the immediate vicinity of the transition point all rays were mixed.

Thus the following phenomena are observed at the transition point of quartz: 1) intensive opalescence; 2) passage of c_p and, undoubtedly, of $\frac{c_p}{T}$ through a sharp maximum; 3) passage of the coefficient of thermal expansion $\left(\frac{\partial l}{\partial T}\right)_p$ through a maximum. All these phenomena are characteristic for both critical and supracritical transitions (in this case occurring near the critical point since for quartz all maxima have high values and sharpness).

The evidence of existence of both phases with macroscopic homogeneity (absence of surfaces of separation), discovered by K. N. Baranskii is the first experimental confirmation of our concept of microheterogeneity. We based this concept on the fact that the maxima of $\frac{c_p}{T}$, $\left(\frac{\partial V}{\partial p}\right)_T$ or $\left(\frac{\partial l}{\partial T}\right)_p$ indicate a strong development of fluctuations in the given system and therefore the possibility of formation within it of regions with energy, density and other properties of the intermediate phase. These phenomena should appear also in the region of decreased stability bounded by quasi-spinodal where there exists a micro-equilibrium among the fluctuational nuclei of both phases which cannot, however, grow to the size of critical nuclei with clearly defined separation boundaries. Therefore, although the phase is macroscopically homogeneous, it is heterogeneous microscopically. In the crystal nuclei of both phases there exist different degrees of anisotropy and their presence can be detected as was done by K. N. Baranskii.

We believe that the experimental evidence cited in this paper makes it possible to affirm that the α-β-transition in quartz is a critical or supracritical transition and that, therefore, continuous transitions are possible between two anisotropic phases which may be called critical or supracritical.

LITERATURE CITED

[1] A. V. Rakovskii, "Theoretical investigations of reversible phase transitions," Vestnik Lomonosovskogo fiz.-khim. ob-va., 2, 2 (1921).

[2] P. W. Bridgman, The Physics of High Pressure [Russian translation] (1952).

[3] L. D. Landau and E. M. Livshits, Statistical Physics [In Russian] (1952).

[4] M. Planck "Verdampfen, Schmelzen und Sublimieren," Ann. Physik. u. Chem., 15, 446-475 (1882).

[5] P. V. Veinmarn, "The main principle of the general theory of the condensation method for obtaining disperse systems," RFKhO, Chast' Khim. 42, 214-226 (1910).

[6] V. K. Semenchenko, "Pseudocritical points and supracritical transitions," Doklady Akad, Nauk SSSR 92, 3, 625-627 (1953).

[7] V. K. Semenchenko, "Supracritical transitions and phase transitions of the II order," Doklady Akad. Nauk SSSR 99, 6, 1045-1048 (1954).

[8] J. Thompson, "Considerations on the abrupt change at boiling or condensing on reference to the continuity of the fluid state of matter," Phil. Mag. 43, 227-234 (1872).

[9] A. Jay, "The thermal expansion of quartz by x-ray measurements," Proc. Roy. Soc. A 142, 237-247 (1933).

[10] P. G. Strelkov, G. I. Kosourov and B. N. Samoilov, "Dilatometer for small samples," Izvest. Akad. Nauk SSSR, Ser. Fiz., 17, 3, 383-388 (1953).

[11] N. N. Sinel'nikov, "Vacuum adiabatic calorimeter and certain new data on inversion of quartz," Doklady Akad. Nauk SSSR, 92, 2, 369-372 (1953).

[12] I. A. Iakovlev, L. F. Mikheeva and T. S. Velichkina, "Molecular dispersion of light and inversion of quartz," Kristallografiia, 1, 1, 123-131 (1956).

[13] K. N. Baranskii, Investigation of the Dependence of the Refractive Index of Quartz on Temperature Near the Inversion Point (Dissertation, Physics Faculty, Moscow State University, 1953).

M. V. Lomonosov State University of Moscow

Received November 27, 1956

OBSERVATIONS ON LAYERED-SPIRAL GROWTH OF CRYSTALS FROM SOLUTIONS

M. I. Kozlovskii

Results of observations on layered-spiral naphthalene crystal growth in a kerosene solution are given in this paper.

The problem of spiral growth was first presented in 1945 by G. G. Lemmlein in his report "Fine contour structure of a crystalline face" given at a meeting of the Mathematical-Physical Dept. of the Academy of Sciences USSR [1]. During the past decade many theoretical and experimental papers have been devoted to the subject, most of them dealing with the spiral growth from a gaseous phase.

The experimental studies of G. G. Lemmlein and E. D. Dukova are of particular interest. By means of cinemicrophotography they were able to study the kinetics of spiral growth of crystals from a gaseous phase and give a correct explanation for the formation of screw dislocations which are the centers of the spirals [2, 3]. The theoretical studies of Frank [4], Burton and Cabrera [5] are also basically related to the growth of crystals in vapors.

Marcelin was the first to note layered growth in 1914 when studying paratoluidine crystal growth in an alcohol solution [6]. Bann and Emmet [7] observed the 1600-4000 A thick layers during crystal growth from solution. However, they did not observe spiral growth. Forty [8] in a survey paper on dislocation in crystals mentions spiral protuberances of the growth when CdI_2 crystals are grown in a solution. Spiral formations were observed by Shubnikov [9] in a study of the nature of diphenylamine crystallization; however, according to him they are associated not with dislocations but with cleavages in the crystal. Spiral crystal growth in solutions was likewise observed in crystals of paraffin, behenic acid, palmitic acid, alcohols and other long chain compounds.

This paper gives the results of our observations, by means of cinemicrophotography, on the spiral growth of crystals in solutions.

We used naphthalene crystals in a kerosene solution.

The apparatus we used was extremely simple (Fig. 1). It consisted of a small cylindrical chamber with a double hermetically sealed glass cover. The bottom of the chamber was also glass. The chamber had an elbow outlet in the shape of a flat tube. Through this tube the chamber was filled with solution. Also a thermocouple and a stirrer were introduced through this tube. The tube was closed with a cotton stopper. The chamber was placed on the heating table of the microscope. A thermostatic liquid, brought in from an ultrathermostat was circulating between the glass panes of the chamber lid. This made possible the regulation at will of the temperature of the upper glass in the chamber. The temperature of the microscope table was set at 3-4°C above the temperature of solution saturation. (In our experiments the solution saturation point was at 32.5°C.)

The temperature of the upper glass of the camera was gradually lowered to 29-28°C. A vigorous growth of laminar naphthalene crystals then took place on the glass. As soon as the crystals began to grow, we increased the temperature of the glass until the growth ceased completely. After that, slightly increasing the temperature, we dissolved the basic portion of deposited crystals keeping only a few crystals for observation. When only 5-6 crystals remained on the glass the dissolving was slowed down, and growth conditions resumed.

We observed the growing crystals under polarized light with a phase contrast condensor. This made it possible to see the layers more distinctly and to determine their thickness qualitatively by the interference color. Observations were carried out on the (001) face of the crystal.

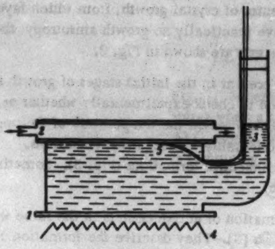

Fig. 1. Chamber diagram:
1) Glass bottom, 2) double glass-lid,
3) elbow tube, 4) heating table,
5) thermocouple.

Changing growth conditions, we were able to observe layers of different thickness starting with layers of several elementary lattice units (the naphthalene unit parameter along the c̲ axis is equal to 8.658 A) giving off first order interference color from light grey up to and ending with layers giving off no color, i.e., thicker than 125 elementary units (h > 1000 A). We also observed the spiral growth of naphthalene crystals in solution. The formation and development of spirals on the (001) face are shown on a movie film (magnified 50 times).

The experiments that we carried out confirmed once again the well known case that thin layers grow faster than thick layers under the very same conditions. This shows that in connection with crystal growth in solution one may speak of the existence of an adsorption layer and of surface diffusion. It has also been proved that with different degrees of supersaturation, layers of equal thickness move with a speed proportional to the supersaturation. Thus with high supersaturation, i.e., with large ΔT in the 3-4° range, growth of thin layers, with speed ranging from 50 to 10-15 microns/sec are prevalent. These layers expand along a straight line front and show the property of anisotropic growth, i.e., the speed of their displacement depends on the direction.

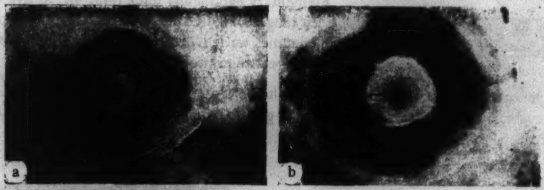

Fig. 2. Concentric layers spreading from one center on the surface of a naphthalene crystal grown in a kerosene solution. 30 ×. (20 seconds elapsed between the photographs a̲ and b̲).

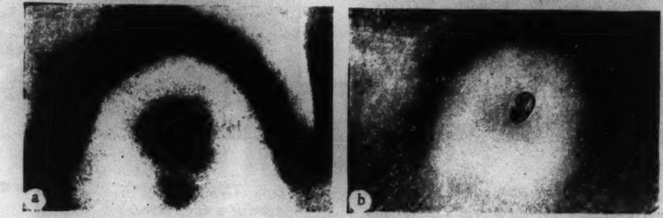

Fig. 3. Growth spirals observed in the centers of concentric layers when supersaturation was decreased during the growth of naphthalene crystals in kerosene solution. 40 ×.

However, if an obstacle in the shape of a step (screw dislocation) or some impurity* is encountered in the path of the rapidly spreading layer, then this obstacle forms a pseudocenter of crystal growth, from which layers begin to spread out in concentric rounded formations. These layers have practically no growth anisotropy; their form approaches a circle. Such layers, showing an obstacle in their centers, are shown in Fig. 2.

G. G. Lammlein showed as far back as 1945 that a spiral must be present in the initial stages of growth in such concentric periodic layers [1]. Using this fact as a basis we decided to check experimentally whether or not a spiral was formed in such a pseudocenter. With this in view we rapidly increased the temperature of the upper glass in the chamber to 32°C, i.e., we decreased the supersaturation considerably. Under these conditions, almost without exception, a spiral was observed in the centers of such concentric formations (Fig. 3). Sometimes instead of one spiral two spirals of opposite sign were observed (Fig. 3,b).

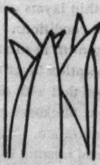

Fig. 4. Schematic drawing of rapidly growing layers whose thickness is that of several elementary lattice units.

We interpret the formation of active centers in the same way as did Lemmlein and Dukova [3]. They describe the formation of a screw dislocation as a result of the closing of the crack (external angle) between two branches of dendritic crystals, placed on different levels one from the other. The height of the step thus formed must be a multiple of the elementary parameter of the cell. Simultaneously they assumed that any crystal, growing under conditions of high supersaturation, grows first in the shape of a skeletal or dendritic crystal. Therefore at the very start of the growth all of the prerequisites for the formation of steps are present. We observed in our experiments that with a rapid crystal growth, the layers grow in the shape of separate tongues when they are several elementary parameters thick (Fig. 4). Active centers are most often formed at the point of junction of two such tongues. Moreover, when the growth is rapid, the thin layers capture the smallest impurity particles, which become, we feel, possible active centers, i.e., obstacles around which spirals may grow, changing with greater superconcentrations into concentric periodic layers.

When supersaturation was decreased we began to notice the formation of clearly defined spiral formations. With very low supersaturations ($\Delta T = 0.5-0.2°C$) the growth of thick layers is generally predominant; their tangential speed depends mostly on supersaturation.

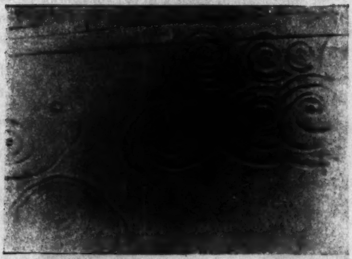

Fig. 5. Spirals on the surface of naphthalene crystals during growth in a weak supersaturated kerosene solution. 30 ×.

Fig. 6. Thin spiral layers, expanding on the surface of a thick layer.

Figure 5 shows the clearly seen spirals whose layer is h > 1000 A thick. These spirals were obtained on active centers when supersaturation was decreased. When we measured their tangential growth speeds we noted

---

* Some foreign particle trapped during the growth of the crystal and which brought about a disruption of the lattice.

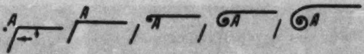

Fig. 7. Scheme of successive stages in the formation of a spiral when a straightline layer goes around an obstacle. A) Obstacle. Arrow indicates direction in which the layer is expanding.

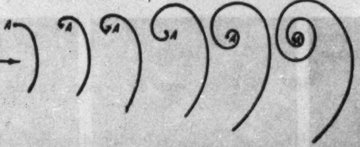

Fig. 8. Scheme of successive stages in the formation of a spiral when a curvilinear layer encounters an obstacle. A) Obstacle. The arrow indicates the direction in which the layer is expanding.

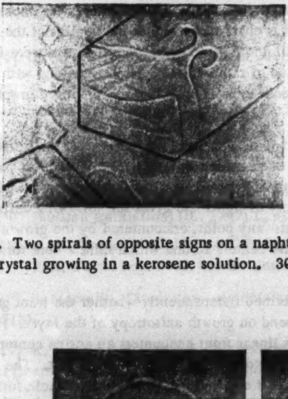

Fig. 9. Two spirals of opposite signs on a naphthalene crystal growing in a kerosene solution. 30 ×.

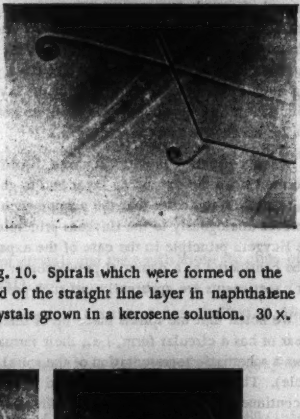

Fig. 10. Spirals which were formed on the end of the straight line layer in naphthalene crystals grown in a kerosene solution. 30 ×.

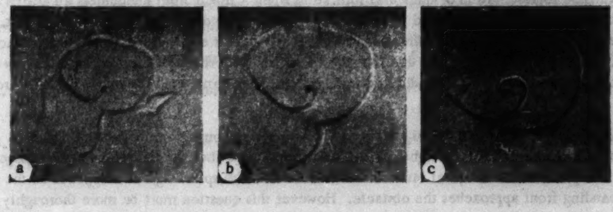

Fig. 11. Formation of a spiral when a circular layer was broken on encounter with an obstacle. 45 ×.
a–c) Film frames.

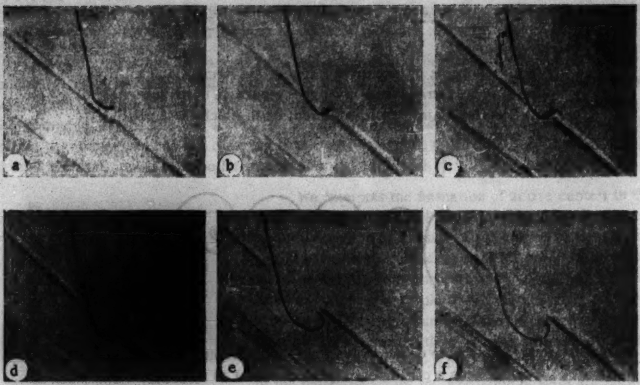

Fig. 12. Formation of a spiral from two straight line layers. 45 ×. a-f) Film frames.

that speed of growth decreases almost to a complete cessation of the layer expansion when supersaturation is decreased. Thus with the same temperature and a gradual decrease of saturation the speed of layer expansion fell from 0.15 microns/sec to 0.08 microns/sec in 10 minutes. It is characteristic that the centers of the spirals in Fig. 5 are located on separate straight lines. This serves as still another proof that these centers were formed during a rapid straight line expansion of the layer during the period of rapid growth. However, along with a predominant growth of thick layers we often observed a simultaneous expansion of rapidly running thin spirals on the surface of the thick layer (Fig. 6).

When we studied in detail separate film frames, we noticed that, as a rule, the spiral with the thick layer was formed when the expanding layer had to go around obstacles encountered in its path. In one of his papers G. G. Lammlein indicates that the phenomenon of going around an obstacle by the expanding layer may be interpreted analogously to the Huygens principle in the wave theory of light. He gives the following definition of the Huygens principle in the case of the expanding growth front: any point, encountered by the growth front may be considered as a potential pseudocenter of growth [10]. The centers around which spirals were formed in our experiments are apparently just such pseudocenters.

We noted that the spirals made up of thick layers may be formed independently whether the front growth is linear or has a circular form, i.e., their formation does not depend on growth anisotropy of the layer. Figure 7 shows a schematic representation of the spiral formation when a linear front encounters an active center (an obstacle). The growing front goes around the obstacle encountered and a spiral is formed around it. The linear front continues to advance in the same direction (up, in Fig. 7) and its edge, going around the obstacle, forms a protuberance. The impression is formed that the spiral is coiled as a result of the formation of new loops and their simultaneous expansion in a radial direction. The spiral thus formed is very much like the Archimedes spiral.

Figure 8 shows the individual stages in the growth of a spiral from a circular expanding layer. The spirals formed may have two signs – left and right. It is usually considered that the sign of a spiral is associated with the sign of the defect present in the crystal lattice. We believe that the spiral sign also depends on the side from which the expanding front approaches the obstacle. However, this question must be more thoroughly studied. Figure 9 shows two spirals (left and right) on the same crystal. In Fig. 10 a spiral formed on the edge of a straight line front is clearly shown. The formation of the spiral of a circular front is also clearly shown in Figs. 6 and 11. Figure 11 shows the different stages of spiral development from a circular layer. Figure 12 shows a series of photographs showing the beginning of spiral formation from two straight line layers, expanding at an angle to each other.

In order to observe the formation of spirals from circular layers we carried out the following experiments. The crystal was dissolved in a low undersaturated solution; during dissolving we observed a motion of the layers, and the direction of the layer motion when being dissolved was opposite to the direction of the motion of the same layer during crystal growth. After the crystal had been considerably dissolved and open holes appeared on its surface, the dissolving was stopped and the slow growth of the crystal was assured. Now we observed the formation of circular, radially expanding layers. When an active center was encountered the circular layers broke and coiled into a spiral. Sometimes a spiral was formed when two layers,on different levels, met. The difference in levels of such layers must be smaller than their thickness otherwise they expand one above the other with no obstruction.

SUMMARY

1. Conditions have been found under which spiral growth of naphthalene crystals in a kerosene solution may be observed.

2. It has been shown that the mechanism of spiral growth in a solution does not differ practically from the mechanism of spiral growth in a gaseous phase.

3. It has been observed that a spiral may be formed from thick layers when the expanding front has to go around obstacles encountered in its path.

4. Qualitative data are given on the speeds of tangential growth of layers depending on the thickness of the layer and on the supersaturation.

LITERATURE CITED

[1] G. G. Lemmlein, "Fine contour structure of a crystalline face," Vestnik AN SSSR 4, 119 (1945).

[2] G. G. Lemmlein and E. D. Dukova, "Study of tangential growth speed of elementary layers in paratoluidine crystals," Kristallografiia 1, 1, 113-118 (1956).

[3] G. G. Lemmlein and E. D. Dukova, "Formation of screw dislocations during the process of crystal growth," Kristallografiia 1, 3, 351-355 (1956).

[4] F. Frank, "Effect of displacement on crystal growth," New Studies in Crystallography and Crystal Chemistry [Russian translation] (IL, 1949) 1, 41-46.

[5] W. K. Burton, N. Cabrera and F. Frank, "The growth of crystals and the equilibrium structure of their surfaces," Phil. Trans. Roy. Soc., London Ser. 243, 299-358, (1951).

[6] R. Marcelin, "Études experimentales sur le développement de cristaux," Ann. de Phys. 9, 10, 189-191 (1918).

[7] K. Bann and G. Emmet, "Formation of layers on crystal faces," New Studies in Crystallography and Crystal Chemistry [Russian translation] (IL, 1949) 1, 89-98.

[8] A. J. Forty, "Direct observations of dislocations in crystals," Advances in Physics 31, 1-60 (1954).

[9] A. V. Shubnikov, "On the nature of diphenylamine crystallization," Kristallografiia 1, 3, 374-375 (1956).

[10] G. G. Lemmlein, "Rounding an obstacle by a growing layer front of a crystal face," Doklady Akad. Nauk SSSR 84, 1166-1169 (1952).

M. V. Lomonosov Moscow State University

Received November 27, 1956

CRYSTALLOGRAPHIC CRITERIA IN SELECTING FLUORSPAR FOR GROWING ARTIFICIAL CRYSTALS OF OPTICAL FLUORITE

G. B. Bokii and O. G. Kozlova

A study of impurities and inclusions in natural fluorspar proves the possibility of obtaining artificial optical fluorite from certain varieties of fluorspar. Morphological criteria for selection have been found. A number of fluorspar deposits are recommended as sources of raw material for artificial growing of optical fluorite crystals.

Optical fluorite crystals possess a number of special optical physico-chemical, mechanical, and other properties which place them among the most valuable optical materials. Fluorite is used in optical instruments for work both in the visible and the invisible regions of the spectrum, in the construction of achromatic systems, in making prisms for spectroscopic equipment, and for other purposes.

In 1953 the problem of growing optical fluorite crystals was solved by the workers of the State Optical Institute, headed by Stepanov and Feofilov [1-2], and following this a search for suitable raw material became necessary. Utilization of shop waste of natural optical fluorite for this purpose is limited. It cannot satisfy the ever-growing demands of the optical industry, especially as production of optical fluorite is very small.

The present work consisted in a study of impurities and inclusions in fluorspar which determine its different technical (not optical) properties and also in finding means of removing these impurities. For this purpose it was necessary to select those deposits in the USSR in which the fluorspar is typical, has all of the various defects, and occurs in a sufficiently large quantity.

Fluorite is a polygenetic mineral [3-4]. Large deposite are hydrothermal. Fluorspar deposits are found in different sedimentary and ingneous rocks. They are not restricted to rocks of a certain type or age. However, the character of the country rock has an effect on the process of ore deposition which in its turn influences the morphology of the ore body, its mineralogical composition and thus the technical properties of fluorspar. Silicate rocks have an entirely different effect from carbonate rocks. Genetically, fluorspar deposits are usually associated with granites. Morphologically, they may be classified as vein, bedded, or irregular deposits. Fluorspar is found associated with quartz, feldspar, barite, sulfides, carbonates, and less frequently with beryl, tourmaline, topaz, micas, cassiterite, etc.

A characteristic feature is observed in the fluorspar deposite of the USSR. The deposits of Central Asia, Kazakhstan, Western Siberia, Eastern Transbaikalia and the region from the Amur River to Cape Chukotsk decrease in age from southwest to northeast (from the Variscan epoch to the Cretaceous).

Characteristics of mineralogy and paragenesis also change. The western fluorspar deposits are polymineralic and are associated with sulfur-bearing minerals. The deposits of Eastern Transbaikalia, on the other hand, are usually associated with different kinds of silica.

The subjects of our investigations were the regions rich in fluorspar in Eastern Transbaikalia and Central Asia (together with Southern Kazakhstan). They differ in the character of deposits.

Fluorspar from a number of deposits was examined in the field, studied in thin sections, and analyzed for rare earths by spectrographic and luminescence methods. After preliminary study part of the material was tested for its suitability as raw material for growing of artificial fluorite crystals.

The impurities in fluorspar are varied and have different effects on the optical properties of the crystals. Such elements as Si, Al, Fe are often called subordinate in the compound CaF_2. They are present in thousandths, sometimes in hundredths, of one percent in high quality natural optical fluorites. The presence of Si and Al in fluorite is due to their close relationship with fluorine. The presence of Na, Cu, Sr, La, Y, and the rare earths is explained by their substitution for Ca ions in the structure of CaF_2. Such impurities, with the exception of some rare earths, do not affect the transparency of fluorite. The presence of heavy metals in fluorspar in almost all deposits is explained by its genesis. These impurities, if they cannot be extracted, often decrease the transparency of fluorite. As for other elements, they usually occur in a dispersed state.

Comparison of spectrographic analyses of 67 samples of fluorspar from Transbaikalia and 56 samples from Central Asia shows a considerable difference in the content of Sr, Be, La, Cu, Pb, and Ba (Table 1).

TABLE 1

Element and its content in fluorspar, %	Number of samples from Transbaikalia containing a given element	Number of samples from Central Asia containing a given element
Sr −0.1	37	None
Be −0.01−0.001	45	9
La −0.01	12	3
Cu −0.001	15	24
Pb −0.01, rarely −0.1	3	11
Ba −0.1	None	5

This difference in the distribution of elements in fluorspar is explained by the difference in the origin of the fluorspars from Transbaikalia, and Central Asia and Kazakhstan. The presence of beryllium (about .001%) in fluorspar from most of the deposits and association with silica indicates possible replacement of silicon by beryllium ions.

A special role in fluorspar as the raw material for growing artificial fluorite crystals is played by the rare earths. It was pointed out by Feofilov [1, 2] that in order to grow colorless and photochemically inert fluorite crystals an addition of rare earths to the raw material is necessary to the amount of .01% of the weight of the crystal. The trivalent ions of the rare earths, having strong electron affinity, decrease formation of color centers. P. P. Feofilov proved the F_2-centered nature of the visible coloration of artificial fluorites.

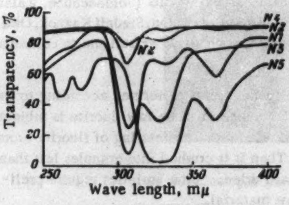

Fig. 1. Transparency of artificial fluorites grown from the fluorspar of the Solonechnoe deposit.
Thickness of plate $d_{No.\ 1} = 39.5$ mm, $d_{No.\ 2} = 4.0$ mm, $d_{No.\ 3} = 34.5$ mm, $d_{No.\ 4} = 4.0$ mm, $d_{No.\ 5} = 39.0$ mm.

Tests show that some fluorspars are rich in the rare earths (Solonechnoe deposit and some others). The presence of absorption bands in the region 307 mμ, 326 mμ and 365 mμ in the ionic spectra of some of the rare earths (Ce^{3+}, Yb^{2+}) makes crystals grown from material containing these elements opaque in the ultra-violet region (Fig. 1). In view of the effect of the rare earths on the optical properties of artificial fluorite a semi-quantitative analysis of fluorspar from 44 localities was made by the luminescence method. The trivalent ions of the rare earths present in the fluorspar as isomorphous admixtures have well defined line spectra which are readily identified. Identification and semi-quantitative analysis of the rare earths in fluorspar were done visually by comparison with standard spectrograms. The standards were obtained from artificial fluorite activated by a single rare earth element of a definite concentration ($\sim 2 \cdot 10^{-3}$%). The results of analyses showed that the variation in concentration of the rare earths is considerable − from zero to $5 \cdot 10^{-3}$% (within the limits of sensitivity of the method, which amounts to $1 \cdot 10^{-5}$%) [5].

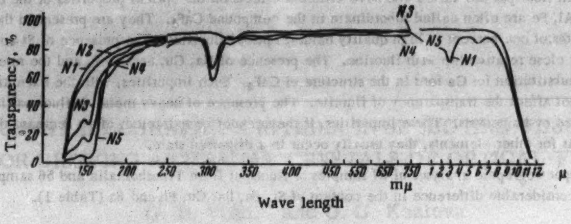

Fig. 2. Transparency of natural and artificial fluorites.
No. 1 natural, d = 1 mm;
No. 2 artificial (from fragments of optical fluorite), d = 1 mm;
No. 3 artificial (from fluorspar of the Solonechnoe deposit), d = 4 mm;
No. 4 artificial (from fluorspar of the Oktiabr'skaia Zhila deposit), d = 4 mm;
No. 5 artificial (from fluorspar of the Taskainar II deposit), d = 4 mm.

The highest concentration of rare earths is found in hydrothermal fluorspar deposited near the source of hydrothermal solutions. In Transbaikalia the decrease in the rare earths content of fluorspar is noticeable with increasing distance from granite, the source of hot solutions. Fluorspar deposits in sedimentary rocks, carbonate rocks excepted, are poor in rare earths. Zonally colored fluorspars are often characterized by different concentrations of the rare earths: green fluorite has the highest concentration; violet, the lowest. The optimum concentration of the rare earths in fluorspar for growing of optical crystals of fluorite occurs in Kul'-i-Kolon, Taskainar and some other deposits.

The impurities in fluorspar from the point of view of the necessity and possibility of their removal can be classed as:1. isomorphous substitutes for the calcium ion (these cannot and sometimes need not be removed); 2. impurities present in the fluorspar in dispersed state, silicates, sulfides and others (these cannot be removed); 3. admixtures of the eutectic type which crystallized simultaneously with fluorite – SiO_2, $BaSO_4$, etc. (impossible to remove) which are admissible in small concentrations; 4. mechanical inclusions of paragenetic minerals which are easily removed if they can be discovered, an exception being barite which is insoluble in acids.

Tests were made on certain varieties of fluorspar from the Transbaikalian deposits (Solonechnoe, Kalangui, Abagaitui) and from four deposits in Central Asia and South Kazakhstan (Kul'-i-Kolon, Srednii Kaznok, Oktiabr'skaia Zhila, Chashly, Taskainar II). This fluorspar, often colored and varying from massive crystalline to columnar, contains admixtures varying in composition and mode of occurrence.

The preparation of the raw material, crushing and cleaning of fluorspar, was performed according to the method devised by GOI. To prepare fluorite granules requires 40 to 50 hours. First the raw fluorite is subjected to quenching by alternate heating to 300-400°C and cooling in water. This insures fracturing of fluorite around inclusions (due to differences in coefficients of thermal expansion). Then it is crushed into granules less than 0.5 mm in diameter, purified in hydrochloric and hydrofluoric acids, and dried. Some varieties require preliminary surface cleaning. Rare earths were not introduced into the raw material.

25 crystals of optical fluorite were grown from fluorspar of the Solonechnoe deposit. The best crystals (as good as natural crystals), so far as dispersion of light and transparency in the visible infrared regions are concerned, are crystals grown from fluorspar with good cleavage and mirror-like surfaces (Fig. 2).

Crystals grown from columnar fluorspar of Kalangui were turbid and terminated with a porcelain-like substance. Columnar fluorspar contains impurities which cannot be removed because of the extreme smallness of the particles. This necessitates grinding the ore into particles unresolvable by the microscope, an impossible and useless procedure in view of the hydrolysis of CaF_2.

The crystals grown from Abagaitui material are opaque. Opacity of crystals grown from coarsely crystalline fluorspar with distinct cleavages is due to the presence of quartz and barite intimately intergrown with the spar. These impurities are also the cause of imperfect cleavage.

Fig. 3. Fluorspar from the Solonechnoe deposit with mirror-like cleavage surfaces.

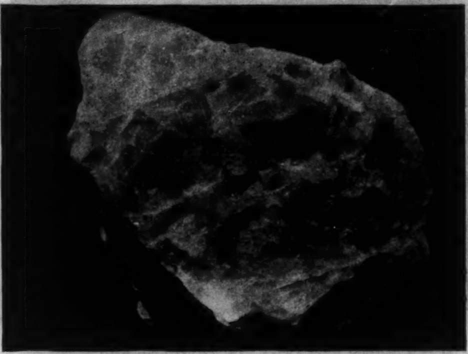

Fig. 4. Fluorspar from the Kul'-i-Kolon deposit.

Tests were made on coarse-grained, poorly crystallized fluorspar from Kul'-i-Kolon. Its semi-opacity is due to the presence of gaseous, liquid and solid inclusions, the latter being mostly barite. These inclusions give the cleavage surfaces of fluorspar a wavy character.

Crystals grown from this fluorspar are transparent but have a higher dispersion than those grown from the Solonechnoe material.

Crystals grown from fluorspar of the western and eastern quarries of Sredny Kaznok contain turbid "sacs" in the center. Lack of transparency is due to the intimate intergrowth of fluorite with barite. The fluorspar is cryptocrystalline to faintly columnar.

Fluorspars from the Oktiabr'skaia Zhila and Chashly deposits are similar in quality. Well developed cleavage and vitreous luster indicate purity of the spar. All associated minerals are easily removed mechanically. Crystals grown from these fluorspars have low dispersion and high transparency for almost the entire spectrum (Fig. 2).

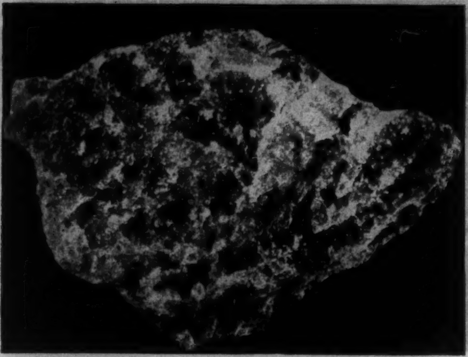

Fig. 5. Fluorspar from Otsolui with poor cleavage.

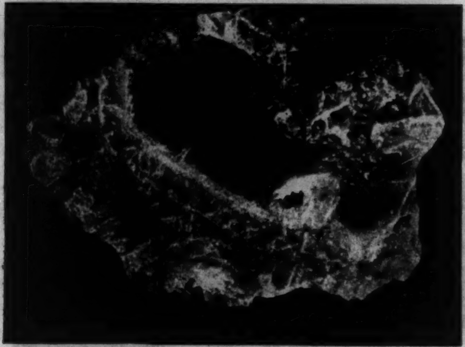

Fig. 6. Fluorspar from Takob with hackly cleavage.

Tests were made on white and violet fractured fluorspar with numerous veinlets of calcite and quartz from Taskainar. These features make the spar nontransparent. Perfect cleavage and mirror-like surfaces indicate purity. The crystals grown from it have much lower dispersion than those grown from the Kul'-i-Kolon material. Transparency for all parts of the spectrum is high (Fig. 2). In order to decrease dispersion of these crystals it is necessary to perfect the separation of fluorspar from quartz and calcite.

Optical characteristics of the artificial crystals of fluorite were obtained from plates 4 mm in thickness polished on both sides. In the ultraviolet part of the spectrum between 125 and 170 mμ measurements were made on the spectrograph SP-41 with a vacuum monochromator and diffraction grating; for the region 170 to 250 mμ, on SP-41 with a fluorite monochromator. Transparency for longer ultraviolet rays (250-390 mμ) of the same samples was measured on SF-4. They were also tested for transparency to infra-red rays up to $\lambda \approx 11\mu$. Transparency and internal dispersion of the fluorite crystals in the visible spectrum were determined on the spectrophotometer of the GOI on polished cylindrical samples with dimensions of the order of ϕ 26 mm × 39 mm.

The limit of transparency to short wave ultraviolet light (160-165 $m\mu$) of fluorite crystals grown from fluorspar is close to that of natural fluorite (130-135 $m\mu$) and of artificial fluorite grown from fragments of optical fluorite (Fig. 2). Samples of artificial crystals from Taskainar do not yield to natural fluorites in transmission of ultraviolet rays in the range of 170 to 390 $m\mu$. Crystals grown from fluorspar of the Solonechnoe and Oktiabr'skaia Zhila deposits have dense absorption bands in the 307 $m\mu$ region which have not yet been explained. These bands are observed also in the natural fluorspar of the Solonechnoe deposit. In the infrared region the artificial fluorite crystals have the same limit of transmission as the natural ones ($\sim$ 10 μ), and differ favorably from the latter in lacking absorption bands of water (near 2.8 and 6.0 μ).

On the basis of analyses and tests the diagnostic features of fluorspar (for field selection) suitable as raw material for growing artificial crystals of optical fluorite are given below.

The diagnostic features are morphological and mineralogical characteristics of fluorspar, structure and cleavage on one hand and admixture of other minerals on the other. Well crystallized fluorspar is generally usable. Depending on the development of cleavage, fluorspar can be classified as follows: first quality – cleavage perfect, mirror-like cleavage surfaces (Fig. 3); second quality – cleavage good, with soft luster on its surfaces (Fig. 4); third quality – cleavage good, with surfaces giving somewhat diffuse reflections.

Unsuitable are fluorspars whose cleavage surfaces diffuse light strongly (Fig. 5), those with hackly cleavages (Fig. 6) and those without cleavage. If fluorspar has the desirable morphological characteristics it is suitable, provided barite is not present as inclusions and the ratio of inclusions to fluorite is not great. Otherwise the process of purification may prove to be uneconomical. The color of fluorspar and its intensity do not affect the quality of artificial crystals. At temperatures above 100°C color disappears. The evaluation of fluorspar must be continued in the laboratory with a microscopic examination in the immersion liquid $n_D \approx 1.434$ (in polarized light). Final conclusions are reached by investigation of optical properties of single crystals grown from the given raw material. Nevertheless, preliminary examination is essential in selecting fluorspar for growing of fluorite crystals transparent through the entire spectrum. Also this examination is sufficient in selecting fluorspar for growing of optical fluorite crystals transparent both in the visible and in the infrared regions of the spectrum.

SUMMARY

1. The possibility of obtaining artificial optical fluorite for certain types of fluorspar has been proved. The solution of this problem gives the USSR a practically unlimited source of this material.

2. Diagnostic features of fluorspar (for selection in the field) suitable as raw material for growing artificial optical fluorite crystals have been found.

3. For growing fluorite crystals transparent both in the visible and in the infrared regions of the spectrum certain kinds of fluorspar from the Solonechnoe, Oktiabr'skaia Zhila and Taskainar II deposits are usable.

4. For growing fluorite crystals transparent in the ultraviolet part of the spectrum use may be made of the Taskainar II fluorspar.

The authors express their sincere gratitude to N. V. Stepanov for his help in this work.

LITERATURE CITED

[1] I. V. Stepanov and P. P. Feofilov, "Two types of luminescence spectra of the rare earths in artificial crystals of fluorite," Doklady Akad. Nauk SSSR, 108, 615-618 (1956).

[2] P. P. Feofilov, "Polarized luminescence of the F-centers in CaF_2," Doklady Akad. Nauk SSSR 92, 545-548 (1953).

[3] V. I. Luchitskii, "Fluorspar in the USSR," Trans. VIMS,* 119 (1937).

[4] N. A. Smolianinov, Fluorspar Deposits of Central Asia [in Russian] (1935).

[5] O. G. Kozlova, "Rare earths in fluorspars of different deposits of the USSR," Geokhimiia 1957, 1.

---

* All-Union Sci. Res. Inst. Mineral Raw Materials.

M. V. Lomonosov State University of Moscow

Received November 20, 1956

EDGE FORMS AND STRIATION ON CRYSTALS

V. I. Mikheev and I. I. Shafranovskii

All the simple edge forms for the lower and middle crystal systems are investigated. Possible types of striations on the crystal faces correspond to these forms. The importance of striae in studying the genesis of crystals is emphasized. The possibility of identifying crystals by their striations is indicated.

In a course on crystallography by A.V. Shubnikov, published in 1923-1925 [1], a diagram was presented showing five different forms of striation on the faces of a cube. Later, this diagram was reproduced in a book by the same author [2]. The diagram in question illustrated the following proposition: "Each of the cubes represents a simple form, since its faces are equal to each other in every respect, but different cubes will differ from each other not only because they are striated differently but by their symmetry... We thus see that crystallography distinguishes five cubes, while geometry is concerned with only one cube."

This proposition later became the starting point for the deduction of physically (crystallographically) different simple forms of crystals [3] and their structural varieties [1]. The diagram showing the striae on different cubes subsequently became very widely used and appeared in elementary textbooks on crystallography. This, however, does not exhaust its importance.

Shubnikov's diagram indicates the strictly systematic character of the striae, demanding careful mathematical treatment for all the simple crystallographic forms, taking the aspects of symmetry into account. Up to the present, the striae on crystal faces have mainly attracted the attention of mineralogists, being a valuable means of identifying minerals (Fig. 2).

Mineralogical literature distinguishes the following forms of striation: 1) growth striation, revealing itself in the stepped character of the faces; 2) solution striation, caused by intense solution of crystals along cleavage cracks; 3) slip striation (deformation), due to the traces of slip planes; 4) twinning striation, corresponding to the traces of twinned intergrowth planes in polysynthetic twins; 5) induction striation, produced in the simultaneous growth of two crystals. Growth striation, associated with the stratified growth of the faces, is in its turn subdivided into combination striation with alternating repetition of two or more crystallographically rational faces, and vicinal zone striation, associated with the alternating repetition of the vicinal faces of one zone.

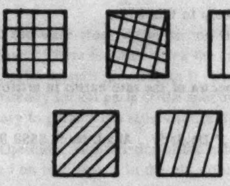

Fig. 1. Possible forms of striation on the faces of five crystallographically different cubes, after A. V. Shubnikov.

From the crystallographic point of view, growth striae are of interest, because they by no means occur always, but only under certain conditions of crystal formation. Valuable mineralogical material illustrating this position was collected by Vernadskii [5]. According to his data, striae on pyrites cubes are observed on crystals of gangue and contact origin, but are absent on crystals occurring in sedimentary rocks; the vertical prismatic striation of topaz is absent on crystals of lythophysa; the well known horizontal

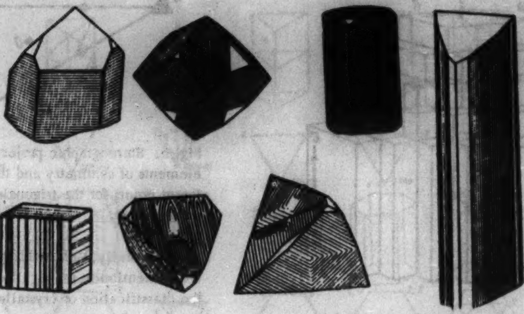

Fig. 2. Characteristic striae on the faces of crystals of different minerals (quartz, diamond, corundum, pyrites, chalcopyrite, arsenopyrites) after E. K. Lazarenko.

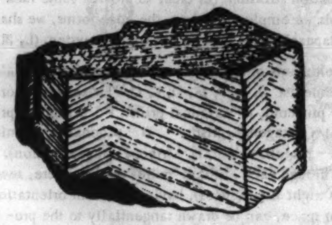

Fig. 3. Oblique striation on prism faces of colorless beryl.

striation of quartz on the $\{10\bar{1}0\}$ faces is not observed at all on quartz from sedimentary rocks. We now know that it is also absent on crystals of synthetic quartz.

According to V. I. Vernadskii, growth striation on mineral crystals depends upon the concentration of the solutions, according to which some crystals may be striated and others not.

In addition, many cases are known where different forms of striation are observed on the same crystal faces. For example, on beryls (aquamarines), the prism faces have vertical striae, whereas on similar faces of colorless beryl, oblique striae, parallel to the $(10\bar{1}0):(11\bar{2}1)$ edge, are observed.

It is evident that beside genetic conditions, striation is determined primarily by purely geometrical causes, connected with the crystal structure (also including symmetry). It is necessary to emphasize the structural importance of striation. It may be recalled that a number of authors, in particular [8, 9], are now advancing the thesis of the influence of chains of strong bonds within the structure on the morphology of crystals. This influence reveals itself in the fact that there are three types of face: flat, stepped and kinked with a complicated structure (Fig. 4). It is evident that stepped faces must have a characteristic combination striation.

Thus, a study of the striation on crystal faces also helps in elucidating the structure of crystals and in particular their genesis.

A prerequisite to the study of any kind of striation is a sound knowledge of striation due to structure, i.e., combination striation. This striation can be derived mathematically on the basis of crystal symmetry. In this case, the striae are always parallel to the crystal edges, and the derivation of the possible forms of striation for specific crystals amounts to a derivation of the crystallographically identical straight lines on the crystal faces.

Such a derivation may be found in part in two of our papers on the edge forms of crystals [10, 11]. We termed the combination of identical crystal edges, derived from the elements of symmetry, simple edge forms (in analogy to the commonly known face forms). The first paper gave the results of the derivation of eighteen simple edge forms of lower systems. In the second, fifty-four edge forms for tetragonal crystals were described. The derivation of edge forms for the trigonal and hexagonal systems is currently being completed. The papers cited gave the examples of crystals of minerals having differentially etched edges.

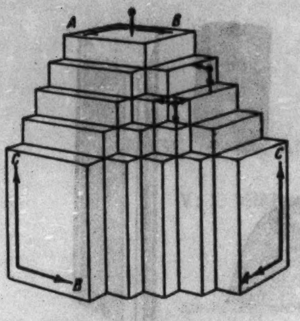

Fig. 4. Diagram showing the structure of the three types of faces: flat, stepped and kinked [8].

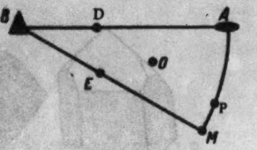

Fig. 5. Stereographic projection of the elements of symmetry and the seven different points for the trigonal-axial form of symmetry.

Recently, Mokievskii and Shafranovskii [12] drew attention to the significance of edge forms in the classification of crystallographic skeletons.

We would here emphasize the fact that simple edge forms and their combinations correspond to the possible types of striation on crystal faces. The complete derivation of such forms will at the same time be the derivation of all the possible types of combination striation. In order to provide some idea of the methods on which this derivation is based and of the symbols we employ to denote the edge forms, we shall discuss the derivation of the simple edge forms for the axial (trapezohedric) form of the trigonal system ($L_3\ 3L_2$).

Figure 5 shows part of the stereographic projection of the elements of symmetry of the given form and also seven different positions of the points corresponding to these elements: B, A, P, M, D, E, O. These points correspond to the gnomostereographic projections of the faces (B – pinacoid, A – trigonal prism, P – ditrigonal prism, M – hexagonal prism, D – trigonal dipyramid, E – rhombohedron, O – trigonal trapezohedron). Through each of these points on the sphere, several straight lines (edges), having different orientations in space, can be drawn tangentially to the projection sphere and consequently located in the planes of the above-mentioned faces (in the derivation, the point B disappears, since the edges derived for it from the given straight line intersect and lie in one plane). A simple edge form will be derived in each case.

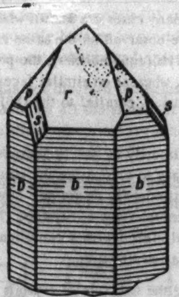

Fig. 6. Striae on the prismatic and dipyramid faces of quartz.

Having considered all the possible cases for the above-mentioned points and deleted the repeated forms, we find all the simple edge forms of the trigonal axial form of symmetry. These forms are denoted by special symbols (Table 1).

In the general case we have assumed, the symbol for the simple edge form is

RNKl (n).

Here, R denotes the trigonal system; N the number of edges of the given form; K denotes the point of contact of the edge with the projection sphere (A, P, M, D, E, O); l the spatial orientation of the edge (h – the edge is horizontal in the plane perpendicular to the principal axis of symmetry; v – the edge is in the vertical plane passing through the principal axis of symmetry; s – the edge lies in an oblique plane); n is the order number of the form with the given symbol.

With the aid of Table 1 it is possible to determine and classify the striations on the faces of crystals of trigonal-trapezohedric form.

TABLE 1

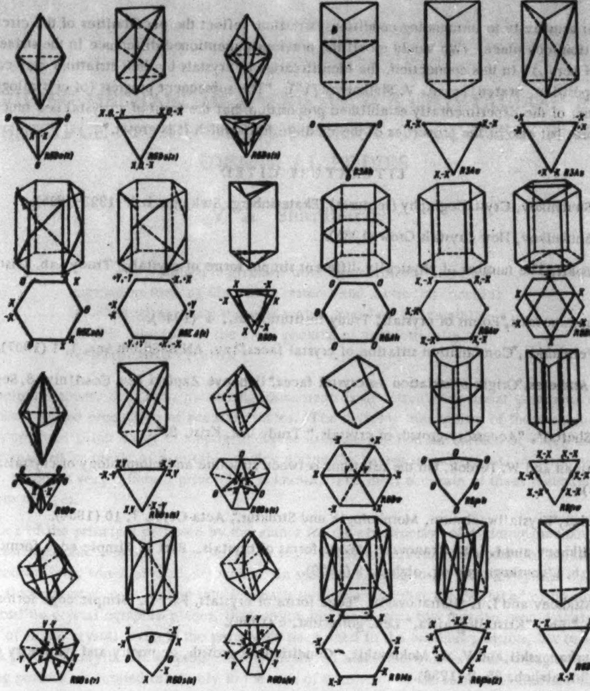

As example, we take the striation of quartz. Comparison of Fig. 6 with Table 1 shows that the horizontal striation on the prismatic faces relates to the simple edge form R6Dh(1), while the oblique striation on the faces of the trigonal dipyramid $\{11\bar{2}\bar{1}\}$ corresponds to the form R6Es(2).

The collation of the various types of striation for crystals of all systems and forms of symmetry, obtained as the result of mathematical deduction, will be of some practical interest. Comparison of the theoretical types of striation of such a collation with the actual striation of a crystal will in some cases enable the knowledge of its form of symmetry to be made more exact and will also reveal the structurally important directions in its structure.

Furthermore, by making use of crystal striations, it ought to be possible to create a specific means of identifying substances from crystal striations, analogous to the well-known criteria of Fedorow [13] and Boldyrev [14]. The angles formed by the striations with the crystal edges are specific constants for crystals of a definite substance and consequently may be used as basis for its identification.

Of course, for identification purposes, special significance will attach to oblique striations (the letter s being their symbol). In addition, the straight striae of h and v type may be used in a number of cases, where these striae intersect oblique edges. It is clear that the crystal edges themselves will also have to be used for identification purposes. The simplest method of measuring plane angles between the striae and edges is to measure them by means of a microscope.

The identification of crystals by their striations will also serve as a means of elucidating the genetic characteristics of crystals.

Due to their sensitivity to surrounding conditions, striations reflect the peculiarities of the circumstance in which crystallization took place. (We would recall the previously mentioned difference in the striae on the prismatic faces of beryl.) In this connection, the identification of crystals by their striations may constitute the answer to the proposition stated by A. V. Shubnikov [15]: "The subsequent progress (of crystallography) will be under the banner of the experimentally established proposition that the form of a crystal is a function not only of its structure, but also of the properties of the medium from which it is grown."

LITERATURE CITED

[1] A. V. Shubnikov, Crystallography (lectures),(Ekaterinburg. Steklogr. izd. 1923-1925).

[2] A. V. Shubnikov, How Crystals Grow (1935).

[3] G. B. Bokii,"The number of physically different simple forms of crystals," Trudy Lab. Kristal. AN SSSR 2 (1940).

[4] I. I. Shafranovskii,"Forms of crystals," Trudy InstitutaKrist., 4 (1948).

[5] V. I. Vernadskii,"Combination striation of crystal faces,"Izv. AN SSSR 6th Ser. 1, 1 (1907).

[6] O. M. Ansheles,"Origin of striation on crystal faces,"Uchenye Zapiski Len. Gos.Univ. 8, Ser. Estest. Nauk, (1943).

[7] N. N. Sheftal', "Accessory growth of crystals," Trudy Inst. Krist. 3.*

[8] P. Hartman and W. Perdok,"On the relations between structure and morphology of crystals. I,"Acta Cryst. 8, I (1955).

[9] W. Kleber,"Krystallwachstum, Morphologie und Struktur.", Acta Cryst. 7, 10 (1954).

[10] V. I. Mikheev and I. I. Shafranovskii, "Edge forms of crystals. Part I. Simple edge forms of lower systems," Miner. sb. L'vovskogo geolog. obshch. 9 (1950).

[11] V. I. Mikheev and I. I. Shafranovskii, "Edge forms of crystals, Part II. Simple edge forms of the tetragonal system," Sb. "Kristallografiia," Len. gorn. inst. 5 (1956).

[12] I. I. Shafranovskii,and V. A. Mokievskii, "Conditions of growth, geometry and symmetry of skeleton crystals," Zap. Min. obshch. 85, 2 (1956).

[13] E. Fedorow, Das Krystallreich, Zapiski Ross. Akad.Nauk (1920).

[14] A.K. Boldyrev,et al., Crystal Identification, Vol. 1, 1st and 2nd parts (1937-1939).**

[15] A. V. Shubnikov and O.M.Shubnikova, "Statistical method as applied to the study of the external form of crystals," Izv. AN SSSR 1926.

Leningrad Mining Institute

Received November 16, 1956

---

* As in original — Publisher's note.

** In Russian.

DIVIDING MECHANISMS BASED ON THE CRYSTALLOGRAPHIC PRINCIPLE OF THE CLOSE PACKING OF GEOMETRICALLY IDENTICAL BODIES

V. A. Shamburov

A description is given of working coordinate dividing engines for making Shubnikov rasters, and a circular machine for dividing accurate circular scales, based on the crystallographic principle of the close packing of geometrically identical bodies (balls).

A principal component of most measuring instruments is the circular or linear graduated scale. Dividing engines are used for the production of accurate scales. The dividing mechanism of these engines produces the intermittent, constant-pitch linear or angular movement of the part, on the surface of which the divisions of the scale are marked by means of a suitable device during the pauses in movement. A large number of dividing mechanisms, based on very different principles, is known. The most accurate of these mechanisms comprise screw or worm devices.

The idea of the principle proposed by the author for the construction of dividing mechanisms originated from the crystallographic concept of the periodic nature of crystal structure composed of identical elements: atoms, molecules, ions, which are "close-packed" in space according to the laws of symmetry. If we imagine a piece of a single crystal to be broken into two parts in such a way that the "surface" of fracture is parallel to one of the possible crystallographic planes, then on joining these parts together, we would again obtain an entire piece of single crystal, even if the parts were not joined in the original position, but in some other position. Such a position may be either progressively displaced along the transfer axes through whole numbers of corresponding periods, or rotated relatively to the axis of symmetry of the surface of fracture through a whole number of angular steps, or it may be displaced and rotated simultaneously. Intermediate positions will be unstable and a single crystal will not be obtained on joining the parts together. Analogously, it is possible to construct a large number of different two-part dividing mechanisms, the contacting elements of whose parts represent mechanical macro-models of the "surfaces" of rupture of the two above-mentioned parts of a single crystal, i.e., they consist of a layer of closely packed, geometrically identical elements, for example balls, rollers, plates, polygons, etc. These elements, in contact with each other and with a retaining ring or frame, form a rigidly connected system. When the two parts of the mechanism are brought into contact with each other, the projecting elements of one of the contacting sides will enter the gaps between the projecting elements of the opposite side.

At the same time, the application of an external force pressing the two parts mechanically together ensures the location of their mutual position, acting in the same way as the interatomic bonding forces when the two parts of a single crystal are joined together in the above-mentioned stable positions. By successively displacing in some way or other the two parts of the mechanism relatively to each other and ensuring positive contact in each located position, it is possible to obtain a series of stepped displacements with intermediate pauses.

From the practical point of view, the greatest interest is presented by two-part dividing mechanisms of this kind, in which the geometrically identical elements are steel balls, such as those used in ball bearings, which can be manufactured commercially with deviations from the mean dimension of a batch not exceeding tenths or even hundredths of a micron.

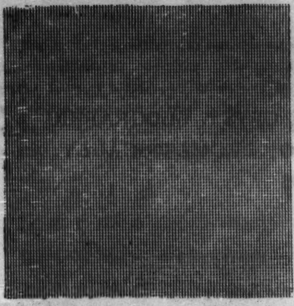

Fig. 1. Shubnikov raster composed of black triangles according to a square grid law.

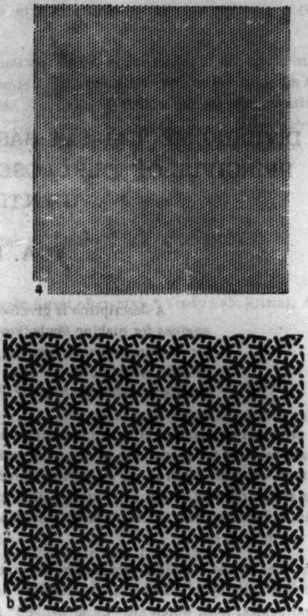

Fig. 2. Shubnikov raster composed of black letters "Γ" according to a hexagonal grid law. a) without axes of symmetry; b) with axes of symmetry.

Using the above-mentioned principle, the author has developed the coordinate dividing engines – ball coordinators [5] – shown in Figs. 3 and 4 for making Shubnikov rasters [1-4] (Figs. 1 and 2) by successive contact printing on a photographic plate 5. The dividing mechanisms of these machines for stepwise displacement of the photographic plate with pauses at the points of a hexagonal (Fig. 3) or square (Fig. 4) grid relatively to a stationary contact printing device 6 consists of two identical parts. The stationary part is a cast-iron verifying plate 1 with a horizontal plane surface. Secured to the plane surface are two pairs of parallel steel strips 2 perpendicular to each other. In the area between the four strips is stuck a layer of closely packed identical steel balls. The balls 3 are situated at the points of a hexagonal(Fig. 3) or square (Fig. 4) grid. The movable part is constructed in exactly the same way but is half the size (see Fig. 5). The balls in both parts are identical, being 12 mm in diameter. On placing the moving plate on the stationary one, the balls come into contact and locate the relative position of the plates, arranging themselves accurately in the gaps of the opposite plate. Even in the event of inaccurate positioning by hand, the plate slips by its own weight into the locating position, i.e., it is self-fixing. In successive pauses of the moving plate into adjacent self-fixed positions, any point on it will occupy in succession a number of positions on the points of a square or hexagonal grid.

In such a two-part ball coordinate dividing mechanism, the successive pauses of the movable plate are produced approximately equal to the pitch by hand (Fig. 3) or by means of an auxiliary automatic mechanism (Fig. 4), and the ball mechanism makes these pauses more accurate, the movable plate with the photographic plate 5 locating itself in the correct position. In the automatic ball coordinate dividing engine (see Fig. 4) the manual operations: stopping the movable plate 4, raising and lowering the lever 5 of the printing device, switching on and off the lamp situated inside tube 6 for the exposures and switching off the machine after the last figure of the raster has been printed, have been made automatic. On testing the accuracy of the automatic ball coordinate dividing engine, it was found that analogous points of the figures of the printed rasters deviated from the points of an ideal square grid by amounts within the limits of 4μ.

The author has developed ball circular dividing mechanisms on the above-mentioned principle. In the simplest case, the mechanism can be constructed in three possible modifications.

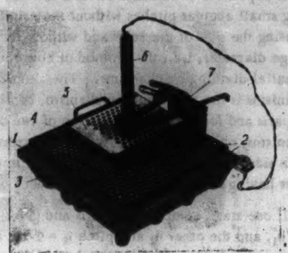

Fig. 3. Manual ball coordinate dividing engine for successive contact printing of hexagonal Shubnikov rasters.

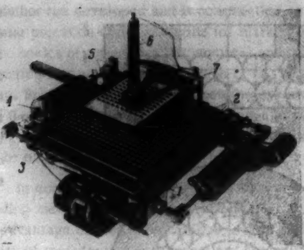

Fig. 4. Automatic ball coordinate dividing engine for successive contact printing of square Shubnikov rasters.

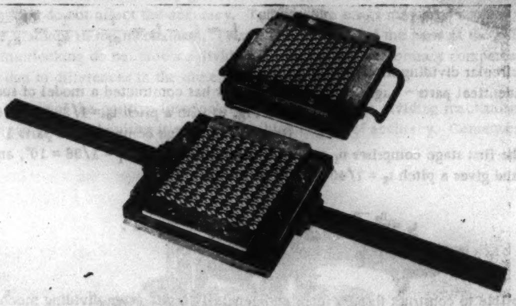

Fig. 5. Movable plates with balls in the inverted position.

In the first modification (see Fig. 6) the parts of the mechanism are two identical closed systems of adjacent identical balls 3 and 4, rigidly held by annular cages 1 and 2, the centers of the balls being situated on circumferences. Each ball of one part is situated between two balls of the other part, and contacts them at points. If the lower cage with its balls is stationary and its axis is vertical, the self-locating position of the movable cage and balls relatively to the stationary cage is effected by the weight of the movable cage itself. By stepwise angular displacement of the movable cage and balls relatively to the stationary cage from one position of location to the next by some means or other, we accomplish the task of various dividing devices, i.e., the problem of constant pitch intermittent angular displacements. The second modification of the mechanism differs from the first in that the size of the balls of one part differs somewhat from that of the balls of the other part (Fig. 7,a). The second modification is the general case and the first and third (Fig, 7, b) modifications are its limit cases. In these three mechanisms, the construction of the cages is shown diagrammatically.

The angular pitch depends upon the number of balls in each cage. If the number of balls in a cage is n, the pitch is t = 1/n'th part of the circumference. For small angular pitches, a large number of balls has to be packed closely in the cage. This leads to the necessity of either increasing the cage diameter, if it is undesirable to reduce the size of the balls, or of decreasing the size of the balls. Either method is restricted in practice by rational limits.

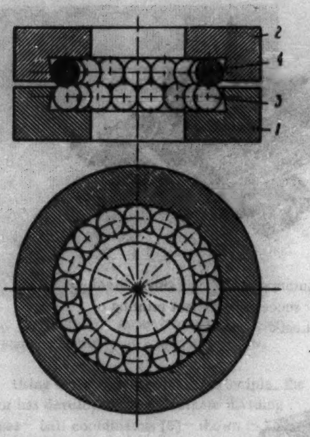

Fig. 6. One-stage ball circular dividing mechanism, consisting of two identical parts — cages with balls.

It is possible to indicate another method of obtaining small angular pitches without materially decreasing the size of the balls and without increasing the cage diameter, i.e., the method of constructing differential dividing mechanisms. The simplest of such mechanisms is the two-stage mechanism, consisting of three parts and forming a combination of two one-stage mechanisms, one cage being common and comprising on both sides two separate centered closed circular systems having different numbers of adjacent balls.

If one stage comprises n_1 balls and gives a pitch $t_1 = 1/n_1$, and the other n_2 and pitch $t_2 = 1/n_2$, as result of the angular displacement by pitch t_1 of the middle part together with the upper part in one direction relatively to the bottom stationary part, and then of the upper part by pitch t_2 in the opposite direction relatively to the middle part, the top part will have rotated by the amount of the pitch t_0, where

$$t_0 = t_1 - t_2 = \frac{1}{n_1} - \frac{1}{n_2} = \frac{n_2 - n_1}{n_1 \cdot n_2}.$$

The author has constructed a model of such a mechanism (see Fig. 8) with a pitch $t_0 = 1/360$ of a circumference. Here the first stage comprises the parts 1 and 2 and the second parts 2 and 3. The first stage comprises $n_1 = 36$ balls and gives a pitch $t_1 = 1/36 = 10°$, and the second comprises $n_2 = 40$ balls and gives a pitch $t_2 = 1/40 = 9°$. The resultant pitch

$$t_0 = \frac{n_2 - n_1}{n_1 \cdot n_2} = \frac{40-36}{40 \cdot 36} = \frac{4}{40 \cdot 36} = \frac{1}{360} = 1°.$$

Similarly, it is possible to construct three-, four- and generally multi-stage dividing mechanisms.

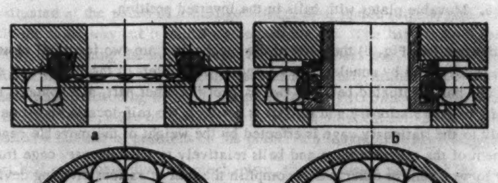

Fig. 7. a) General case of a one-stage ball circular dividing mechanism with different balls in the cages; b) the limit case of such a mechanism.

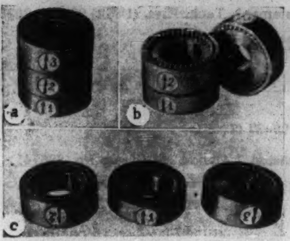

Fig. 8. Model of a two-stage circular ball dividing mechanism.
a) In the assembled form; b) top cage removed; c) dismantled.

On the basis of the two-stage ball dividing mechanism, the author has developed and is constructing an automatic circular precision dividing engine for marking the graduations on the scales of surveying, astronomical and other angle measuring instruments; a photograph of this machine is shown in Fig. 9. The theoretically expected accuracy of the machine is of the order of 1". The minimum angular pitch of the dividing mechanism is 20'. Larger pitches, multiples of 20', can be obtained.

In conclusion, a number of qualities and features of ball dividing mechanisms will be mentioned. In the first place, the advantage of these mechanisms is their simplicity, availability of manufacture, cheapness and the practical possibility of ensuring a high degree of accuracy of dividing work, much higher than in existing dividing engines. The wear of the contacting parts of the dividing mechanisms in service does not reduce their accuracy, but on the contrary, increases it somewhat, due to running in. In the circular dividing mechanisms, there are no accurate rotary guide members (spindles and bearings), and different temperature conditions of working do not affect the accuracy. Temperature errors may arise only as the result of the existence of a temperature gradient in the mechanism. Elastic deformations of the parts at the points of contact of the balls due to positive interlocking do not produce dividing errors, but on the contrary compensate to some extent the effect of errors, due to differences in the dimensions of the balls.

Under the effect of the positive interlocking of the parts of the dividing mechanism, self-location and self-centering of the circular mechanisms is ensured to a high degree of accuracy. Consequently, these mechanisms may be used not only as dividing mechanisms, but also as accurate locating and centering mechanisms. The plane, cylindrical, conical and spherical surfaces of the elements alone require precision manufacture.

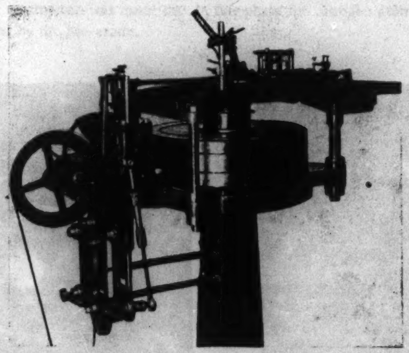

Fig. 9. Automatic circular ball dividing engine for marking the graduations on precision circular scales.

The individual part (cage with balls) of a circular dividing mechanism may be used as an index dial with locator, and the plane dividing mechanism as a coordinate plate. The circular ball dividing mechanism may be used instead of a standard graduated scale in instruments for the investigation of errors and checking the accuracy of the graduation divisions on circular scales.

LITERATURE CITED

[1] A. V. Shubnikov, "The effects of the superposition of grid systems," J. Tech. Phys. (USSR) 22, 12, 2038 (1952).

[2] A. V. Shubnikov, "Moire," Priroda 2, 83-88 (1927).

[3] A. V. Shubnikov, Symmetry [In Russian] (1940).

[4] A. V. Shubnikov, "Advances in raster optics," Priroda 6, 20-27 (1953).

[5] V. A. Shamburov, "Dividing device for angular or linear division," Authors certificate No. 86674, Class $\frac{49B,\ 13}{42B,\ 15}$.

Institute of Crystallography,
Academy of Sciences, USSR

Received November 27, 1956

BRIEF COMMUNICATIONS

ELECTRON DIFFRACTION STUDY OF MOLYBDENUM NITRIDES

Z. G. Pinsker, S. V. Kaverin and N. V. Troitskaia*

Preliminary electron diffraction studies of nitration and of the structure of molybdenum nitrides were carried out. Conditions under which a cubic Mo$_2$N nitride is formed have been noted as well as the presence of two hexagonal phases (of a compound $\sim$MoN with lattice constants: (I) $a = 5.72$, $c = 5.60$ A and (II) $a = 5.665$, $c = 5.52$). The first of these phases shows a layered structure and apparently contains a smaller quantity of nitrogen than the second.

Even though the alloys of the Mo–N system are technically important they have not been widely studied. X-rays have shown the presence in this system of four phases: α, β, γ and δ [1].

The α-phase: practically pure molybdenum;

the β-phase: stable above 600°C;

the γ-phase: at 6.8 weight % an Mo$_2$N compound is formed with a cubic face-centered cell: $a = 4.155$-4.160 A;

the δ-phase: at 50 atomic % nitrogen an MoN compound is formed with a simple hexagonal cell: $a = 2.86$ and $c = 2.804$ A. Later [2] doubling of the a and c axes was noted. Space group D_{6h}^4. On the basis of a geometric analysis the assumption was made that in this phase the nitrogen atoms are placed in the centers of trigonal prisms, formed by the Mo atoms.

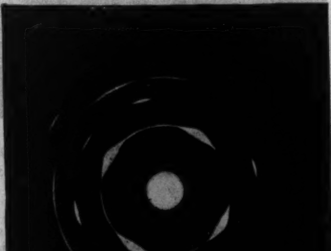

Fig. 1. Electron diffraction pattern of a monocrystalline molybdenum film.

Fig. 2. Electron diffraction pattern of a polycrystalline film of cubic molybdenum nitride.

---

[*] N. B. Kostrova, a student at Gor'kii State University also took part in the study.

In preparing our samples for this study we used as a basic material molybdenum films obtained by the sublimation of the metal in a vacuum with condensation on NaCl crystal faces. In order to obtain monocrystalline molybdenum films, the NaCl crystal was preheated at 345° for 15 minutes and subsequently (after film sputtering) at 450° for 2.5 hours (Fig. 1). We also studied Mo films sublimated on a molybdenum plate stripped with a thin skin.

The nitration process was carried out in an atmosphere of dry ammonia. The nitration temperature range was between 500-780°C, the duration of nitration was between 40-60 minutes. The samples were cooled in a constant flow of ammonia for a period of 2-3 hours.

Ammonia pressure above the metal was decreased by diluting it with a neutral gas and this made it possible to suppress certain nitride compound formation reactions. This technique was used in experiments in which ammonia was predissociated.

The maximum degree of predissociation, equal to 95%, was quite sufficient for the formation of the γ-phase at 750°C (Fig. 2, 3). In a series of experiments, aiming at a greater dissociation of ammonia, iron filings were placed in the boat and the samples placed on top of them. In order to obtain samples of a pure γ-phase, a predissociation of ammonia was carried out and nitration took place without iron filings.

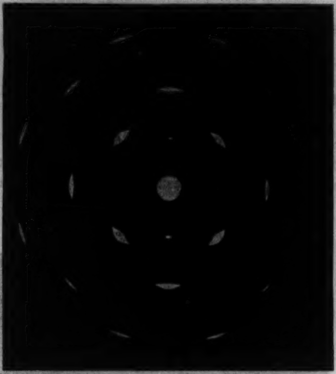

Fig. 3. Electron diffraction pattern of a monocrystalline film of cubic molybdenum nitride.

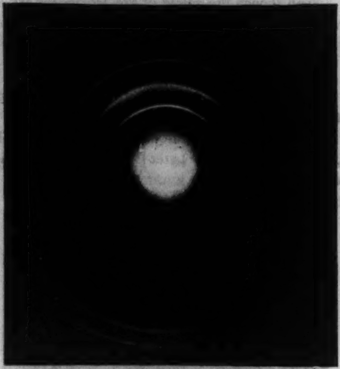

Fig. 4. Diffraction pattern of the reflection from a polycrystalline film of hexagonal nitride (with a NaCl standard).

Mo samples sublimated on a molybdenum plate were nitrated at 700°C for 1-2 hours. In all cases a hexagonal γ-phase was obtained (Fig. 4). In contrast to the x-ray method, the electron diffraction studies of monocrystalline Mo_2N samples showed weak reflections from planes with mixed indices.

When the γ-Mo_2N structures were being studied the experimental intensities of the reflections were determined by photometering of individual diffraction patterns and visually by means of pictures taken with short exposures. The average intensity values obtained by the two methods were used in the calculations.

In the process of deciphering the Mo_2N structure, values were calculated of Φ^2 and Φ along the space diagonal and the cube edge. Maxima were then observed in the center of the cell and in the centers of the edges. A comparison of experimental and theoretical values of the structure amplitudes (Table 1) was subsequently carried out.

Theoretical amplitudes were calculated on the assumption that one atom of nitrogen is placed regularly at the center of the cube and the second one statistically in other octahedral free spaces ($\frac{1}{2}00$, $0\frac{1}{2}$, $00\frac{1}{2}$).

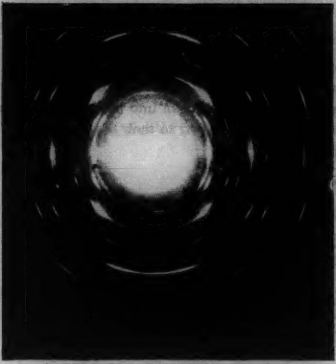

Fig. 5. Diffraction pattern of a type of a diagonal special spatial configuration[•] of a layered hexagonal molybdenum nitride.

TABLE 1

Exp. no.	*hkl*	Theor. Φ_{hkl}	Exp. Φ_{hkl}	Δ
1	100	—1.36	—4.03	2.67
2	110	1.23	6.38	5,16
3	111	24,64	24.70	0,06
4	200	27,76	27.60	0.16
5	220	18,97	22.20	3,24
6	311	12.43	14.95	2.52
7	222	15,08	12,10	2,98
8	231	0.47	2.66	2.19
9	400	12,08	11.25	0,83
10	313	8.46	10.80	2.34
11	240	10.19	13.30	3.11
12	224	8.83	11.76	3.44
13	531	5.24	7.80	2.56
14	620	5.84	7.40	1.56

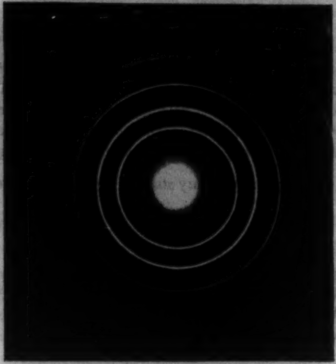

Fig. 6. Diffraction pattern of a polycrystalline film of hexagonal molybdenum nitride.

The experimental values $|\Phi|$ were normalized with the theoretical by multiplication by the magnitude

$$\frac{1}{2}\Big\{(\Phi_{111})\text{ theor.}/(\Phi_{111})\text{ exp.} + (\Phi_{200})\text{ theor.}/(\Phi_{200})\text{ exp.}\Big\}.$$

It is important to note that a relatively good agreement of the intensities does not indicate a regularity in the arrangement of the nitrogen atoms in view of their insignificant scattering properties. In connection with this let us note that the experimental value for the intensity of reflection 110 is greater than the intensity of reflection 100, but theoretically the intensities have a reverse ratio.

When studying δ-nitrides we found two phases with slightly differing periods. When there is an insufficiency of atomic nitrogen, a laminar special spatial configuration[•] δ-MoN with lattice constants a = 5.72, c = 5.60 A is usually formed in experiments with predissociation (700°C, 1 hour, 90% dissociation). Qualitative study of the diffraction patterns taken at an angle (Fig. 5) shows two cells; strong reflections (with $l = 2n$, $n = 0, 1, 2,\ldots$) correspond to a cell with periods half as large and the weak reflections (with $l = 2n + 1$) give the superlattice. As long as the scattering property of nitrogen atoms is at least 6 times less than that of molybdenum, and the reflections, corresponding to the superlattice, are sufficiently strong, there is no doubt that molybdenum takes part in the formation of weak reflections. This means that part of the molybdenum atoms are shifted from their individual positions, which leads to a two-fold increase in the period. The reason for these shifts is still unknown, for each cell has 8 prisms and in each prism there is an atom of nitrogen.

The δ-phase lattice may be represented as consisting of packets each one of which is formed by three atoms layers (MoNMo). The indexing of the pattern taken at an angle of 70° gives reflections which fit into the space group D_{6h}^{4} with the exception of reflection 221.

[•] "Texture;" see footnote on p. 86 — Publisher.

We observed a second hexagonal phase (Fig. 6) with higher atomic nitrogen content. Its lattice constants are

$$a = 5.665,\ c = 5.520\ \text{A}.$$

In this case the introduction of a greater quantity of nitrogen does not increase but rather decreases the lattice periods. This decrease may be due to the following situation. The structure of the layered phase of δ-MoN is not the closest packing ($c/a = 0.98$). The introduction of additional nitrogen into the prisms between (Mo−N−Mo) packets leads not to the pushing apart of molybdenum atoms but rather to their drawing closer together, which is apparently associated with a change in the bond forces.

This is a preliminary study of the molybdenum-nitrogen system.

LITERATURE CITED

[1] Strukturbericht, Band II, 793 (1937).

[2] N. Schönberg, "Contribution to the knowledge of the molybdenumnitrogen and the tungstennitrogen systems," Acta Chem. Scand. 8, 2, 204-207 (1954).

Gor'kii State University
Gor'kii Physico-Technical Research Institute
Institute of Crystallography, Acad. Sci. USSR

Received November 27, 1956

ELECTRON DIFFRACTION STUDY BY REFLECTION OF POWDER SAMPLES OF CELADONITE

B. B. Zviagin and R. A. Shakhova

Powder samples of clay minerals are usually studied by electron diffraction in transmission. The preparations made from suspensions by means of precipitation of the substance onto a backing form grain-oriented polycrystals; when these are studied at an oblique angle to the electron beam, diffraction patterns appear with a well known distribution of reflections along ellipses. These diffraction patterns have a considerable defect: they do not show the 00l basal reflections. However these reflections are very important for the identification of minerals, the study of mixtures, and are indispensable for harmonic synthesis.

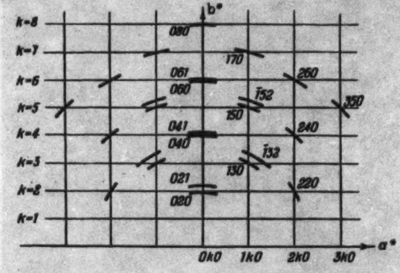
b*
k=8
k=7
k=6
k=5
k=4
k=3
k=2
k=1
080
170
061
060
260
152̄
150
350
041
040
240
132̄
130
021
020
220
0k0
1k0
2k0
3k0
a*

Fig. 1. Distribution diagram of reflections belonging to a texture with a b* axis.

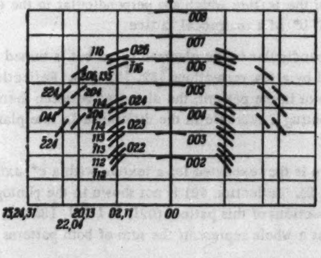
c*
008
007
006
005
004
003
002
116
026
1̄16
206,135
224
204
114
024
044
206
1̄14
023
2̄24
113
1̄13
022
112
1̄12
15,24,31
20,13
22,04
02,11
00

Fig. 2. Distribution diagram of reflections belonging to a texture with a c* axis.

In 1955 the possibility of studying clay minerals by reflection was experimentally proved in paper [1]. The preparations were made by precipitating particles of the substance to be studied onto perfectly polished surfaces of stainless steel. The diffraction patterns, thus obtained, contained the 00l basal reflections.

At VSEGEI [All-Union Geol. Sci. Res. Inst.] a similar study was carried out on celadonite, a mineral with a very perfect and relatively simple structure. It was to be expected that in this case, corresponding to the study of a texture with an inclination angle of 90°, each ellipse would be transformed into a pair of parallel straight lines and the diffraction pattern would show a straight texture with a c* texture axis.

However, the diffraction pattern which was obtained was considerably more complicated. When it

Fig. 3. Electron diffraction reflection pattern of celadonite.

Fig. 4. Electron-microscope picture of celadonite (13,000 ×).

was analyzed it was shown that the main reflections belong to a pattern of a straight texture with a b^* axis (see diagram, Fig. 1) and is obtained largely from those particles of the texture which are perpendicular to the electron beam in plane ab, and thus basically it represents the plane $a^* b^*$ of a reciprocal lattice.

Diffraction of those particles whose ab plane is not perpendicular to the electron beam but is turned at a certain angle around the axis of the b^* texture, is represented by a few reflections $\overset{\pm}{1}32$, $\overset{\pm}{1}52$ etc). Reflection pairs 020-021, 040-041, 060-061 and 080-081 are clearly shown in the pattern; the distances between them naturally decrease as one goes away from the center, representing a decrease in the difference in interplanar spacings.

The other and less clearly discernible part of the pattern is that expected for a texture with a c^* axis and contains basal reflections 002, 003, 004 etc. (see diagram, Fig. 2). Reflection 001 is not shown in the photograph as it lies in the shadow region of the sample. The other reflections of this pattern ($02l$, $\overset{\pm}{1}1l$, $\overset{\pm}{2}0l$, $\overset{\pm}{1}3l$, etc.) are placed along parallel straight lines. The diffraction pattern as a whole represents the sum of both patterns (Fig. 3).

These special features of the diffraction pattern are due to the fact that celadonite particles, as shown by the electron-microscope, are in the shape of long ribbons (Fig. 4). When such particles are precipitated out of a suspension they usually arrange themselves parallel to the backing not only along the plane of these ribbons but also along their long edge, which, in accordance with the diffraction pattern, must coincide with the $\underline{a}$ axis. The transverse direction of the ribbon naturally coincides with the $\underline{b}$ axis, and the $\underline{c}$ axis is inclined to the plane of the ribbon at a certain angle. The elementary celadonite cell ($a = 5.20$, $b = 9.00$, $c = 10.25$ A and $\beta^* = 100.1°$) was determined from transmission patterns of textures.

The results obtained show that, depending on their shape and orientation in reference to the direction of the electron beam, the particles of thinly dispersed layer silicates do not take part equally in the formation of the diffraction pattern. In connection with this, with a nonisometric particle shape additional reflections may appear in the reflection pictures of powder samples of such materials, which in the case of celadonite were even more clear than the reflections of the patterns expected for textures with a c^* axis.

It must be noted that the study of such samples by reflection is complicated by the fact that the diffusion halos from polished surfaces of the backing partially coincide with certain basal reflections.

The authors are deeply grateful to K. M. Malkova for lending them samples of celadonite.

LITERATURE CITED

[1] R. P. Mitra and M. V. R. K. Rao, "Basal reflection of electron waves by oriented aggregates of clay minerals," Naturwissenschaften, 42, 5, 119-120 (1955).

All-Union Scientific-Research Geological Institute

Received November 5, 1956

ON THE CHANGE IN THE NATURE OF THE CHEMICAL BOND WHEN THE COORDINATION NUMBER IS CHANGED

S. S. Batsanov and V. I. Pakhomov

Dependence of the nature of the chemical bond on changes in the structure of a substance is usually associated in crystal chemistry with changes in the interatomic distances.

It is known that with an increase of the coordination number the interatomic distances increase in inorganic crystals. According to Pauling [1] the ionic character of the bond increases. This Pauling explains in the following manner. In a gaseous state, for example in the NaCl molecule, there is one bond of an intermediate nature. During crystallization of this substance only one such bond can operate between Na^+ and Cl^- ions, whereas the other bonds must be ionic. As long as all the interatomic distances in the NaCl coordination polyhedron are equivalent, one may consider all the bonds equal, and then each one of them will show a degree of covalency inversely proportional to the increase in the coordination number in the crystal in relation to the gas.

TABLE 1

Change in the Radii of the Alkali Metals with Degree of Ionization

	Ionization %									
	10	20	30	40	50	60	70	80	90	100
1,57 Na	1.44_5 21.2	1.33_5 15.3	1.28 12.7	1.22 10.2	1.16_5 9.3	1,12 7.6	1.08 6.8	1.04_5 5.9	1.01 5.9	0.98 (0.98) Å 5.1 %
2,09 K	1.93 21.3	1.80_5 16.7	1.71 12.7	1.63 10.7	1.56_5 8.7	1.50_5 8.0	1.45_5 6.6	1.41 6.0	1.37 5.3	1.34 (1.33) Å 4.0%
2,25 Rb	2.09_5 19.6	1.96_5 16.5	1.86 13.3	1.77 11.4	1.70 8.9	1.64 7.6	1.58_5 7.0	1.53_5 6.3	1.49_5 5.1	1.46 (1.49) Å 4.4%
2,63 Cs	2.41 22.7	2.25 16.5	2.12_5 12.9	2.02_5 10.3	1.94 8.8	1.86_5 7.7	1.80_5 6.2	1.75 5.7	1.70 5.2	1.66 (1.65) Å 4.1%
Average	21.2	16.2	12.9	10.6	8.9	7.7	6.6	6.0	5.4	4.4%

TABLE 2

Change in the Radii of Halogen Atoms with Degree of Ionization

	Ionization %										
	0	10	20	30	40	50	60	70	80	90	100
F	0.72	0.74_5 3.5	0.77 3.5	0.80 4.2	0.83_5 4.9	0.88 6.3	0.93 7.0	0.99_5 9.1	1.03_5 12.6	1.21_5 18.2	1.43_5Å 30.8%
Cl	1.00	1.03_5 2.2	1.07_5 2.6	1.12_5 3.2	1.18_5 3.8	1.25 4.2	1.34 5.7	1.45_5 7.3	1.62_5 10.9	1.90 17.6	2.56_5Å 42.5%
Br	1.14	1.18 1.4	1.22_5 1.5	1.28 1.9	1.35 2.4	1.43 2.7	1.53_5 3.6	1.68 4.9	1.90 7.5	2.32 14.3	4.075Å 59.8%

In the case of organic substances Schomaker and Stevenson [2] proposed the following formula for the computation of interatomic distances: $r_{AB} = r_A + r_B - 0.09\ (x_A - x_B)$ where $r_{A,B}$ are the covalent radii, $x_{A,B}$ are the electronegativity of atoms A and B. From this formula it is seen that the interatomic distances will decrease (in comparison to the sum of the covalent radii) as the difference in the electronegativity of the atoms increases, i.e., the greater the ionic character of the bond.

Thus the Pauling method and the Schomaker-Stevenson method give contradictory results; an increase in the ionic character of the bond in the first case is accompanied by an increase in the interatomic distances and in the second case by their decrease. It must be noted that the authors mentioned above do not restrict in any way the region of applicability of their formulas.

With Sanderson's [3, 4] work as a basis, this contradiction may be resolved and a quantitative relation may be derived for the dependence of the interatomic distances on the ionic character of the bond. According to Sanderson, the radius of an atom is associated in the following manner with its electronegativity:

$r = \sqrt[3]{\dfrac{Z}{4.19 \cdot EN \cdot ED_{in}}}$; here EN is the electronegativity of the atom, Z is the number of its electrons and ED_{in} is the electron density for the isoelectronic inert gas atom. Using the numerical values for these magnitudes, given in the above mentioned papers of Sanderson, one can calculate dimensions for atoms in the intermediate bond states.

In Table 1 in the first lines are given values of the radii of the alkali metals (starting at 10% ionic character) from purely covalent to purely ionic; in the second line are given the changes in radii as portions of the total change of radius on complete ionization of the atom. In the last column of the table the Goldschmidt

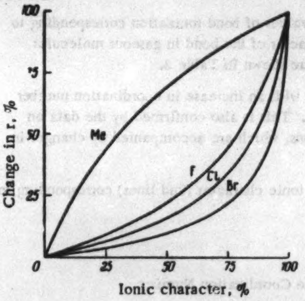

Fig. 1. Change in the radii of atoms with degree of ionization.

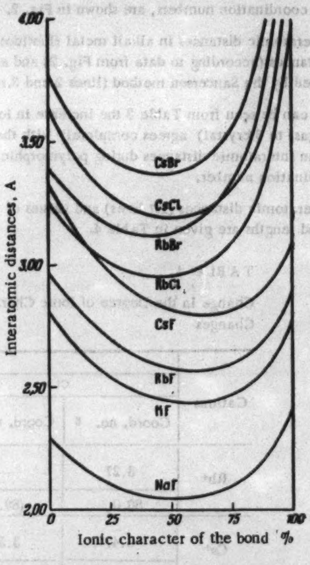

Fig. 2. Change in interatomic distances with bond ionization.

TABLE 3

Changes in Degree of Ionic Character During Crystallization

Anion	Cations			
	Na^+	K^+	Rb^+	Cs^+
F	2.31 95.0 76.0	2.67 95.5 78.0	2 82 96.5 78.0	3.00_5 Å 96.0% 80.5%

values of the ionic radii of the alkali metals [5] are given in brackets.

It can be seen from the Table that the agreement between the ionic radii, calculated according to Sanderson, and the empirical ionic radii is practically complete.

The analogously calculated change in the radii of the halogens arranged as to degree of ionization is given in Table 2.

In this case the agreement between the anion radii, calculated theoretically, and the empirical radii is considerably worse. It may be assumed that this is due to the fact that the Sanderson theory does not take into account the polarization of the ions. In the case of cations polarization is insignificant and there this defect in the theory is not apparent in the values of the radii; the anion polarization is, however, so great that it can not be disregarded. For this reason we shall subsequently only deal with alkali metal fluorides (with the exception of Li) in which the ion deformation is insignificant.

The data of Tables 1 and 2 are graphically represented in Fig. 1. From the graph it is clearly seen that, up to 50% ionic bond character i.e., in the case of predominantly covalent substances, as the polarization of the bond increases, the "cations" decrease in size more than the "anions" increase. Over 50% (highly ionic substances) the reverse is seen: the radius of the "anions" increases more rapidly than the radius of the "cations" decreases. This solves the contradiction mentioned in the beginning of this article, especially in the case of substances with predominantly covalent bonds (organic substances) where, as the polarization of the bond increases, the interatomic distances are shortened, whereas in the case of inorganic substances as the ionic character increases, the interatomic distances increase.

Curves of the change in interatomic distances with changes in the polarity of the bond for alkali metal fluorides, as well as chlorides and bromides of such metals which in a crystalline state show structures with different coordination numbers, are shown in Fig. 2. The curves are drawn from the data of Tables 1 and 2.

Interatomic distances in alkali metal fluorides (first lines), values of bond ionization corresponding to these distances (according to data from Fig. 2) and also ionic character of the bond in gaseous molecules determined by the Sanderson method (lines 2 and 3, respectively) are shown in Table 3.

As can be seen from Table 3 the increase in ionic character with an increase in coordination number from 1 (gas) to 6 (crystal) agrees completely with the Pauling rule. This is also confirmed by the data on changes in interatomic distances during polymorphic transformations, which are accompanied by changes in the coordination number.

Interatomic distances (1st lines) and values of the degree of ionic character (2nd lines) corresponding to these bond lengths are given in Table 4.

TABLE 4

Change in the Degree of Ionic Character When the Coordination Number Changes

Cations	Anions			
	Cl		Br	
	Coord. no. 6	Coord. no. 8	Coord. no. 6	Coord. no. 8
Rb^+	3.27	—	3.43	3.53 Å
	86.0	(89.5)	79.7	84 (84.5) %
Cs^+	3.47	3.56	3.61_5	3.71 Å
	85.5	89.0 (89.1)	78.5	92 (84) %

Absolute values of the ionic character are here apparently somewhat lower due to the fact that the polarization of the anions was not taken into account, but relative changes are sufficiently accurate as in both modifications we have to do with equal cations. As can be seen from Table 4 the Pauling rule holds true here as well (values of the degree of ionic character according to Pauling are given in brackets).

Thus we can draw the general conclusion that when the coordination number is increased in alkali metal halides the degree of bond covalency decreases as the coordination number increases.

LITERATURE CITED

[1] L. Pauling, Nature of the Chemical Bond [Russian translation] (1947).

[2] V. Schomaker and D. Stevenson,"Some revisions of the covalentic radii," J. Amer. Chem. Soc. 63, 37-40 (1941).

[3] R. Sanderson, "Electronegativities in inorganic chemistry, I," J. Chem. Educ. 29, 539-544 (1952).

[4] R. Sanderson, "Electronegativities in inorganic chemistry, IV," J. Chem. Educ. 31, 140-141 (1955).

[5] V. Goldschmidt, Crystal Chemistry [Russian translation] (1937).

M. V. Lomonosov Moscow State University Received Octover 22, 1956

ON THE VIBRATIONAL "STRUCTURE" OF ABSORPTION SPECTRA OF CRYSTALS WHOSE COLORATION IS DUE TO ISOMORPHIC IMPURITIES

S. V. Grum-Grzhimailo and M. G. Enikeeva

Pekar and Krivoglaz [1] have shown that the shape of the band absorption by impurities in dielectrics may be represented as the product of two frequency functions. The first frequency function factor is represented by a smooth bell shaped curve and describes the smooth contours of the absorption spectrum. In the case of previously studied crystals whose coloration was due to isomorphic impurities the absorption band has the form of a Gauss error curve; such absorption bands exist in the case of the ruby (chromium colored corundum) [2] and corundum colored by vanadium.

The second factor in the above mentioned expression for the form of the absorption band describes a vibratory "structure" of the absorption bands.

In the studies carried out earlier at the Institute of Crystallography of the Academy of Sciences, USSR, the vibrational "structure" was found in absorption spectra of corundum colored by chromium and vanadium impurities [3, 4]. The study was carried out in the visible portion of the spectrum in polarized light on a ISP-51 spectrograph at low temperatures (100°K).

In ruby containing 0.1% Cr_2O_3 as an impurity, the "structure" which appears around 170°K was observed on the long wave length side of the absorption band as five supplementary maxima in the ordinary ray only. In corundum, colored by vanadium, the "structure" appearing at higher temperatures than in the case of the ruby, was observed in both the ordinary and the extraordinary ray. Here the maxima of the "structure" absorption in corundum are displaced in relation to the ruby towards the long wave length end of the spectrum, which corresponds with the displacement of the maximum of the wide absorption band [4].

"Structure" bands in corundum, colored by chromium and vanadium, are located at equal distances from each other, with approximately two hundred bands per centimeter. These distances correspond approximately with the natural lattice vibration of corundum, found by Krishnan [5] when studying the infrared absorption spectrum of corundum. Such correspondence leads us to assume that these bands are produced by an interaction of the electron transitions in the impurity ions with the vibrations of the crystal lattice, which agrees with the theoretical conclusions of Pekar and Krivoglaz [1].

Using the same apparatus we studied, in the visible portion of the spectrum at a temperature of 100°K, samples of corundum containing various percentages of chromium oxide (see paper [6] for a description of the samples) with weak and intense colorations; the latter contained about 2% Cr_2O_3. For all of these samples, approximately 1-2 mm thick, "structure" bands in the absorption spectra were also observed in the ordinary ray only, and their position in the spectrum does not depend, within the limit of measurement error, on the amount of chromium they contain. With larger amounts of impurity and more intensive coloration, the spectrograms show a smaller number of "structure" bands.

We also studied absorption spectra of corundum, colored by the isomorphic impurities such as nickel, manganese and titanium. Samples of corundum containing titanium and manganese were synthesized at the Chernorechensk chemical factory where it was impossible to grow a large piece of intensely colored corundum (with large quantities of Mn and Ti the corundum crystals shatter).

In the low temperature absorption spectra of these corundum samples up to 10 mm thick, weakly colored by titanium to a pinkish-violet hue, and by manganese to a pink color, "structure" was not observed. In the absorption spectra of samples up to 100 mm thick, made up to two or three half-pieces, with polished sides, parallel to the optical axis, "structure" bands were observed in the ordinary ray. The position of these bands is the same as that for samples with manganese impurities and samples with titanium impurities and corresponds to the positions of the "structure" bands in ruby. We assume that the "structure" bands observed in the absorption spectra are due to chromium. This is confirmed by the curves of the absorption spectra of these samples which show that their color is affected not only by the Ti and Mn but also by chromium* impurities found in the crystals (absorption maxima, characteristic of ruby are seen in the curve).

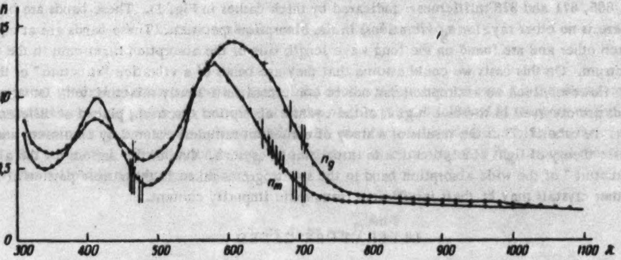

Fig. 1. Curve of the absorption spectrum of cyanite.
Extinction coefficient K is plotted along the ordinate, wave lengths in millimicrons are plotted along the abscissa.

In a corundum sample, colored yellow by nickel, 5 indistinct narrow bands were observed in the ordinary ray, located in the yellow and red portions of the spectrum at varying distances one from the other. Therefore these bands can not be considered as bands produced by a combination of electron transitions with ionic lattice vibrations. In blue corundums (sapphires) studied, 2 mm thick, no narrow absorption bands were found in the spectrum.

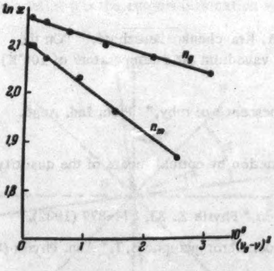

Fig. 2. Graph of ln κ as a function of $(\nu_0-\nu)^2$. $\kappa(\nu)$ is the coefficient of absorption; ν_0 is the frequency corresponding to the maximum of absorption [1, 2] in the red part of the spectrum (n_g) and in the yellow part of the spectrum (n_m).

We studied the absorption spectra of natural minerals in our collection at a temperature of 100°K: emerald, cyanite, red spinel, pyrope, kotschubeite, all colored by chromium; pink tournaline colored by manganese; garnet, beryl and tourmaline colored by iron (the samples were plane parallel plates from 1 to 3 mm thick).

In the absorption spectra of some of the samples narrow absorption bands characteristic of trivalent chromium [7, 8] were observed. Narrow bands were found in the absorption spectrum of dark blue cyanite (a plane parallel plate 9 × 3.5 × 1.2 mm). Two planes (100) perpendicular to an acute bisector of this plate were polished. The cyanite sample, which we studied, came from the Kamenka river in the Cheliabinsk district (from the Mineralogical Museum of the Acad. Sci. USSR); it showed a blue coloration for light vibration along n_g and a less intensive greenish-blue coloration for light vibration along n_m.

---

* A small amount of chromium is always present in all of our corundum samples synthesized at ChKhZ (Chernorechensk Chemical Factory).

The curves of the absorption spectrum for cyanite are shown in Fig. 1 (absorption measurements were taken on a SF-4 spectrophotometer in polarized light). They are characteristic for minerals whose coloration is due to Cr^{3+}. They have two wide bell shaped maxima. Calculations showed that they have the form of the Gauss error curve because all of the experimental values of a number proportional to the logarithm of the absorption coefficient, fall on a straight line, if the square of the difference between the frequency of light and the frequency of the absorption maximum are plotted along the abscissa (see Fig. 2 and [2]), which should agree with the Pekar and Davydov theory [9, 10]. In cyanite, as in corundum, the ions of trivalent chromium replace trivalent aluminum which fills the oxygen octahedrons [11]. A row of narrow absorption bands appears in the red portion of the cyanite absorption spectrum. Dashes in Fig. 1 indicate their position in the spectrum.

For light which had gone through the crystal with n_m vibrations, there are 5 bands among the narrow bands (λ = 655, 660, 665, 671 and 676 millicrons – indicated by thick dashes in Fig. 1). These bands are highly polarized. There is no other ray (for n_g vibrations) in the absorption spectrum. These bands are at equal distances from each other and are found on the long wave length side of the absorption maximum in the yellow end of the spectrum. On this basis we could assume that they are bands of a vibration "structure" of the absorption spectrum. However, such an assumption can not be considered sufficiently substantiated. Other narrow absorption bands are observed in the blue region of the cyanite absorption spectrum, placed at different distances one from the other.* Thus the results of a study of corundum samples, colored by chromium and vanadium, confirm the basic theory of light absorption due to impurities in crystals. One of the reasons for the absence of a vibration "structure" of the wide absorption band in the spectrograms taken in the visible portion of the spectrum for other crystals may be their insufficient isomorphic impurity content.

LITERATURE CITED

[1] M. A. Krivoglaz and S. I. Pekar, "Shape of impurity light absorption spectra and luminiscence in dielectrics," Trudy In-ta fiziki AN Ukrain SSR 4, 37 (1953).

[2] B. N. Grechushnikov and S. V. Grum-Grzhimailo, "On light absorption by impurities in crystals," Trudy In-ta kristallografii, II, 179 (1955).

[3] B. N. Grechushnikov and P. P. Feofilov, "Vibrational structure in the absorption spectrum of ruby," J. Exptl.-Theoret. Phys. (USSR) 29, 3 (8) 384 (1955).**

[4] S. V. Grum-Grzhimailo, B. N. Grechushnikov, and R. A. Kravchenko-Berezhnoi, "On the vibrational structure of absorption spectrum of corundum, colored by vanadium (at a temperature of 100°K)," Trans. of the 10th Conference on Spectroscopy [In Russian] Vol. 4.

[5] R. S. Krishnan, "Raman spectrum of alumina and the luminescence of ruby," Proc. Ind. Acad. Sci., Sec. A 26, 6, 450-459 (1947).

[6] S. V. Grum-Grzhimailo and E. I. Utkina, "On the determination by optical means of the quantity of chromium in ruby," Trudy In-ta kristallografii 8, 99 (1953).

[7] O. Deutschbein, "Über die Spektren des Chroms in Kristallen," Physik Z. 33, 874-877 (1932).

[8] O. Deutschbein, "Die linienhafte Emission und Absorption der Chromphosphore, I," Ann. Physik (5), 14, 712-728, 1932; II, Ann. Physik (7), 14, 729-754 (1932).

[9] S. I. Pekar, "Theory of luminescence and light absorption by impurities in dielectrics," J. Exptl.-Theoret. Phys. (USSR) 29, 197 (1953).

[10] A. S. Davydov, "Theory of absorption, dispersion and diffusion of light by solutions," J. Exptl.-Theoret. Phys. (USSR) 24, 196, 197 (1953).

[11] N. V. Belov, "Essays on structural mineralogy," Coll. L'vov Min. Society 10, 7, 10 (1956).

Institute of Crystallography, Acad. Sci. USSR Received November 26, 1956

---

* Narrow absorption bands in cyanite are observed also at room temperature, but with low temperatures they are more pronounced.

**[Soviet Physics – JETP, p. 388].

MACROSCOPIC EDGE DISLOCATIONS IN A CORUNDUM CRYSTAL

V. L. Indenbom and G. E. Tomilovskii

The optical method of stress analysis is one of the methods that can be used for the direct detection of edge dislocations in crystals which are transparent in the visible [1] and infrared [2] regions of the spectrum. In a cylindrical coordinate system whose axis coincides with the line of the edge dissociation, the radial stress distribution σ_r, the tangential stress distribution σ_θ and the shear stress distribution $\tau_{r\theta}$ around the dislocation are described by the following expressions [3]:

$$\sigma_r = \sigma_\vartheta = -D\frac{\sin\vartheta}{r}, \tag{1}$$

$$\tau_{r\vartheta} = D\frac{\cos\vartheta}{r}. \tag{2}$$

Here ϑ is measured from the slip plane OS (Fig. 1) and $D = \frac{bG}{2\pi(1-\mu)}$, where G is the shear modulus, μ is Poisson's ratio, b is the Burgers dislocation vector (for simplicity we omit the anisotropy of the elastic properties of the crystal). When the isotropic crystal is studied along the line of dislocation between crossed Nicols, the intensity of the illumination of each section will be defined by the square of the shear stresses taken in the system of coordinates whose axes coincide with the axes of the polarizer and analyzer.

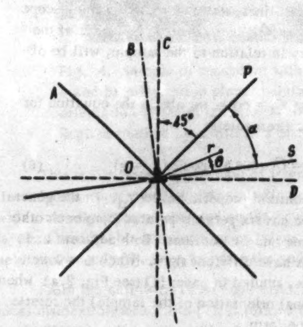

Fig. 1. Observation of edge dislocation by the polarizing-optical method.
OS is the dislocation slip plane;
OP is the axis of the polarizer; OA is the axis of the analyzer (OA ⊥ OP); OP and OC are isoclines (OC ⊥ OD); OB is the neutral line (OB ⊥ OS).

Calculating by means of (1) and (2) the value of the shear stresses τ_α in a coordinate system, rotated in relation to the slip plane by the angle α (see Fig. 1) we obtain

$$\tau_\alpha = \frac{D}{r}\cdot\cos\theta\cdot\cos 2(\vartheta-\alpha). \tag{3}$$

When $\alpha = \vartheta$, Expression (3), as expected, coincides with Equation (2). Equating τ_α to zero we obtain two solutions:

$$\theta = \frac{\pi}{2} \tag{4}$$

(the so called "neutral line" which remains dark when the the sample is rotated between crossed Nicols) and

$$\vartheta = \alpha \pm \frac{\pi}{4}, \tag{5}$$

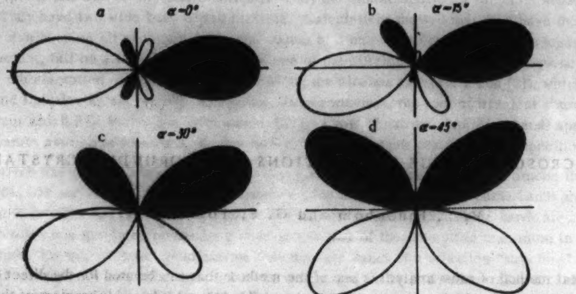

Fig. 2. Equal shear stress rosettes, τ = const, for edge dislocation. a) In a coordinate system one of whose axes coincides with the slip plane ($\alpha = 0$); b) when $\alpha = 15°$; c) when $\alpha = 30°$; d) with diagonal orientation ($\alpha = 45°$); $\tau >$ const regions are blackened.

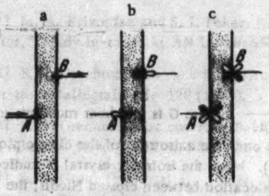

Fig. 3. Diagram of the formation of macroscopic edge dislocations (a) when shear is inhibited, (b) with corresponding illumination rosettes for orientation of the polarizer (or analyzer) planes parallel to the boundary of the interlayer, (c) with diagonal orientation. Direction of slip is indicated by arrows. A positive, B negative edge dislocations. Regions are noted with different signs of the optical path difference. Crossed Nicols.

i.e., two mutually perpendicular isoclines, dark lines moving on the sample as it is rotated between crossed Nicols. It is interesting to note that in this case the isoclines are always placed in a diagonal position in reference to the axes of the polarizer-analyzer. Thus we reach the following interesting conclusion: when an isotropic crystal is examined between crossed Nicols along the line of edge dislocations a cross of mutually perpendicular isoclines, stationary under a microscope and a straight neutral line, crossing the center of the cross, stationary in relation to the sample, will be observed.

Assuming τ_α = const we obtain the equation for the equal shear stress rosette

$$r = C \cdot \cos\vartheta \cdot \cos 2(\vartheta - \alpha), \qquad (6)$$

where C is a constant proportional to τ_α. In the general case the rosette has six petals separated from each other by a neutral line and by isoclines. Both adjacent and opposing petals have different signs. When $\alpha = 0$ we obtain a rosette, studied in paper [1] (see Fig. 2, a), when $\alpha = 45°$ (diagonal orientation of the sample) the rosette equation has the form

$$r = C \cdot \cos\vartheta \cdot \sin 2\vartheta. \qquad (7)$$

Here one of the isoclines joins with the neutral line and the petal which had previously been between them disappears (see Fig. 2, d).* In Fig. 2, b and c such rosettes have been drawn, corresponding to the intermediate cases $\alpha = 15°$ and $\alpha = 30°$.

---

* Let us note that the equal shear stress rosettes look like the anti-symmetrical black-white figures, studied in a general way by Shubnikov [4].

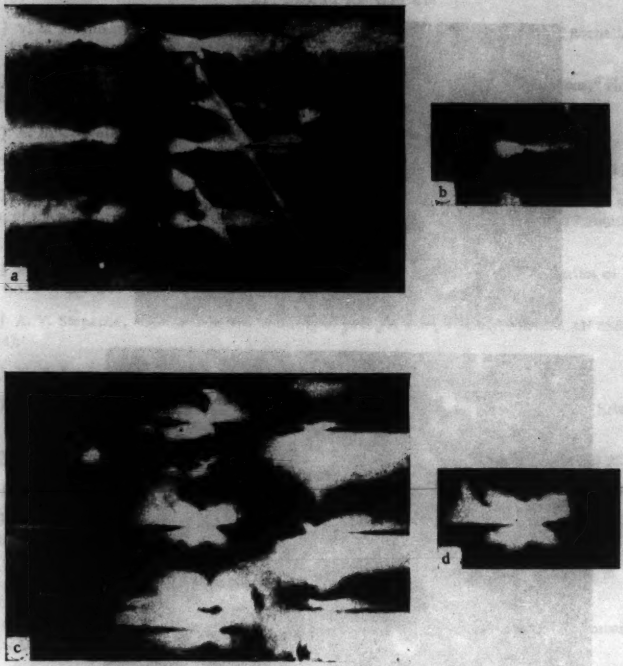

Fig. 4. Sample of corundum with blocked shear. Crossed Nicols.
a and b) Polarization plane parallel to the boundary of the interlayer; c and d) diagonal orientation of the polarizer.
Regions marked by arrows in a and c are enlarged in b and d.

This is illustrated by the case of interior stresses, caused by blocked shear, an interesting case in itself. One of the authors, when studying plastic deformation in synthetic corundum crystals [5], obtained a sample with clear slip lines, interrupted on the boundary between the monocrystal and the differently oriented interlayer. Considerable interior stresses, whose role and significance were qualitatively analyzed in the Klassen-Nekliudova study [6], were found at the end of the slip lines in polarized light.

From the definition of an edge dislocation as a frontal boundary of the slip plane region, along which the local dislocation took place [7], it follows that the shear, inhibited at the boundary of the block, causes (macroscopic [8]) edge dislocation (Fig, 3, a). In this case the dislocations, placed at opposite sides of the interlayer, have different signs. The optical effects, which can be observed between crossed Nicols at the boundary of the slip lines (lines of equal shear stresses correspond to the lines of equal illuminations) are diagramatically shown in Fig. 3, b and c, by means of the rosettes shown in Fig. 2.

In Figs. 4 and 5 are shown photographs between crossed Nicols of the above mentioned corundum crystal with blocked shear. The sample was oriented by means of the Fedorov table, in such a way that the principal axes of the monocrystal and the interlayer coincided approximately with the direction of the microscope axis. Thus the plane of the pictures may be considered (approximately) as the basic plane of the crystal, which, as

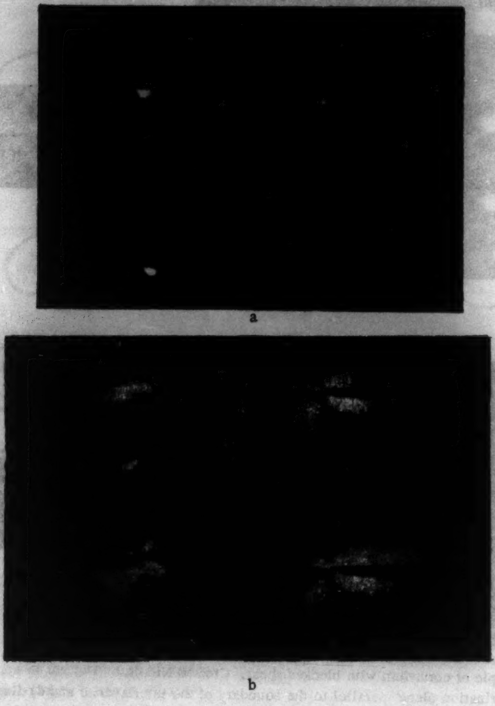

Fig. 5.* Same sample as in Fig. 4. Shifting of the colors when a sensitive plate is introduced:
a) polarization plane parallel to the interlayer boundary; b) diagonal orientation of the polarizer.

is well known [9], is practically isotropic. A certain analogy may be observed between the illumination rosettes shown in Figs. 4 and 5 and the illustrated results of the calculations shown in Figs. 2 and 3. By means of a sensitive plate it was shown that the signs of the stresses actually correspond to the diagrams in Fig. 3,b and c. In the photographs taken, one sign of the shear stresses corresponds to an intensification of the colors and the other to their reduction.

We may assume that a more detailed quantitative study of the phenomenon will establish the size and character of the distribution of interior stresses caused by blocked shear. This is particularly interesting because at the present time such stresses are considered very important in theories on the strength of crystalline materials [10, 11]. Developing of ideas of A. V. Stepanov on the connection between the processes of plastic deformation and destruction [12], the authors assume that dangerous local concentrations of stresses occur due to blocked shear and not to the Griffith cracks.

---

* This figure could not be reproduced in color — Publisher.

LITERATURE CITED

[1] V. L. Indenbom and M. A. Chernysheva, "Edge dislocation ring in a crystal of Rochelle salt," Doklady Akad. Nauk SSSR 111, 596 (1956).

[2] W. L. Bond and J. Andrus,"Photographs of the stress field around edge dislocations," Phys. Rev. 101, 1211 (1956).

[3] A. H. Cottrell, Dislocations and plastic flow in crystals. (Oxford, 1953) p. 34 .

[4] A. V. Shubnikov, Symmetry and Antisymmetry of Terminal Figures [In Russian] (1951).

[5] G. E. Tomilovskii, "Experimental study of synthetic corundum crystal: the effect of nonhomogeneous structure, of surface condition and of thermal treatment on its strength"(Dissertation) [In Russian] Institute of Crystallography, Acad. Sci. USSR (1953).

[6] M. V. Klassen-Nekliudova, "Results of an optical study of the mechanical properties of corundum," Tr. Inst. Krist. 8, 159-160 (1953).

[7] A. V. Stepanov, "On the dislocation theory of strength and plasticity," Izvest. AN SSSR, OTN, 9, 90-107 (1954).

[8] W. T. Read, Dislocations in Crystals (1953) p. 2.

[9] I. M. Sil'vestrova, "Determination of elastic moduli in white sapphire," Tr. Inst. Krist. 8, 283-290 (1953).

[10] A. N. Stroh, "The formation of cracks as a result of plastic flow," Proc. Roy. Soc. 223, 404-414 (1954).

[11] N. J. Petch, "The ductile fracture of polycrystalline α-iron," Phil. Mag. 1, 2, 186-190 (1956).

[12] A. V. Stepanov, "Über den Zusammenhang der Deformationarbeit mit Schmälzwärme," Physik. Z. d. Sow. 2, 537-540, (1932); "On the reasons for premature rupture," Izvest. AN SSSR, Otd. Matem. i Est. Nauk 797-813 (1937).

Institute of Crystallography
Acad. Sci. USSR

Received November 20, 1956

GROWING UNIFORM CRYSTALS OF ROCHELLE SALT FROM STRONGLY SUPERSATURATED SOLUTIONS

N. V. Aliavdin, N. N. Sheftal' and Z. I. Frolova

The present communication concerns an investigation into the possibility of rapidly producing Rochelle salt crystals from strongly supersaturated solutions of high concentration. Industry, by the use of dynamic growing methods, produces large single crystals of Rochelle salt of a weight of the order of 3-4 kg. Usually these crystals are grown in the course of say three or four weeks from slightly supersaturated solutions. If the rate of growth is increased by the use of a higher degree of supersaturation, the result is a disturbance in the crystal uniformity. Our investigations have shown that in experimental conditions, the rate of growth of uniform crystals of Rochelle salt can be increased several times by increasing the supersaturation and temperature beyond the thermodynamic limit of stability of the crystallizing salt.

The work of van't Hoff [1] and van Leeuwen [2] showed that at a temperature above 41°C, Rochelle salt solutions are unstable and begin to dissociate into the separate sodium and potassium tartrates. Sodium tartrate has a lower solubility than Rochelle salt and readily separates out from its solution. This process is rapidly intensified with increase in temperature, 55°C being the point of complete dissociation of Rochelle salt into the individual tartrates. Above this temperature, only a mixture of the tartrates crystallizes out.

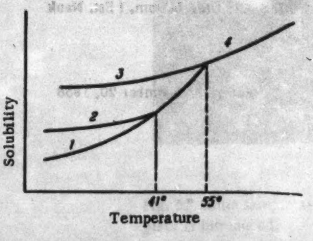

Fig. 1. Solubility curve: 1) Rochelle salt + + sodium tartrate, 2) Rochelle salt, 3) Rochelle salt + potassium tartrate, 4) sodium tartrate + + potassium tartrate.

These relationships are illustrated by the solubility diagram (Fig. 1) [2]. This diagram defines the regions of thermodynamic stability of crystallizing Rochelle salt, and its components, sodium and potassium tartrates.

The separation of sodium tartrate from the solution renders difficult the crystallization of Rochelle salt and completely arrests the growth of uniform crystals. The growth of Rochelle salt crystals by cooling is therefore conducted from a temperature of 40°C or slightly above, since dissociation is only slight from weakly supersaturated solutions in the vicinity of 41°C.

We have studied the cause of dissociation and the conditions of the metastable state of Rochelle salt solutions. We found that dissociation of the salt is due not only to increase in temperature, but also to the presence in the solution of undetectable nuclei of the individual tartrates. If a solution of the salt is subjected to fairly long heating at a temperature above 100°C, the nuclei are destroyed and crystals of Rochelle salt are produced on seeds from such a solution in the range 41-56°C. The presence of nuclei of the individual tartrates in the solution may lead to its dissociation even in the temperature region below 41°C. Thus, the dissociation of highly concentrated solutions at 18°C has been confirmed experimentally. In well heated solutions, the tartrates did not appear even when the solutions were maintained for some time both in the conversion temperature range and at room temperature.

The dissociation of solutions containing nuclei of the individual tartrates depends upon the concentration of the solution: the higher the concentration, the greater is the probability of dissociation. This dependence is also understandable in essence: in a molecule of Rochelle salt $KNaC_4H_4O_6 \cdot 4H_2O$, there are four molecules of water and in the molecules of the tartrates of sodium $Na_2C_4H_4O_6 \cdot 2H_2O$ and potassium $K_2C_4H_4O_6 \cdot \frac{1}{2}H_2O$ together, there are only two and a half molecules of water.

In our initial experiments, the growth of crystals of Rochelle salt was carried out in the range 46-50°C in special flat closed molds (Fig. 2), as well as in test tubes having a capacity of 150 cc. The conditions of the

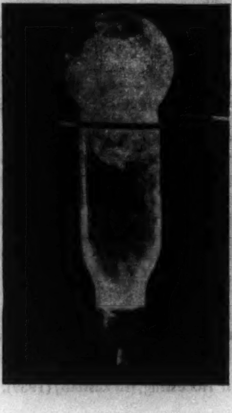

Fig. 2. Single crystal plate grown in a special vessel.

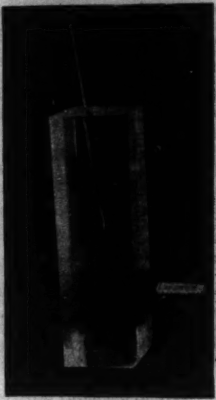

Fig. 3. Uniform single crystal of Rochelle salt weighing 971 g grown in 63 hours.

process were not rigid: temperature fluctuations of several degrees were permitted, the concentration of the solution was varied, salt from different batches was dissolved, etc. In these conditions, adding 3-10% of water to the salt melt, heating the solution to boiling, followed by cooling to a temperature of 46-50°C and crystallization failed to give uniform crystals of more than half a gram in weight. Usually the small crystal, formed from the seed, was intersected by cracks and lacked uniformity. Reducing the supersaturation within the indicated limits merely resulted in a slight procrastination of the destruction of the small single crystal.

The effect of impurities was then tried in order to preserve uniformity of the crystals in unfavorable growth conditions. The literature contains descriptions of cases of the production of large good quality crystals under the stimulating action of impurities [3]. After trying a number of substances, including some colloids, we decided upon a linseed colloidal extract of complex organic structure, possessing high stability compared with other colloids in a wide range of pH concentration. The extract is used in industry for a number of purposes and has been the subject of special investigations [4]. The addition of a 10% alkaline colloidal solution of this extract to the melt of Rochelle salt instead of water ensured uniform growth of the crystals in the above-mentioned conditions. It was thus possible to produce good crystals weighing up to 60 g, grown at a mean rate of growth of 2 mm/hour along the b axis in one direction (Fig. 2). It was subsequently found that with considerable reduction in supersaturation, and particularly with an initial crystallization temperature of 52-52.5°C, uniform crystals could be grown without the colloidal impurity, but with an addition of 10% of water only and at practically half the rate.

For better comparison of the last results with known data, the confining vessels in which the crystals were initially grown were replaced by ordinary crystallizers with revolving crystal holders. In conditions of free growth at a temperature of 52.5°C and with the addition of 10% water, good crystals weighing up to 971 g were obtained at a rate of growth along the c axis of the order of 3 mm/hour. A uniform crystal weighing 971 g was obtained in 63 hours from a point seed (Fig. 3). Growth was from a 4.9 kg solution with a fall in temperature from 52.5 to 51°C. In industry, a crystal weighing 1 kg is grown in 12-13 days.

Crystals grown in the above-mentioned conditions are appreciably elongated on the c axis. Taking the length of the crystal along the c axis as unity, the dimensions along the a axis are 0.32-0.33 and along the b axis 0.41-0.42. The shape of the crystal is formed by the $\{110\}$, $\{210\}$, $\{001\}$ faces, which are not always adjoined by the subordinate faces $\{100\}$ and $\{010\}$. The $\{110\}$ face is developed much more than in crystals grown in the normal way.

As a result of this work, it has thus been shown possible to produce uniform crystals of Rochelle salt on seeds in conditions of its thermodynamic instability during crystallization.

It may therefore be assumed possible to grow large uniform crystals of other substances in conditions of thermodynamic instability.

To increase the rate of growth of crystals in industry, increasing the initial temperature of crystallization to above 43°C is to be recommended. The danger of the appearance of tartrates in this case may be avoided by boiling the solution in the crystallizer.

The authors wish to express their thanks to M. V. Gavrilova and G. B. Netesov for assistance in the experimental work.

LITERATURE CITED

[1] J. H. van't Hoff, Lectures on the Formation and Dissociation of Double Salts, [Russian translation] (1937).

[2] J. D. van Leeuwen, "On the dissociation of Rochelle salt and the corresponding ammonium compounds," Z. phys. Chem., 23, 33-55 (1897).

[3] F. Ehrlich, "On the influencing of the crystal growth of sal ammoniac by pectin," Z. anorg. u. allg. Chem., 203, 1-2, 26-33 (1932).

[4] A. M. Goldovskii, Chemistry of Oil Seeds and Products of their Processing, [in Russian] (1939).

Institute of Crystallography,
Academy of Sciences, U.S.S.R.

Received August 23, 1956

HYDROTHERMAL SYNTHESIS OF SCHEELITE

I. N. Anikin

The author in collaboration with G. B. Bokii previously investigated the solubility of $CaWO_4$ in water and aqueous solutions of some chlorides [1]. The hydrothermal origin and close genetic association of scheelite with quartz in nature leads one to expect successful results from the hydrothermal synthesis of scheelite crystals. The present communication gives the first results of an investigation into the solubility of $CaWO_4$ and its crystallization from water and aqueous solutions of some electrolytes – $CaCl_2$, Na_2WO_4, LiCl, NaCl, NH_4OH, LiOH, NaOH – at pressures of 300-320 atmos and temperatures of 350-500°C.

The experiments were carried out in an autoclave having a capacity of 110 cc, permitting the use of pressures of up to 350 atmos; the autoclave was fitted with a pressure gauge. It was heated in an electric resistance furnace with a vertical temperature gradient, the temperature being measured by chromel-alumel thermocouples at the bottom and in the upper part of the autoclave on its external surface. The difference between these temperatures during the course of the experiments was 40-50°C.

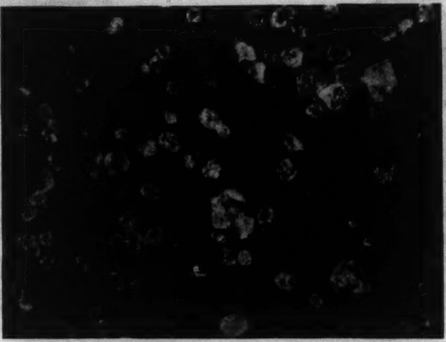

Fig. 1. Synthetic hydrothermal scheelite. × 18.

Four to six single crystal seeds of synthetic scheelite [2] were suspended from a frame in the autoclave at different levels. The seeds were weighed before and after the experiment; the structure of their surface was examined under the microscope. This permitted assessment of the solubility, deposition and transport of substance during the experiment. The autoclave, filled to 60-70% with the above-mentioned 4-6% solutions, remained in the furnace at constant temperature and pressure for 10-12 hours, whereupon the furnace was switched off and the autoclave rapidly cooled. In this way, from the loss in weight of the seeds introduced into the autoclave, it was possible to form a rough estimate of, and compare, the dissolving capacities of the solvents selected.

It was found that the solubility of scheelite in pure water and in solutions of $CaCl_2$, Na_2WO_4, NH_4OH and LiCl is practically nonexistent, amounting only to a few milligrams per 100 g of solvent. Evidently, compared with normal conditions [1], there is no increase in solubility. A somewhat higher solubility is observed in a solution of NaCl (tenths of a milligram per 100 g of solvent), and still higher in a solution of LiOH, but as yet far from sufficient to permit its use for the crystallization of $CaWO_4$ from such solutions.

The solubility of scheelite in a solution of NaOH (a 4% solution was used) was found to be quite considerable. In this case, the seeds of $CaWO_4$, situated in the lower, hotter part of the autoclave, dissolved almost completely (weight of seeds about 3g), and then on cooling, the scheelite crystallized in the form of a fine-grain deposit on the remaining seeds and on the windows of the autoclave in its lower part. Qualitative chemical analysis failed to reveal any appreciable amounts of calcium and tungsten in the solution left after the experiment.

For the purpose of producing larger crystals, an amorphous powder of $CaWO_4$ was dissolved and the cooling time was increased. After first maintaining the temperature at 380°C and the pressure at 300 atmos for several days (50 hours), gradual cooling took place. The result of such re-crystallization was the production of well-faced transparent crystals of scheelite (Fig. 1). The crystals were distributed in the form of nodes over the walls in the bottom part of the autoclave. The average size of the crystals was 0.3-0.5 mm; they have a pseudo-octahedric habit; well developed $e' \{112\}$ faces; some of the crystals show $p \{011\}$ faces. In some crystals, fine gas-liquid inclusions can be seen under the microscope. When the crystals are exposed to x-rays, a blue luminescence is observed.

After the experiment, the solution had a dark brown color, and the crystals were covered with a thin gray coating, attributed to the influence of the autoclave material. It is evident that further experiments will have to be carried out with the use of a silver-lined autoclave.

LITERATURE CITED

[1] G. B. Bokii and I. N. Anikin, "Determination of the solubility of scheelite in water and aqueous solutions," Zhurn. Neorg. Khim. 1, 8, 1926-1928 (1956).

[2] I. N. Anikin, "The possibility of the crystallization of calcium tungstate from the system $CaWO_4$–LiCl." Doklady Akad. Nauk SSSR 110, 4, 645-646 (1956).

Institute of General and Inorganic
Chemistry

Received November 3, 1956

THE PROBLEM OF THE EFFECT OF MECHANICAL AGITATION AND ULTRASONIC VIBRATIONS ON THE PROCESS OF IMPURITY TRAPPING BY SINGLE CRYSTALS

E. M. Akulenok, Kh. S. Bagdasarov and V. Ia. Khaimov-Mal'kov

We have made some experiments to study the effect of agitation on the process of molecular impurity trapping by the faces of single crystals.

The experiments were carried out on single crystals of alumino-potassium alums. Methylene blue dye was used as impurity. Since impurity consisting of this dye is generally trapped by the cube faces of alumino-potassium alums, these faces were subjected to examination.

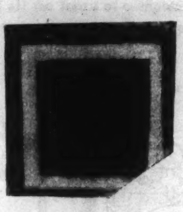

Fig. 1.

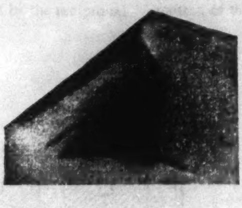

Fig. 2.

In some experiments, agitation was effected by means of a rotary stirrer and in others by means of ultrasonics, a qualitative connection between the trapping of impurity and the degree of agitation being obtained.

Figure 1 shows the photograph of the polished surface of a single crystal with impurity, grown in the following conditions. The crystal first grew in static conditions and then the solution was agitated by means of a stirrer, the speed of rotation of which was increased and diminished in steps. In Fig. 1, the dark colored areas, corresponding to minimum intensity of agitation, have maximum impurity content.

With a view to utilizing the acoustic currents set up in liquids by the action of ultrasonic vibrations, experiments were made to study the effect of ultrasonics on the trapping of impurities by a single crystal. Irradiation was carried out for 8 hours at a frequency of 2 cps.* The approximate intensity of the ultrasonic vibrations in the solution was 0.1 w/cm^2. The polished surface of a single crystal grown in conditions of ultrasonic irradiation is shown in Fig. 2.

For comparison, the crystal was first grown in static conditions (the dark area in Fig. 2, corresponds to this), and then the ultrasonic field was applied.

The similarity of the effect of mechanical agitation (Fig. 1) and that of ultrasonic irradiation (Fig. 2) leads one to believe that the character of the effect is identical in both cases. The nature of the phenomena described permits the conclusion that the quantity of impurity trapped by a single crystal decreases with increase in the intensity of agitation of the solution.

---

* As in original – Publisher's note.

It is considered that the phenomenon may be used for controlling the process of impurity trapping in crystallization from either a solution or a melt.

The author thanks A. V. Shubnikov for the interest shown in this work.

Institute of Crystallography
Academy of Sciences, U.S.S.R.

Received November 27, 1956

NEW METHOD OF PRODUCING VERY HIGH GAS PRESSURES

S. S. Boksha

In the course of some work on the crystallization of substances at very high pressures, it was found that none of the available methods of producing high pressures was able to ensure the required pressure and purity of the compressed gas. We were thus compelled to make a search for new methods of producing very high gas pressures.

The gas compressors currently used in industry and in laboratory practice may be divided into two main groups, according to the principle on which the compression of the gas is effected in them. The first group includes piston and rotary compressors, in which volume compression is used. To the second group belong centrifugal turbocompressors, axial compressors and also injection compressors. In compressors of the last-mentioned type, compression of the gas takes place by the conversion of the kinetic energy of the gas stream into pressure energy. Of all the forms of compressors for producing high pressures, piston compressors alone have found application. In these compressors, the compression of the gas is produced by the reciprocal motion of the pistons.

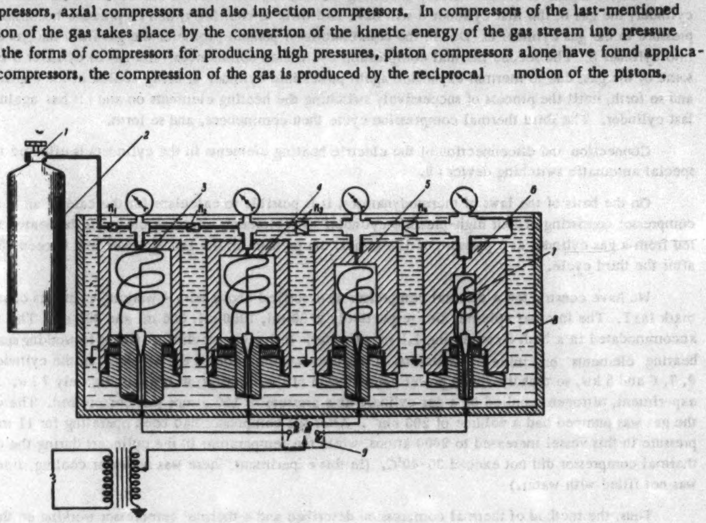

Fig. 1. Diagram of pistonless thermal compressor.

Piston compressors for pressures of 100-1000 atmos are utilized in industry and are perfectly satisfactory in operation, but compressors for 1500-5000 atmos cannot yet be regarded as standard, but as special, complicated equipment, principally of laboratory type [1]. This is due to the considerable constructional and technical difficulties encountered in the design and manufacture of such compressors. Piston compressors also suffer from a number of other drawbacks: 1) contamination of the compressed gas with lubricant substances; 2) low productivity; 3) comparatively low operating reliability; 4) high cost and 5) necessity for skilled attention. All these negative qualities of piston compressors arise from the presence of seals for the moving pistons and piston rods.

The present article describes a pistonless thermal compressor, in which the drawbacks enumerated above have been completely or partly eliminated. In this compressor, the only moving parts are valves.

The working principle of the thermal compressor is the utilization of the expansion of gases when they are heated. The mode of operation of such a compressor can be appreciated by a consideration of Fig. 1. The diagram shows four high-pressure cylinders 3-6, situated in a cooling bath 8 and connected together by steel tubing with systems of valves K_1-K_4, which pass the gas only in one direction (in the diagram from left to right). Each cylinder is equipped with an internal electric heating element 7.

On opening the valve 1, the entire installation is filled with gas at a pressure approximately equal to the pressure of the gas in the gas cylinder 2. The electric heating element in cylinder 3 is then switched on. The gas in this cylinder, due to thermal expansion, passes partly into the next cylinders 4-6, thereby increasing the pressure in them by a certain amount. The gas in these cylinders will be at approximately room temperature, since on its passage through the capillaries, it gives up its heat to the cooling bath 8. The element in cylinder 3 is then switched off and the element in cylinder 4 is switched on. The gas in this cylinder expands by heating, and a certain portion of it, cooling on the way, passes into cylinders 5 and 6, thereby increasing the pressure in them to a certain value. The procedure is continued until all the cylinders have been used.

Figure 1 shows four cylinders, but their number may be increased or reduced according to the demands which the compressor has to meet. On heating the gas in the last cylinder, the first compression cycle is completed.

When the process of successively switching the heating elements on and off has been carried to the last cylinder, the gas in the first cylinder 3 will have had time to cool fully, and its pressure becomes less than the pressure in the gas cylinder 2. Due to the equalization of pressure, some of the gas from the gas cylinder 2 passes into cylinder 3. The second thermal compression cycle then commences: the gas in cylinder 3 is again heated, some of the gas, due to thermal expansion again passes into cylinder 4, being cooled in the capillaries on the way, and so forth, until the process of successively switching the heating elements on and off has again reached the last cylinder. The third thermal compression cycle then commences, and so forth.

Connection and disconnection of the electric heating elements in the cylinders is effected by means of special automatic switching devices 9.

On the basis of the laws of thermodynamics, it is possible to calculate for the case of an ideal gas and a compressor consisting of four high-pressure cylinders with elements enabling the gas to be heated to 800°C and fed from a gas cylinder at a pressure of 150 atmos, the pressure in the last cylinder will exceed 2500 atmos, even after the third cycle.

We have constructed a thermal compressor as described above with 4 working cylinders of stainless steel mark Ia1T. The internal volumes are, respectively 2130 ml, 1360 ml, 500 ml and 480 ml. The cylinders are accommodated in a bath 8 containing 1.5 m^3 of water. Inside each cylinder, filling its working space are nichrome heating elements on mica insulators. The power consumption of the elements in the cylinders is respectively 9, 7, 6 and 5 kw, so that the mean power consumption of the installation is approximately 7 kw. In a control experiment, nitrogen supplied by a gas cylinder at a pressure of 150 atmos was compressed. The vessel into which the gas was pumped had a volume of 200 cm^3. After the compressor had been operating for 11 minutes, the pressure in this vessel increased to 2000 atmos, while the temperature in the cylinders during the coperation of the thermal compressor did not exceed 30-40°C. (In this experiment, there was no water cooling, since the bath 8 was not filled with water.)

Thus, the method of thermal compression described and a thermal compressor working on this method of compressing gas permit:

1) the production of much higher gas pressures than is allowed by methods existing heretofore, in view of the absence of seals for moving pistons and piston rods;

2) the elimination of the use of lubricant, and hence the production of compressed gas uncontaminated by lubricant substances;

3) a considerable cheapening and simplification of both the manufacture and service of compressors.

By such a method, it is possible to compress not only gases but steam-gas mixtures, for which purpose it is merely necessary to use heating elements which do not oxidize at a high temperature, for example platinum heating elements.

We consider that the method we have developed for producing very high gas pressures may be employed in both laboratory practice and in industry.

LITERATURE CITED

[1] B. A. Korndorf, The Technique of High Pressures in Chemistry (1952) [In Russian].

Institute of Crystallography
Academy of Sciences, U.S.S.R.

Received October 30, 1956

We consider that the method we have developed for producing very high gas pressures may be employed in both laboratory practice and in industry.

LITERATURE CITED

[1] E. A. [illegible], The Technique of High Pressures in Chemistry (1952) [In Russian].

Institute of Crystallography,
Academy of Sciences USSR

Received December 28, 1956

SOVIET PHYSICS—CRYSTALLOGRAPHY VOL. 2, NO. 1 JANUARY-FEBRUARY, 1957

(Translation of the journal "Crystallography" of the USSR, Vol. 2, No. 1
published by the American Institute of Physics, September, 1958)

CONTENTS

	Page	Russ. Page
Aleksei Vasil'evich Shubnikov	1	5
Symmetry and Various Kinds of Antisymmetry of Finite Bodies. A. M. Zamorzaev, E. I. Sokolov	5	9
Generalization of Fedorov Groups. A. M. Zamorzaev	10	15
Mosaics for 46 Plane (Shubnikov) Antisymmetry Groups and for 15 (Fedorov) Color Groups. N. V. Belov and E. N. Belova	16	21
Symmetry, Antisymmetry and Pseudosymmetry of Nucleation Surfaces. V. A. Mokievskii and I. I. Shafranovskii	19	23
On the Theory of the Radial Distribution Method. B. K. Vainshtein	24	29
X-Ray Examination of Captax (2-Mercaptobenzothiazole). Iu. Tashpulatov, Z. V. Zvonkova and G. S. Zhdanov	33	38
Metallographic and X-Ray Diffraction Study of Alloys in the Antimony-Iridium System. R. N. Kuz'min, G. S. Zhdanov and N. N. Zhuravlev	42	48
The Crystal Structures of Diphenyliodonium Halides. T. L. Khotsianova	45	51
Electrical Properties and Real Structure of Single-Crystal Germanium Films Produced by Evaporation in Vacuum. G. A. Kurov, S. A. Semiletov and Z. G. Pinsker	53	59
Neutron Diffraction Study of Iron—Nickel Alloys of the Permalloy Class. B. G. Liashchenko, D. F. Litvin, I. M. Puzei and Iu. G. Abov	59	64
The State of Fixation of the Cations of Methylene Blue on the Crystals of Montmorillonite and the Capacity of the Latter to Form Oriented Aggregates. N. E. Vedeneeva and L. I. Tsukerman	68	74
Anomalous Bisectrix Dispersion in Organic Pigment Crystals. N. M. Melankholin	75	78
On the Possibility of Optical Detection of Dauphine Twinning in Quartz. V. L. Indenbom	79	83
Symmetry and Piezoelectric Properties of Crystals and "Textures". I. S. Zheludev	86	89
On the Superposition of Symmetry Groups in Crystal Physics. V. A. Koptsik	95	99
Wood as a Piezoelectric Texture. V. A. Bazhenov	104	108
Piezoelectric Shear Modulus of Polarized Barium Titanate. S. V. Bogdanov, B. M. Vul and R. Ia. Razbash	111	115
Dielectric and Piezoelectric Properties of Polarized Ceramic $BaTiO_3$ in its Various Ferroelectric Phases. L. A. Shuvalov	115	119
Electrophotography on Photoelectrets. V. M. Fridkin	125	130
Plastic Deformation of Crystals Caused by Rotation of the Lattice Without Formation of Glide Lines. M. V. Klassen-Nekliudova and A. A. Urusovskaia	128	134

(continued)

CONTENTS (continued)

	Page	Russ. Page
Propagation of Elastic Shear Waves in a Crystal Bent Around a Specific Direction. K. S. Aleksandrov	134	140
Phase Transitions and Critical Phenomena in Anisotropic Phases. V. K. Semenchenko	139	145
Observations on Layered-Spiral Growth of Crystals from Solutions. M. I. Kozlovskii . .	146	153
Crystallographic Criteria in Selecting Fluorspar for Growing Artificial Crystals of Optical Fluorite. G. B. Bokii and O. G. Kozlova	152	158
Edge Forms and Striation on Crystals. V. I. Mikheev and I. I. Shafranovskii	158	166
Dividing Mechanisms Based on the Crystallographic Principle of the Close Packing of Geometrically Identical Bodies. V. A. Shamburov.	163	172

Brief Communications

	Page	Russ. Page
Electron Diffraction Study of Molybdenum Nitrides. Z. G. Pinsker, S. V. Kaverin and N. V. Troitskaia	169	179
Electron Diffraction Study by Reflection of Powder Samples of Celadonite. B. B. Zviagin and R. A. Shakhova	173	181
On the Change in the Nature of the Chemical Bond When the Coordination Number is Changed. S. S. Batsanov and V. I. Pakhomov	176	183
On the Vibrational "Structure" of Absorption Spectra of Crystals Whose Coloration is Due to Isomorphic Impurities. S. V. Grum-Grzhimailo and M. G. Enikeeva.	180	186
Macroscopic Edge Dislocations in a Corundum Crystal. V. L. Indenbom and G. E. Tomilovskii.	183	190
Growing Uniform Crystals of Rochelle Salt From Strongly Supersaturated Solutions. N. V. Aliavdin, N. N. Sheftal' and Z. I. Frolova	188	193
Hydrothermal Synthesis of Scheelite. I. N. Anikin	191	195
The Problem of the Effect of Mechanical Agitation and Ultrasonic Vibrations on the Process of Impurity Trapping by Single Crystals. E. M. Akulenok, Kh. S. Bagdasarov and V. Ia. Khaimov-Mal'kov.	193	197
New Method of Producing Very High Gas Pressures. S. S. Boksha	195	198

SIGNIFICANCE OF ABBREVIATIONS MOST FREQUENTLY ENCOUNTERED IN SOVIET CRYSTALLOGRAPHY LITERATURE

AN SSSR	*Academy of Sciences, USSR*
FIAN	*Physics Institute, Academy of Sciences USSR*
GITI	*State Scientific and Technical Press*
GITTL	*State Press for Technical and Theoretical Literature*
GOI	*State Optical Institute*
GONTI	*State United Scientific and Technical Press*
Gosfizkhimizdat	*State Physical Chemistry Press*
Gozkhimizdat	*State Chemistry Press*
GOST	*All-Union State Standard*
Goztekhizdat	*State Technical Press*
GTTI	*State Technical and Theoretical Press*
GUPIAE	*State Office for Utilization of Atomic Energy*
IF KhI	*Institute of Physical Chemistry Research*
IFP	*Institute of Physical Problems*
IK	*Institute of Crystallography*
IL	*Foreign Literature Press*
IPF	*Institute of Applied Physics*
IPM	*Institute of Applied Mathematics*
IREA	*Institute of Chemical Reagents*
ISN (Izd. Sov. Nauk)	*Soviet Science Press*
IIaP	*Institute of Nuclear Studies*
Izd	*Press (publishing house)*
KISO	*Solar Research Commission*
LETI	*Leningrad Electrotechnical Institute*
LFTI	*Leningrad Institute of Physics and Technology*
LIM	*Leningrad Institute of Metals*
LITMiO	*Leningrad Institute of Precision Instruments and Optics*
MATI	*Moscow Aviation Technology Institute*
MGU	*Moscow State University*
Metallurgizdat	*Metallurgy Press*
MOPI	*Moscow Regional Pedagogical Institute*
NIAFIZ	*Scientific Research Association for Physics*
NIFI	*Scientific Research Institute of Physics*
NIIMM	*Scientific Research Institute of Mathematics and Mechanics*
NII ZVUKSZAPIOI	*Scientific Research Institute of Sound Recording*
NIKFI	*Scientific Institute of Motion Picture Photography*
OIIaI	*Joint Institute of Nuclear Studies*
ONTI	*United Scientific and Technical Press*
OTI	*Division of Technical Information*
OTN	*Division of Technical Science*
RIAN	*Radium Institute, Academy of Sciences of the USSR*
SPB	*All-Union Special Planning Office*
Stroiizdat	*Construction Press*
TsNIIChERMET	*Central Scientific Research Institute for Ferrous Metallurgy*
URALFTI	*Ural Institute of Physics and Technology*

NOTE: Abbreviations not on this list and not explained in the translation have been transliterated, no further information about their significance being available to us.—*Publisher.*

The expanded program of the American Institute of Physics comprises translation of six leading Soviet physics journals, as listed below. These translations, by competent, qualified scientists, provide all research laboratories and libraries with accurate and up-to-date information of the results of research in the U.S.S.R.

Soviet Physics—Technical Physics

A translation of the "Journal of Technical Physics" of the Academy of Sciences of the U.S.S.R. The translation began with the 1956 issues. Twelve issues per year, approximately 3,000 Russian pages. Annually $75.00 domestic, $79.00 foreign. Libraries* $35.00 domestic, $39.00 foreign. Back numbers, all issues $8.00.

Soviet Physics—Acoustics

A translation of the "Journal of Acoustics" of the Academy of Sciences of the U.S.S.R. The translation began with the 1955 issues. Four issues per year, approximately 400 Russian pages. Annually $12.00 domestic, $14.00 foreign. (No library discounts.) Back numbers, all issues $4.00.

Soviet Physics—Doklady

A translation of all of the "Physics Sections" of the Proceedings of the Academy of Sciences of the U.S.S.R. The translation began with the 1956 issues. Six issues per year, approximately 1,500 Russian pages. Annually $35.00 domestic, $38.00 foreign. Libraries* $15.00 domestic, $18.00 foreign. Back numbers for Volumes 1 and 2, $5.00 per issue; Volume 3 and subsequent, $7.00 per issue.

Soviet Physics—JETP

A translation of the "Journal of Experimental and Theoretical Physics" of the Academy of Sciences of the U.S.S.R. The translation began with the 1955 issues. Twelve issues per year, approximately 4,000 Russian pages. Annually $75.00 domestic, $79.00 foreign. Libraries* $35.00 domestic, $39.00 foreign. Back numbers, all issues $8.00.

Soviet Physics—Crystallography

A translation of the journal "Crystallography" of the Academy of Sciences of the U.S.S.R. The translation began with the 1957 issues. Six issues per year, approximately 1,000 Russian pages. Annually $25.00 domestic, $27.00 foreign. Libraries* $10.00 domestic, $12.00 foreign. Back numbers, all issues $5.00.

Soviet Astronomy—AJ

A translation of the "Astronomical Journal" of the Academy of Sciences of the U.S.S.R. The translation began with the 1957 issues. Six issues per year, approximately 1,100 Russian pages. Annually $25.00 domestic, $27.00 foreign. Libraries* $10.00 domestic, $12.00 foreign. Back numbers, all issues $5.00.

Subscriptions should be addressed to the American Institute of Physics, 335 East 45th Street, New York 17, N.Y.

---

* For libraries of non-profit academic institutions.